Conductivity of strongly pumped superconductors:
An electron-phonon system far from equilibrium

Dissertation
zur Erlangung des akademischen Grades
Dr. rer. nat.
der Fakultät Physik
der Technischen Universität Dortmund

vorgelegt von
Dipl. Phys. Holger Krull
geboren in Dortmund

Lehrstuhl für Theoretische Physik 1
Fakultät Physik
Otto-Hahn-Str. 4
D-44221 Dortmund
Technische Universität Dortmund

-2014-

technische universität
dortmund

1. Gutachter:	Prof. Dr. G. S. Uhrig
2. Gutachter:	Prof. Dr. D. Manske
Vorsitzender der Prüfungskommission:	Prof. Dr. C. Westphal
Vertreterin der wiss. Mitarbeiter:	Dr. B. Siegmann

Abgabedatum:	09. 12. 2014
Tag der Disputation:	29. 01. 2015

Abstract

The study of nonequilibrium physics is of great interest, because one can capture novel phenomena and properties which are hidden at equilibrium, e.g., one can study relaxation processes. A common way to study the nonequilibrium dynamics of a sample is a pump-probe experiment. In a pump probe experiment an intense laser pulse, the so called pump pulse, excites the sample and takes it out of equilibrium. After a certain delay time a second pulse, the probe pulse, measures the actual state of the sample.

In this thesis, we theoretically study the pump-probe response of superconductors. On the one hand we are interest in the effect of a pump pulse and on the other hand we want to provide the pump-probe response, such that experimental measurement can be easily interpreted. In order to do this, we use the density matrix formalism to compute the pump-probe response of the system. In the density matrix formalism equations of motion are set up for expectation values of interest.

In order to study the dynamics induced by a pump pulse, we compute the temporal evolution of the quasiparticle densities and the mean phonon amplitude. We find that the induced dynamics of the system depends on characteristics of the pump pulse. For short pulses, the system is pushed into the nonadiabatic regime. In this regime, the order parameter is lowered during the pump pulse and shows a $1/(\sqrt{t})$-decaying oscillations afterwards. In addition, coherent phonons are generated, which is resonantly enhanced if the frequency of the order parameter oscillation is equal to the phonon frequency. For long pulses, the system is pushed into the adiabatic regime. In this regime, the order parameter is lowered during the pulse and remains almost constant afterwards. Further, there is almost no generation of coherent phonons.

For the pump-probe response we compute the conductivity induced by the probe pulse. The conductivity is a typical observable in real pump-probe experiments. Hence, it is possible to compare the theoretical conductivity with a measured one. We find that the dynamics of the superconductor is reflected in oscillation of the conductivity as function of delay time between pump and probe pulse. This oscillation provides information of the frequency and decay time of the algebraically decaying order-parameter oscillations. Further, the dynamics of the coherent phonons is reflected by an oscillation of conductivity as function of delay time at the phonon frequency.

Kurze Zusammenfassung

Die Physik jenseits vom Gleichgewicht ist ein sehr spannendes Forschungsfeld, weil man neuartige Phänomene und Eigenschaften erfassen kann, die im Gleichgewicht nicht beobachtbar sind. Zum Beispiel können Relaxationsprozesse untersucht werden. Eine gängige Methode zur Untersuchung von Systemen im Nicht-Gleichgewicht ist das sogenannte „pump-probe-Experiment“. In solchen Experimenten bringt ein Laserpuls, der sogenannte „pump pulse“, die Probe aus dem Gleichgewicht. Nach einer Verzögerungszeit misst ein zweiter Laserpuls, der sogenannte „probe pulse“, den aktuellen Zustand der Probe.

In der vorliegenden Arbeit wird das Ergebnis eines solchen Experimentes an einem Supraleiter theoretisch untersucht. Zum einen wird die vom „pump pulse“ erzeugte Dynamik berechnet, zum anderen wird eine typische Messgröße, die Leitfähigkeit, berechnet. Mit dieser Größe ist es möglich die theoretischen Resultate mit denen eines Experiments zu vergleichen. Zur Berechnung wird der Dichtematrixformalismus verwendet. In dieser Methode wird die zeitliche Entwicklung von Erwartungswerten, welche von Interesse sind, berechnet.

Um den Effekt des „pump pulse“ zu untersuchen, wird die zeitliche Entwicklung der Quasiteilchendichten und der mittleren Phononamplitude bestimmt. Die Dynamik dieser Größen hängt von den Eigenschaften des Laserpulses ab. Kurze Laserpulse bringen den Supraleiter ins nichtadiabatische Regime. In diesem Regime wird der Wert des Ordnungsparameters während des Laserpulses abgesenkt und oszilliert danach mit einer $1/(\sqrt{t})$-abfallenden Schwingung. Zusätzlich werden kohärente Phononen erzeugt. Wenn die Phononfrequenz gleich der Frequenz der Ordnungsparameterschwingung ist, wird die kohärente Erzeugung der Phononen verstärkt. Lange Laserpulse hingegen bringen das System ins adiabatische Regime, in welchem der Ordnungsparameter nach dem Puls nicht oszilliert. Des Weitern werden kaum kohärente Phononen erzeugt.

Zusätzlich wird die Leitfähigkeit, die durch den „probe pulse“ induziert wird, berechnet. Die Leitfähigkeit ist eine typische Messgröße eines Experiments und damit ist ein direkter Vergleich zwischen theoretischen und experimentiellen Resultaten möglich. Es wird gezeigt, dass die Leitfähigkeit die Dynamik des System in Schwingungen als Funktion der Verzögerungszeit wiederspiegeln. Diese Schwingungen geben Aufschluss über die Frequenz und den Abfall der Ordnungsparameterschwingung. Zusätzlich beinhaltet die Leitfähigkeit Hinweise auf die Dynamik der Gitterionen. Schwingungen in der Leitfähigkeit als Funktion der Verzögerungszeit bei der Absorptionfrequenz, die gleich der Phononfrequenz ist, spiegeln die Dynamik des Gitters wieder.

Contents

1 Introduction

The study of nonequilibrium dynamics is of special interest, because it reveals a lot of new interesting phenomena such as an induced oscillation of the order parameter of a superconductor. Further, one can study excitation processes, relaxation processes, or thermalization. In this thesis, we are interested in the nonequilibrium dynamics of superconductors induced by a short intense pump pulse. The nonequilibrium dynamics of superconductors has been subject of considerable interest for a long time [1, 2]. Due to a permanent development of experimental as well as theoretical methods, one is able to study the ultrafast time response of a superconductor to nonadiabatic perturbations.

On the experimental side the recent advances of femtoseconds terahertz laser technology [3] lead to many experimental studies focused on the ultrafast time response of superconductors [4–19]. Terahertz laser pulses have a pump energy $\hbar\omega$ which is of the order of the superconducting gap. So one can excite some quasiparticles without destroying the superconducting state.

One common experimental method to investigate the nonequilibrium dynamics induced by a laser pulse is the THz-pump and THz-probe spectroscopy. An intense THz-pump pulse excites the superconductor and induces nonequilibrium dynamics. A second less intense pulse, the probe pulse, measures the actual state of the superconductor after a certain delay time. For instance, the optical conductivity or the transmittivity as function of the absorption frequency ω and the delay time δt provides information about the nonequilibrium dynamics [4–6]. In addition, the reflectivity can also be used as an observable [12, 13]. But not only optical measurement parameter can be used. In the **t**ime **r**esolved **a**ngular **r**esolved **p**hoto**e**mission **s**pectroscopy (trARPES) the photoelectron is used as measurement parameter [15].

On the theory side, intense effort has been devoted to describe the nonequilibrium dynamics of a superconductor. Early attempts were based on the **t**ime-**d**ependent **G**inzburg **L**andau theory (TDGL) [1, 20] or Boltzmann kinetic equation [1, 21, 22]. The TDGL reduces the problem to the time evolution of a single collective order parameter. It is only applicable if a local thermal equilibrium compatible with an instantaneous value of the order parameter is established faster than the time scale of the order parameter variation. This requirement limits the possible applications to special situations, e.g. one has to be close to the critical temperature.

The Boltzmann kinetic equation uses the quasiparticle distribution function as dynamical variables, but the evolution of anomalous expectation values are left out, i.e., coherences between different quasiparticle states. This approach is only valid if external parameters change slowly on the order parameter time scale. In other words, this method is only applicable if adiabatic perturbations are considered.

Further, models based on effective chemical potential μ^* and temperature T^* are used to describe the nonequilibrium dynamics [23]. The excited quasiparticle distribution is described as equilibrium distribution with an effective temperature or potential, respectively. But similiar to the TDGL one has to assume quasi-equilibrium and compute the time evolution of a single collective order parameter only.

Another possible description of the kinetics of a superconductor with a laser pulse is obtained with the help of phenomenological Rothwarf and Taylor model [24]. In this method, rate equations for the quasiparticle and phonon distribution are set up using phenomenological parameters, e.g., a parameter for pair breaking recombination. This method is again only valid for adiabatic perturbation.

The above methods are used to describe the nonequilibrium dynamics of superconductors, but they cannot be applied to compute the nonadiabatic dynamics of a superconductor. Hence, another method is needed to describe the nonadiabatic dynamics of a superconductor.

For example one can use approaches just as the time dependent dynamical mean field theory [25, 26], the time dependent density matrix renormalization [27], the time dependent numerical renormalization group [28], and the forward backward continuous unitary transformation [29]. But for the study of the nonequilibrium dynamics of a superconductor in the superconducting phase, the above methods are not so easily implemented.

In this thesis, the **d**ensity **m**atrix **f**ormalism (DMF) is used to describe the nonequilibrium dynamics of superconductors [30–36]. This method yields equations of motion for the expectation values of interest. Especially, a mean field BCS Hamiltonian which interacts with a laser field can be computed essentially exactly [30]. This method can describe the dynamics of a superconductor induced by an adiabatic as well as by a nonadiabatic perturbation. If a non-bilinear Hamiltonian is considered, the DMF approach has to be truncated to get a closed set of equations of motion.

Of course, the DMF approach is not the only method which is used to describe the nonequilibrium dynamics of superconductors. If the superconductor is perturbed by a quench even an analytic solution can be derived [37–41]. These analyses as well as DMF simulations [30–36] predicted an $1/\sqrt{t}$-decaying oscillation of the order parameter if the perturbation are in a nonadiabatic fashion. This order parameter oscillation can be interpreted as Higgs mode in a superconductor [42].

Recently, the order parameter oscillations are actually measured in THz-pump and THz-probe spectroscopy of thin Niobium nitride films by Matsunaga *et al.* [4–6]. They used a pump pulse of a duration of $\tau = 90\,\text{fs}$ which yields a nonadiabatic excitation of the superconductor and measured a damped oscillation in the transmittivity as well as oscillation in the conductivity as function of delay time [6].
The recent developments motivate to study the outcome of a pump-probe experiment theoretically. To this end, we simulate such kinds of experiments for superconductors. Here, we consider not only the pure BCS Hamiltonian but rather an additional coupling to phonons. The additional phonon coupling is considered to study the effect of the nonequilibrium quasiparticle dynamics on the lattice ions. The lattice dynamics induced by a pump pulses has been studied experimentally for semiconductors [43–45] as well as for high-temperature superconductors [14, 46, 47]. First, we will study the dynamics of the system induced by the pump pulse, e.g. order parameter oscillation or generation of coherent phonons in the nonadiabatic regime. Second, the response of the probe pulse is computed. In addition, the response is analyzed for signatures of the dynamics induced by the pump pulse. As a result, a direct comparison between theoretical predictions and the experimental results is possible.

This thesis is organized as follows.
In Sect. 2 the employed method, namely the density matrix formalism, is introduced. In addition to the main ideas of it this method is also applied to a simple test model to present its advantages and disadvantages. For a better appreciation of the strength of the DMF a comparison with two other approaches, namely the quantum master equation [48, 49] and the iterated equation of motion methods [50, 51], are presented for the toy model. In Sect. 3, the models under study are presented. It is a mean field type BCS Hamiltonian with or without a coupling to additional phonons which is perturbed by laser pulses. In Sect. 4 some numerical details about the implementation of the DMF are discussed. The equations of motion and some details about the numerical implementation, e.g., the discretization mesh, are presented. The dynamics induced by pump pulse is discussed in Sect. 5. Here, the response of the system for various pump pulse condition is studied. Afterwards, the pump-probe response of the dynamics is studied to find signatures of the pumped dynamics. To this end, some information about the implementation and the results of the simulations are discussed. Finally, we conclude and give an outlook to interesting further investigations in Sect. 7.

2 Methods

In this section, the method is introduced which is applied in this thesis to simulate the nonequilibrium dynamics of a superconductor. The method is the **d**ensity **m**atrix **f**ormalism (DMF). The main task of this technique is to derive **e**quations **o**f **m**otion (EoM) of certain (quasi-) particle densities. The DMF approach was successfully applied to describe the nonequilibrium dynamics induced by a pump pulse to semiconductors [52–55] as well as to superconductors [30–36, 56]. One advantage of this method is that one can compute the interaction of a light field with a BCS mean field superconductor essentially exactly [30], except for inaccuracies due to discretization, and cover all dynamical regimes of the system. The exact description is caused by the mean field type Hamiltonian of the superconductor.

Certainly, if the system is described by a non-bilinear Hamiltonian, e.g. a Hamiltonian with electron-phonon coupling, the method yields an infinite hierarchy of equations of expectation values higher and higher order [33, 53]. In order to obtain a closed system of equations it is necessary to break this hierarchy. In this thesis, we use the so called correlation expansion [53]. The method and the correlation expansion are introduced in Sect. 2.1.

Depending on the order of the expansion different expectation values can be computed more or less accurately. For instance, in the so called first order of the correlation expansion the generation of coherent phonons can be described whereas a damping of these phonons due to electron-phonon scattering or electron-electron scattering is not computable [33]. The influence of different orders of the correlation expansion is tested first on a simpler model than the BCS Hamiltonian coupled to additional phonons. As simple toy model, we considered the spin boson model in the limit of pure dephasing without tunneling [48, 57], see Sect. 2.3. This model couples to Bosons via a linear coupling. The same kind of coupling is used to describe the coupling between superconductor and phonons in this thesis. In addition, the toy model is exact solvable. Hence, the toy model is well suited to test how the correlation expansion works. Further, we compare the resulting dynamics of different orders of the correlation expansion with other approaches to verify the accuracy of the correlations expansion.

For comparison, we solve a quantum master equation in Lindblad form [48, 49]. The quantum master equation is a standard approach to derive the temporal evolution of an open quantum system. The main ideas and the results are presented in Sect. 2.3.2.

One other but related approach to the DMF is the **i**terated **e**quation **o**f **m**otion method (iEoM) introduced by Hamerla and Uhrig [50, 51]. This method derives a systematically controlled expansion of Heisenberg equation of motion. The iEoM derives equation of motion for operators instead of expectation values as in the DMF. It has been successfully applied to describe the dynamics of a quenched Heisenberg Hamiltonian [50, 51, 58, 59]. The systematically controlled expansion of this method is used to verify the correlation expansion of the DMF. The method is introduced in Sect. 2.2 and also applied to the toy model, see Sect. 2.3.3.

2.1 Density matrix formalism

In the **d**ensity **m**atrix **f**ormalism (DMF) we set up the **e**quation **o**f **m**otion (EoM) for the expectation value of interest by

$$i\hbar\frac{\mathrm{d}}{\mathrm{d}t}\left\langle A\right\rangle = i\hbar\frac{\mathrm{d}}{\mathrm{d}t}\mathrm{Tr}\left(\rho A\right) = \mathrm{Tr}\left(\rho i\hbar\frac{\mathrm{d}}{\mathrm{d}t}A\right) = \mathrm{Tr}\left(\rho\left[A,H\right]\right) = \left\langle\left[A,H\right]\right\rangle, \tag{2.1}$$

where A denotes an operator, H the system Hamiltonian, and $[A, H]$ the corresponding commutator. As has been shown in the above equation, the time derivative of the expectation value can be rewritten into the time derivative of the corresponding operator. The time derivative of an operator is given by the Heisenberg equation of motion. This leads to the commutator in Eq. (2.1).

The method consists of two parts, the first is to set up the equations of motion for the expectation values of interest. The second part is to solve the equation of motion. The second task is accomplished numerically by using a standard Runge Kutta algorithm of 4th order [60].

To set up the EoM for an expectation value $\langle A\rangle$ one has to commute the corresponding operator with the Hamiltonian, see Eq. (2.1). If the Hamiltonian is not bilinear the commutation leads to additional expectation values, whose temporal evolution must be known. So to compute the temporal evolution of these new expectation values one have to use Eq. (2.1) once more which leads again to new values. In the end this yields an infinite hierarchy of equation of motion. To keep the system closed, the differential equation system has to be truncated in some way. To do so, the correlation expansion [53] is used.

In the correlation expansion, correlation between a specific number of particles are neglected at some point. Thereto, we factorize an expectation value including two operators A and B according to

$$\langle AB\rangle = \langle AB\rangle^c + \langle A\rangle \langle B\rangle , \tag{2.2}$$

where c denotes the correction of the factorized parts. The idea of this expansion is that the contribution of the corrections including a certain number of operators become smaller and it can be neglected.

In the numerical implementation we use the EoM of the correlations instead of the EoM of the full expectation value. The EoM of the correlations can be calculated with the help of the EoM of the full expectation value and their factorized parts. For the expectation values $\langle AB\rangle$ the EoM of the correction can be set up via

$$i\hbar\frac{\mathrm{d}}{\mathrm{d}t}\langle AB\rangle = i\hbar\frac{\mathrm{d}}{\mathrm{d}t}\langle AB\rangle^c + \left(i\hbar\frac{\mathrm{d}}{\mathrm{d}t}\langle A\rangle\right)\langle B\rangle + \langle A\rangle\left(i\hbar\frac{\mathrm{d}}{\mathrm{d}t}\langle B\rangle\right) \tag{2.3}$$

$$i\hbar\frac{\mathrm{d}}{\mathrm{d}t}\langle AB\rangle^c = i\hbar\frac{\mathrm{d}}{\mathrm{d}t}\langle AB\rangle - \left(i\hbar\frac{\mathrm{d}}{\mathrm{d}t}\langle A\rangle\right)\langle B\rangle - \langle A\rangle\left(i\hbar\frac{\mathrm{d}}{\mathrm{d}t}\langle B\rangle\right) . \tag{2.4}$$

Due to this the numerical effort is reduced, because the EoM for the correlations simplifies.

In this work, the additional electron-phonon coupling leads to this infinite hierarchy of equations for the BCS superconductor. The first commutation of a fermionic density operator for example leads to the phonon assisted quantities like

$$\left\langle c^\dagger_{\mathbf{k}} c_{\mathbf{k}} b_{\mathbf{p}}\right\rangle = \left\langle c^\dagger_{\mathbf{k}} c_{\mathbf{k}} b_{\mathbf{p}}\right\rangle^c + \left\langle c^\dagger_{\mathbf{k}} c_{\mathbf{k}}\right\rangle \left\langle b_{\mathbf{p}}\right\rangle . \tag{2.5}$$

Here, $c_{\mathbf{k}}$ stands for a fermionic annihilation operator and $b_{\mathbf{p}}$ for a bosonic annihilation operator. In addition, the factorization of these correlation is presented. If we are only interested in the generation of coherent phonons, the correction of these phonon assisted quantities are neglected, e.g.

$$\left\langle c^\dagger_{\mathbf{k}} c_{\mathbf{k}} b_{\mathbf{p}}\right\rangle \approx \left\langle c^\dagger_{\mathbf{k}} c_{\mathbf{k}}\right\rangle \left\langle b_{\mathbf{p}}\right\rangle ,$$

which leads to a closed system and the temporal evolution of the mean phonon amplitude $\left\langle b_{\mathbf{p}}\right\rangle$ can be computed. This truncation is called first order in the correlation expansion, although we do not expand in powers of a small parameter. In particular, the correlation expansion is no expansion in the electron-phonon coupling. As will be discussed in Sect. 5.2.1 the correlation expansion can lead to equations of motion which include contributions of higher order in $g_{\mathbf{p}}$. As a results we can observe a

decaying lattice displacement even in this order. Even though, all effects arising from electron-phonon or electron-electron scattering processes are neglected.
To include processes like electron-phonon or electron-electron scattering, one has to compute the so called second order of the correlation expansion. In this order, the temporal evolution of the phonon assisted correlations is taken into account. This leads to new expectations values including two fermionic and two bosonic operators or four fermionic operators. These new values are again factorized and the corrections including four operators are neglected. Beside the temporal evolution of the coherent phonons, we are now able to compute the one of the incoherent phonon densities. The incoherent phonons density is given by

$$\left\langle b_{\mathbf{k}}^{\dagger} b_{\mathbf{k}} \right\rangle^{c} = \left\langle b_{\mathbf{k}}^{\dagger} b_{\mathbf{k}} \right\rangle - \left\langle b_{\mathbf{k}}^{\dagger} \right\rangle \left\langle b_{\mathbf{k}} \right\rangle . \tag{2.6}$$

To describe the nonequilibrium dynamics of the superconductor coupled to additional phonons we restrict our calculation to the second order of the correlation expansion, i.e., including the temporal evolution of the phonon assisted correlations and the incoherent phonon densities.

2.2 Iterated equation of motion

The iEoM approach leads a systematically controlled expansion of Heisenberg equation of motion. So instead of directly deriving the temporal evolution of certain expectation values as in the density matrix formalism, the temporal evolution of certain operators are computed. If the time dependence of these operators are known one can easily determine the temporal evolution of the corresponding observable by computing the expectation value regarding the initial state.
The approach consists of two parts. The first part is to set up the equations of motion for a set of operators and the second one is to solve these equations. For the second part a Runge Kutta algorithm of 4th order is used again, as in the DMF approach. The derivation of the equations of motion is presented in this section. In order to demonstrate the functionality of this method by an example, we apply it on the toy model, see Sect. 2.3.3.
To derive the equation of motion for an operator the Heisenberg equation of motion is used, given by

$$i\hbar \frac{\mathrm{d}}{\mathrm{d}t} A_{\mathbf{k}} = \left[A_{\mathbf{k}} \ , \ H \right] . \tag{2.7}$$

Depending on the Hamiltonian the commutator may leads to a shift in $\mathbf{k}$ of the operator or to additional operators. A shift in k-space arises from Hamiltonians like the Hamiltonian of the pump pulse, see Sect. 3.3. In the toy model no part of the Hamiltonian leads to a shift in k-space, see Sect. 2.3.

An additional operator is put as extra contribution into the ansatz of the time dependent operator. The ansatz of an operator reads in general

$$A_{\mathbf{k}}(t) = \sum_{\delta} a_{0,\mathbf{k}+\delta}(t) A_{\mathbf{k}+\delta} + \sum_{\delta} a_{1,\mathbf{k}+\delta}(t) A_{\text{new},\mathbf{k}+\delta} + \dots, \tag{2.8}$$

where $A_{\mathbf{k}}$ denotes the operator and A_{new} an arbitrary new operator resulting from the commutator calculation. The time dependence of the operator is put into the prefactors $a_{i,\mathbf{k}+\delta}(t)$. The initial condition of these prefactors are given by $a_{0,\mathbf{k}}(0) = 1$ otherwise $a_{i,\mathbf{k}+\delta}(0) = 0$. For $t = 0$ the ansatz is given by the operator itself

$$A_{\mathbf{k}}(t = 0) = a_{0,\mathbf{k}}(0) A_{\mathbf{k}} = A_{\mathbf{k}}. \tag{2.9}$$

If an extra contribution enters the ansatz one has to consider it in the Heisenberg EoM, which means the corresponding commutator has to be computed. Of course this will produce additional contributions to the ansatz and a truncation is necessary. In this thesis, we truncate using an expansion in the electron-phonon coupling strength with an additional self-consistent truncation. This means that the ansatz only consists of contributions which are of the order $O(g_{\mathbf{p}}^{n})$. Here, n denotes the maximal order of the electron-phonon coupling which is considered. All contributions of higher orders are neglected.

To apply the additional self-consistent truncation, one has to commute the contribution which are proportional to $g_{\mathbf{p}}^{n}$ once more with the Hamiltonian. This leads to a connection to already existing contribution as well as to additional contribution of order $O(g_{\mathbf{p}}^{n+1})$. Then, the new contributions to the ansatz are neglected but connection to contributions which already existed are kept in the differential equation system. It has been successfully shown that this kind of truncation leads to better results [50,51]. How this self-consistent truncation influences the calculation will be also shown for the toy model in Sect. 2.3.3.

If the computation of the commutator is closed, a differential equation system for the prefactors can be set up by comparing the coefficients. The differential equation system can be now solved with a standard Runge Kutta algorithm numerically.

If the Hamiltonian is time independent this approach works as explained above, but if this is not the case the approach changes a bit. For a time dependent Hamiltonian the time evolution operator U is given by

$$U(t,t_0) = T\left[\exp\left(-i\int_{t_0}^{t} H(t')\mathrm{d}t'\right)\right], \tag{2.10}$$

where T is the time ordering operator. The derivation of U is given by

$$i\hbar\frac{\partial}{\partial t}U(t,t_0) = H(t)U(t,t_0) \tag{2.11}$$

For $t_0 = 0$ the Heisenberg picture for an operator A is given by

$$A(t) = U^\dagger(t)A(0)U(t) \tag{2.12}$$

and the time evolution reads

$$\frac{\mathrm{d}}{\mathrm{d}t}A(t) = \left(\frac{\mathrm{d}}{\mathrm{d}t}U^\dagger(t)\right)A(0)U(t) + U^\dagger(t)A(0)\left(\frac{\mathrm{d}}{\mathrm{d}t}U(t)\right) \tag{2.13}$$

$$= \frac{i}{\hbar}[U^\dagger(t)H(t)U(t), U^\dagger(t)A(0)U(t)] \tag{2.14}$$

$$\Rightarrow i\hbar\frac{\mathrm{d}}{\mathrm{d}t}A(t) = [U^\dagger(t)A(0)U(t), U^\dagger(t)H(t)U(t)] = [A(t),\tilde{H}(t)] \tag{2.15}$$

with $\tilde{H}(t) = U^\dagger(t)H(t)U(t)$. This short calculation shows, that the ansatz for the time dependent operators must also be applied to the Hamiltonian. But similar to the operator ansatz, the Hamiltonian is restricted to be correct up to the order of interest in the expansion parameter. All higher contributions of the Hamiltonian are neglected. Hence, not only the operator ansatz becomes larger but the structure of the Hamiltonian becomes more complicated.

Further, the numerical effort raises for a time-dependent Hamiltonian, because to compute the temporal evolution of a certain operator one needs the evolution of all operators of the Hamiltonian, i.e, the equation of motion of a prefactor for a certain operator possess also prefactors of another operator. This can be seen in the equations of motion of the BCS Hamiltonian perturbed by a quench, see App. B. Here, the prefactors $a_i(t)$ of $\alpha^\dagger_{\mathbf{k}}$ mix with the prefactors $b_i(t)$ of $\beta^\dagger_{\mathbf{k}}$. Instead for the time independent Hamiltonians, only prefactors of the same operator couple with each other, for instance see Eq. (2.54). As a results, we can compute the evolution of a certain operator of interest only. All in all a time dependent Hamiltonian makes the iEoM approach numerically more costly.

In contrast, the toy model is described by a time independent Hamiltonian, see Eq. (2.16). So the standard iEoM as explained above can be applied easily. The controlled expansion of the iEoM will help to understand the effect of the correlation expansion of the DMF, as will be shown in the toy model analysis.

2.3 Toy Model

The spin boson model in the limit of pure dephasing without tunneling [48] is chosen to test the accuracy of the correlation expansion of the DMF. This model is often used to study the influence of decoherence in quantum computers, e.g. see Refs. [61–63] and references therein. The Hamiltonian of this model is given by

$$H = \underbrace{\frac{\hbar\omega_0}{2}\sigma_z}_{=H_S} + \underbrace{\sum_{\mathrm{k}} \hbar\omega_{\mathrm{k}} b^\dagger_{\mathrm{k}} b_{\mathrm{k}}}_{=H_B} + \underbrace{\sigma_z \sum_{\mathrm{k}} g_{\mathrm{k}} \left(b^\dagger_{\mathrm{k}} + b_{\mathrm{k}}\right)}_{=H_I}, \tag{2.16}$$

where $b^\dagger_{\mathrm{k}}(b_{\mathrm{k}})$ is the bosonic creation(annihilation)-operator, ω_{k} the boson frequency, g_{k} the spin-boson coupling strength, and σ_z the Pauli matrix

$$\sigma_z = \begin{pmatrix} 1 & 0 \\ 0 & -1 \end{pmatrix}. \tag{2.17}$$

The Hamiltonian describes a two-level system H_S interacting with a bosonic environment H_B. The coupling between system and environment is described by the interaction Hamiltonian H_I.

As initial condition we set the temperature $T = 0$. The initial state of the spin sub-system should be a superposition of the ground-state $|g\rangle$ and excited-state $|e\rangle$

$$|\psi(t=0)\rangle = \frac{1}{\sqrt{2}} \left(|g\rangle + |e\rangle\right). \tag{2.18}$$

Thus, the corresponding initial reduced density operator ρ_S of the spin system is given by

$$\rho_S(t=0) = \begin{pmatrix} \rho_{S,1,1} & \rho_{S,1,2} \\ \rho_{S,2,1} & \rho_{S.2,2} \end{pmatrix} = \frac{1}{2} \begin{pmatrix} 1 & 1 \\ 1 & 1 \end{pmatrix}. \tag{2.19}$$

The considered toy model serves to illustrate how truncation affects the solution of the DMF approach, which will be introduced in the following. For a quantitative comparison the dynamics of the toy model are computed exactly.

2.3.1 Exact Solution of the spin boson model

One advantage of the toy model is that it is exact solvable [48, 61]. In this section, we sketch calculation of the exact solution. A detailed calculation can be find for example in Ref. [48].
The Pauli matrix σ_z is a conserved quantity for this model, since it commutes with the Hamiltonian $[\sigma_z\ ,\ H] = 0$. As a results, the populations $\rho_{S,1,1}$ and $\rho_{S,1,1}$ are constant in time [48].
To determine the coherence $\rho_{1,2} = \rho^*_{2,1}$ it is advantageous to use the interaction picture. In the interaction picture, the interaction Hamiltonian is given by

$$\tilde{H}_I(t) = \sum_{\mathbf{k}} g_{\mathbf{k}} \sigma_z \left(b_{\mathrm{k}} e^{-i\omega_k t} + b^\dagger_{\mathrm{k}} e^{i\omega_k t} \right) \tag{2.20}$$

and the time-evolution operator is given by

$$\tilde{U}(t) = T \left[\exp \left(-\frac{i}{\hbar} \int_0^t \mathrm{d}s \tilde{H}_I(s) \right) \right] = \phi(t) V(t), \tag{2.21}$$

here $\phi(t)$ is an overall time-dependent phase factor. The operator $V(t)$ is given by

$$V(t) = \exp \left(\sigma_z \sum_{\mathbf{k}} \frac{g_{\mathbf{k}}}{\omega_{\mathbf{k}}} \left[\left\{ 1 - e^{i\omega_{\mathbf{k}} t} \right\} b^\dagger_{\mathrm{k}} - \left\{ 1 - e^{-i\omega_{\mathbf{k}} t} \right\} b_{\mathrm{k}} \right] \right). \tag{2.22}$$

The time evolution is governed by this operator. The temporal evolution of the coherence are given by

$$\tilde{\rho}_{s,1,2}(t) = \langle 1 | \tilde{\rho}_s(t) | 2 \rangle = \langle 1 | \mathrm{Tr}_B \left\{ V(t) \tilde{\rho}_{tot}(0) V^{-1}(t) \right\} | 2 \rangle , \tag{2.23}$$

with the density matrix ρ_{tot} of the complete system. This can be exactly calculated under two standard assumption [61]. First the spin and the environment are initially uncorrelated

$$\rho_{tot} = \rho_S \otimes \rho_B. \tag{2.24}$$

Second, the environment is initially in thermal equilibrium at temperature T

$$\rho_B = \frac{1}{Z_B} \exp\left(-\beta H_B\right). \tag{2.25}$$

Where, $\beta = 1/(k_B T)$ and Z_B is the environment partition function.
With this assumptions we can rewrite Eq. (2.23) into

$$\tilde{\rho}_{s,1,2}(t) = \rho_{1,2}(0)e^{\Gamma(t)}, \tag{2.26}$$

with the decoherence function $\Gamma(t)$ [48]

$$\Gamma(t) = \mathrm{Tr}_B\left\{V(t)\rho(0)V^{-1}(t)\right\} = -\sum_{\mathbf{k}} \frac{4|g_{\mathbf{k}}|^2}{\omega_{\mathbf{k}}^2}\coth\left(\frac{\omega_{\mathbf{k}}}{2k_BT}\right)\left[1-\cos(\omega_{\mathbf{k}}t)\right]. \tag{2.27}$$

As a next step the continuum limit is used. It is given by

$$\sum_{\mathbf{k}} g_{\mathbf{k}}^2 \to \int_0^\infty \mathrm{d}\omega_{\mathbf{k}} F(\omega_{\mathbf{k}}). \tag{2.28}$$

Here, $F(\omega_{\mathbf{k}})$ is the spectral function of the bath. For the spectral function one can use an ohmic function [57], which reads [48]

$$F(\omega_{\mathbf{k}}) = \frac{\alpha}{2}\omega_{\mathbf{k}} \exp\left(-\frac{\omega_{\mathbf{k}}}{\omega_c}\right). \tag{2.29}$$

It shows a linear increase with slope $\frac{\alpha}{2}$ for small frequencies and an exponential frequency cutoff at the cutoff frequency ω_c.
Further, we are interested in the special case at $T = 0$. Hence, $\Gamma(t)$ reads

$$\Gamma(t) = -\int_0^\infty \mathrm{d}\omega \frac{2\alpha}{\omega}\exp\left(-\frac{\omega_{\mathbf{k}}}{\omega_c}\right)(1-\cos(\omega t)) = -\alpha\ln\left(1+\omega_c^2t^2\right). \tag{2.30}$$

Finally, the temporal evolution of the reduced density matrix is given by

$$\rho_{S,1,1}(t) = \frac{1}{2} \tag{2.31a}$$

$$\rho_{S,1,2}(t) = \frac{1}{2}\left(1+\omega_c^2t^2\right)^{-\alpha}\exp(-i\omega_0 t) \tag{2.31b}$$

$$\rho_{S,2,1}(t) = \frac{1}{2}\left(1+\omega_c^2t^2\right)^{-\alpha}\exp(i\omega_0 t) \tag{2.31c}$$

$$\rho_{S,2,2}(t) = \frac{1}{2}. \tag{2.31d}$$

The trace is preserved, but the coherences decay.

Knowing $\rho_S(t)$ we can compute the expectation values of interest to compare the results to the other methods. They are given by

$$\langle\sigma_z\rangle = \mathrm{Tr}\left\{\rho_S(t)\sigma_z\right\} = 0 \tag{2.32}$$

$$\langle\sigma_+\rangle = \frac{1}{2}\left(1+\omega_c^2t^2\right)^{-\alpha}\exp\left(i\omega_0 t\right) \tag{2.33}$$

$$\langle\sigma_-\rangle = \frac{1}{2}\left(1+\omega_c^2t^2\right)^{-\alpha}\exp\left(-i\omega_0 t\right). \tag{2.34}$$

2.3.2 Results for Quantum Master Equation

By way of comparison to the DMF results, we also compute the dynamics of the toy model using a quantum master equation. In this method, the temporal evolution of a system which is coupled to an environment is determined. For the toy model the system is given by H_S and the environment by H_B, see Eq. (2.16). Then the temporal evolution of the reduced density matrix ρ_S can be written in the following form[1]

$$\frac{\mathrm{d}}{\mathrm{d}t}\rho_S = -\frac{i}{\hbar}\left[H_S + H_{LS}\ ,\ \rho_S\right] + \gamma_0(t)\left(\sigma_z\rho_S\sigma_z - \frac{1}{2}\left\{\sigma_z\sigma_z\ ,\ \rho_S\right\}\right), \tag{2.35}$$

where H_{LS} describes the Lamb shift Hamiltonian

$$H_{LS} = \lambda_0(t)\sigma_z\sigma_z. \tag{2.36}$$

The Lamb shift Hamiltonian is cancelled in this calculation, because $\sigma_z\sigma_z = \mathbb{1}$.

The decay rate $\gamma_0(t)$ and the Lamb-shift coupling $\lambda_0(t)$ are given by the real or imaginary part of a function $\Gamma(t,\omega)$

$$\gamma_0(t) = 2\Re\left[\Gamma(t,0)\right] \tag{2.37}$$

$$\lambda_0(t) = \Im\left[\Gamma(t,0)\right]. \tag{2.38}$$

The function $\Gamma(t,\omega)$ is defined to be the correlation of the bosonic bath

$$\Gamma(t,\omega) = \int_0^t \mathrm{d}t' \exp(i\omega t')\mathrm{Tr}_B\left\{B^\dagger(t')B\ (t)\right\}, \tag{2.39}$$

---

[1] A detailed derivation of this equation including all assumptions and approximations can be found in Ref. [49].

with the bath operator $B(t) = g_{\mathbf{k}} \left(b_{\mathrm{k}}^{\dagger}(t) + b_{\mathrm{k}}(t) \right)$.
For zero temperature all modes of the bosonic bath are in the ground state and the Bose distribution is zero for all momenta. Then $\Gamma(t, \omega)$ reads

$$\Gamma(t, \omega) = \int_0^t \mathrm{d}t' \sum_{\mathbf{k}} g_{\mathbf{k}}^2 \exp\left(i(\omega - \omega_{\mathbf{k}})t' \right). \tag{2.40}$$

Applying the continuum limit, see Eq. (2.28), and using the spectral function of Eq. (2.29), the decay rate reads

$$\gamma_0(t) = \frac{\alpha \omega_c^2 t}{1 + \omega_c^2 t^2}. \tag{2.41}$$

With this we can set up the equation of motion for a non-Markovian master equation. Note, for the Markovian master equation the decay rates do not depend on the time and can be computed by letting $t \to \infty$ [49]. In this case γ_0 is equal to zero.
For the non-Markovian case, the equations of motion are given by

$$\frac{\mathrm{d}}{\mathrm{d}t} \rho_{S,1,1}(t) = 0 \tag{2.42a}$$
$$\frac{\mathrm{d}}{\mathrm{d}t} \rho_{S,1,2}(t) = \left(-i\omega_0 - 2\gamma_0(t) \right) \rho_{S,1,2}(t) \tag{2.42b}$$
$$\frac{\mathrm{d}}{\mathrm{d}t} \rho_{S,2,1}(t) = \left(i\omega_0 - 2\gamma_0(t) \right) \rho_{S,2,1}(t) \tag{2.42c}$$
$$\frac{\mathrm{d}}{\mathrm{d}t} \rho_{S,2,2}(t) = 0 \tag{2.42d}$$

and can be easily solved analytically. For the temporal evolution of the reduced density matrix we obtain

$$\rho_{S,1,1}(t) = \frac{1}{2} \tag{2.43a}$$
$$\rho_{S,1,2}(t) = \frac{1}{2} \left(1 + \omega_c^2 t^2 \right)^{-\alpha} \exp(-i\omega_0 t) \tag{2.43b}$$
$$\rho_{S,2,1}(t) = \frac{1}{2} \left(1 + \omega_c^2 t^2 \right)^{-\alpha} \exp(i\omega_0 t) \tag{2.43c}$$
$$\rho_{S,2,2}(t) = \frac{1}{2}. \tag{2.43d}$$

The dynamics obtained with the non-Markovian master equation result in the same as the exact solution. This is caused by the simple model.

However, the Markovian solution

$$\rho_{S,1,1}(t) = \frac{1}{2} \tag{2.44a}$$

$$\rho_{S,1,2}(t) = \frac{1}{2} \exp(-i\omega_0 t) \tag{2.44b}$$

$$\rho_{S,2,1}(t) = \frac{1}{2} \exp(i\omega_0 t) \tag{2.44c}$$

$$\rho_{S,2,2}(t) = \frac{1}{2} \tag{2.44d}$$

shows only an oscillation in the coherences and no decay. Hence, the Markovian approximation not suffices to describe the dynamics of the system.
Finally, the expectation values for the non-Markovian dynamics read

$$\langle \sigma_z \rangle = \mathrm{Tr}\left\{\rho_S(t)\sigma_z\right\} = 0 \tag{2.45}$$

$$\langle \sigma_+ \rangle = \frac{1}{2}\left(1 + \omega_c^2 t^2\right)^{-\alpha} \exp\left(i\omega_0 t\right) \tag{2.46}$$

$$\langle \sigma_- \rangle = \frac{1}{2}\left(1 + \omega_c^2 t^2\right)^{-\alpha} \exp\left(-i\omega_0 t\right). \tag{2.47}$$

2.3.3 Results for the iEoM

Before the DMF is applied to the toy model, the results for the iterative equation of motion approach are derived. The iEoM uses a controlled expansion in the electron-phonon coupling strength $g_{\mathbf{k}}$ instead of the correlation expansion in the DMF. Due to this a comparison between these both truncations is of interest.
For the toy model the Hamiltonian is time independent. In the first order in $g_{\mathbf{k}}$, the ansatz for the operators is given by

$$\sigma_z(t) = s_0^z(t)\sigma_z \tag{2.48}$$

$$b_{\mathbf{k}}(t) = \alpha_{0,\mathbf{k}}(t) b_{\mathbf{k}} + \alpha_{1,\mathbf{k}}(t) g_{\mathbf{k}} \sigma_z \tag{2.49}$$

$$\sigma_+(t) = s_0^+(t)\sigma_+ + \sum_{\mathbf{k}} \left(s_{1,\mathbf{k}}^+(t) g_{\mathbf{k}} \sigma_+ b_{\mathbf{k}}^\dagger + s_{2,\mathbf{k}}^+(t) g_{\mathbf{k}} \sigma_+ b_{\mathbf{k}} \right). \tag{2.50}$$

The result for $\sigma_-(t)$ can easily be computed by Hermitian conjugation of the result of $\sigma_+(t)$.

The ansatz yields the following equations

$$i\hbar\frac{\mathrm{d}}{\mathrm{d}t}\sigma_z(t) = i\hbar\frac{\mathrm{d}}{\mathrm{d}t}s_0^z(t)\sigma_z = 0 \tag{2.51}$$

$$\begin{aligned} i\hbar\frac{\mathrm{d}}{\mathrm{d}t}b_{\mathbf{k}} &= i\hbar\frac{\mathrm{d}}{\mathrm{d}t}\alpha_{0,\mathbf{k}}(t)b_{\mathbf{k}} + i\hbar\frac{\mathrm{d}}{\mathrm{d}t}\alpha_{1,\mathbf{k}}(t)g_{\mathbf{k}}\sigma_z \\ &= \hbar\omega_{\mathbf{k}}\alpha_{0,\mathbf{k}}(t)b_{\mathbf{k}} + \alpha_{0,\mathbf{k}}(t)g_{\mathbf{k}}\sigma_z \end{aligned} \tag{2.52}$$

$$\begin{aligned} i\hbar\frac{\mathrm{d}}{\mathrm{d}t}\sigma_+(t) &= i\hbar\frac{\mathrm{d}}{\mathrm{d}t}s_0^+(t)\sigma_+ + \sum_{\mathbf{k}}\left(i\hbar\frac{\mathrm{d}}{\mathrm{d}t}s_{1,\mathbf{k}}^+(t)g_{\mathbf{k}}\sigma_+b_{\mathbf{k}}^\dagger + i\hbar\frac{\mathrm{d}}{\mathrm{d}t}s_{2,\mathbf{k}}^+(t)g_{\mathbf{k}}\sigma_+b_{\mathbf{k}}\right) \\ &= -\hbar\omega_0 s_0^+(t)\sigma_+ - \sum_{\mathbf{k}} 2g_{\mathbf{k}}s_0^+(t)\left(\sigma_+b_{\mathbf{k}}^\dagger + \sigma_+b_{\mathbf{k}}\right) \\ &\quad - \sum_{\mathbf{k}}\hbar\omega_0 g_{\mathbf{k}}\left(s_{1,\mathbf{k}}^+(t)\sigma_+b_{\mathbf{k}}^\dagger + s_{2,\mathbf{k}}^+(t)\sigma_+b_{\mathbf{k}}\right) \\ &\quad + \sum_{\mathbf{k}}\hbar\omega_{\mathbf{k}} g_{\mathbf{k}}\left(-s_{1,\mathbf{k}}^+(t)\sigma_+b_{\mathbf{k}}^\dagger + s_{2,\mathbf{k}}^+(t)\sigma_+b_{\mathbf{k}}\right) \\ &\quad - \sum_{\mathbf{k}} g_{\mathbf{k}}^2\left(s_{1,\mathbf{k}}^+(t) + s_{2,\mathbf{k}}^+(t)\right)\sigma_+. \end{aligned} \tag{2.53}$$

Here, the red colored part represents the additional contributions of the self-consistent truncation. A comparison of the coefficients leads to the equations of motion for the prefactors, which read

$$i\hbar\frac{\mathrm{d}}{\mathrm{d}t}s_0^z(t) = 0 \tag{2.54a}$$

$$i\hbar\frac{\mathrm{d}}{\mathrm{d}t}\alpha_{0,\mathbf{k}}(t) = \hbar\omega_{\mathbf{k}}\alpha_{0,\mathbf{k}}(t) \tag{2.54b}$$

$$i\hbar\frac{\mathrm{d}}{\mathrm{d}t}\alpha_{1,\mathbf{k}}(t) = \alpha_{0,\mathbf{k}}(t) \tag{2.54c}$$

$$i\hbar\frac{\mathrm{d}}{\mathrm{d}t}s_0^+(t) = -\hbar\omega_0 s_0^+(t) - \sum_{\mathbf{k}} g_{\mathbf{k}}^2\left(s_{1,\mathbf{k}}^+(t) + s_{2,\mathbf{k}}^+(t)\right) \tag{2.54d}$$

$$i\hbar\frac{\mathrm{d}}{\mathrm{d}t}s_{1,\mathbf{k}}^+(t) = -\hbar\left(\omega_0 + \omega_{\mathbf{k}}\right)s_{1,\mathbf{k}}^+(t) - 2s_0^+(t) \tag{2.54e}$$

$$i\hbar\frac{\mathrm{d}}{\mathrm{d}t}s_{2,\mathbf{k}}^+(t) = -\hbar\left(\omega_0 - \omega_{\mathbf{k}}\right)s_{2,\mathbf{k}}^+(t) - 2s_0^+(t). \tag{2.54f}$$

First, we ignore the self-consistency contribution and arrive following results

$$s_0^z(t) = 1, \tag{2.55a}$$
$$\alpha_{0,\mathbf{k}}(t) = \exp(-i\omega_{\mathbf{k}}t) \tag{2.55b}$$
$$\alpha_{1,\mathbf{k}}(t) = \frac{1}{\hbar\omega_{\mathbf{k}}}\left(\exp(-i\omega_{\mathbf{k}}t) - 1\right) \tag{2.55c}$$
$$s_0^+(t) = \exp(i\omega_0 t) \tag{2.55d}$$
$$s_{1,\mathbf{k}}^+(t) = \frac{2}{\hbar\omega_{\mathbf{k}}}\left(-\exp(-i\omega_{\mathbf{k}}t) + 1\right)\exp(i\left(\omega_{\mathbf{k}} + \omega_0\right)t) \tag{2.55e}$$
$$s_{2,\mathbf{k}}^+(t) = \frac{2}{\hbar\omega_{\mathbf{k}}}\left(\exp(i\omega_{\mathbf{k}}t) - 1\right)\exp(i\left(-\omega_{\mathbf{k}} + \omega_0\right)t). \tag{2.55f}$$

With this knowledge we are able to compute the expectation values of interest. Note, the initial condition are given at $T = 0$ and the density matrix of H_S is given by Eq. (2.19). So the expectation values are

$$\langle\sigma_z(t)\rangle = s_0^z(t)\langle\sigma_z\rangle = 0 \tag{2.56}$$
$$\left\langle a_{\mathbf{k}}(t)\right\rangle = \alpha_{0,\mathbf{k}}(t)\left\langle a_{\mathbf{k}}\right\rangle + g_{\mathbf{k}}\alpha_{1,\mathbf{k}}(t)\langle\sigma_z\rangle = 0 \tag{2.57}$$
$$\langle\sigma_+(t)\rangle = \frac{1}{2}s_0^+(t) = \frac{1}{2}\exp(i\omega_0 t). \tag{2.58}$$

The first order truncation without self-consistent loop leads to the same results as the Markovian quantum master equation.

Considering the self-consistent truncation, we solve the equations of motion numerically. To do so, we have to discretized the coupling strength and the phonon energies. Thereto, we discretize the spectral function of the environment, see Eq. (2.29). The spectral function is divided into different intervals $[\omega_m, \omega_{m+1}]$. In addition, we can rewrite H_B and H_I into [64]

$$H_B = \sum_n \hbar w_n b_n^\dagger b_n \tag{2.59}$$
$$H_I = \sigma_z \sum_n \gamma_n \left(b_n^\dagger + b_n\right) \tag{2.60}$$

with

$$\gamma_n^2 = \int_{\omega_n}^{\omega_{n+1}} F(\omega)\mathrm{d}\omega \tag{2.61}$$

$$w_n = \gamma_n^{-2} \int_{\omega_n}^{\omega_{n+1}} F(\omega)\omega\mathrm{d}\omega. \tag{2.62}$$

Here, γ_n describes the coupling between the environment and the two-level system and w_n sets the energy of the environment. With this we are able to solve the equations of motion numerically.

The resulting evolution of $\langle\sigma_+\rangle$ is depicted in Fig. 2.1. If we apply the self-consistent truncation, we are able to capture the dephasing of $\langle\sigma_+\rangle$. The results are in perfect agreement with the exact results for small coupling strength, i.e., small values of α. For increasing α the results deviate stronger from the exact results. This behavior is reasonable, because we expand around orders of the coupling strength. Further, we observe that the results are in good agreement with the exact one for short times, even for larger α. However, with increasing time the iEoM-results starts to deviate from the exact results.

To improve the long time behavior of the calculation we go a step further in the expansion. If we consider the pure second order truncation without self-consistent truncation we get the same results as for the first order truncation with self-consistent truncation. This can be seen by comparing Eqs. (2.54) with Eqs. (2.64) and ignoring the red contribution of Eqs. (2.64b) and (2.64c). This is caused by the simple toy model and is not a generic feature. Hence, we consider the $O(g_{\mathbf{k}}^2)$ expansion with self-consistent truncation. The equation of motion for σ_+ reads

$$
\begin{aligned}
i\hbar\frac{\mathrm{d}}{\mathrm{d}t}\sigma_+(t) = {} & i\hbar\frac{\mathrm{d}}{\mathrm{d}t}s_0^+(t)\sigma_+ + \sum_{\mathbf{k}}\left(i\hbar\frac{\mathrm{d}}{\mathrm{d}t}s_{1,\mathbf{k}}^+(t)g_{\mathbf{k}}\sigma_+b_{\mathbf{k}}^\dagger + i\hbar\frac{\mathrm{d}}{\mathrm{d}t}s_{2,\mathbf{k}}^+(t)g_{\mathbf{k}}\sigma_+b_{\mathbf{k}}\right) \qquad (2.63)\\
& + \sum_{\mathbf{k},\mathbf{q}}\Bigg(i\hbar\frac{\mathrm{d}}{\mathrm{d}t}s_{3,\mathbf{k},\mathbf{q}}^+(t)g_{\mathbf{k}}g_{\mathbf{q}}\sigma_+b_{\mathbf{k}}^\dagger b_{\mathbf{q}} + i\hbar\frac{\mathrm{d}}{\mathrm{d}t}s_{4,\mathbf{k},\mathbf{q}}^+(t)g_{\mathbf{k}}g_{\mathbf{q}}\sigma_+b_{\mathbf{k}}^\dagger b_{\mathbf{q}}\\
& \qquad + i\hbar\frac{\mathrm{d}}{\mathrm{d}t}s_{5,\mathbf{k},\mathbf{q}}^+(t)g_{\mathbf{k}}g_{\mathbf{q}}\sigma_+b_{\mathbf{k}}^\dagger b_{\mathbf{q}}\Bigg)\\
& = -\hbar\omega_0 s_0^+(t)\sigma_+ - \sum_{\mathbf{k}} 2g_{\mathbf{k}}s_0^+(t)\left(\sigma_+b_{\mathbf{k}}^\dagger + \sigma_+b_{\mathbf{k}}\right)\\
& - \sum_{\mathbf{k}}\hbar\omega_0 g_{\mathbf{k}}\left(s_{1,\mathbf{k}}^+(t)\sigma_+b_{\mathbf{k}}^\dagger + s_{2,\mathbf{k}}^+(t)\sigma_+b_{\mathbf{k}}\right)\\
& + \sum_{\mathbf{k}}\hbar\omega_{\mathbf{k}} g_{\mathbf{k}}\left(-s_{1,\mathbf{k}}^+(t)\sigma_+b_{\mathbf{k}}^\dagger + s_{2,\mathbf{k}}^+(t)\sigma_+b_{\mathbf{k}}\right)\\
& - \sum_{\mathbf{k}} g_{\mathbf{k}}^2\left(s_{1,\mathbf{k}}^+(t) + s_{2,\mathbf{k}}^+(t)\right)\sigma_+\\
& - 2\sum_{\mathbf{k},\mathbf{q}} g_{\mathbf{k}}g_{\mathbf{q}}\left[s_{1,\mathbf{k}}^+\left(\sigma_+b_{\mathbf{q}}^\dagger b_{\mathbf{k}}^\dagger + \sigma_+b_{\mathbf{k}}^\dagger b_{\mathbf{q}}\right) + s_{2,\mathbf{k}}^+\left(\sigma_+b_{\mathbf{q}}^\dagger b_{\mathbf{k}} + \sigma_+b_{\mathbf{q}}b_{\mathbf{k}}\right)\right]\\
& + \sum_{\mathbf{k},\mathbf{q}}\hbar g_{\mathbf{k}}g_{\mathbf{q}}\Big[\left(-\omega_0 - \omega_{\mathbf{k}} + \omega_{\mathbf{q}}\right)s_{3,\mathbf{k},\mathbf{q}}^+ + \left(-\omega_0 + \omega_{\mathbf{k}} + \omega_{\mathbf{q}}\right)s_{4,\mathbf{k},\mathbf{q}}^+\\
& \qquad + \left(-\omega_0 - \omega_{\mathbf{k}} - \omega_{\mathbf{q}}\right)s_{5,\mathbf{k},\mathbf{q}}^+\Big]\\
& - \sum_{\mathbf{k},\mathbf{q}} g_{\mathbf{k}}g_{\mathbf{q}}s_{3,\mathbf{k},\mathbf{q}}^+\left(g_{\mathbf{k}}\sigma_+b_{\mathbf{q}} + g_{\mathbf{q}}\sigma_+b_{\mathbf{k}}^\dagger\right)\\
& - \sum_{\mathbf{k},\mathbf{q}} g_{\mathbf{k}}g_{\mathbf{q}}s_{4,\mathbf{k},\mathbf{q}}^+\left(g_{\mathbf{k}}\sigma_+b_{\mathbf{q}} + g_{\mathbf{q}}\sigma_+b_{\mathbf{k}}\right)\\
& - \sum_{\mathbf{k},\mathbf{q}} g_{\mathbf{k}}g_{\mathbf{q}}s_{5,\mathbf{k},\mathbf{q}}^+\left(g_{\mathbf{k}}\sigma_+b_{\mathbf{q}}^\dagger + g_{\mathbf{q}}\sigma_+b_{\mathbf{k}}^\dagger\right).
\end{aligned}
$$

A comparison of the coefficients leads to following equations of motion for the prefactors

$$i\hbar\frac{\mathrm{d}}{\mathrm{d}t}s_0^+(t) = -\hbar\omega_0 s_0^+(t) - \sum_{\mathbf{k}} g_{\mathbf{k}}^2\left(s_{1,\mathbf{k}}^+(t) + s_{2,\mathbf{k}}^+(t)\right) \tag{2.64a}$$

$$i\hbar\frac{\mathrm{d}}{\mathrm{d}t}s_{1,\mathbf{k}}^+(t) = -\hbar\left(\omega_0 + \omega_{\mathbf{k}}\right)s_{1,\mathbf{k}}^+(t) - 2s_0^+(t) - \sum_{\mathbf{q}} g_{\mathbf{q}}^2\left(s_{3,\mathbf{k},\mathbf{q}}^+(t) + s_{5,\mathbf{k},\mathbf{q}}^+(t) + s_{5,\mathbf{q},\mathbf{k}}^+(t)\right) \tag{2.64b}$$

$$i\hbar\frac{\mathrm{d}}{\mathrm{d}t}s_{2,\mathbf{k}}^+(t) = -\hbar\left(\omega_0 - \omega_{\mathbf{k}}\right)s_{2,\mathbf{k}}^+(t) - 2s_0^+(t) - \sum_{\mathbf{q}} g_{\mathbf{q}}^2\left(s_{3,\mathbf{k},\mathbf{q}}^+(t) + s_{4,\mathbf{k},\mathbf{q}}^+(t) + s_{4,\mathbf{q},\mathbf{k}}^+(t)\right) \tag{2.64c}$$

$$i\hbar\frac{\mathrm{d}}{\mathrm{d}t}s_{3,\mathbf{k},\mathbf{q}}^+(t) = \hbar\left(-\omega_0 - \omega_{\mathbf{k}} + \omega_{\mathbf{q}}\right)s_{3,\mathbf{k},\mathbf{q}}^+(t) - 2\left(s_{1,\mathbf{k}}^+(t) + s_{2,\mathbf{q}}^+(t)\right) \tag{2.64d}$$

$$i\hbar\frac{\mathrm{d}}{\mathrm{d}t}s_{4,\mathbf{k},\mathbf{q}}^+(t) = \hbar\left(-\omega_0 + \omega_{\mathbf{k}} + \omega_{\mathbf{q}}\right)s_{4,\mathbf{k},\mathbf{q}}^+(t) - 2s_{2,\mathbf{q}}^+(t) \tag{2.64e}$$

$$i\hbar\frac{\mathrm{d}}{\mathrm{d}t}s_{5,\mathbf{k},\mathbf{q}}^+(t) = \hbar\left(-\omega_0 - \omega_{\mathbf{k}} - \omega_{\mathbf{q}}\right)s_{5,\mathbf{k},\mathbf{q}}^+(t) - 2s_{1,\mathbf{q}}^+(t). \tag{2.64f}$$

The results of the second order with self-consistent truncation are also depicted in Fig. 2.1. It shows an enhancement of the first order calculation. For the second order also larger values of α can be computed accurately. All in all with increasing order we are able to describe the temporal evolution of the toy model more precisely for larger couplings and longer times.

2.3.4 Results for the DMF

In this section, we apply the DMF approach on the toy model. Especially, we are interested in the temporal evolution of the following expectation values

$$\langle \sigma_z \rangle , \quad \left\langle b_{\mathbf{k}} \right\rangle , \quad \text{and } \langle \sigma_+ \rangle . \tag{2.65}$$

The expectation value $\langle \sigma_- \rangle$ can be computed by a complex conjugation of $\langle \sigma_+ \rangle$. The equations of motion, set up by using Eq. (2.1), are given by

$$i\hbar \frac{\mathrm{d}}{\mathrm{d}t} \langle \sigma_z \rangle = 0 \tag{2.66}$$

$$i\hbar \frac{\mathrm{d}}{\mathrm{d}t} \left\langle b_{\mathbf{k}} \right\rangle = \hbar\omega_{\mathbf{k}} \left\langle b_{\mathbf{k}} \right\rangle + g_{\mathbf{k}} \langle \sigma_z \rangle \tag{2.67}$$

$$i\hbar \frac{\mathrm{d}}{\mathrm{d}t} \langle \sigma_+ \rangle = -\hbar\omega_0 \langle \sigma_+ \rangle - \sum_{\mathbf{k}} 2g_{\mathbf{k}} \left(\left\langle \sigma_+ b_{\mathbf{k}} \right\rangle + \left\langle \sigma_+ b^\dagger_{\mathbf{k}} \right\rangle \right) . \tag{2.68}$$

Due to the electron-phonon coupling, the phonon assisted quantities read

$$\left\langle \sigma_+ b_{\mathbf{k}} \right\rangle \text{ and } \left\langle \sigma_+ b^\dagger_{\mathbf{k}} \right\rangle . \tag{2.69}$$

For the first order in the correlation expansion, the corrections of the factorized phonon assisted quantities are neglected, e.g.

$$\left\langle \sigma_+ b_{\mathrm{k}} \right\rangle = \langle \sigma_+ \rangle \left\langle b_{\mathrm{k}} \right\rangle + \left\langle \sigma_+ b_{\mathrm{k}} \right\rangle^c \approx \langle \sigma_+ \rangle \left\langle b_{\mathrm{k}} \right\rangle . \tag{2.70}$$

The resulting closed system reads

$$i\hbar \frac{\mathrm{d}}{\mathrm{d}t} \langle \sigma_z \rangle = 0 \tag{2.71}$$

$$i\hbar \frac{\mathrm{d}}{\mathrm{d}t} \left\langle b_{\mathbf{k}} \right\rangle = \hbar\omega_{\mathbf{k}} \left\langle b_{\mathbf{k}} \right\rangle + g_{\mathbf{k}} \langle \sigma_z \rangle \tag{2.72}$$

$$i\hbar \frac{\mathrm{d}}{\mathrm{d}t} \langle \sigma_+ \rangle = -\hbar\omega_0 \langle \sigma_+ \rangle - \sum_{\mathbf{k}} 2g_{\mathbf{k}} \left(\langle \sigma_+ \rangle \left\langle b_{\mathbf{k}} \right\rangle + \langle \sigma_+ \rangle \left\langle b^\dagger_{\mathbf{k}} \right\rangle \right) \tag{2.73}$$

and can be easily solved by using the initial conditions

$$\langle \sigma_z \rangle (t=0) = 0 \ \Rightarrow \ \langle \sigma_z \rangle (t) = 0 \tag{2.74}$$

$$\left\langle b_{\mathbf{k}} \right\rangle (t=0) = 0 \ \Rightarrow \ \left\langle b_{\mathbf{k}} \right\rangle (t) = 0 \tag{2.75}$$

$$\langle \sigma_+ \rangle (t=0) = \frac{1}{2} \ \Rightarrow \ \langle \sigma_+ \rangle (t) = \frac{1}{2} \exp(i\omega_0 t). \tag{2.76}$$

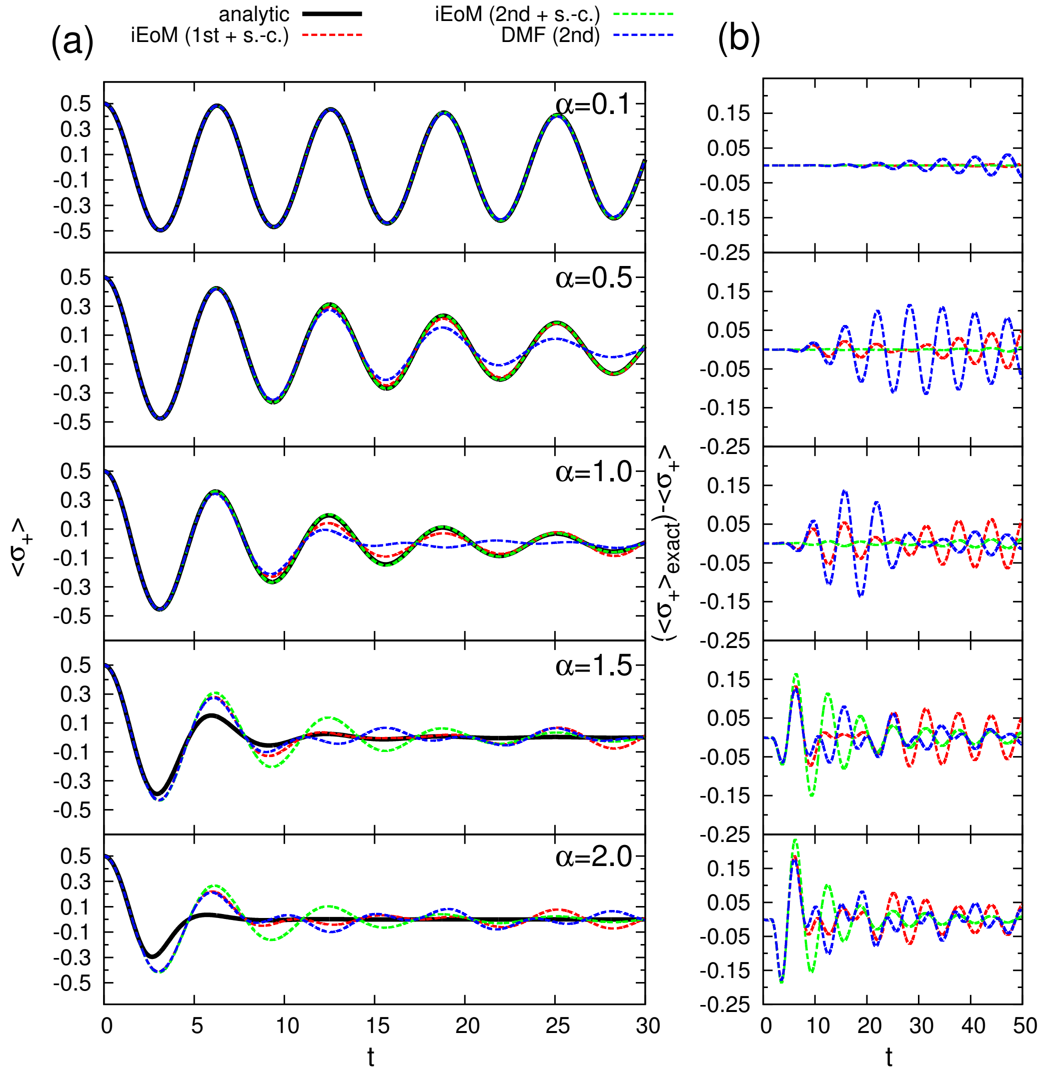

Figure 2.1: In panel (a), the temporal evolution of $\langle\sigma_+\rangle$ is presented for $\omega_0 = 1$, $\omega_c = 0.1$, and various $\alpha \in \{0.1, 0.5, 1, 1.5, 2\}$. The exact results are depicted as solid black lines, the DMF-results as dotted blue lines, the first order with self-consistent truncation iEoM-results as dotted red lines, and the second order with self-consistent truncation iEoM-results as dotted blue lines. In panel (b) the deviation from the exact results is depicted for the DMF and iEoM results.

The results of DMF in first order are in perfect agreement with the Markovian dynamics, just as the results for the iEoM in first order without the self-consistent truncation. The constant behavior of $\langle\sigma_z\rangle(t)$ as well as the oscillation of $\langle\sigma_+\rangle(t)$ is captured. Again the decay of $\langle\sigma_+\rangle(t)$ of the exact solution cannot be captured.
In the second order of the correlation expansion the temporal evolution of the phonon assisted quantities, e.g. $\langle\sigma^+ a_\mathrm{k}\rangle$, is taken into account. This means one has to apply Eq. (2.1) to these quantities. For the toy model one obtains

$$\begin{aligned} i\hbar\frac{\mathrm{d}}{\mathrm{d}t}\left\langle\sigma_+ b_\mathbf{k}\right\rangle &= \hbar\left(-\omega_0+\omega_\mathbf{k}\right)\left\langle\sigma_+ b_\mathbf{k}\right\rangle - g_\mathbf{k}\left\langle\sigma_+\right\rangle \\ &\quad -\sum_{\mathbf{k}'}2g_{\mathbf{k}'}\left(\left\langle\sigma_+ b^\dagger_{\mathbf{k}'}b_\mathbf{k}\right\rangle+\left\langle\sigma_+ b_{\mathbf{k}'}b_\mathbf{k}\right\rangle\right) \end{aligned} \tag{2.77}$$

$$\begin{aligned} i\hbar\frac{\mathrm{d}}{\mathrm{d}t}\left\langle\sigma_+ b^\dagger_\mathbf{k}\right\rangle &= -\hbar\left(\omega_0+\omega_\mathbf{k}\right)\left\langle\sigma_+ b^\dagger_\mathbf{k}\right\rangle - g_\mathbf{k}\left\langle\sigma_+\right\rangle \\ &\quad -\sum_{\mathbf{k}'}2g_{\mathbf{k}'}\left(\left\langle\sigma_+ b^\dagger_{\mathbf{k}'}b^\dagger_\mathbf{k}\right\rangle+\left\langle\sigma_+ b^\dagger_\mathbf{k}b_{\mathbf{k}'}\right\rangle\right). \end{aligned} \tag{2.78}$$

As already mentioned, this leads to higher order expectation correlations including a spin operator and two bosonic operators. These quantities have to be factorized according to

$$\left\langle\sigma_+ b^\dagger_{\mathbf{k}'}b_\mathbf{k}\right\rangle = \left\langle\sigma_+ b^\dagger_{\mathbf{k}'}b_\mathbf{k}\right\rangle^c + \left\langle\sigma_+\right\rangle\left(\left\langle b^\dagger_{\mathbf{k}'}b_\mathbf{k}\right\rangle^c+\left\langle b^\dagger_{\mathbf{k}'}\right\rangle\left\langle b_\mathbf{k}\right\rangle\right). \tag{2.79}$$

For the purpose of the correlation expansion we neglect all corrections including one spin operator and two bosonic operators for the second order in the correlation expansion. As one can see in the factorization, the temporal evolution of the incoherent phonon density is needed. Due to $\left\langle a^\dagger_\mathbf{k}\right\rangle = 0 = \left\langle a_\mathbf{k}\right\rangle$ the incoherent phonon density is equal to the full phonon density. The temporal evolution of this quantity is given by

$$i\hbar\frac{\mathrm{d}}{\mathrm{d}t}\left\langle a^\dagger_\mathbf{k}a_\mathbf{p}\right\rangle = \hbar\left(\omega_\mathbf{p}-\omega_\mathbf{k}\right)\left\langle a^\dagger_\mathbf{k}a_\mathbf{p}\right\rangle + g_\mathbf{p}\left\langle\sigma_z a^\dagger_\mathbf{k}\right\rangle - g_\mathbf{k}\left\langle\sigma_z a_\mathbf{p}\right\rangle \tag{2.80}$$

$$i\hbar\frac{\mathrm{d}}{\mathrm{d}t}\left\langle a_\mathbf{k}a_\mathbf{p}\right\rangle = \hbar\left(\omega_\mathbf{p}+\omega_\mathbf{k}\right)\left\langle a_\mathbf{k}a_\mathbf{p}\right\rangle + g_\mathbf{p}\left\langle\sigma_z a_\mathbf{k}\right\rangle + g_\mathbf{k}\left\langle\sigma_z a_\mathbf{p}\right\rangle. \tag{2.81}$$

To compute the temporal evolution of the quantities above one needs

$$i\hbar\frac{\mathrm{d}}{\mathrm{d}t}\left\langle\sigma_z a_{\mathbf{k}}\right\rangle = \hbar\omega_{\mathbf{k}}\left\langle\sigma_z a_{\mathbf{k}}\right\rangle + g_{\mathbf{k}}\underbrace{\left\langle\sigma_z^2\right\rangle}_{=1} \tag{2.82}$$

$$\Rightarrow\left\langle\sigma_z a_{\mathbf{k}}\right\rangle = -\frac{g_{\mathbf{k}}}{\hbar\omega_{\mathbf{k}}}(1-\exp(-i\omega_{\mathbf{k}}t)), \tag{2.83}$$

with $\left\langle a^\dagger_{\mathbf{k}} a_{\mathbf{p}}\right\rangle(t)$ and $\left\langle a_{\mathbf{k}} a_{\mathbf{p}}\right\rangle(t)$ given by

$$\left\langle a^\dagger_{\mathbf{k}} a_{\mathbf{p}}\right\rangle = \frac{g_{\mathbf{k}}g_{\mathbf{p}}}{\hbar^2\omega_{\mathbf{k}}\omega_{\mathbf{p}}}\left(1-e^{i\omega_{\mathbf{k}}t}-e^{-i\omega_{\mathbf{p}}t}+e^{-i(\omega_{\mathbf{p}}-\omega_{\mathbf{k}})t}\right) \tag{2.84}$$

$$\left\langle a_{\mathbf{k}} a_{\mathbf{p}}\right\rangle = \frac{g_{\mathbf{k}}g_{\mathbf{p}}}{\hbar^2\omega_{\mathbf{k}}\omega_{\mathbf{p}}}\left(1-e^{-i\omega_{\mathbf{k}}t}-e^{-i\omega_{\mathbf{p}}t}+e^{-i(\omega_{\mathbf{p}}+\omega_{\mathbf{k}})t}\right). \tag{2.85}$$

To solve the complete differential equation system, we have to solve the equations of motion for the phonon assisted quantities and $\langle\sigma_+\rangle$. This task is done numerically. Thereto, we use the same discretization as for the iEoM equations, see Sect. 2.3.3. The temporal evolution of $\langle\sigma_+\rangle$ is depicted in Fig. 2.1. Additionally to the oscillation of the first order calculation, we observe a damping of $\langle\sigma_+\rangle$. For small values of α it is in good agreement with the exact results. With increasing α the deviation increases, too. Interestingly, the results of the iEoM seems to be more accurate than the results of the DMF. For the DMF approach the damping is always stronger and with this the deviation compared to the exact curve is larger.

The study of the toy model shows that the correlation expansion is no expansion in the electron-phonon coupling strength. In fact an infinite order in the coupling strength is taken into account if an expectation value enters its own equation of motion in a contribution proportional to the coupling strength. This infinite order in $g_{\mathbf{k}}$ does not enhance the results. On the contrary, the iEoM with self-consistent truncation leads to better results. This is maybe caused by the fact that neglecting some correlations leads to a larger error than truncate in order of a small parameter and add some self-consistency contributions as in the iEoM.

Although the iEoM approach leads to better results for the toy model, we use the DMF method to compute the pump pulse induced nonequilibrium dynamics of a superconductor. This is due to the fact that the DMF approach is successfully applied to compute the pump pulse response of superconductors [30–35, 56]. As already mentioned before, one can compute the effect of a pump pulse exactly due to the mean field approximation [30], except of inaccuracies due to discretization.

Additionally, the BCS Hamiltonian is time dependent, due to the mean field description, see Sect. 3.1. With this the iEoM approach is numerically more complicated for this model than the DMF. This is another reason why the DMF is the method of choice. Nevertheless, the iEoM was applied to the BCS model for a testing purpose, namely for the BCS Hamiltonian which is perturbed by a quench, see Sect.5.1.

3 Models

In this section, the model is introduced which is used to describe the nonequilibrium dynamics of a superconductor. A standard $s-$wave BCS mean field Hamiltonian H_{sc} is considered. To study the effects of the induced quasiparticle dynamics on the lattice ions, the superconductor is coupled to additional phonons, which are not involved in the pairing mechanism. We take optical as well as acoustic phonons into account. Note, in this work either optical or acoustic phonons are considered. The phonons, described by the free phonon Hamiltonian H_{ph}, are coupled to the superconductor via a Fröhlich-Hamiltonian H_{Fr}.

To bring this model out of equilibrium we examine two different approaches. First, an intense laser pulse, the pump pulse, is used. The coupling between this external electromagnetic field to the superconductor is given by the Hamiltonian H_{em}. To simulate a pump probe experiment a second weaker pulse, the probe pulse, is also considered. Its coupling can be likewise described by H_{em}.

The second approach will be a quench, e.g. a sudden reduction of the coupling constant of the order parameter. Applying a quench instead of a light pulse move us a little bit away from the aim to describe pump probe experiment as accurately as possible, but it has some numerical advantages. Details will be presented in Sect. 4. Further, it will be shown that the applied quenches yield the same dynamics as a short pump pulse, see Sect. 5.1. The different quenches are introduced in Sect. 3.4. All in all, the model Hamiltonian is given by

$$H = H_{\mathrm{sc}} + H_{\mathrm{ph}} + H_{\mathrm{Fr}} + H_{\mathrm{em}}. \tag{3.1}$$

Only parts of the model Hamiltonian are taken into account depending on the model or the perturbation. In the following sections the different parts of the model Hamiltonian are discussed in detail.

3.1 BCS superconductor

For the superconductor a standard mean field type BCS Hamiltonian is used [65,66]. The Hamiltonian is given by

$$H_{\mathrm{sc}} = \sum_{\mathbf{k},\sigma} \epsilon_{\mathbf{k}} c^{\dagger}_{\mathbf{k},\sigma} c_{\mathbf{k},\sigma} - \sum_{\mathbf{k}\in W} \left(\Delta_{\mathbf{k}} c^{\dagger}_{\mathbf{k},\uparrow} c^{\dagger}_{-\mathbf{k}\downarrow} + \Delta^{*}_{\mathbf{k}} c_{-\mathbf{k},\downarrow} c_{\mathbf{k},\uparrow} \right). \tag{3.2}$$

Here, $c_{\mathbf{k},\sigma}$ is the annihilation operator of an electron with momentum $\mathbf{k}$ and spin σ, $\epsilon_{\mathbf{k}} = \frac{\hbar^2 \mathbf{k}^2}{2m} - E_{\mathrm{F}}$ is the dispersion, m is the effective electron mass, and E_{F} denotes the Fermi energy. The second sum is over the set W of all $\mathbf{k}$ vectors with $|\epsilon_{\mathbf{k}}| \leq \hbar\omega_c$, where ω_c is a cutoff frequency. The superconducting order parameter $\Delta_{\mathbf{k}}$ is given self-consistently by

$$\Delta_{\mathbf{k}} = \sum_{\mathbf{k}' \in W} \frac{W_0(\mathbf{k}, \mathbf{k}')}{N} \left\langle c_{-\mathbf{k}',\downarrow} c_{\mathbf{k}',\uparrow} \right\rangle, \tag{3.3}$$

with the interaction coupling $W_0(\mathbf{k}, \mathbf{k}')$ and the number of lattice sites N. The order parameter is one of the main quantities to describe the temporal evolution of the electronic system, e.g. see Sect. 5.

The expectation value $\left\langle c_{-\mathbf{k}',\downarrow} c_{\mathbf{k}',\uparrow} \right\rangle$ is given by

$$\left\langle c_{-\mathbf{k}',\downarrow} c_{\mathbf{k}',\uparrow} \right\rangle = \frac{\Delta_{\mathbf{k}'}}{2E_{\mathbf{k}'}}(1 - 2f(E_{\mathbf{k}'})), \tag{3.4}$$

where $f(E_{\mathbf{k}'})$ denotes the Fermi distribution and $E_{\mathbf{k}'} = \sqrt{\epsilon_{\mathbf{k}'}^2 + |\Delta_{\mathbf{k}'}|^2}$. Eq. (3.4) is true as can be seen by applying the Bogoliubov transformation, see Sect. 3.1.1. For $T = 0$ Eq. (3.3) simplifies to the self-consistency equation

$$\Delta_{\mathbf{k}} = \sum_{\mathbf{k}' \in W} \frac{W_0(\mathbf{k}, \mathbf{k}')}{N} \frac{\Delta_{\mathbf{k}'}}{2E_{\mathbf{k}'}}. \tag{3.5}$$

In this thesis, we consider a $s-$wave order parameter. This results in a momentum independent coupling strength

$$W_0(\mathbf{k}, \mathbf{k}') = W_0 \tag{3.6}$$

and with this the order parameter is also momentum independent

$$\Delta_{\mathbf{k}} = \Delta. \tag{3.7}$$

The standard s-wave BCS Hamiltonian ensues, which is well known in literature [66]. For the simulation of the dynamics it is advantageous to perform a Bogoliubov transformation of the electronic operators. This transformation diagonalizes the Hamiltonian H_{sc} in the initial state. The Bogoliubov transformation is presented in the following section.

3.1.1 Bogoliubov transformation

A Bogoliubov transformation [67,68] is used to introduce the new fermionic operators $\alpha_{\mathbf{k}}$ and $\beta_{\mathbf{k}}$. The transformation is given by

$$\begin{pmatrix} c_{\mathbf{k},\uparrow} \\ c^\dagger_{-\mathbf{k},\downarrow} \end{pmatrix} = \begin{pmatrix} u^*_{\mathbf{k}} & v_{\mathbf{k}} \\ -v^*_{\mathbf{k}} & u_{\mathbf{k}} \end{pmatrix} \begin{pmatrix} \alpha_{\mathbf{k}} \\ \beta^\dagger_{\mathbf{k}} \end{pmatrix}, \quad \begin{pmatrix} \alpha_{\mathbf{k}} \\ \beta^\dagger_{\mathbf{k}} \end{pmatrix} = \begin{pmatrix} u_{\mathbf{k}} & -v_{\mathbf{k}} \\ v^*_{\mathbf{k}} & u^*_{\mathbf{k}} \end{pmatrix} \begin{pmatrix} c_{\mathbf{k},\uparrow} \\ c^\dagger_{-\mathbf{k},\downarrow} \end{pmatrix} \tag{3.8}$$

Here, $u_{\mathbf{k}}$ and $v_{\mathbf{k}}$ are set to

$$u_{\mathbf{k}} = \sqrt{\frac{1}{2}\left(1 + \frac{\epsilon_{\mathbf{k}}}{E_{\mathbf{k}}}\right)} \tag{3.9}$$

$$v_{\mathbf{k}} = \frac{\Delta_0}{|\Delta_0|}\sqrt{\frac{1}{2}\left(1 - \frac{\epsilon_{\mathbf{k}}}{E_{\mathbf{k}}}\right)}, \tag{3.10}$$

with $E_{\mathbf{k}} = \sqrt{\epsilon^2_{\mathbf{k}} + |\Delta_0|^2}$ and the initial value of the order parameter Δ_0. Note, the coefficients $u_{\mathbf{k}}$ and $v_{\mathbf{k}}$ are time independent and fulfil the relation $|u|^2_{\mathbf{k}} + |v|^2_{\mathbf{k}} = 1$. This leads to a diagonal Hamiltonian for the initial condition. The temporal evolution of quasiparticle densities will be computed with respect to a fixed time-independent Bogoliubov-de Gennes basis.

The transformation of the Hamiltonian H_{sc} can be easily applied if it is rewritten in the following way

$$H_{\text{sc}} = \sum_{\mathbf{k}} \begin{pmatrix} c^\dagger_{\mathbf{k},\uparrow} & c_{-\mathbf{k},\downarrow} \end{pmatrix} \begin{pmatrix} \epsilon_{\mathbf{k}} & -\Delta \\ -\Delta^* & -\epsilon_{\mathbf{k}} \end{pmatrix} \begin{pmatrix} c_{\mathbf{k},\uparrow} \\ c^\dagger_{-\mathbf{k},\downarrow} \end{pmatrix}. \tag{3.11}$$

Note, the order parameter $\Delta = \Delta(t)$ depends on time.

Now, the Bogoliubov transformation is applied

$$\sum_{\mathbf{k}} \begin{pmatrix} u_{\mathbf{k}} & -v_{\mathbf{k}} \\ v^*_{\mathbf{k}} & u^*_{\mathbf{k}} \end{pmatrix} \begin{pmatrix} \epsilon_{\mathbf{k}} & -\Delta \\ -\Delta^* & -\epsilon_{\mathbf{k}} \end{pmatrix} \begin{pmatrix} u^*_{\mathbf{k}} & v_{\mathbf{k}} \\ -v^*_{\mathbf{k}} & u_{\mathbf{k}} \end{pmatrix} = \begin{pmatrix} R_{\mathbf{k}} & C_{\mathbf{k}} \\ C^*_{\mathbf{k}} & -R_{\mathbf{k}} \end{pmatrix}, \tag{3.12}$$

where

$$R_{\mathbf{k}} = \epsilon_{\mathbf{k}}(1 - 2|v_{\mathbf{k}}|^2) + v_{\mathbf{k}} u^*_{\mathbf{k}} \Delta^* + v^*_{\mathbf{k}} u^*_{\mathbf{k}} \Delta \tag{3.13}$$

$$C_{\mathbf{k}} = 2\epsilon_{\mathbf{k}} v_{\mathbf{k}} u_{\mathbf{k}} + \Delta^* |v_{\mathbf{k}}|^2 - \Delta |u_{\mathbf{k}}|^2. \tag{3.14}$$

To simplify the expression for $R_{\mathbf{k}}$ and $C_{\mathbf{k}}$, the relations $u_{\mathbf{k}} = \sqrt{\frac{1}{2}\left(1 + \frac{\epsilon_{\mathbf{k}}}{E_{\mathbf{k}}}\right)}$, $v_{\mathbf{k}} = \frac{\Delta_0}{|\Delta_0|}\sqrt{\frac{1}{2}\left(1 - \frac{\epsilon_{\mathbf{k}}}{E_{\mathbf{k}}}\right)}$, and $v_{\mathbf{k}} u_{\mathbf{k}} = \frac{|\Delta_0|}{2E_{\mathbf{k}}}$ are used. With these, one can rewrite $R_{\mathbf{k}}$ and $C_{\mathbf{k}}$ into

$$R_{\mathbf{k}} = \frac{\epsilon_{\mathbf{k}}^2 + \mathrm{Re}(\Delta^* \Delta_0)}{E_{\mathbf{k}}} \tag{3.15}$$

$$C_{\mathbf{k}} = \Delta_0^* \left(\frac{\epsilon_{\mathbf{k}}}{E_{\mathbf{k}}} \left(1 - \mathrm{Re}\left(\frac{\Delta}{\Delta_0} \right) \right) + i\,\mathrm{Im}\left(-\frac{\Delta}{\Delta_0} \right) \right). \tag{3.16}$$

Finally, the Hamiltonian H_{sc} is given by

$$H_{\mathrm{sc}} = \sum_{\mathbf{k} \notin W} |\epsilon_k| \left(\alpha_{\mathbf{k}}^\dagger \alpha_{\mathbf{k}} + \beta_{\mathbf{k}}^\dagger \beta_{\mathbf{k}} \right) + \sum_{\mathbf{k} \in W} \left(R_{\mathbf{k}} \left(\alpha_{\mathbf{k}}^\dagger \alpha_{\mathbf{k}} + \beta_{\mathbf{k}}^\dagger \beta_{\mathbf{k}} \right) + C_{\mathbf{k}} \alpha_{\mathbf{k}}^\dagger \beta_{\mathbf{k}}^\dagger + C_{\mathbf{k}}^* \beta_{\mathbf{k}} \alpha_{\mathbf{k}} \right). \tag{3.17}$$

If the order parameter is equal to the initial one the coefficients $R_{\mathbf{k}}$ and $C_{\mathbf{k}}$ are given by $R_{\mathbf{k}} = E_{\mathbf{k}}$ and $C_{\mathbf{k}} = 0$ and the Hamiltonian is diagonal by construction.

The order parameter is rewritten into terms of the presented transformation as the Hamiltonian. It is given by

$$\Delta(t) = \sum_{\mathbf{k} \in W} \frac{W_0}{N} \big(v_{\mathbf{k}} u_{\mathbf{k}} \left(- \left\langle \alpha_{\mathbf{k}}^\dagger \alpha_{\mathbf{k}} \right\rangle - \left\langle \beta_{\mathbf{k}}^\dagger \beta_{\mathbf{k}} \right\rangle + 1 \right) + u_{\mathbf{k}}^2 \left\langle \beta_{\mathbf{k}} \alpha_{\mathbf{k}} \right\rangle - v_{\mathbf{k}}^2 \left\langle \alpha_{\mathbf{k}}^\dagger \beta_{\mathbf{k}}^\dagger \right\rangle \big). \tag{3.18}$$

3.2 Coupling to phonons

In order to study the response of the lattice on the nonequilibrium dynamics of the Bogoliubov quasiparticles, the BCS superconductor is additionally coupled to phonons.

Thereto, a free phonon Hamiltonian and a Hamiltonian which describes the coupling is needed. In this study, the Fröhlich Hamiltonian is used for the electron-phonon coupling [69].

The free phonon Hamiltonian is given by

$$H_{\mathrm{ph}} = \sum_{\mathbf{p}} \hbar\omega_{\mathbf{p}} \left(b^{\dagger}_{\mathbf{p}} b_{\mathbf{p}} + \frac{1}{2} \right), \tag{3.19}$$

where $b_{\mathbf{p}}$ denotes the bosonic annihilation operator of a phonon with wave vector $\mathbf{p}$ and frequency $\omega_{\mathbf{p}}$. Here, only a phonon mode of low energy around $\hbar\omega_{\mathbf{p}} \lesssim 2\Delta_0 = 2.7\,\mathrm{meV}$ is taken into account. This mode does not generate the superconductivity. The pairing interaction is assumed to be mediated by other bosons at higher energies, for instance by spin fluctuations or by phonons at high energies of the order of the Debye energy $\hbar\omega_{\mathrm{D}} \approx 30$ meV [36]. This energy scale is much larger than the energy scale of the Bogoliubov quasiparticles so these other bosons influence the low-energy dynamics only indirectly via virtual processes, and hence, they do not need to be treated explicitly. The corresponding electron-boson couplings are assumed to be integrated out and enter in the mean-field treatment of superconductivity via $W_0(\mathbf{k}, \mathbf{k}')$.

We considered only one phonon mode within the simulation, because phonons with a frequency near the frequency of the order parameter oscillation are generated at most as discussed in Sect. 5.2. All other modes are of less importance.

The Fröhlich Hamiltonian reads

$$H_{\mathrm{Fr}} = \sum_{\mathbf{k},\mathbf{p}\sigma} \frac{g_{\mathbf{p}}}{\sqrt{N}} c^{\dagger}_{\mathbf{k}+\mathbf{p},\sigma} c_{\mathbf{k},\sigma} \left(b_{\mathbf{p}} + b^{\dagger}_{-\mathbf{p}} \right). \tag{3.20}$$

Here, $g_{\mathbf{p}}$ denotes the electron-phonon coupling strength. According to the BCS Hamiltonian H_{sc}, the Hamiltonian H_{Fr} has to be transformed with the same Bogoliubov transformation. The transformed Hamiltonian is given by

$$\begin{aligned} H_{\mathrm{Fr}} = \sum_{\mathbf{p},\mathbf{k}} \frac{g_{\mathbf{p}}}{\sqrt{N}} \left(b_{\mathbf{p}} + b^{\dagger}_{-\mathbf{p}} \right) \times \qquad\qquad\qquad\qquad\qquad\qquad (3.21) \\ \times \left(L^{-}_{\mathbf{k},\mathbf{p}} \left[\alpha^{\dagger}_{\mathbf{k}+\mathbf{p}} \alpha_{\mathbf{k}} + \beta^{\dagger}_{\mathbf{k}} \beta_{\mathbf{k}+\mathbf{p}} \right] + M^{+}_{\mathbf{k},\mathbf{p}} \left[\beta_{\mathbf{k}+\mathbf{p}} \alpha_{\mathbf{k}} + \alpha^{\dagger}_{\mathbf{k}+\mathbf{p}} \beta^{\dagger}_{\mathbf{k}} \right] + 2\delta_{\mathbf{p},0} |v_{\mathbf{k}}|^2 \right). \end{aligned}$$

Following shortcuts are used to write this expression in a concise way

$$L^{\pm}_{\mathbf{k},\mathbf{p}} = u_{\mathbf{k}} u_{\mathbf{k}+\mathbf{p}} \pm v_{\mathbf{k}} v_{\mathbf{k}+\mathbf{p}} \tag{3.22}$$

$$M^{\pm}_{\mathbf{k},\mathbf{p}} = v_{\mathbf{k}} u_{\mathbf{k}+\mathbf{p}} \pm u_{\mathbf{k}} v_{\mathbf{k}+\mathbf{p}}. \tag{3.23}$$

Up to now, the Hamiltonians describing the coupling to the phonons are formulated generally. The exact form of the phonon frequency and the coupling strength depends on the kind of the considered phonons.

For optical phonons we assume the phonon frequency and the electron-phonon coupling strength to be in Holstein form, i.e. that both quantities are momentum independent. With this we set $\omega_{\mathbf{p}} = \omega_{\text{ph}}$ and $g_{\mathbf{p}} = g_{\text{ph}}$.

For acoustic phonons the frequency and the coupling strength depend on the phonon wave vector. The frequency depends on the absolute value of the wave vector and is given by

$$\omega_{\mathbf{p}} = v|\mathbf{p}|, \tag{3.24}$$

with the phonon velocity v.

The coupling constant $g_{\mathbf{p}}$ is proportional to [70]

$$g_{\mathbf{p}} \sim V(\mathbf{k}_1 - \mathbf{k}_2)(\mathbf{k}_1 - \mathbf{k}_2)\frac{1}{\sqrt{\omega_{\text{p}}}}, \tag{3.25}$$

where $V(\mathbf{k}_1 - \mathbf{k}_2)$ is the Fourier transformed potential and $\omega_{\text{ph}} = v|\mathbf{p}|$ is the phonon dispersion. The difference $(\mathbf{k}_1 - \mathbf{k}_2)$ of the electron momenta is given by

$$(\mathbf{k}_1 - \mathbf{k}_2) = \mathbf{p} + K, \tag{3.26}$$

where K stands for possible Umklapp processes. If we now assume, that there are no Umklapp processes, K can be set to $K = 0$. Further, $\mathbf{p}$ should be small so that the potential is set to be constant $[V(\mathbf{k}_1 - \mathbf{k}_2) = V(\mathbf{p}) \to \text{const}]$. With this $g_{\mathbf{p}}$ is approximately given by

$$g_{\mathbf{p}} \sim V(0)\mathbf{p}\frac{1}{\sqrt{v|\mathbf{p}|}} = a\sqrt{|\mathbf{p}|}. \tag{3.27}$$

A new observable of interest enters the system if phonons are included, namely the lattice displacement $U(r,t)$. The lattice displacement is connected to the mean phonon amplitude $\langle b_{\mathbf{p}} \rangle$ and is given by

$$U(r,t) = \sum_{\mathbf{p}} \sqrt{\frac{\hbar}{2M\omega_{\mathbf{p}}N}} \left(\langle b_{\mathbf{p}} \rangle + \left\langle b^{\dagger}_{-\mathbf{p}} \right\rangle \right) e^{i\mathbf{pr}}, \tag{3.28}$$

where M denotes the reduced mass of the lattice ions.

3.3 Coupling to an electromagnetic light field

In order to push the system out of equilibrium a short intensive light pulse is used, the pump pulse. This pulse injects a nonthermal distribution of the Bogoliubov quasiparticles, see Sect. 5 or Refs. [30–36].

The considered pump pulse is of Gaussian shape with the photon frequency ω_0, **f**ull **w**idth at **h**alf **m**aximun (FWHM) τ_0, the photon wave vector $\mathbf{q}_0 = |\mathbf{q}_0|\vec{e}_x = \omega_0/(c)\vec{e}_x$, and the amplitude $\mathbf{A}_0 = |\mathbf{A}_0|\vec{e}_y$. Using the Coulomb gauge, the pulse is characterized by the transverse vector potential

$$\mathbf{A}_{\mathbf{q}}(t) = \mathbf{A}_0 e^{-\left(\frac{2\sqrt{\ln 2}t}{\tau_0}\right)^2} \left(\delta_{\mathbf{q},\mathbf{q}_0} e^{-i\omega_0 t} + \delta_{\mathbf{q},-\mathbf{q}_0} e^{i\omega_0 t}\right). \tag{3.29}$$

Note, this equation describes a laser pulse with definite wave vector, but finite uncertainty in its energy $\Delta E \approx \hbar/(2\tau_0)$. Nevertheless, we expect that the results remain qualitatively unchanged for more realistic pulse shapes with a broader distribution of wave vectors, because the wave vector $|\mathbf{q}_0|$ is much smaller than the Fermi momentum.

The nonequilibrium response in the simulation is measured by a probe pulse. This pulse follows the pump pulse after a certain delay time δt. The probe pulse has the same shape as the pump pulse, see Eq. (3.29), but it has a much weaker intensity. For the probe pulse, we label the probe pulse momentum with $|\mathbf{q}_{\mathrm{pr}}| = \omega_{\mathrm{pr}}/(c)$ and the probe pulse width with τ_{pr}. For the delay time we consider positive as well as negative delay times, corresponding cases that the probe pulse precedes the pump pulse $\delta t < 0$ or follows it $\delta t > 0$.

The photon energy of the pump pulse is set to a value, which is slightly larger than twice the initial order parameter $2|\Delta_0| \approx 3$meV of the superconductor. Due to this the pump pulse can excite the superconductor. Further, we assume that the pump pulse is centered in time at $t = 0\,\mathrm{ps}$. The probe pulse is taken to be very short in time and the energy is chosen to be slightly smaller than $2|\Delta_0|$. Due to the short pulse width the superconductor is probed with a broad range of frequencies. Further, both pulses are cut off where their amplitude is only a thousandth of their maximum amplitude. No overlap of the both pulses is considered, that means $|\delta t| > (\tau_{\mathrm{p}} + \tau_{\mathrm{probe}})$. An example of the temporal evolution of a pump pulse with $\tau_0 = 0.5\,\mathrm{ps}$ and a probe pulse $\tau_{\mathrm{pr}} = 0.25\,\mathrm{ps}$ is given in Fig. 3.1. Here, a delay time of $\delta t = 2\,\mathrm{ps}$ is used.

The coupling of the pulse to the system is given by the standard minimal coupling.

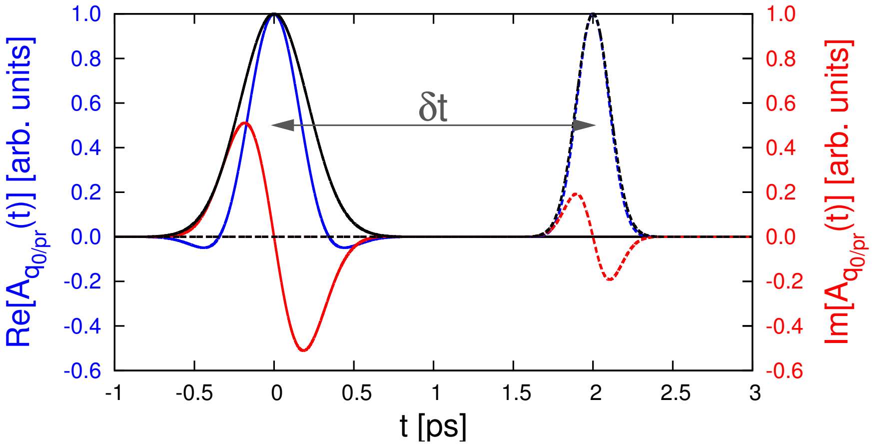

Figure 3.1: Temporal evolution of the pump vector potential $A_{\mathbf{q}_0}(t)$ (solid lines) and probe vector potential $A_{\mathbf{q}_{\rm pr}}(\mathrm{t})$ (dashed lines) with pulse widths $\tau_0 = 0.5$ ps and $\tau_{\rm pr} = 0.25$ ps, respectively. The black solid (dashed) line represents the Gaussian envelope of the pump (probe) pulse. The blue and red lines show the real and imaginary parts of the vector potentials, respectively. The pump pulse is centered at $t = 0$ ps and the probe pulse at $t = \delta t = 2$ ps.

The corresponding Hamiltonian reads

$$H_{\rm em} = H_{\rm em}^{(1)} + H_{\rm em}^{(2)} \tag{3.30}$$

$$H_{\rm em}^{(1)} = \frac{e\hbar}{2m} \sum_{\mathbf{k},\mathbf{q},\sigma} (2\mathbf{k}+\mathbf{q})\mathbf{A}_{\mathbf{q}}(t) c^\dagger_{\mathbf{k}+\mathbf{q},\sigma} c_{\mathbf{k},\sigma}, \tag{3.31}$$

$$H_{\rm em}^{(2)} = \frac{e^2}{2m} \sum_{\mathbf{k},\mathbf{q},\sigma} \left(\sum_{\mathbf{q}'} \mathbf{A}_{\mathbf{q}-\mathbf{q}'}(t)\mathbf{A}_{\mathbf{q}'}(t) \right) c^\dagger_{\mathbf{k}+\mathbf{q},\sigma} c_{\mathbf{k},\sigma}. \tag{3.32}$$

Again, this Hamiltonian has to be transformed by means of the Bogoliubov transformation of Eq. (3.8). The transformed Hamiltonian reads

$$\begin{aligned} H_{\rm em}^{(1)} = \frac{e\hbar}{2m} \sum_{\mathbf{k},\mathbf{q},\sigma} (2\mathbf{k}+\mathbf{q})\mathbf{A}_{\mathbf{q}}(t) \Big(& (u^*_{\mathbf{k}} u_{\mathbf{k}+\mathbf{q}} + v^*_{\mathbf{k}} v_{\mathbf{k}+\mathbf{q}}) \alpha^\dagger_{\mathbf{k}+\mathbf{q}} \alpha_{\mathbf{k}} \\ & - (u^*_{\mathbf{k}+\mathbf{q}} u_{\mathbf{k}} + v^*_{\mathbf{k}+\mathbf{q}} v_{\mathbf{k}}) \beta^\dagger_{\mathbf{k}} \beta_{\mathbf{k}+\mathbf{q}} + (u_{\mathbf{k}+\mathbf{q}} v_{\mathbf{k}} - u_{\mathbf{k}} v_{\mathbf{k}+\mathbf{q}}) \alpha^\dagger_{\mathbf{k}+\mathbf{q}} \beta^\dagger_{\mathbf{k}} \\ & + (u^*_{\mathbf{k}} v^*_{\mathbf{k}+\mathbf{q}} - u^*_{\mathbf{k}+\mathbf{q}} v^*_{\mathbf{k}}) \beta_{\mathbf{k}+\mathbf{q}} \alpha_{\mathbf{k}} \Big) \end{aligned} \tag{3.33}$$

$$
\begin{aligned}
H^{(2)}_{\mathrm{em}} = \frac{e^2}{2m} \sum_{\mathbf{k},\mathbf{q},\sigma} \left(\sum_{\mathbf{q}'} \mathbf{A}_{\mathbf{q}-\mathbf{q}'}(t) \mathbf{A}_{\mathbf{q}'}(t) \right) \Bigg[& (u^*_{\mathbf{k}} u_{\mathbf{k}+\mathbf{q}} - v^*_{\mathbf{k}} v_{\mathbf{k}+\mathbf{q}}) \alpha^\dagger_{\mathbf{k}+\mathbf{q}} \alpha_{\mathbf{k}} \\
& + (u^*_{\mathbf{k}+\mathbf{q}} u_{\mathbf{k}} - v^*_{\mathbf{k}+\mathbf{q}} v_{\mathbf{k}}) \beta^\dagger_{\mathbf{k}} \beta_{\mathbf{k}+\mathbf{q}} + (u_{\mathbf{k}+\mathbf{q}} v_{\mathbf{k}} + u_{\mathbf{k}} v_{\mathbf{k}+\mathbf{q}}) \alpha^\dagger_{\mathbf{k}+\mathbf{q}} \beta^\dagger_{\mathbf{k}} \\
& + (u^*_{\mathbf{k}} v^*_{\mathbf{k}+\mathbf{q}} + u^*_{\mathbf{k}+\mathbf{q}} v^*_{\mathbf{k}}) \beta_{\mathbf{k}+\mathbf{q}} \alpha_{\mathbf{k}} \Bigg] .
\end{aligned}
\tag{3.34}
$$

Due to the fact that the probe pulse is much weaker than the pump pulse, it is only treated in linear approximation, i.e., only the linear coupling $H^{(1)}_{\mathrm{em}}$ is taken into account. The Hamiltonian of second order $H^{(2)}_{\mathrm{em}}$ is neglected. The pump pulse instead has a high intensity and as a consequence both linear and nonlinear part of the Hamiltonian have to be considered. In order to simulate the effect of the probe pulse further approximations are used, which will be discussed in Sect. 6.2.

3.4 Quenches

As can be seen in Eq. (3.33), the pump pulse leads to a shift of quasiparticles in **k**-space. So expectation values are excited which are non-diagonal in **k**, e.g. $\left\langle \alpha^\dagger_{\mathbf{k}} \alpha_{\mathbf{k}+\mathbf{q}} \right\rangle$. Due to this the temporal evolution of these expectation values has to be computed. The shift of quasiparticles is determined by the photon momentum. Due to this the discretization of the Brillouin zone depends on the photon momentum, for further details see Sect. 4.3.

Certainly a diagonal perturbation, which pushes the system out of equilibrium without shifting quasiparticles, reduces the numerical effort due to a less strict discretization mesh. This is one reason why quenches are taken into account.

To perturb the electronic system two different kinds of quenches are defined.

First, a quench is considered, which suddenly changes the value of the coupling strength W_0, see Eq. (3.3). This quench is called "interaction quench". The new coupling strength $\tilde{W}_0$ is given by

$$
\tilde{W}_0 = a W_0, \tag{3.35}
$$

with the parameter $a \in [0, 1]$. Applying this quench makes the initial state to be no longer the equilibrium state of the system, which induces collective dynamics.

A light pulse excites quasiparticles and the quasiparticle densities become finite, e.g., see Sect. 5.1. This is used for the second considered quench. For this quench the normal expectation values $\left\langle \alpha^{\dagger}_{\mathbf{k}}\alpha_{\mathbf{k}} \right\rangle$ and $\left\langle \beta^{\dagger}_{\mathbf{k}}\beta_{\mathbf{k}} \right\rangle$ become finite in a Gaussian shape around the Fermi momentum. This quench is called "occupation quench". The Gaussian shape is chosen, because a short pump pulse leads to similar expectation values, see Sect. 5.1. As parameter of this quench one can choose the amplitude and the FWHM.

As can be seen in Sect. 5.1, both quenches yield nearly the same dynamics of the electronic subsystem as a short pump pulse, so both can be used as a good approximation of a perturbation by a pump pulse.

The main reason why we applied quenches is that we want to test the effect of different discretization, see Sect. 4.3, and other numerical implementation details with a simpler system. As already mentioned a quench simplifies the equations of motion drastically, see Sect. 4.1.

4 Equations of motions and implementation

In this section, some details of the numerical implementation are presented. First, the equations of motion to describe the nonequilibrium dynamics are introduced. To solve the system of differential equations a standard Runge-Kutta 4th order algorithm is used [60].

In order to solve the equations of motion numerically one has to discretize the **B**rillouin **z**one (BZ), i.e. choose the **k**-values, which are taken into account. How this is done is described in Sect. 4.3.

In this section, we only concentrate on the numerical implementation of the system perturbed by a pump pulse or a quench. The implementation of the probe pulse is discussed in Sect. 6.1.

4.1 Equations of motion

Observables such as the order parameter, see Eq. (3.3), are fully determined by the temporal evolution of quasiparticle densities such as $\left\langle \alpha^{\dagger}_{\mathbf{k}} \alpha_{\mathbf{k}'} \right\rangle$. The temporal evolution of these expectation values is given by the equation of motion which follows from the DMF approach. Due to the non bilinear Fröhlich Hamiltonian of the system a truncation is needed to obtain a closed system. Here, the equations of motion up to the second order in the correlation expansion are presented. The presented equations can easily be simplified to the equations for other system, e.g., the pure superconductor without additional phonons.

In the following, the differential equations of the normal quasiparticle density $\left\langle \alpha^{\dagger}_{\mathbf{k}} \alpha_{\mathbf{k}'} \right\rangle$, the phonon assisted correlation $\left\langle \alpha^{\dagger}_{\mathbf{k}} \alpha_{\mathbf{k}'} b_{\mathbf{p}} \right\rangle^{c}$, the mean phonon amplitude $\langle b_{\mathbf{p}} \rangle$, and the incoherent phonon density $\left\langle b^{\dagger}_{\mathbf{p}} b_{\mathbf{p}'} \right\rangle$ are shown. The equations, which are not explicitly shown in this section, are of similar form. They are given in Appendix A.2.

For the normal quasiparticle density $\left\langle \alpha^\dagger_{\mathbf{k}} \alpha_{\mathbf{k}'} \right\rangle$, the equation of motion reads

$$i\hbar \frac{\mathrm{d}}{\mathrm{d}t} \left\langle \alpha^\dagger_{\mathbf{k}} \alpha_{\mathbf{k}'} \right\rangle = (R_{\mathbf{k}'} - R_{\mathbf{k}}) \left\langle \alpha^\dagger_{\mathbf{k}} \alpha_{\mathbf{k}'} \right\rangle + C_{\mathbf{k}'} \left\langle \alpha^\dagger_{\mathbf{k}} \beta^\dagger_{\mathbf{k}'} \right\rangle - C^*_{\mathbf{k}} \left\langle \beta_{\mathbf{k}} \alpha_{\mathbf{k}'} \right\rangle \tag{4.1a}$$

$$+ \frac{e\hbar}{2m} \sum_{\mathbf{q}'=\pm\mathbf{q}_0} 2\mathbf{k}\mathbf{A}_{\mathbf{q}'} \Bigg(- L^+_{\mathbf{k},\mathbf{q}'} \left\langle \alpha^\dagger_{\mathbf{k}+\mathbf{q}'} \alpha_{\mathbf{k}'} \right\rangle + \tag{4.1b}$$

$$+ L^+_{\mathbf{k}',-\mathbf{q}'} \left\langle \alpha^\dagger_{\mathbf{k}} \alpha_{\mathbf{k}'-\mathbf{q}'} \right\rangle - M^-_{\mathbf{k}',-\mathbf{q}'} \left\langle \alpha^\dagger_{\mathbf{k}} \beta^\dagger_{\mathbf{k}'-\mathbf{q}'} \right\rangle + M^-_{\mathbf{k},\mathbf{q}'} \left\langle \beta_{\mathbf{k}+\mathbf{q}'} \alpha_{\mathbf{k}'} \right\rangle \Bigg)$$

$$+ \frac{e^2}{2m} \sum_{\mathbf{q}'=0,\pm2\mathbf{q}_0} \left(\sum_{\mathbf{q}_i=\pm\mathbf{q}_0} \mathbf{A}_{\mathbf{q}'-\mathbf{q}_i} \mathbf{A}_{\mathbf{q}_i} \right) \Bigg(- L^-_{\mathbf{k},\mathbf{q}'} \left\langle \alpha^\dagger_{\mathbf{k}+\mathbf{q}'} \alpha_{\mathbf{k}'} \right\rangle + \tag{4.1c}$$

$$+ L^-_{\mathbf{k}',-\mathbf{q}'} \left\langle \alpha^\dagger_{\mathbf{k}} \alpha_{\mathbf{k}'-\mathbf{q}'} \right\rangle + M^+_{\mathbf{k}',-\mathbf{q}'} \left\langle \alpha^\dagger_{\mathbf{k}} \beta^\dagger_{\mathbf{k}'-\mathbf{q}'} \right\rangle - M^+_{\mathbf{k},\mathbf{q}'} \left\langle \beta_{\mathbf{k}+\mathbf{q}'} \alpha_{\mathbf{k}'} \right\rangle \Bigg)$$

$$+ \sum_{\mathbf{p}} \frac{g_{\mathbf{p}}}{\sqrt{N}} \left(\left\langle b^\dagger_{-\mathbf{p}} \right\rangle + \langle b_{\mathbf{p}} \rangle \right) \Bigg(- L^-_{\mathbf{k},\mathbf{p}} \left\langle \alpha^\dagger_{\mathbf{k}+\mathbf{p}} \alpha_{\mathbf{k}'} \right\rangle + \tag{4.1d}$$

$$+ L^-_{\mathbf{k}',-\mathbf{p}'} \left\langle \alpha^\dagger_{\mathbf{k}} \alpha_{\mathbf{k}'-\mathbf{p}} \right\rangle - M^+_{\mathbf{k},\mathbf{p}} \left\langle \beta_{\mathbf{k}+\mathbf{p}} \alpha_{\mathbf{k}'} \right\rangle + M^+_{\mathbf{k}',-\mathbf{p}} \left\langle \alpha^\dagger_{\mathbf{k}} \beta^\dagger_{\mathbf{k}'-\mathbf{p}} \right\rangle \Bigg)$$

$$+ \sum_{\mathbf{p}} \frac{g_{\mathbf{p}}}{\sqrt{N}} \Bigg(- L^-_{\mathbf{k},\mathbf{p}} \left(\left\langle \alpha^\dagger_{\mathbf{k}+\mathbf{p}} \alpha_{\mathbf{k}'} b_{\mathbf{p}} \right\rangle^c + \left\langle \alpha^\dagger_{\mathbf{k}+\mathbf{p}} \alpha_{\mathbf{k}'} b^\dagger_{-\mathbf{p}} \right\rangle^c \right) + \tag{4.1e}$$

$$+ L^-_{\mathbf{k}',-\mathbf{p}'} \left(\left\langle \alpha^\dagger_{\mathbf{k}} \alpha_{\mathbf{k}'-\mathbf{p}} b_{\mathbf{p}} \right\rangle^c + \left\langle \alpha^\dagger_{\mathbf{k}} \alpha_{\mathbf{k}'-\mathbf{p}} b^\dagger_{-\mathbf{p}} \right\rangle^c \right) -$$

$$- M^+_{\mathbf{k},\mathbf{p}} \left(\left\langle \beta_{\mathbf{k}+\mathbf{p}} \alpha_{\mathbf{k}'} b_{\mathbf{p}} \right\rangle^c + \left\langle \beta_{\mathbf{k}+\mathbf{p}} \alpha_{\mathbf{k}'} b^\dagger_{-\mathbf{p}} \right\rangle^c \right) +$$

$$+ M^+_{\mathbf{k}',-\mathbf{p}} \left(\left\langle \alpha^\dagger_{\mathbf{k}} \beta^\dagger_{\mathbf{k}'-\mathbf{p}} b_{\mathbf{p}} \right\rangle^c + \left\langle \alpha^\dagger_{\mathbf{k}} \beta^\dagger_{\mathbf{k}'-\mathbf{p}} b^\dagger_{-\mathbf{p}} \right\rangle^c \right) \Bigg).$$

Here, the line (4.1a) follows from the commutator $\left[\alpha^\dagger_{\mathbf{k}} \alpha_{\mathbf{k}'} \ , \ H_{\mathrm{sc}}\right]$ and describes the temporal evolution of the pure superconductor. If we only consider a superconductor which is perturbed by a quench, we only need to take this line into account. The lines (4.1b) and (4.1c) result from $\left[\alpha^\dagger_{\mathbf{k}} \alpha_{\mathbf{k}'} \ , \ H_{\mathrm{em}}\right]$. They have to be considered if the system is perturbed by the pump pulse instead of a quench. The last two lines (4.1d) and (4.1e) are derived from $\left[\alpha^\dagger_{\mathbf{k}} \alpha_{\mathbf{k}'} \ , \ H_{\mathrm{Fr}}\right]$. They must be considered if the system is coupled to additional phonons. Here, the phonon assisted quantities are already factorized, e.g. $\left\langle \alpha^\dagger_{\mathbf{k}} \alpha_{\mathbf{k}'} b_{\mathbf{p}} \right\rangle = \left\langle \alpha^\dagger_{\mathbf{k}} \alpha_{\mathbf{k}'} b_{\mathbf{p}} \right\rangle^c + \left\langle \alpha^\dagger_{\mathbf{k}} \alpha_{\mathbf{k}'} \right\rangle \langle b_p \rangle$. For the first order in the correlation expansion, i.e., neglecting the corrections of the phonon assisted quantities, only line (4.1d) must be kept.

If only the first order in the expansion is considered, the equation of motion for the mean phonon amplitude is needed to obtain a closed system. It is given by

$$\begin{aligned} i\hbar\frac{\mathrm{d}}{\mathrm{d}t}\left\langle b_{\mathbf{p}}\right\rangle &= \hbar\omega_{-\mathbf{p}}\left\langle b_{\mathbf{p}}\right\rangle \qquad \text{(4.2a)} \\ &+ \frac{1}{\sqrt{N}}\sum_{\mathbf{k}} g_{-\mathbf{p}}\Bigg(L^{-}_{\mathbf{k},-\mathbf{p}}\left(\left\langle \alpha^{\dagger}_{\mathbf{k}-\mathbf{p}}\alpha_{\mathbf{k}}\right\rangle + \left\langle \beta^{\dagger}_{\mathbf{k}}\beta_{\mathbf{k}-\mathbf{p}}\right\rangle\right) \qquad \text{(4.2b)} \\ &\qquad + M^{+}_{\mathbf{k},-\mathbf{p}}\left(\left\langle \alpha^{\dagger}_{\mathbf{k}-\mathbf{p}}\beta^{\dagger}_{\mathbf{k}}\right\rangle + \left\langle \beta_{\mathbf{k}-\mathbf{p}}\alpha_{\mathbf{k}}\right\rangle\right) + 2\delta_{0,-\mathbf{p}}|v_{\mathbf{k}}|^{2}\Bigg). \end{aligned}$$

Here, line (4.2a) result from $\left[b_{\mathbf{p}}\ ,\ H_{\mathrm{ph}}\right]$ and line (4.2b) from $\left[b_{\mathbf{p}}\ ,\ H_{\mathrm{Fr}}\right]$.

For the second order in the expansion the temporal evolution of the phonon assisted quantities must be known. The equations of motion for the full phonon assisted quantities consist of expectation values including four operators, e.g. four fermionic ones or two fermionic and two bosonic ones. For example, the factorization of such correlations is given by

$$\begin{aligned} \left\langle \alpha^{\dagger}_{\mathbf{k}}\alpha_{\mathbf{k}'}b^{\dagger}_{\mathbf{p}}b_{\mathbf{p}'}\right\rangle &= \left\langle \alpha^{\dagger}_{\mathbf{k}}\alpha_{\mathbf{k}'}b^{\dagger}_{\mathbf{p}}b_{\mathbf{p}'}\right\rangle^{c} + \left\langle \alpha^{\dagger}_{\mathbf{k}}\alpha_{\mathbf{k}'}b_{\mathbf{p}'}\right\rangle^{c}\left\langle b^{\dagger}_{\mathbf{p}}\right\rangle + \left\langle \alpha^{\dagger}_{\mathbf{k}}\alpha_{\mathbf{k}'}b^{\dagger}_{\mathbf{p}}\right\rangle^{c}\left\langle b_{p'}\right\rangle \qquad (4.3) \\ &+ \left\langle \alpha^{\dagger}_{\mathbf{k}}\alpha_{\mathbf{k}'}\right\rangle\left(\left\langle b^{\dagger}_{\mathbf{p}}\right\rangle\left\langle b_{p'}\right\rangle + \left\langle b^{\dagger}_{\mathbf{p}}b_{\mathbf{p}'}\right\rangle^{c}\right). \end{aligned}$$

All other factorizations are given in Appendix A.1. Note that $\left\langle \alpha^{\dagger}_{\mathbf{k}}\alpha_{\mathbf{k}'}\right\rangle = \left\langle \alpha^{\dagger}_{\mathbf{k}}\alpha_{\mathbf{k}'}\right\rangle^{c}$ and $\left\langle b_{p}\right\rangle = \left\langle b_{p}\right\rangle^{c}$. As mentioned in Sect. 2.1 it is much faster to compute the temporal evolution of the correlation instead of the full expectation values. This is caused by a reduced equation of motion of the correlation, e.g. the EoM for the correlation $\left\langle \alpha^{\dagger}_{\mathbf{k}}\alpha_{\mathbf{k}'}b_{\mathbf{p}}\right\rangle^{c}$ is defined by

$$\begin{aligned} i\hbar\frac{\mathrm{d}}{\mathrm{d}t}\left\langle \alpha^{\dagger}_{\mathbf{k}}\alpha_{\mathbf{k}'}b_{\mathbf{p}}\right\rangle^{c} &= i\hbar\frac{\mathrm{d}}{\mathrm{d}t}\left\langle \alpha^{\dagger}_{\mathbf{k}}\alpha_{\mathbf{k}'}b_{\mathbf{p}}\right\rangle \qquad (4.4) \\ &- \left(i\hbar\frac{\mathrm{d}}{\mathrm{d}t}\left\langle \alpha^{\dagger}_{\mathbf{k}}\alpha_{\mathbf{k}'}\right\rangle\right)\left\langle b_{p}\right\rangle - i\hbar\left\langle \alpha^{\dagger}_{\mathbf{k}}\alpha_{\mathbf{k}'}\right\rangle\frac{\mathrm{d}}{\mathrm{d}t}\left\langle b_{p}\right\rangle, \end{aligned}$$

and reads

$$
\begin{aligned}
& i\hbar\frac{\mathrm{d}}{\mathrm{d}t}\left\langle\alpha^\dagger_{\mathbf{k}}\alpha_{\mathbf{k}'}b_{\mathbf{p}}\right\rangle^c = \qquad\qquad (4.5)\\
& (-R_{\mathbf{k}}+R_{\mathbf{k}'}+\hbar\omega_p)\left\langle\alpha^\dagger_{\mathbf{k}}\alpha_{\mathbf{k}'}b_{\mathbf{p}}\right\rangle^c + C_{\mathbf{k}'}\left\langle\alpha^\dagger_{\mathbf{k}}\beta^\dagger_{\mathbf{k}'}b_{\mathbf{p}}\right\rangle^c - C^*_{\mathbf{k}}\left\langle\beta_{\mathbf{k}}\alpha_{\mathbf{k}'}b_{\mathbf{p}}\right\rangle^c\\
& +\frac{e\hbar}{2m}\sum_{\mathbf{q}'=\pm\mathbf{q}_0}2\mathbf{k}\mathbf{A}_{\mathbf{q}'}\Big(-L^+_{\mathbf{k},\mathbf{q}'}\left\langle\alpha^\dagger_{\mathbf{k}+\mathbf{q}'}\alpha_{\mathbf{k}'}b_{\mathbf{p}}\right\rangle^c + L^+_{\mathbf{k}',-\mathbf{q}'}\left\langle\alpha^\dagger_{\mathbf{k}}\alpha_{\mathbf{k}'-\mathbf{q}'}b_{\mathbf{p}}\right\rangle^c\\
& \qquad\qquad - M^-_{\mathbf{k}',-\mathbf{q}'}\left\langle\alpha^\dagger_{\mathbf{k}}\beta^\dagger_{\mathbf{k}'-\mathbf{q}'}b_{\mathbf{p}}\right\rangle^c + M^-_{\mathbf{k},\mathbf{q}'}\left\langle\beta_{\mathbf{k}+\mathbf{q}'}\alpha_{\mathbf{k}'}b_{\mathbf{p}}\right\rangle^c\Big)\\
& +\frac{e^2}{2m}\sum_{\mathbf{q}'=0,\pm2\mathbf{q}_0}\left(\sum_{\mathbf{q}_i=\pm\mathbf{q}_0}\mathbf{A}_{\mathbf{q}'-\mathbf{q}_i}\mathbf{A}_{\mathbf{q}_i}\right)\Big(-L^-_{\mathbf{k},\mathbf{q}'}\left\langle\alpha^\dagger_{\mathbf{k}+\mathbf{q}'}\alpha_{\mathbf{k}'}b_{\mathbf{p}}\right\rangle^c\\
& \qquad + L^-_{\mathbf{k}',-\mathbf{q}'}\left\langle\alpha^\dagger_{\mathbf{k}}\alpha_{\mathbf{k}'-\mathbf{q}'}b_{\mathbf{p}}\right\rangle^c + M^+_{\mathbf{k}',-\mathbf{q}'}\left\langle\alpha^\dagger_{\mathbf{k}}\beta^\dagger_{\mathbf{k}'-\mathbf{q}'}b_{\mathbf{p}}\right\rangle^c - M^+_{\mathbf{k},\mathbf{q}'}\left\langle\beta_{\mathbf{k}+\vec{}}\alpha_{\mathbf{k}'}b_{\mathbf{p}}\right\rangle^c\Big)\\
& +\sum_{\mathbf{r}}\frac{g_{-\mathbf{q}}}{\sqrt{N}}\Big\{L^-_{\mathbf{k},-\mathbf{p}}\Big[\left\langle\alpha^\dagger_{\mathbf{k}}\alpha_{\mathbf{r}}\right\rangle\left(\delta_{\mathbf{r}-\mathbf{p},\mathbf{k}'}-\left\langle\alpha^\dagger_{\mathbf{r}-\mathbf{p}}\alpha_{\mathbf{k}'}\right\rangle\right)+\left\langle\alpha^\dagger_{\mathbf{k}}\beta^\dagger_{\mathbf{r}}\right\rangle\left\langle\beta_{\mathbf{r}-\mathbf{p}}\alpha_{\mathbf{k}'}\right\rangle\Big]\\
& \qquad\qquad + M^+_{\mathbf{r},-\mathbf{p}}\Big[\left\langle\alpha^\dagger_{\mathbf{k}}\beta^\dagger_{\mathbf{r}}\right\rangle\left(\delta_{\mathbf{r}-\mathbf{p},\mathbf{k}'}-\left\langle\alpha^\dagger_{\mathbf{r}-\mathbf{p}}\alpha_{\mathbf{k}}\right\rangle\right)-\left\langle\alpha^\dagger_{\mathbf{k}}\alpha_{\mathbf{r}}\right\rangle\left\langle\beta_{\mathbf{r}-\mathbf{p}}\alpha_{\mathbf{k}'}\right\rangle\Big]\Big\}\\
& +\sum_{q}\frac{g_{\mathbf{q}}}{\sqrt{N}}\Big\{\\
& -L^-_{\mathbf{k},\mathbf{q}}\Big[\left\langle\alpha^\dagger_{\mathbf{k}+\mathbf{q}}\alpha_{\mathbf{k}'}b_{\mathbf{p}}\right\rangle^c\left(\langle b_{\mathbf{q}}\rangle+\left\langle b^\dagger_{-\mathbf{q}}\right\rangle\right)+\left\langle\alpha^\dagger_{\mathbf{k}+\mathbf{q}}\alpha_{\mathbf{k}'}\right\rangle\left(\left\langle b^\dagger_{-\mathbf{q}}b_{\mathbf{p}}\right\rangle^c+\langle b_{\mathbf{q}}b_{\mathbf{p}}\rangle^c\right)\Big]\\
& +L^-_{\mathbf{k}',-\mathbf{q}}\Big[\left\langle\alpha^\dagger_{\mathbf{k}}\alpha_{\mathbf{k}'-\mathbf{q}}b_{\mathbf{p}}\right\rangle^c\left(\langle b_{\mathbf{q}}\rangle+\left\langle b^\dagger_{-\mathbf{q}}\right\rangle\right)+\left\langle\alpha^\dagger_{\mathbf{k}}\alpha_{\mathbf{k}'-\mathbf{q}}\right\rangle\left(\left\langle b^\dagger_{-\mathbf{q}}b_{\mathbf{p}}\right\rangle^c+\langle b_{\mathbf{q}}b_{\mathbf{p}}\rangle^c\right)\Big]\\
& -M^+_{\mathbf{k},\mathbf{q}}\Big[\left\langle\beta_{\mathbf{k}+\mathbf{q}}\alpha_{\mathbf{k}'}b_{\mathbf{p}}\right\rangle^c\left(\langle b_{\mathbf{q}}\rangle+\left\langle b^\dagger_{-\mathbf{q}}\right\rangle\right)+\left\langle\beta_{\mathbf{k}+\mathbf{q}}\alpha_{\mathbf{k}'}\right\rangle\left(\left\langle b^\dagger_{-\mathbf{q}}b_{\mathbf{p}}\right\rangle^c+\langle b_{\mathbf{q}}b_{\mathbf{p}}\rangle^c\right)\Big]\\
& +M^+_{\mathbf{k}',-\mathbf{q}}\Big[\left\langle\alpha^\dagger_{\mathbf{k}}\beta^\dagger_{\mathbf{k}'-\mathbf{q}}b_{\mathbf{p}}\right\rangle^c\left(\langle b_{\mathbf{q}}\rangle+\left\langle b^\dagger_{-\mathbf{q}}\right\rangle\right)+\left\langle\alpha^\dagger_{\mathbf{k}}\beta^\dagger_{\mathbf{k}'-\mathbf{q}}\right\rangle\left(\left\langle b^\dagger_{-\mathbf{q}}b_{\mathbf{p}}\right\rangle^c+\langle b_{\mathbf{q}}b_{\mathbf{p}}\rangle^c\right)\Big]\Big\}.
\end{aligned}
$$

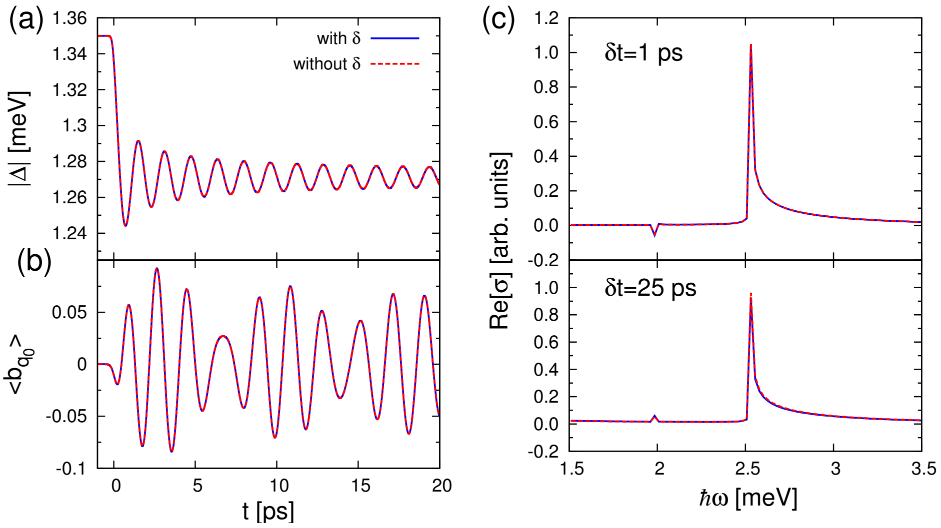

Figure 4.1: The temporal evolution is depicted for the order parameter (a), the mean phonon amplitude $\left\langle b_{\mathbf{q}_0}\right\rangle$, and the real part of the conductivity for two delay times. The blue line presents the results using Eq. (4.2) and the red dotted line presents the results neglecting the contribution proportional to $\delta_{0,\mathbf{p}}$.

As can be seen in the above equation the incoherent phonon density enters and has to be computed by

$$
\begin{aligned}
i\hbar\frac{\mathrm{d}}{\mathrm{d}t}\left\langle b^\dagger_{\mathbf{p}}b_{\mathbf{q}}\right\rangle^c &= \hbar\left(\omega_{-\mathbf{q}}-\omega_{\mathbf{p}}\right)\left\langle b^\dagger_{\mathbf{p}}b_{\mathbf{q}}\right\rangle^c \\
&\quad+\frac{1}{\sqrt{N}}\sum_k\Big\{g_{-\mathbf{q}}\Big[L^-_{\mathbf{k},-\mathbf{q}}\left(\left\langle\alpha^\dagger_{\mathbf{k}-\mathbf{q}}\alpha_{\mathbf{k}}b^\dagger_{\mathbf{p}}\right\rangle^c+\left\langle\beta^\dagger_{\mathbf{k}}\beta_{\mathbf{k}-\mathbf{q}}b^\dagger_{\mathbf{p}}\right\rangle^c\right) \\
&\qquad\qquad+M^+_{\mathbf{k},-\mathbf{q}}\left(\left\langle\alpha^\dagger_{\mathbf{k}-\mathbf{q}}\beta^\dagger_{\mathbf{k}}b^\dagger_{\mathbf{p}}\right\rangle^c+\left\langle\beta_{\mathbf{k}-\mathbf{q}}\alpha_{\mathbf{k}}b^\dagger_{\mathbf{p}}\right\rangle^c\right)\Big] \\
&\qquad-g_{\mathbf{p}}\Big[L^-_{\mathbf{k},\mathbf{p}}\left(\left\langle\alpha^\dagger_{\mathbf{k}+\mathbf{p}}\alpha_{\mathbf{k}}b_{\mathbf{q}}\right\rangle^c+\left\langle\beta^\dagger_{\mathbf{k}}\beta_{\mathbf{k}+\mathbf{p}}b_{\mathbf{q}}\right\rangle^c\right) \\
&\qquad\qquad+M^+_{\mathbf{k},\mathbf{p}}\left(\left\langle\alpha^\dagger_{\mathbf{k}+\mathbf{p}}\beta^\dagger_{\mathbf{k}}b_{\mathbf{q}}\right\rangle^c+\left\langle\beta_{\mathbf{k}+\mathbf{p}}\alpha_{\mathbf{k}}b_{\mathbf{q}}\right\rangle^c\right)\Big]\Big\}.
\end{aligned}
\tag{4.6}
$$

The temporal evolution of $\left\langle b_{\mathbf{p}}b_{\mathbf{p}}\right\rangle^c$ is presented in Appendix A.2.
The above equations together with the equations in Appendix A.2 form a closed set of differential equations.

4.2 Parameter and initial condition

Before the equations of motion can be solved, some parameters for the numerical simulations have to be fixed.

The simulation starts from the BCS ground state at zero temperature $T = 0\,\mathrm{K}$. Thus, the quasiparticle densities are zero at the beginning of the simulation. If the electron-phonon coupling is included we assume the BCS ground state and the bosonic vacuum to be the starting state of the simulation. Normally, due to the electron-phonon coupling the BCS ground state is no longer the real ground state of the system, but for small coupling strength $g_{\mathbf{p}}$ this assumption should be valid. This initial state is not the groundstate as can be seen in the equation of motion of the mean phonon amplitude, see Eq. (4.2). The Kronecka delta $\delta_{0,\mathbf{p}}$ induces a dynamic of $\left\langle b_0 \right\rangle$ even without any perturbation, namely an oscillation given by

$$\left\langle b_0 \right\rangle = -\left(\sum_{\mathbf{k}} \frac{g_0}{\sqrt{N}} \frac{2|v_{\mathbf{k}}|^2}{\hbar\omega_{(\mathbf{p}=0)}} \right) \left(1 - \exp\left(-i\omega_{(\mathbf{p}=0)} t\right)\right) . \tag{4.7}$$

In the following, we neglect the contribution proportional to $\delta_{0,\mathbf{p}}$ and take into account that we make a mistake in computing $\left\langle b_0 \right\rangle (t)$. With this Eq. (4.2) simplifies to

$$\begin{aligned} i\hbar \frac{\mathrm{d}}{\mathrm{d}t} \left\langle b_{\mathbf{p}} \right\rangle = \hbar\omega_{-\mathbf{p}} \left\langle b_{\mathbf{p}} \right\rangle + \frac{1}{\sqrt{N}} \sum_{\mathbf{k}} g_{-\mathbf{p}} \Bigg(& L^-_{\mathbf{k},-\mathbf{p}} \left(\left\langle \alpha^\dagger_{\mathbf{k}-\mathbf{p}} \alpha_{\mathbf{k}} \right\rangle + \left\langle \beta^\dagger_{\mathbf{k}} \beta_{\mathbf{k}-\mathbf{p}} \right\rangle \right) \\ & + M^+_{\mathbf{k},-\mathbf{p}} \left(\left\langle \alpha^\dagger_{\mathbf{k}-\mathbf{p}} \beta^\dagger_{\mathbf{k}} \right\rangle + \left\langle \beta_{\mathbf{k}-\mathbf{p}} \alpha_{\mathbf{k}} \right\rangle \right) \Bigg) . \end{aligned} \tag{4.8}$$

This approximation is valid if we consider acoustic phonons, because in this case $g_0 = 0$ and the neglected contribution does not enter the equation of motion. For optical phonons the approximation is also justified, because we get almost the same results for quantities such as the order parameter, the conductivity, and all other mean phonon amplitudes $\left\langle b_{\mathbf{p}\neq 0} \right\rangle (t)$. For example, Fig. 4.1 shows the results of a simulation using a pump pulse with $|\mathbf{A}_0| = 7 \cdot 10^{-8}\,\mathrm{Js/(Cm)}$ and $\tau_0 = 0.5\,\mathrm{ps}$, a phonon energy of $\hbar\omega_{\mathrm{ph}} = 2\mathrm{meV}$, and a coupling strength of $g_{\mathrm{ph}} = 0.2\,\mathrm{meV}$. A detailed discussion of the presented results is given in Sects. 5 and 6.

Motivated by the numbers for lead (Pb) [71] the initial order parameter is set to $\Delta_0 = 1.35\,\mathrm{meV}$. The Fermi energy is given by $E_{\mathrm{Fermi}} = 9479\,\mathrm{meV}$, the cutoff energy by $\hbar\omega_{\mathrm{c}} = 8.3\,\mathrm{meV}$, and the effective mass by $m = 1.9m_0$, with the free electron mass

superconductor		laser pulses	
Δ_0	$1.35\,\mathrm{meV}$	$\hbar\omega_0$	$3\,\mathrm{meV}$
E_{Fermi}	$9479\,\mathrm{meV}$	$\hbar\omega_{\mathrm{pr}}$	$2.5\,\mathrm{meV}$
$\hbar\omega_{\mathrm{c}}$	$8.3\,\mathrm{meV}$	τ_{pr}	$0.25\,\mathrm{ps}$
m	$1.9m_0$	-	-

Table 4.1: Parameters for numerical simulation.

m_0.

For the laser pulses we use following parameters. First, the pump pulse is centered at $t = 0\,\mathrm{ps}$. The pump pulse energy, which is slightly larger than the gap, is set to $\hbar\omega_0 = 3\,\mathrm{meV}$. The probe pulse energy is set to $\hbar\omega_{\mathrm{pr}} = 2.5\,\mathrm{meV}$ and the pulse width to $\tau_{\mathrm{pr}} = 0.25\,\mathrm{ps}$.

The fixed parameters are additionally listed in Tab. 4.1. All other parameters of the system, e.g., the pump pulse width, are varied. The actual value of these parameters is given in the corresponding sections.

4.3 Discreatization

In order to solve the closed set of differential equations introduced in the previous sections numerically, we have to restrict the number of considered points in momentum space. The discretization meshes are presented in the following. For the superconductor with or without coupled phonons we use the same mesh.

In general, we take only expectation values with indices $\mathbf{k}$ and $\mathbf{k}+\mathbf{q} \in W$, e.g., $\left\langle \alpha^{\dagger}_{\mathbf{k}} \alpha_{\mathbf{k}+\mathbf{q}} \right\rangle$, into account. This means that we concentrate on the $\mathbf{k}$-values where the attractive interaction takes place. Expectation values with $\mathbf{k} \in W$ and $\mathbf{k}+\mathbf{q} \notin W$ or vice versa are neglected.

For simplicity, the simulations are done in two dimensions. A sketch of the two dimensional momentum space is depicted in Fig. 4.2. For all cases, especially for the superconductor without phonons, we perform a quasi-one-dimensional calculation to reduce the numerical effort. It has been shown that this quasi-one-dimensional simulation yields a good approximation for two- and three-dimensional systems [30]. For example, the temporal evolution of the order parameter for the quasi-one-dimensional, as explained in the following, and a two dimensional mesh, i.e. a radial symmetric mesh as depicted in Fig. 4.2(b), are shown in Fig. 4.3(a). Here,

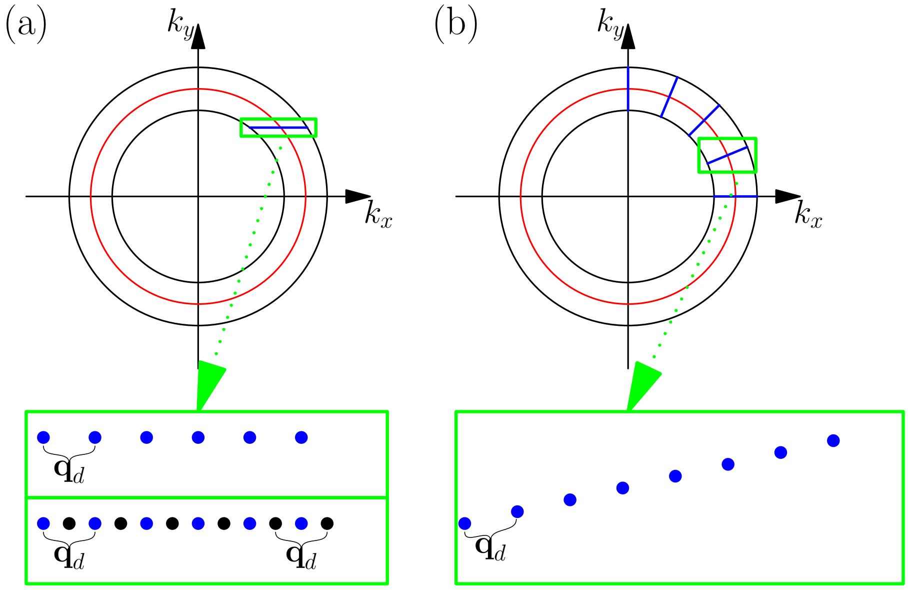

Figure 4.2: Sketch of the discretization mesh. In panel (a) the quasi-one-dimensional mesh and in panel (b) the two-dimensional mesh is sketched. The red circle denotes the Fermi momentum $\mathbf{k}_F$ and the black circles the momenta $\mathbf{k}_F \pm \mathbf{k}_c$, where $\mathbf{k}_c$ is the cutoff momentum. The blue lines depict the position of discretization points. A zoom to the discretization points is presented in the green boxes. The distance between two discretization points, blue dots, is given by $\mathbf{q}_d$. The black dots denote the nested mesh.

the system, consisting only of the BCS Hamiltonian H_{sc}, was perturbed by a interaction quench with $a = 0.9$, see Eq. (3.35). For both meshes the evolution of order parameter matches perfectly.

The quasi-one-dimensional mesh is constructed by choosing discretization points on a line parallel to k_x for a fixed value of k_y, see Fig. 4.2. The distance between two $\mathbf{k}$-points is given by the momentum $\mathbf{q}_d$. The pump pulse couples only in k_x-direction. Due to this the discretization is chosen in this direction. The coupling in k_y-direction enters only over the order parameter and is weak compared to the coupling to the light field.

If a quench is considered, only expectation values diagonal in $\mathbf{k}$, e.g. $\left\langle \alpha^\dagger_{\mathbf{k}} \alpha_{\mathbf{k}} \right\rangle$, have to be considered. As a result $\mathbf{q}_d$ can be chosen arbitrarily. Nevertheless, the numbers of discretization points determine the maximal time $t_{\max}$ up to which the simulation can be computed accurately. The temporal evolution of the order parameter for various numbers of discretization points is depicted in Fig. 4.3(b). Here, the system was perturbed by an interaction quench with $a = 0.9$, see Eq. (3.35). This figure shows, that the maximal time, up to which a smooth $1/\sqrt{t}$-decay is visible, increases

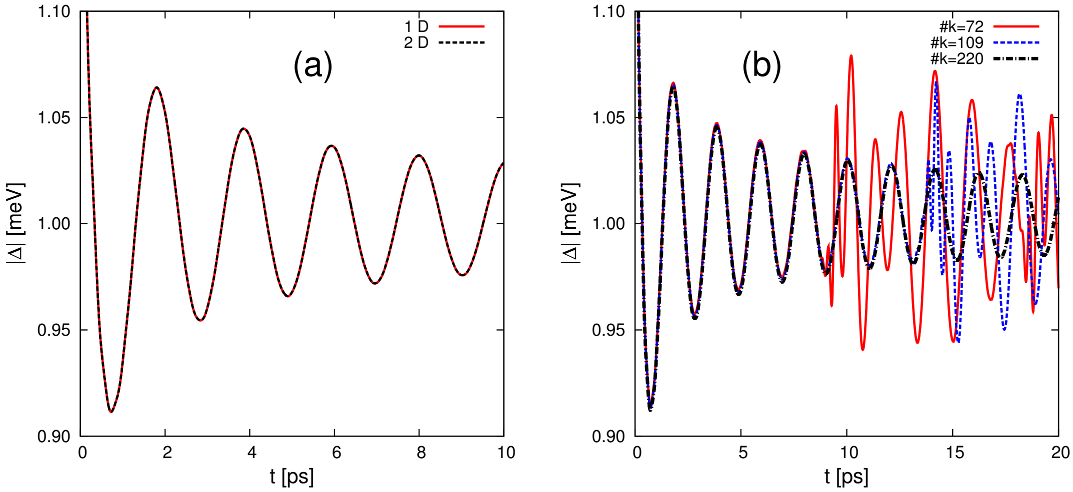

Figure 4.3: Temporal evolution of the order parameter after a quench $\tilde{W}_0 = aW_0$ with $a = 0.9$. In panel (a) the results for a quasi 1 D mesh and a 2 D mesh are shown. In panel (b) the results for a 1 D mesh with various numbers of **k**-points are depicted.

with increasing numbers of **k**-values. The decay is due to destructive interference between expectation values with different momenta, see Sect. 5.1. If the number of **k**-values is too small this behavior cannot be captured correctly.

Once the pump pulse is used as perturbation, also the expectation values with momenta $\mathbf{k}$ and $(\mathbf{k}+\mathbf{q})$ have to be considered, but it suffices to use only the momenta $\mathbf{k}+n\mathbf{q}_0$ with an integer n. This can be easily seen in the equation of motion of the normal density in Eq. (4.1). The external electromagnetic field breaks translational invariance and may add or subtract the pump pulse momentum $\mathbf{q}_0$. As consequence the distance $\mathbf{q}_d$ of the discretization mesh is also determined by the pump pulse momentum, i.e. $\mathbf{q}_d = \mathbf{q}_0$. For small amplitudes $|\mathbf{A}_0|$ the off-diagonal elements decrease rapidly as n increases due to the contribution at $(\mathbf{k},\ \mathbf{k}+n\mathbf{q}_0) = O(|\mathbf{A}_0|^{|n|})$ [30]. Thus, we set all entries with $n > 4$ to zero. With this choice of the $\mathbf{k}$, $\mathbf{k}+\mathbf{q}$ values, we are able to solve the equations of motion. Due to the small value of $\mathbf{q}_0$ compared to $\mathbf{k}_{\mathrm{Fermi}}$ the number of discretization points is large so that simulations up to $t_{\max} \approx 100$ps are possible. To expand the maximal time of the simulation a second pattern can be nested into the old one as depicted in Fig. 4.2. This new pattern couples to the old one over the order parameter only, but not to the pump pulse.

If also phonons are considered, the same mesh is used. For the phonon momenta we set $\mathbf{p} = m\mathbf{p}_0 = m\mathbf{q}_0$ with an integer m. As for the integer n we restrict $m \leq 4$. This restriction is well justified as can be seen in the equations of motion for the mean phonon amplitude, see Eq. (4.2). This equation describes a driven harmonic oscillator, for details see Sect. 5.2. For $m > 4$ the driving force includes only quasi-particle densities with $n > 4$ and are thus zero. Considering the initial condition, see previous section, yields that $\left\langle b^{\dagger}_{\mathbf{p}} \right\rangle (t)$ remains zero for $m > 4$. Processes which excite expectation values $\left\langle \alpha^{\dagger}_{\mathbf{k}} \alpha_{\mathbf{k}+\mathbf{p}} \right\rangle$ with $\mathbf{p} \neq m\mathbf{q}_0$ are not taken into account in order of the correlation expansion.

5 Nonequilibriun Dynamics

In this section, the nonequilibrium dynamics of a superconductor induced by a quench or a pump pulse are discussed. Thereto, we mainly concentrate on the temporal evolution of the order parameter and of the lattice displacement. The main findings of the induced dynamics may be found as a signature of the pump probe response, e.g. the optical conductivity. This will be discussed in Sect. 6.

We start our investigation with the s-wave superconductor without any additional phonon couplings. The dynamics of this system induced either by an interaction quench [37–41, 72] or by an ultrafast pump pulse [30–32] has already been topic of various studies. Here, we reproduce the main findings and take a closer look to some more details, e.g. the transition between the nonadiabatic regime and the adiabatic regime of the system, see Sect. 5.1. Further, we use this investigation to establish the numerical implementation.

Finally, a s-wave superconductor coupled to additional phonons is considered. Here, the generation of coherent and incoherent optical phonons as well as of coherent acoustic phonons is analyzed. The investigation of the coherent optical phonons is discussed based on previous studies of Schnyder *et al.* [33]. Again, the previous findings are reproduced and further aspects are studied, see Sect. 5.2

5.1 Superconductor in absence of phonons

A pump pulse with $\hbar\omega_0 > 2\Delta_0$ acting on a superconductor excites Bogoliubov quasiparticles. This breaks Cooper-pairs and thereby leads to a lowering of the absolute value of the order parameter. The way the pump pulses excite the Bogoliubov quasiparticle depends on the width and the intensity of the pump pulse. In Fig. 5.1, the occupation of the normal quasiparticle densities $\left\langle \alpha^\dagger_{\mathbf{k}} \alpha_{\mathbf{k}} \right\rangle$ just after the pulse acts on the system is shown for various pump pulse width. The corresponding normal densities $\left\langle \beta^\dagger_{\mathbf{k}} \beta_{\mathbf{k}} \right\rangle$ look the same and are not explicitly shown. Although the simulations are performed in a fixed, time independent Bogoliubov-de Gennes basis which is determined by the initial order parameter, it is always possible to transform to an instantaneous Bogoliubov space in which the Hamiltonian is actually diagonal. The presented densities are given in this instantaneous Bogoliubov space. The basis is

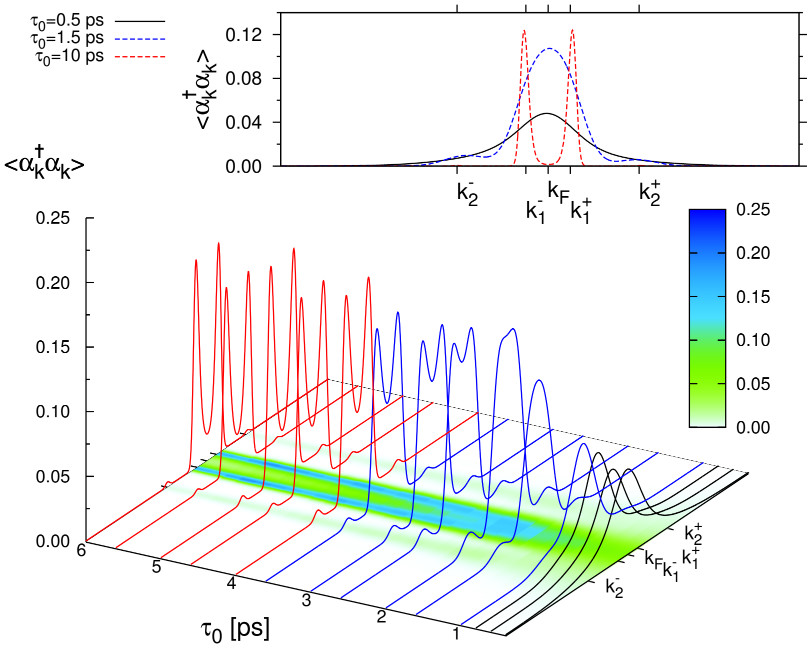

Figure 5.1: Quasiparticle occupation just after the pump pulse acts on the system in the instantaneous Bogoliubov space, see Eq. (5.1), for various pulse widths. The pump pulse intensity is kept almost constant at $|\mathbf{A}_0|^2\tau \approx 4\cdot 10^{-27}\,\mathrm{J^2s^3/(C^2m^2)}$. The momentum $\mathrm{k_F} = 2.17315\cdot 10^{10}\,1/(\mathrm{m})$ denotes the Fermi momentum, the momenta $\mathrm{k}_1^+ = 2.17323\cdot 10^{10}\,1/(\mathrm{m})$ and $\mathrm{k}_1^- = 2.17307\cdot 10^{10}\,1/(\mathrm{m})$ correspond to $E_{\mathbf{k}_1^\pm} = \frac{\hbar\omega_0}{2}$, and $\mathrm{k}_2^+ = 2.17345\cdot 10^{10}\,1/(\mathrm{m})$ and $\mathrm{k}_2^- = 2.17285\cdot 10^{10}\,1/(\mathrm{m})$ correspond to $E_{\mathbf{k}_2^\pm} = \hbar\omega_0$. The inset compares the occupation for three specific pulse widths ($\tau_0 = 0.5, 1.5,$ and $10\,\mathrm{ps}$). The results of the adiabatic regime is presented by red lines, whereas the black depicts the results for the nonadiabatic regime. The intermediate regime is colored in blue.

changed via

$$\begin{pmatrix}\tilde{\alpha}_{\mathbf{k}}\\ \tilde{\beta}_{\mathbf{k}}^\dagger\end{pmatrix} = \begin{pmatrix}\tilde{u}_{\mathbf{k}} & -\tilde{v}_{\mathbf{k}}\\ \tilde{v}_{\mathbf{k}}^* & \tilde{u}_{\mathbf{k}}^*\end{pmatrix}\begin{pmatrix}u_{\mathbf{k}}^* & v_{\mathbf{k}}\\ -v_{\mathbf{k}}^* & u_{\mathbf{k}}\end{pmatrix}\begin{pmatrix}\alpha_{\mathbf{k}}\\ \beta_{\mathbf{k}}^\dagger\end{pmatrix} \tag{5.1}$$

with

$$\tilde{u}_{\mathbf{k}} = \sqrt{\frac{1}{2}\left(1+\frac{\epsilon_{\mathbf{k}}}{E_{\mathbf{k}}(\Delta)}\right)} \qquad \text{and} \qquad \tilde{v}_{\mathbf{k}} = \frac{\Delta}{|\Delta|}\sqrt{\frac{1}{2}\left(1-\frac{\epsilon_{\mathbf{k}}}{E_{\mathbf{k}}(\Delta)}\right)}. \tag{5.2}$$

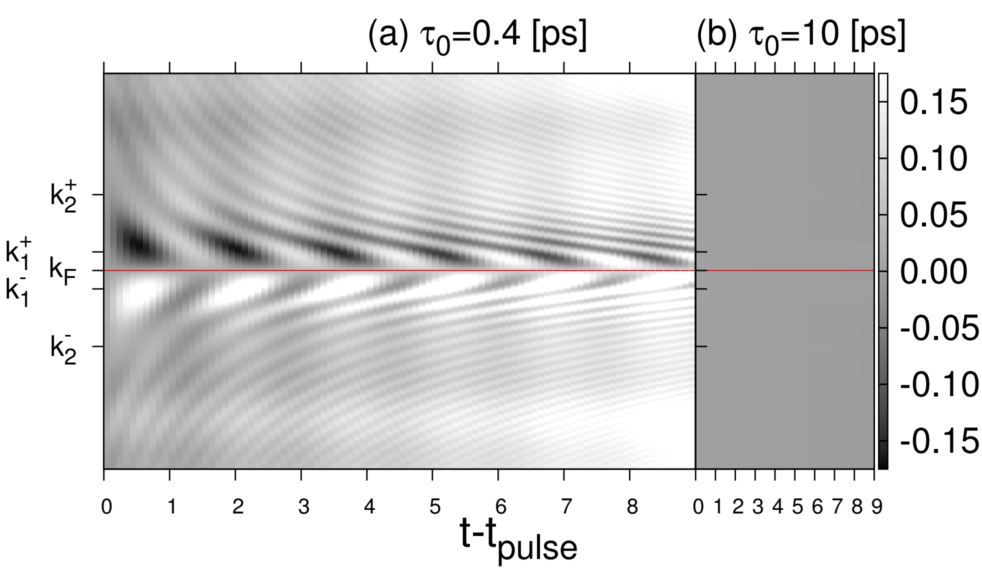

Figure 5.2: The relative deviation δ, as explained in the text, versus time t and momentum $\mathbf{k}$ for the nonadiabatic, panel (a), and the adiabatic regime, panel (b). The red solid line denote the Fermi momentum $\mathrm{k_F} = 2.17315 \cdot 10^{10}\,1/(\mathrm{m})$. The momenta $\mathrm{k}_1^+ = 2.17323 \cdot 10^{10}\,1/(\mathrm{m})$ and $\mathrm{k}_1^- = 2.17307 \cdot 10^{10}\,1/(\mathrm{m})$ correspond to $E_{\mathbf{k}_1^\pm} = \frac{\hbar\omega_0}{2}$, and $\mathrm{k}_2^+ = 2.17345 \cdot 10^{10}\,1/(\mathrm{m})$ and $\mathrm{k}_2^- = 2.17285 \cdot 10^{10}\,1/(\mathrm{m})$ correspond to $E_{\mathbf{k}_2^\pm} = \hbar\omega_0$.

Here, $\tilde{u}_\mathbf{k}$ and $\tilde{v}_\mathbf{k}$ depend on the actual value of the order parameter and $E_\mathbf{k}(\Delta) = \sqrt{\epsilon_\mathbf{k}^2 + |\Delta|^2}$.

For a large pulse duration two strong sharp peaks symmetrical around the Fermi momentum $\mathbf{k} = \mathbf{k}_{\mathrm{Fermi}}$ appear. These two peaks arise from processes which are linear in the vector potential. The position of these maxima correspond approximately to half the pump pulse energy $\frac{1}{2}\hbar\omega_0$. It can be interpreted as the absorption of one photon.

Further, two smaller peaks can be observed. The positions of the weaker peaks correspond approximately to the pump pulse energy $\hbar\omega_0$. These peaks originate from processes quadratic in the vector potential. In other words, it can be interpreted as the absorption of two photons.

With decreasing pulse width the two strong peaks deform gradually into one narrow peak around $\mathbf{k} = \mathbf{k}_{\mathrm{Fermi}}$. The weaker peaks are still visible. On further decreasing of the duration the narrow peak become wider resulting into one broad peak around $\mathbf{k} = \mathbf{k}_{\mathrm{Fermi}}$. This broad peak is caused by the larger uncertainty in the pump energy for shorter pulse durations.

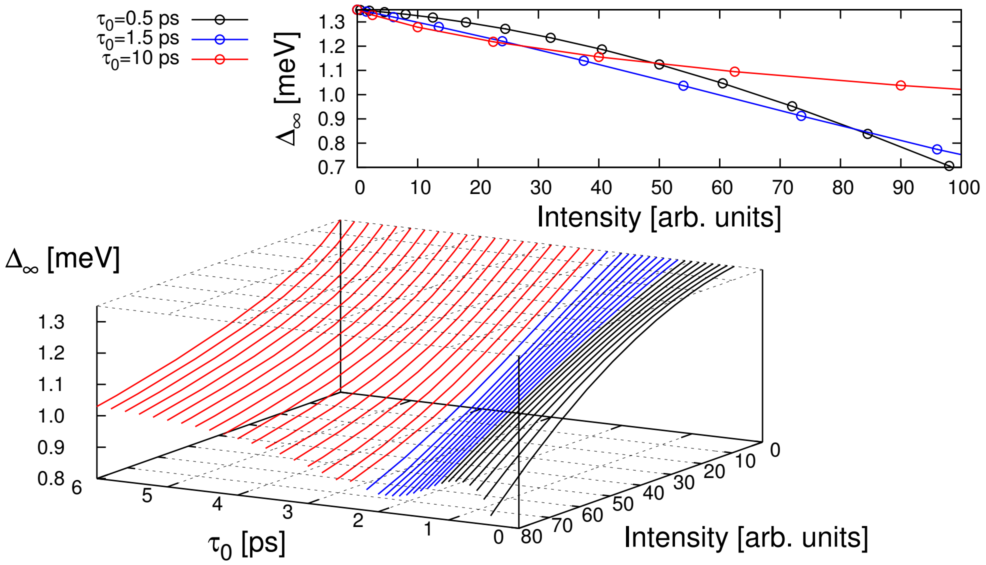

Figure 5.3: The asymptotical value Δ_∞ as function of pump pulse intensity for different pump pulse widths. The inset shows the same for three specific pulse widths ($\tau_0 = 0.5, 1.5,$ and $10\,\mathrm{ps}$). The results of the adiabatic regime are presented by red lines whereas the black lines depict the results for the nonadiabatic regime. The intermediate regime is colored in blue.

The shape of the quasiparticle distribution depends on the pulse duration just as the temporal evolution of the densities. For longer pulses, the normal densities are almost time independent after the pulse acts, whereas for short pulses the densities show a rapid oscillation. In this case, quasiparticle densities with different momenta oscillates differently. This behavior is sketched in Fig. 5.2. It shows the relative deviation

$$\delta = \frac{\left\langle \alpha_{\mathbf{k}}^{\dagger}\alpha_{\mathbf{k}}\right\rangle (t) - \left\langle \alpha_{\mathbf{k}}^{\dagger}\alpha_{\mathbf{k}}\right\rangle (t_{\mathrm{pulse}})}{\left\langle \alpha_{\mathbf{k}}^{\dagger}\alpha_{\mathbf{k}}\right\rangle (t_{\mathrm{pulse}})} \tag{5.3}$$

between the normal quasiparticle densities at time t and the densities just after the pulse $t = t_{\mathrm{pulse}}$. The oscillation in the quasiparticle distribution for short pulses is clearly visible in δ, left panel in Fig. 5.2, whereas δ is constant for longer pulses, right panel in Fig. 5.2.

This behavior can be understood by the fact that the pulse excites normal Bogoliubov densities and anomalous Bogoliubov densities, e.g. $\left\langle \alpha_{\mathbf{k}}^{\dagger}\beta_{\mathbf{k}}^{\dagger}\right\rangle$ [30]. In the case of longer pulses, the anomalous densities vanish almost completely in the instantaneous Bogoliubov space. As a consequence, the derivatives of $\left\langle \alpha_{\mathbf{k}}^{\dagger}\alpha_{\mathbf{k}}\right\rangle$,$\left\langle \beta_{\mathbf{k}}^{\dagger}\beta_{\mathbf{k}}\right\rangle$, and $\left\langle \alpha_{\mathbf{k}}^{\dagger}\beta_{\mathbf{k}}^{\dagger}\right\rangle$ become zero, see Eqs. (4.1), (A.4), and (A.5), because the prefactors $C_{\mathbf{k}}$ become zero in the instantaneous Bogoliubov space. Thus, a stationary state is reached.

For shorter pulses the anomalous Bogoliubov densities remain finite even in the instantaneous Bogoliubov space. As a result the derivative of $\left\langle \alpha_{\mathbf{k}}^{\dagger}\beta_{\mathbf{k}}^{\dagger}\right\rangle$ is not zero. This leads to a change in $\left\langle \alpha_{\mathbf{k}}^{\dagger}\beta_{\mathbf{k}}^{\dagger}\right\rangle$, which influences the order parameter and with this the Hamiltonian is consequently no longer diagonal. Hence, the normal Bogoliubov densities will also change and the system is in a nonstationary state far from equilibrium. The oscillation of the densities generates also an oscillation of the order parameter, e.g. see Fig. 5.4, which will be discussed in more detail in the following.

Beside the pulse duration the intensity of the pump pulse influences its impact. For increasing intensity the absolute value of the order parameter is lowered stronger, because more quasiparticles are excited. In Fig. 5.3 the value of the order parameter at $\Delta(t \to \infty) = \Delta_\infty$ is plotted versus the width and intensity of the pump pulse. For short pulses Δ_∞ decreases very steeply compared to longer pulses. This behavior is in perfect agreement with experimental results of Matsunaga *et al.* [6]. They performed THz-pump and THz probe spectroscopy on thin NbN films with a pump pulse duration of 90 fs. They also observed the asymptotic gap value versus the pump intensity. It shows the same steep decrease as our theoretical results. More details about these experimental results can be found in Sect. 6.3, where we compare the theoretically computed pump probe response with the experimental one.

With increasing pulse duration the decrease of Δ_∞ flattens, see Fig. 5.3. For $\tau_0 \approx \tau_\Delta$ the decrease is almost linear. This behavior can be explained by the quasiparticle distribution induced by the pump pulse. For a larger pulse two strong sharp peaks appear in the quasiparticle occupation. The additional excitation of quasiparticles becomes more and more difficult because of Pauli's exclusion principle. This is called Pauli blocking. In contrast, a short pulse creates a rather broad maxima in the quasiparticle occupation. This means that the occupation is distributed on many states and Pauli blocking is not efficient. As for the quasiparticle occupation a smooth crossover between the two dynamical regimes can be seen in the shift of Δ_∞.

We want shortly conclude, that depending on the pulse duration the system tune into two dynamical regimes. Between the two regimes a smooth crossover exist, which will be discussed later.

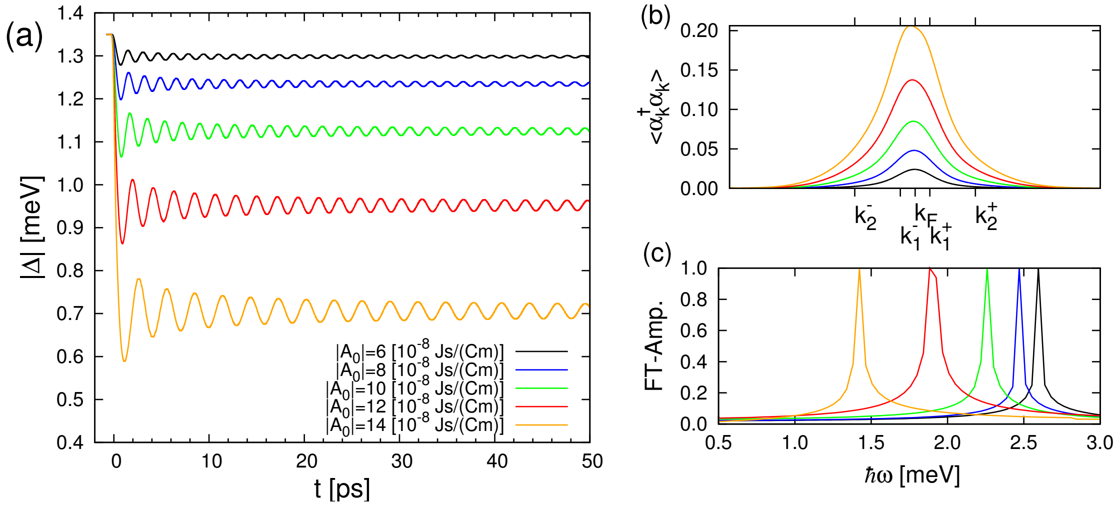

Figure 5.4: (a) Temporal evolution of the order parameter for a pump pulse with pulse width $\tau_0 = 0.5\,\mathrm{meV}$ and various light field amplitudes. (b) Quasiparticle occupation just after the pulse acts on the system in the instantaneous Bogoliubov space, see Eq. (5.1). The momentum $\mathrm{k_F} = 2.17315 \cdot 10^{10}\,1/(\mathrm{m})$ denotes the Fermi momentum, the momenta $\mathrm{k}_1^+ = 2.17323 \cdot 10^{10}\,1/(\mathrm{m})$ and $\mathrm{k}_1^- = 2.17307 \cdot 10^{10}\,1/(\mathrm{m})$ correspond to $E_{\mathbf{k}_1^\pm} = \frac{\hbar\omega_0}{2}$, and $\mathrm{k}_2^+ = 2.17345 \cdot 10^{10}\,1/(\mathrm{m})$ and $\mathrm{k}_2^- = 2.17285 \cdot 10^{10}\,1/(\mathrm{m})$ correspond to $E_{\mathbf{k}_2^\pm} = \hbar\omega_0$. (c) Fourier spectra of (a).

If the pump pulse width τ_0 is larger than the dynamical time scale of the superconductor $\tau_0 > \tau_\Delta = \frac{\pi\hbar}{|\Delta|}$ the system is tuned into the adiabatic regime, depicted as red lines in Figs. 5.1- 5.3. In this regime, the order parameter is lowered during the pulse and remains constant afterwards, because a stationary state is reached.

If $\tau_0 < \tau_\Delta$ the system is tuned into the nonadiabatic regime, where the expectation value and consequently the order parameter show an oscillation after the pulse [30–34, 36]. This regime is highlighted as black curves in Figs. 5.1- 5.3. In the nonadabtic regime the system is in a non-stationary state far from equilibrium.

Between both regimes a crossover takes place. This crossover is labeled as intermediate regime and depicted as blue lines in Figs. 5.1- 5.3.

In the following the temporal evolution of the order parameter is studied for the three defined dynamical regimes. We concentrate mostly on the nonadiabatic regime, although the evolution for the intermediate and adiabatic regime are also discussed.

5.1.1 Nonadiabatic regime ($\tau \ll \tau_\Delta$)

As mentioned in the previous section the rapid oscillation in the quasiparticle occupation causes an oscillation of the order parameter. In Fig. 5.4 the temporal evolution of the order parameter for a short pulse width of $\tau_0 = 0.5\,\mathrm{ps}$ is shown. First, the order parameter is lowered during the pulse and oscillates afterwards with one specific frequency. As can be seen in the corresponding Fourier spectra, the frequency of the oscillation is given by $\omega_{\Delta_\infty} = \frac{2\Delta_\infty}{\hbar}$, where Δ_∞ is the value of $|\Delta|$ asymptotically reached. The fact that the order parameter oscillates with only one frequency can also be seen in temporal evolution of the expectation values in Fig. 5.2(a). Here, we see that the oscillation around $\mathbf{k}_{\mathrm{Fermi}}$, i.e., $E(\mathbf{k}_{\mathrm{Fermi}}) = |\Delta|$ dominates and its frequency is given by ω_{Δ_∞}. The other frequencies of the expectation value oscillations are canceled out due to destructive interference. Interestingly, the order parameter oscillation is decaying, although the simulations are performed in the collisionless regime, i.e., without relaxation processes, so that no damping of the oscillation is included. The observed decay is no true relaxation but caused by destructive interference among quasiparticle densities with different momenta.

Upon increasing pump pulse intensity the absolute value of the order parameter decreases, which is caused by the stronger excitation of quasiparticles, see Fig. 5.4(b). In addition, the amplitude of the oscillation increases with increasing intensity.

This finding is again in perfect agreement with the experimental results of Matsunaga *et al.* [6]. The observed changed of the transmission oscillates with $\omega_{\Delta_\infty} = \frac{2\Delta_\infty}{\hbar}$ reflecting the oscillation of the order parameter. A more precise discussion about the results of Matsunaga *et al.* [6] is given in Sect. 6.3

For a more detailed description of the decay of the order parameter oscillation, we study the nonequilibrium dynamics for a superconductor which is perturbed by a quench. In comparison, in Fig. 5.5 the evolutions of the order parameter induced by an interaction quench, by an occupation quench, and by a pump pulse with $\tau_0 = 0.5\,\mathrm{ps}$ are depicted. The results of the interaction quench were computed by both the DMF approach and iEoM method, leading to the same dynamics. The derivation of the equation of motion for the iEoM is given in App. B. In general, the order parameter behaves similar for the quenches and for the pump pulse excitation. In particular, the absolute value of $|\Delta|$ is lowered while the pulse or the quench acts, respectively. As for the laser pulse, the lowering of $|\Delta(t)|$ induced by the occupation quench is caused by an excitation of quasiparticles. For the interaction quench the lowering is given due to the new coupling constant. As can be easily seen in the self-consistent equation, see Eq. (3.5), the order parameter is lowered to $\Delta = a\Delta_0$. Afterwards, the order parameter oscillates and shows a decay.

Hence, we observe that the order parameter behaves similar when it is perturbed by a quench or a pump pulse. This is of great advantage in order to describe the

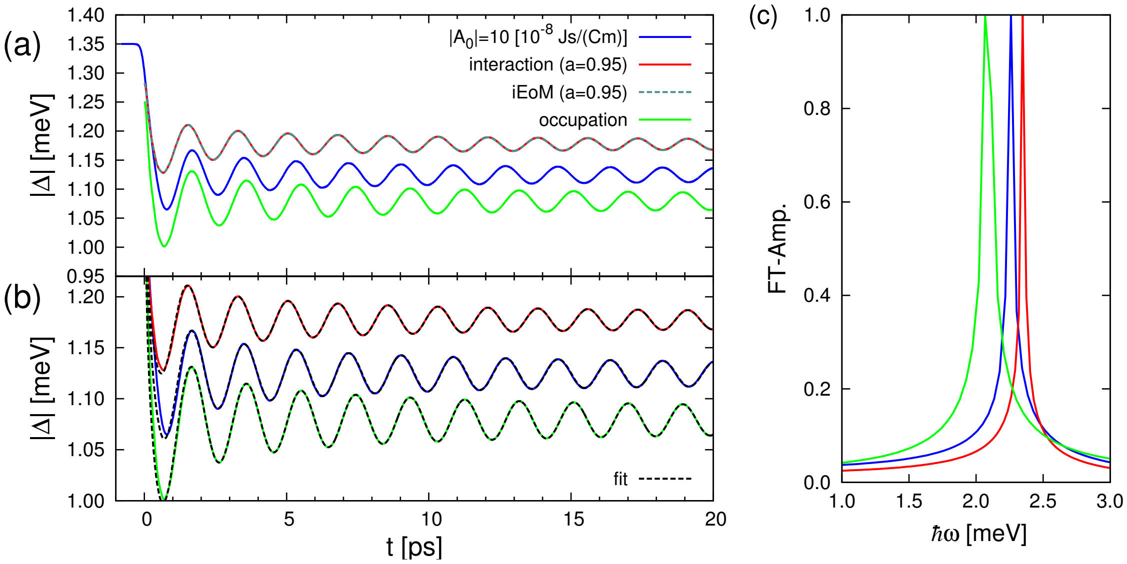

Figure 5.5: (a) Temporal evolution of the order parameter for various perturbation. (b) Comparison of the numerical with the analytical solution, see Eq. (5.12). (c) Fourier spectra of (a).

evolution of $|\Delta(t)|$ more precisely, because for an interaction quench as perturbation it is possible to derive an analytical solution for the order parameter dynamics [37, 40, 41, 72].

5.1.2 Analytical solution

To derive an analytical solution the BCS Hamiltonian is mapped to an Anderson pseudo spin Hamiltonian [73], given by

$$H_{\text{BCS}} = \sum_{\mathbf{k}} 2\epsilon_{\mathbf{k}} \mathbf{s}^z_{\mathbf{k}} - \frac{W_0}{N} \sum_{\mathbf{k},\mathbf{p}} \mathbf{s}^+_{\mathbf{k}} \mathbf{s}^-_{\mathbf{p}}. \tag{5.4}$$

Here, the spin components are given by

$$s^i_{\mathbf{k}} = \frac{1}{2} \left(c^\dagger_{\mathbf{k},\uparrow}, c_{-\mathbf{k},\downarrow} \right) \sigma_i \begin{pmatrix} c_{\mathbf{k},\uparrow} \\ c^\dagger_{-\mathbf{k},\downarrow} \end{pmatrix}. \tag{5.5}$$

The mean field decomposition is exact due to the infinite range of the interaction. As a results the effective field seen by each pseudospin in Eq. 5.4 can be replaced by its expectation value. The effective magnetic field is given by

$$\mathbf{b}_{\mathbf{k}} = 2\left(-\Delta_x, -\Delta_y, \epsilon_j\right) \tag{5.6}$$

with the order parameter

$$\Delta(t) = \Delta_x - i\Delta_y = \frac{W_0}{N}\sum_{\mathbf{k}} \left\langle s_{\mathbf{k}}^- \right\rangle = \frac{W_0}{N}\sum_{\mathbf{k}} \left(\langle s_{\mathbf{k}}^x\rangle - i\,\langle s_{\mathbf{k}}^y\rangle\right). \tag{5.7}$$

Its equation of motion is a Bloch equation

$$\frac{\mathrm{d}}{\mathrm{d}t}\mathbf{s}_{\mathbf{k}} = \mathbf{b}_{\mathbf{k}} \times \mathbf{s}_{\mathbf{k}} \tag{5.8}$$

describing a precession about the magnetic field $\mathbf{b}_{\mathbf{k}}$. Since the above equations are linear in $\mathbf{s}_{\mathbf{k}}$, we can use the expectation value with respect to the time-dependent state of the system. As a results we can use classical spins instead of quantum spins [72].

Up to now we have only rewritten the task of solving the equations of motion, but there are still infinitely many evolutions of classical spins to be calculated, which is normally intractable analytically.

To solve this problem analytically Volkov and Kogan [37] linearize the Bloch equations around the ground state yielding

$$|\Delta(t)| = \Delta_{\text{initial}} + a\frac{\cos\left(2\Delta_{\text{initial}}t + \Phi\right)}{\sqrt{t}} \ . \tag{5.9}$$

This describes the behavior for small deviations from the equilibrium. To describe the dynamics far from equilibrium Yuzbashyan *et al.* [40,41,72] use the integrability of the Hamiltonian [74].

By rewrite the pseudospin Hamiltonian to

$$H_{BCS} = -\frac{W_0}{N}\sum \epsilon_j H_j + const. \tag{5.10}$$

it can be shown that the Hamiltnoian is integrable [40]. The Hamiltnoian H_j is given by [40]

$$H_j = \sum_l \frac{\mathbf{s}_j \mathbf{s}_l}{\epsilon_j - \epsilon_l} - \frac{N s_j^z}{W_0}. \tag{5.11}$$

The Hamiltonian H_j is known as Gaudin magnets. In addition, all H_j Poisson commutes which each other, i.e. $\{H_j, H_i\} = 0$. As a result the Gaudin magnet Hamiltonian is integrable [75,76]. Hence, the pseudospin Hamiltonian Poisson commutes with all H_j's and as a result the H_j's are the integral of motions for H_{BCS}, i.e., H_{BCS} is integrable.
With this knowledge they computed

$$|\Delta(t)| = \Delta_\infty + a\frac{\cos\left(2\Delta_\infty t + \Phi\right)}{\sqrt{t}} \ , \tag{5.12}$$

for the temporal evolution of the order parameter. Compared to the results of Volkov and Kogan the frequency is given by $\omega_{\Delta_\infty} = \frac{2\Delta_\infty}{\hbar}$ instead of $\omega_{\Delta_0} = \frac{2\Delta_0}{\hbar}$.
A comparison between the analytical, see Eq. (5.12), and the numerical results reveals a perfect agreement, also for pump pulse and occupation quench perturbation. This is displayed in Fig. 5.5(b).

We conclude that the dynamics of the order parameter induced by a short pump pulse is perfectly described by Eq. (5.12). In addition, a quench can be used to approximately describe the effect of a short pump pulse.

5.1.3 Adiabatic regime ($\tau \gg \tau_\Delta$) and intermediate regime

For a larger pump pulse width $\tau_0 \gg \tau_\Delta$, e.g. $\tau_0 = 10\,\text{ps}$, the system is in the adiabatic regime. The corresponding evolution of the order parameter is presented in Fig. 5.6(a). During the pulse the absolute value of $|\Delta|$ is reduced and afterwards it remains almost constant, i.e., it does not oscillate like in the nonadiabatic regime. The only effect which appears by increasing the intensities is to lower Δ_∞, but $|\Delta(t)|$ does not show any oscillation. This is in perfect agreement with the temporal evolution of the quasiparticle densites.

The simulation for the intermediate regime is performed for a pump pulse width $\tau_0 = 1.5\,\text{ps}$, see Fig. 5.7. This value of τ is chosen, because it is close to the dynamical time scale of the superconductor $\tau_0 \approx \tau_\Delta$. In this regime, an oscillation of the order parameter can be detected after the pulse, too. Again the oscillation can be described with Eq. (5.12). The corresponding frequencies, see Fourier spectra in Fig. 5.7(c), fit again $\omega_{\Delta_\infty} = \frac{2|\Delta_\infty|}{\hbar}$, but compared to the oscillation of the nonadiabatic regime the amplitude is much smaller. With increasing pulse width the amplitude decreases, see also Fig. 5.8, so that finally the adiabatic regime is

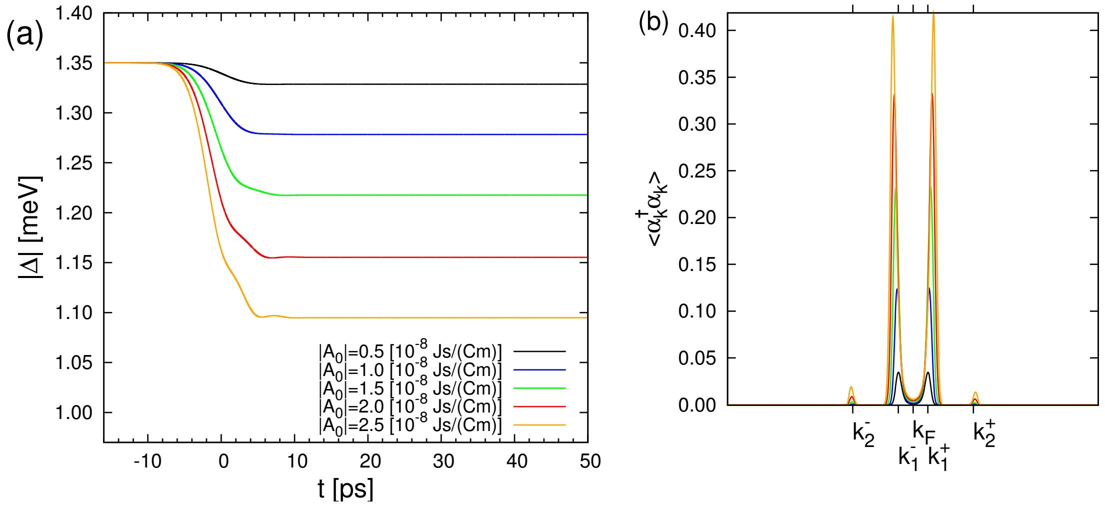

Figure 5.6: (a) Temporal evolution of the order parameter for a pump pulse with pulse width $\tau_0 = 10\,\mathrm{meV}$ and various light field amplitudes. (b) Quasiparticle occupation just after the pulse in the instantaneous Bogoliubov space, see Eq. (5.1). The momentum $\mathrm{k_F} = 2.17315 \cdot 10^{10}\,1/(\mathrm{m})$ denotes the Fermi momentum, the momenta $\mathrm{k}_1^+ = 2.17323{\cdot}10^{10}\,1/(\mathrm{m})$ and $\mathrm{k}_1^- = 2.17307{\cdot}10^{10}\,1/(\mathrm{m})$ correspond to $E_{\mathbf{k}_1^\pm} = \frac{\hbar\omega_0}{2}$, and $\mathrm{k}_2^+ = 2.17345 \cdot 10^{10}\,1/(\mathrm{m})$ and $\mathrm{k}_2^- = 2.17285 \cdot 10^{10}\,1/(\mathrm{m})$ correspond to $E_{\mathbf{k}_2^\pm} = \hbar\omega_0$.

reached.

If the pump pulse intensity increases the amplitude of the order parameter oscillation increases. In other words, by increasing the intensity an oscillation of $|\Delta(t)|$ can be generated, even for a pump pulse width equal or larger than the dynamical time scale. This is due to nonlinear effects of the pump pulse [35]. The impact of the nonlinear effect increases with increasing intensity, as can be seen in the quasiparticle occupation in Fig. 5.7(b). The two photon peaks in the distribution enhance with increasing intensity .

The intensity dependence of the amplitude a of $|\Delta(t)|$ for various pump pulse widths is depicted in Fig. 5.8. The amplitude has been obtained by fitting Eq. (5.12) to the simulated data. The amplitude of the order parameter oscillation increases monotonically with increasing intensity. The increase is almost linear for short pulses. This was to be expected, because short pulses $\tau_0 \ll \tau_\Delta$ always induce nonadiabatic dynamics.

For longer pulses we observe an increasing of the amplitude with increasing intensity. This time the slope of the increase is near zero at the beginning and increases with higher intensities. Longer pulses normally induce only adiabatic dynamics, but with higher intensity the pulse excites oscillations. Upon increasing pump pulse intensity

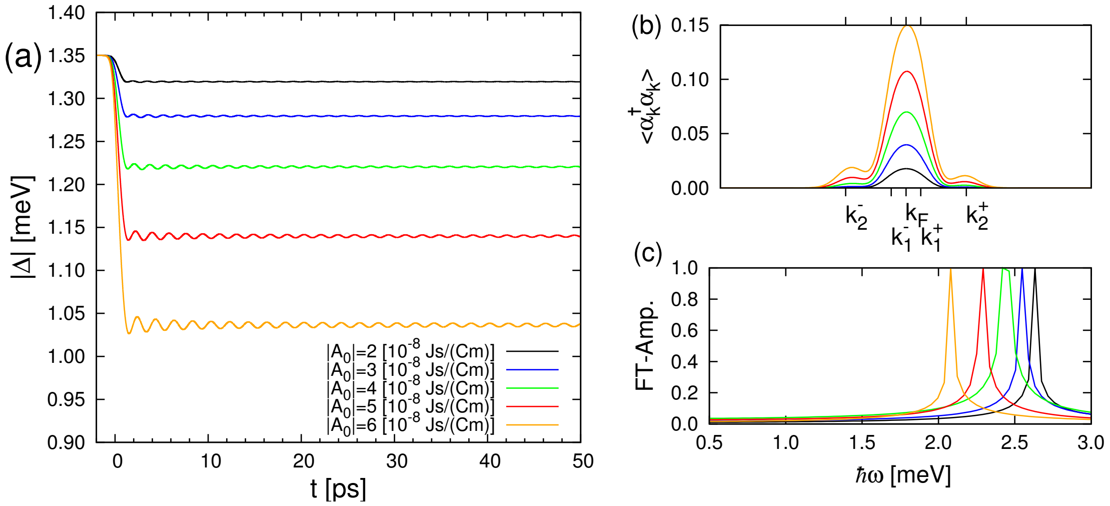

Figure 5.7: (a) Temporal evolution of the order parameter for a pump pulse with pulse width $\tau_0 = 1.5\,\text{meV}$ and various light field amplitudes. (b) Quasiparticle occupation just after the pulse in the instantaneous Bogoliubov space, see Eq. (5.1). The momentum $\mathrm{k_F} = 2.17315 \cdot 10^{10}\,1/(\mathrm{m})$ denotes the Fermi momentum, the momenta $\mathrm{k}_1^+ = 2.17323{\cdot}10^{10}\,1/(\mathrm{m})$ and $\mathrm{k}_1^- = 2.17307{\cdot}10^{10}\,1/(\mathrm{m})$ correspond to $E_{\mathbf{k}_1^\pm} = \frac{\hbar\omega_0}{2}$, and $\mathrm{k}_2^+ = 2.17345 \cdot 10^{10}\,1/(\mathrm{m})$ and $\mathrm{k}_2^- = 2.17285 \cdot 10^{10}\,1/(\mathrm{m})$ correspond to $E_{\mathbf{k}_2^\pm} = \hbar\omega_0$. (c) Fourier spectra of (a).

the nonlinear effects become more important. As a result the nonadiabatic dynamics can be reached even if the pump pulse width is not shorter than the dynamical time scale [35].

The previous investigations help to define specific pulse widths for the three dynamical regimes. If not otherwise specified the following values are used for the further investigation

$$\tau_{\text{non}} = 0.5\,\text{ps} \tag{5.13}$$

$$\tau_{\text{adi}} = 20\,\text{ps} \tag{5.14}$$

$$\tau_{\text{int}} = 1.5\,\text{ps}, \tag{5.15}$$

where τ_{non} denotes the width for the nonadiabatic regime, τ_{adi} for the adiabatic regime, and τ_{int} for the intermediate regime.

5.2 Superconductor in presence of optical phonons

In this section, we investigate the dynamics of the s-wave superconductor, which is additionally coupled to optical phonons.

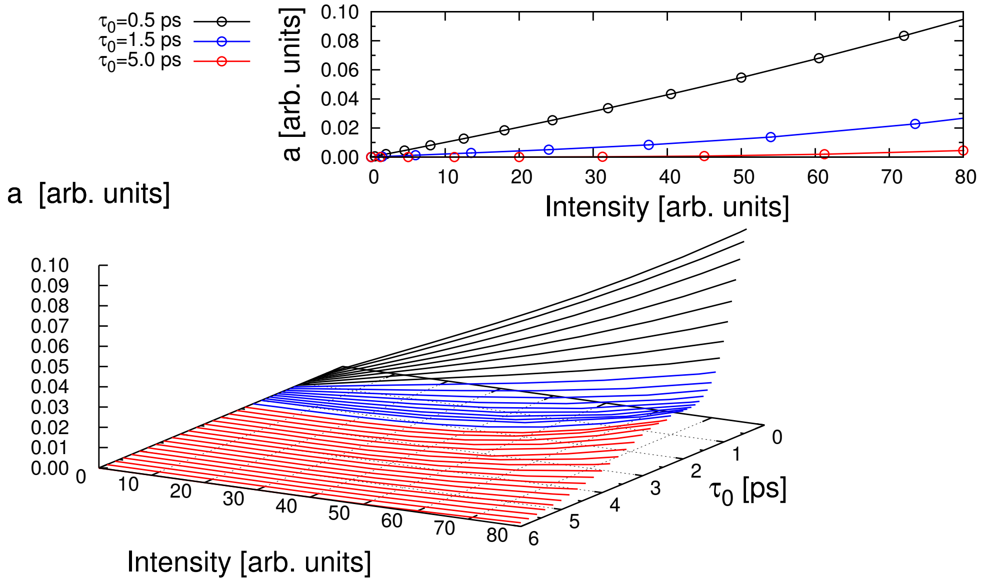

Figure 5.8: Amplitude a of the order parameter oscillation, see Eq. (5.12), as function of pump pulse intensity and different pump pulse width. The results of the adiabatic regime is presented by red lines whereas the black depict the results for the nonadiabatic regime. The intermediate regime is colored in blue.

The induced dynamics of the Bogoliubov quasiparticle densities leads to a generation of phonons. Here, we split the phonon dynamics into two parts, namely the coherent phonon part and the incoherent phonon part. The phonon density, given by

$$\left\langle b^\dagger_{\mathbf{p}} b_{\mathbf{p}} \right\rangle = \underbrace{\left\langle b^\dagger_{\mathbf{p}} \right\rangle \left\langle b_{\mathbf{p}} \right\rangle}_{N_{\text{coh.}}} + \underbrace{\left\langle b^\dagger_{\mathbf{p}} b_{\mathbf{p}} \right\rangle^c}_{N_{\text{incoh.}}}, \tag{5.16}$$

can be separated into a coherent and incoherent part. The coherent part is given by the mean phonon amplitude and the incoherent part by the correction of the phonon density.

First, we study only the generation of coherent phonons, which means that we neglect the incoherent part $N_{\text{incoh.}} = 0$. The dynamics are given by the first order correlation expansion. Here, we investigate the generation of the coherent phonon for various initial condition, e.g. different pump pulses or phonon energies.

Second, we include the incoherent phonons into the system, which induces a computing of the second order of the correlation expansion. With this we take processes like electron-phonon scattering into account, which were neglected in the first order calculation.

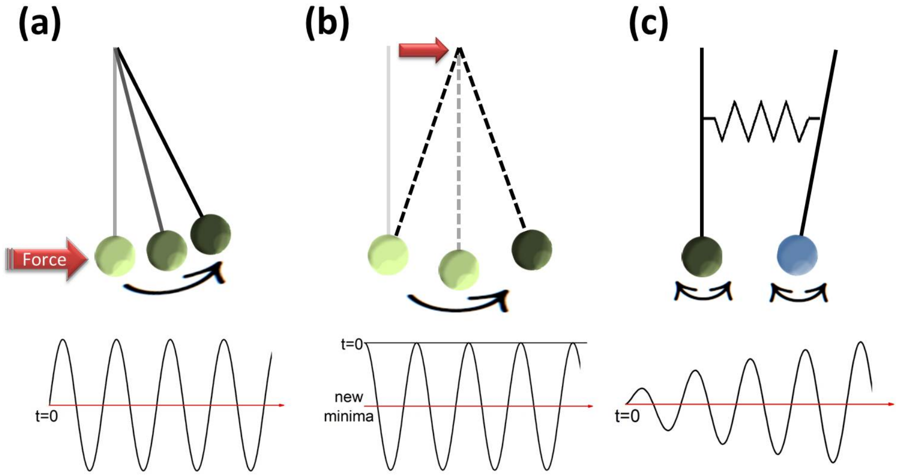

Figure 5.9: Sketches of the three generation mechanism of coherent phonons as discussed for semiconductors. Depicted are (a) the impulsive mechanism, (b) the DECP, and (c) the resonant phonon generation in a simple pendulum picture. The temporal evolution of the oscillation is depicted below.

5.2.1 Coherent phonons

The generation of coherent phonons by pump pulses has been studied for various materials, like semiconductors [43–45, 77], semiconductor quantum wells [54, 55, 78–80], superlattices [81, 82], and high-temperature superconductors [14, 46, 47]. The generation of coherent phonons in BCS superconductor is studied theoretically by Schnyder *et al.* [33], on which our following studies are based on.

For semiconductors several generation mechanism are discussed. For example, in the **impulsive mechanism** an effective coupling from the laser field to the lattice ions is assumed [44]. This coupling leads to a force acting on the ions and they start to oscillate. This mechanism is sketched in a simple pendulum picture in Fig. 5.9(a). In the **d**isplacive **e**xcitation of **c**oherent **p**honons (**DECP**) mechanism [45, 77] the generation of coherent phonons happens by an excited electronic state. It leads to a different position of the potential minimum for the lattice ions than in the groundstate and hence give rise to an oscillation around the new minimum, see sketch in Fig. 5.9(b).

In both mechanism the dynamics of the electronic subsystem is neglected. If the electronic subsystem oscillates close to or exact with the phonons frequency, its dynamics cannot be neglected. In this case, a resonant enhanced generation of coherent phonons can be obtained, see sketch in Fig. 5.9(c). This **resonant phonon generation** has been observed experimentally in semiconductor quantum wells [79]

as well as in superlattices [81,82].
In this section, we study the generation of coherent phonons in BCS superconductors. The temporal evolution of the mean phonon amplitude is described by a driven oscillator

$$i\hbar \frac{\mathrm{d}}{\mathrm{d}t} \left\langle b_{\mathbf{p}} \right\rangle = \hbar\omega_{\mathrm{ph}} \left\langle b_{\mathbf{p}} \right\rangle \tag{5.17}$$

$$+ \underbrace{\sum_{\mathbf{k}} \frac{g_{\mathrm{ph}}}{\sqrt{N}} \left[L^{-}_{\mathbf{k},-\mathbf{p}} \left(\left\langle \alpha^{\dagger}_{\mathbf{k}-\mathbf{p}} \alpha_{\mathbf{k}} \right\rangle + \left\langle \beta^{\dagger}_{\mathbf{k}} \beta_{\mathbf{k}-\mathbf{p}} \right\rangle \right) + M^{+}_{\mathbf{k},-\mathbf{p}} \left(\left\langle \alpha^{\dagger}_{\mathbf{k}-\mathbf{p}} \beta^{\dagger}_{\mathbf{k}} \right\rangle + \left\langle \beta_{\mathbf{k}-\mathbf{p}} \alpha_{\mathbf{k}} \right\rangle \right) \right]}_{=F_{\mathbf{p}}(t)}$$

$$= \hbar\omega_{ph} \left\langle b_{\mathbf{p}} \right\rangle + F_{\mathbf{p}}(t), \tag{5.18}$$

with the driving force $F_{\mathbf{p}}(t)$, which is a function of the Bogoliubov quasiparticles densities. In general, the evolution of the mean phonon amplitude is given by

$$\left\langle b_{\mathbf{p}} \right\rangle (t) = \frac{-i}{\hbar} \int_{-\infty}^{\infty} \mathrm{d}t' F_{\mathbf{p}}(t') e^{i\omega_{ph}(t'-t)}. \tag{5.19}$$

Knowing the evolution of the driving force, we are able to compute $\left\langle b_{\mathbf{p}} \right\rangle (t)$, but $F_{\mathbf{p}}(t)$ is not explicit known. Due to the fact that the driving force is a function of quasiparticle densities, we know that its dynamics depend on the parameters of the pump pulse, e.g. the pump pulse width. As discussed in Sect. 5.1 the temporal evolution of the quasiparticle densities differs depending on the characteristics of the pump pulse. In general, the quasiparticle densities oscillate, except for the adiabatic regime where the temporal evolution of the quasiparticle densities is almost constant. As a consequence the driving force will be an oscillating one for the nonadiabatic regime whereas it is almost constant in the adiabatic regime.
The phononic dynamics also influences the quasiparticle dynamics, for instance see Eq. (4.1). Thus, the dynamics of the quasiparticle densities can be changed by the feedback of the phonon dynamics. How strong the phonons influence the quasiparticle subsystem depend for instance on the electron-phonon coupling strength and how strong coherent phonons are generated. Therefore, the exact dynamics of the driving force cannot be generally known.
To understand better how the driving force influences the coherent phonons, we concentrate on the numerical simulation. Thereto, we have to identify initial conditions which are worthwhile to observe, because new model parameters enter the simulation, namely the phonon frequency ω_{ph} and the electron-phonon coupling strength g_{ph}. To do so, we perform a simulation for various initial conditions and identify the

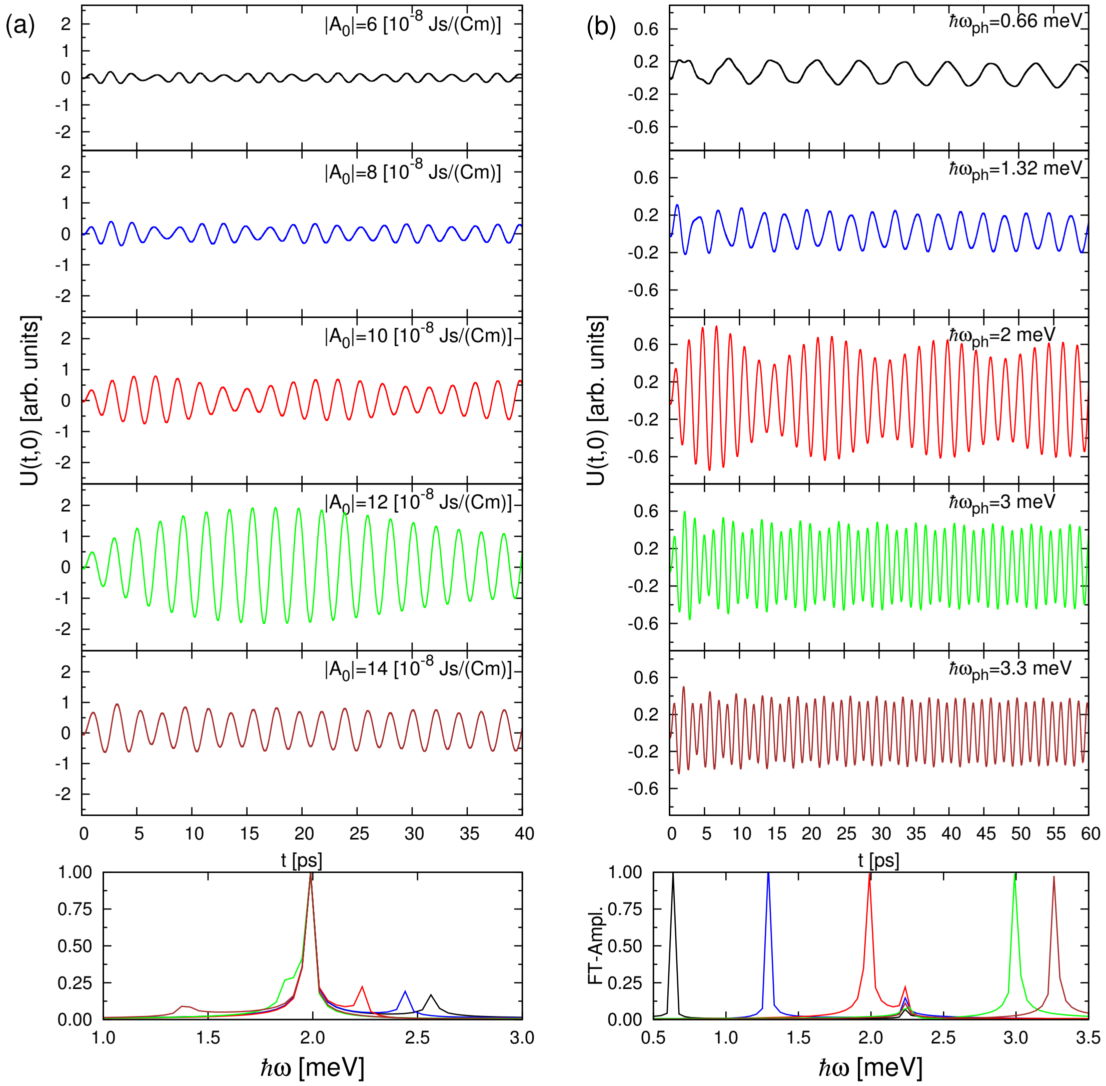

Figure 5.10: Temporal evolution of the lattice displacement $U(t, 0)$ for various initial conditions. In panel (a) the amplitude dependences of $U(t, 0)$ for $\hbar\omega_{\mathrm{ph}} = 2\,\mathrm{meV}$ and $g_{\mathrm{ph}} = 0.1\,\mathrm{meV}$ are depicted and in panel (b) the phonon energy dependence for $|\mathbf{A}_0| = 10 \cdot 10^{-8}\,\mathrm{Js/(Cm)}$. The corresponding Fourier spectra are presented in the lowest plots.

most interesting sets of it, which will be discussed in more detail later.

We use the lattice displacement as observable. It is proportional to the real part of the mean phonon amplitude, see Eq. (3.28), and is well suited for a description of the generation of coherent phonons.

For the overview, we fix the pump pulse width to $\tau_0 = 0.5\,\mathrm{ps}$ corresponding to the nonadiabatic regime. As will be shown later, the dynamics of this regime generates coherent phonons most effectively. Further, the coupling strength g_{ph} is for now set to $g_{\mathrm{ph}} = 0.1\,\mathrm{meV}$.

To study the dependence of the lattice displacement $U(t, 0)$ on the pump pulse amplitude, in other words on the frequency of the order parameter, the phonon frequency is fixed to $\hbar\omega_{\mathrm{ph}} = 2\,\mathrm{meV}$. In Fig. 5.10(a) the temporal evolution of the lattice displacement is depicted for various pump pulse amplitudes. For the phonon frequency dependence, we fix the pump pulse amplitude to $|\mathbf{A}_0| = 10 \cdot 10^{-8}\,\mathrm{Js/(Cm)}$ and computed $U(t, 0)$ for various phonon frequencies. The corresponding lattice displacements are presented in Fig 5.10(b).

In general, the lattice displacement is a superposition of two oscillations. One is oscillating with the phonon frequency, as can be seen by the strong sharp peak in the Fourier spectra at $\omega = \omega_{\mathrm{ph}}$. The other one oscillates with the frequency of the order parameter oscillation ω_{Δ_∞}, see second weaker peak in the Fourier spectra. This shows, that the evolution of the driving force is in general given by the pure quasiparticle subsystem dynamics without any feedback of the phonon subsystem. Hence, it oscillates like the order parameter with only one frequency given by ω_{Δ_∞}. For the amplitude of the lattice displacement we observe, that it increases drastically if both frequencies of $U(t, 0)$ are close to each other, i.e. $\omega_{\mathrm{ph}} \approx \omega_{\Delta_\infty}$. The observed generation of coherent phonons can be interpreted in terms of the resonant phonon generation mechanism. Hence, the temporal evolution of the coherent phonons should show for example a beating phenomena if both frequencies of the lattice displacement are close to each other and an enhanced generation at resonance. Due to this, the resonant, i.e. $\omega_{\mathrm{ph}} = \omega_{\Delta_\infty}$, and near resonant case will be discussed in more detail below. In addition, it shows that the ansatz of using only one phonon mode is justified, because the phonon mode which is near resonant with ω_{Δ_∞} influences the lattice displacement at most and the others are of less importance.

If the phonon energy is much smaller than the asymptotic value of the gap $\hbar\omega_{\mathrm{ph}} \ll 2\Delta_\infty$, e.g. see black curve in Fig. 5.10(a), the dynamical time scale $\tau_{\Delta_\infty} = \frac{\pi\hbar}{\Delta_\infty}$ is much shorter than the phonon period $\tau_{\mathrm{ph}} = \frac{2\pi}{\omega_{\mathrm{ph}}}$. For this case, the generation

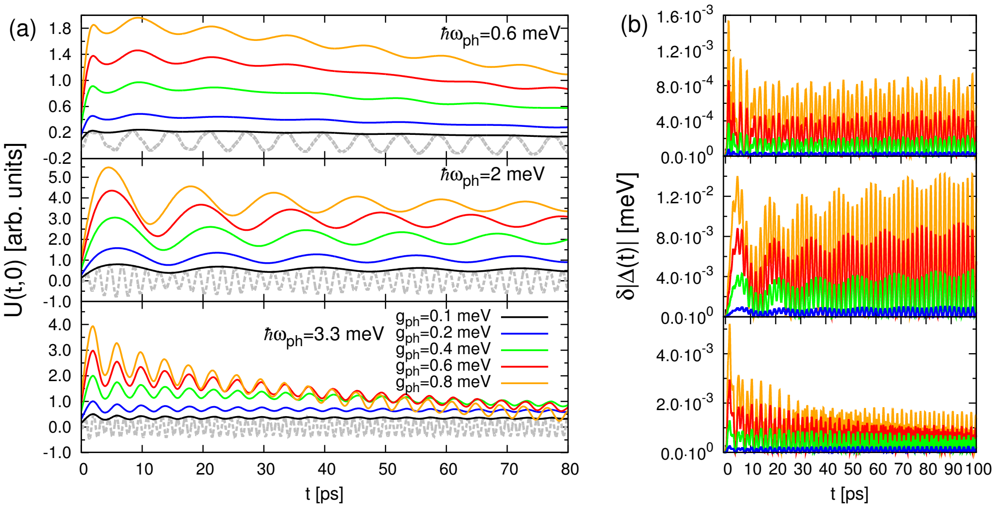

Figure 5.11: (a) Temporal evolution of the envelope of $U(t,0)$. The results for three different phonon frequencies and various coupling strengths are depicted in panel (a). The deviation $|\Delta(t)_{g_{\mathrm{ph}}=0.1} - \Delta(t)_{g_{\mathrm{ph}}=a}|$ with $a \in \{0.2, 0.4, 0.6, 0.8\}$ for the three different phonon frequencies is depicted in panel (b).

of coherent phonons is similar to the DECP mechanism. The lattice displacement oscillates almost with one frequency given by ω_{ph}. Further, it oscillates around a new minimum unequal the initial value $U(0, t_{\mathrm{initial}}) = 0$. The generation of coherent phonons are weaker compared to the case where $\omega_{\mathrm{ph}} \approx \omega_{\Delta_\infty}$. Due to this we mostly concentrate on the resonant generation.

The dependence on the coupling strength is depicted in Fig. 5.11. Here, the lattice displacement is shown for a pump pulse of $|\mathbf{A}_0| = 10 \cdot 10^{-8}\,\mathrm{Js/(Cm)}$, three different phonon energies $\hbar\omega_{\mathrm{ph}} = 0.6\,\mathrm{meV}$, $2\,\mathrm{meV}$, and $3.3\,\mathrm{meV}$, and various coupling strengths.

In panel (a) the envelope of $U(t,0)$ is shown. With increasing coupling strength the amplitude of the lattice displacement increases. Interestingly, for $\hbar\omega_{\mathrm{ph}} = 3.3\,\mathrm{meV}$ the lattice displacement shows some decay with increasing coupling strength. For phonon energies smaller than the initial gap this behavior is not visible. The decay is only observed for $\hbar\omega_{\mathrm{ph}} > 2\Delta$ and will be discussed in more detail below.

In addition, the contributions proportional to g_{ph} of the equation of motion for the quasiparticle densities, e.g. see Eq. (4.1), become more and more important if the coupling strength and the value of mean phonon amplitude increase. Thus, the phonon dynamics strongly influence the quasiparticle dynamics. As a consequence, this leads to a change of temporal evolution of the order parameter. For small coupling strength the contributions proportional to g_{ph} in the equations of motion for the quasiparticle densities are negligible small. In Fig. 5.11(b) the deviation $\delta\Delta(t) = |\Delta_{g_{\mathrm{ph}}=0.1\,\mathrm{meV}}(t) - \Delta_{g_{\mathrm{ph}}}(t)|$ of the order parameter with $g_{\mathrm{ph}} = 0.1\,\mathrm{meV}$ and the larger coupling strengths are depicted. With increasing coupling strength the deviations of $\Delta(t)$ increase. This is most visible for the resonant case, because in this case the generation of coherent phonons is large. If $\hbar\omega_{\mathrm{ph}} > 2\Delta_0$ the deviation of the order parameter decreases for increasing time. This is caused by the decaying amplitude of the lattice displacement and as a result the contributions proportional to g_{ph} become weaker.

We state that if the coupling strength g_{ph} is small the quasiparticle dynamics are almost independent of the phononic dynamics. But with increasing coupling strength the phononic subsystem influence more and more the quasiparticle subsystem.

Due to the above investigation, the following frequency regimes are chosen to study the generation of coherent phonons in more detail

$$\omega_{\mathrm{ph}} \approx \omega_{\Delta_\infty} < \omega_0 \tag{5.20}$$

$$\omega_{\Delta_\infty} < \omega_{\mathrm{ph}}. \tag{5.21}$$

In words, we observe the case when the phonon and order parameter oscillation frequency are near or at resonance and the case where the phonon energy is larger than the initial gap.

5.2.2 Coherent phonons: $\omega_{\mathrm{ph}} \approx \omega_{\Delta_\infty} < \omega_0$

The temporal evolution of the lattice displacement for the case where the order parameter oscillation frequency is near the phonon frequency is depicted in Fig. 5.12. Here, the results for the three dynamical regimes, namely the nonadiabatic, the intermediate, and the adiabatic regime, are presented. For the phonons we set the energy to $\hbar\omega_{\mathrm{ph}} = 2\,\mathrm{meV}$ and the coupling strength to $g_{\mathrm{ph}} = 0.1\,\mathrm{meV}$.

For the **nonadiabatic regime** a pump pulse with $\tau_0 = 0.5\,\mathrm{ps}$ and various pump pulse amplitudes are used. The amplitudes are chosen in such a way that the induced order parameter oscillation has a frequency near the phonon frequency. As mentioned before, the lattice displacement oscillates with two frequencies, namely ω_{ph} and ω_{Δ_∞}. Both frequencies can be observed as two sharp peaks in the corresponding Fourier spectra. Due to the fact that these frequencies are very similar a pronounced beating phenomenon can be detected.

For the **intermediate regime**, a pump pulse with $\tau_0 = 1.5\,\mathrm{ps}$ is used. The lattice dynamics show the same behavior as in the nonadiabatic case as displayed in

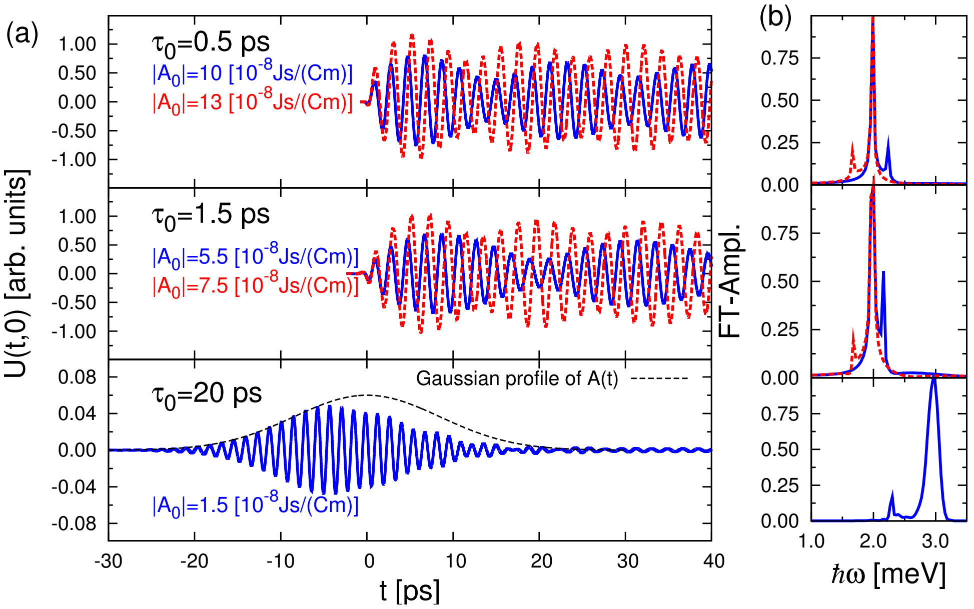

Figure 5.12: Panel (a) shows the temporal evolution of the lattice displacement $U(t,0)$ near resonance $\omega_{\rm ph} \approx \omega_{\Delta_\infty}$ for coupling strength $g_{\rm ph} = 0.1\,\rm meV$ and $\hbar\omega_{\rm ph} = 2\,\rm meV$. The results for the three dynamical regime are depicted. In panel (b) the corresponding Fourier spectra are shown. For $\tau_0 = 20, \rm ps$ (adiabatic regime) additionally the Gaussian shape of the pump pulse is included.

Fig. 5.12. However, the generation of coherent phonons is weaker compared to the nonadiabatic case, as the smaller amplitude of $U(0,t)$ shows. This is in good agreement with the observed evolution of the order parameter in this regime. Compared to the nonadiabatic order parameter oscillation the oscillation in the intermediate regime has a smaller amplitude. This yields a weaker driving force and leads to a weaker generation of the coherent phonons.

In the **adiabatic regime**, the order parameter is almost constant. The coherent phonons are still driven by an oscillating forcing term, but with a much smaller amplitude, see Fig. 5.12. In this figure, the lattice displacement for a pump pulse with $\tau_0 = 20\,\rm ps$ is depicted. Furthermore, we observed that during the pump pulse the lattice displacement shows a large transient oscillation. The frequency of this oscillation is given by the pump pulse frequency ω_0, see strong peak at $\hbar\omega = 3\,\rm meV$ in the Fourier spectra. After this transient oscillation the weak generation of coherent phonons is observed, but compared to the both other regimes this generation is negligibly small.

If the phonon energy lies in the interval $0 < \hbar\omega_{\rm ph} < 2\Delta_0$ we are able to bring the system into perfect resonance by adjusting the pump pulse intensity. In Fig. 5.13

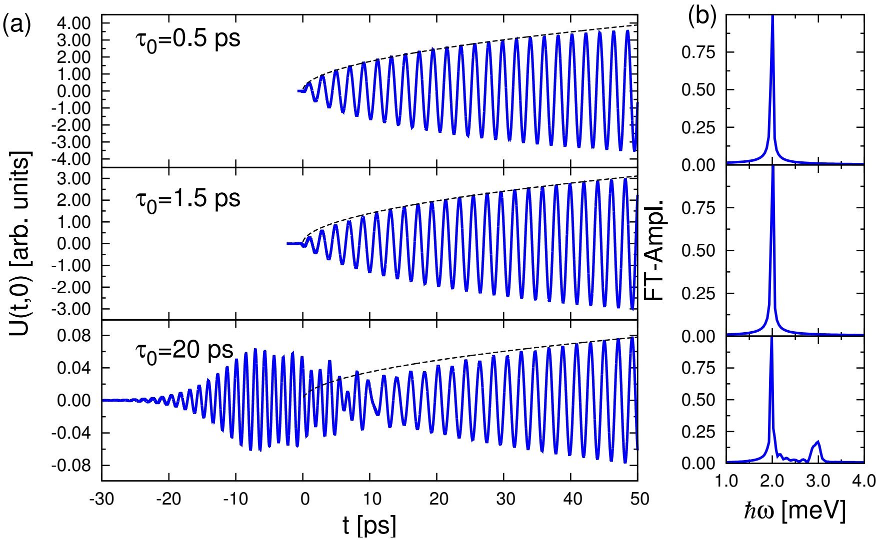

Figure 5.13: In panel (a), the temporal evolution of the lattice displacement $U(t,0)$ at resonance $\omega_{\mathrm{ph}} = \omega_{\Delta_\infty}$ is shown for coupling strength $g_{\mathbf{p}} = 0.1\,\mathrm{meV}$ and $\hbar\omega_{\mathrm{ph}} = 2\,\mathrm{meV}$. The results for the three dynamical regime are depicted. The dotted black lines present the function $f(t) = a\sqrt{t}$ and agrees well with the envelope of $U(t,0)$. In panel (b), the Fourier spectra of the lattice displacement are shown.

the results for the resonant case for all dynamical regimes are presented. In this case, the lattice displacement oscillates with only one frequency as displayed by the sharp peak at $\omega = \omega_{\mathrm{ph}}$ in the corresponding Fourier spectrum. Certainly, an additional transient oscillation still appears in the adiabatic regime. Furthermore, the amplitude of the lattice displacement grows with $\sqrt{t}$ in contrast to the $\frac{1}{\sqrt{t}}$-decay. We conclude that the system is not yet in the stationary state up to the times studied. Even in the adiabatic regimes the $\sqrt{t}$ increase can be observed, albeit with a much smaller amplitude.

The $\sqrt{t}$ increase can also be seen in the general solution of the lattice displacement. To see this, the real part of the general solution of Eq. (5.19) is needed. It reads

$$U_{\mathbf{p}}(0,t) \propto \int \mathrm{d}t' F_{\mathbf{p}}(t') \sin\left(\omega_{\mathrm{ph}}(t'-t)\right). \tag{5.22}$$

Here, $U_{\mathbf{p}}(0,t)$ is the contribution of phonon momentum $\mathbf{p}$ to the total displacement given by $U(0,t) = \sum_{\mathbf{p}} U_{\mathbf{p}}(0,t)$. If we now assume small coupling strengths, the driving force is determined by the dynamics of the quasiparticle subsystem characterized by the evolution of the order parameter. Hence, we approximate the driving force as

$$F_{\mathbf{p}}(t) = \Theta(t)\left(A_{\mathbf{p}} + B_{\mathbf{p}}\frac{\cos\left(\omega_{\Delta_\infty t}\right)}{\sqrt{(t)}}\right), \tag{5.23}$$

where $\Theta(t)$ denotes the Heavyside stepfunction. With this driving force we solve Eq. (5.22) for the resonant case $\omega_{\mathrm{ph}} = \omega_{\Delta_\infty}$. The result reads

$$\begin{aligned} U_{\mathbf{p}}(0,t) \propto &-\frac{A_{\mathbf{p}}}{\omega_{\mathrm{ph}}}\left(1-\cos(\omega_{\mathrm{ph}}t)\right) - B_{\mathbf{p}}\sqrt{t}\sin(\omega_{\mathrm{ph}}t) \\ &+ \frac{B_{\mathbf{p}}\sqrt{\pi}}{\sqrt{\omega_{\mathrm{ph}}}}\left(\cos(\omega_{\mathrm{ph}}t)S\left(\frac{2\sqrt{\omega_{\mathrm{ph}}t}}{\sqrt{\pi}}\right) - \sin(\omega_{\mathrm{ph}}t)C\left(\frac{2\sqrt{\omega_{\mathrm{ph}}t}}{\sqrt{\pi}}\right)\right), \end{aligned} \tag{5.24}$$

where S and C denote the two Fresnel integrals given by

$$S(x) = \int_0^x \sin\left(\frac{1}{2}\pi t^2\right)\mathrm{d}t \tag{5.25}$$

$$C(x) = \int_0^x \cos\left(\frac{1}{2}\pi t^2\right)\mathrm{d}t. \tag{5.26}$$

As t increases the second term dominates and the lattice displacement shows a $\sqrt{t}$ increase agreeing perfectly with the numerics.

5.2.3 Coherent phonons: $2\Delta_0 < \hbar\omega_{\mathbf{ph}}$

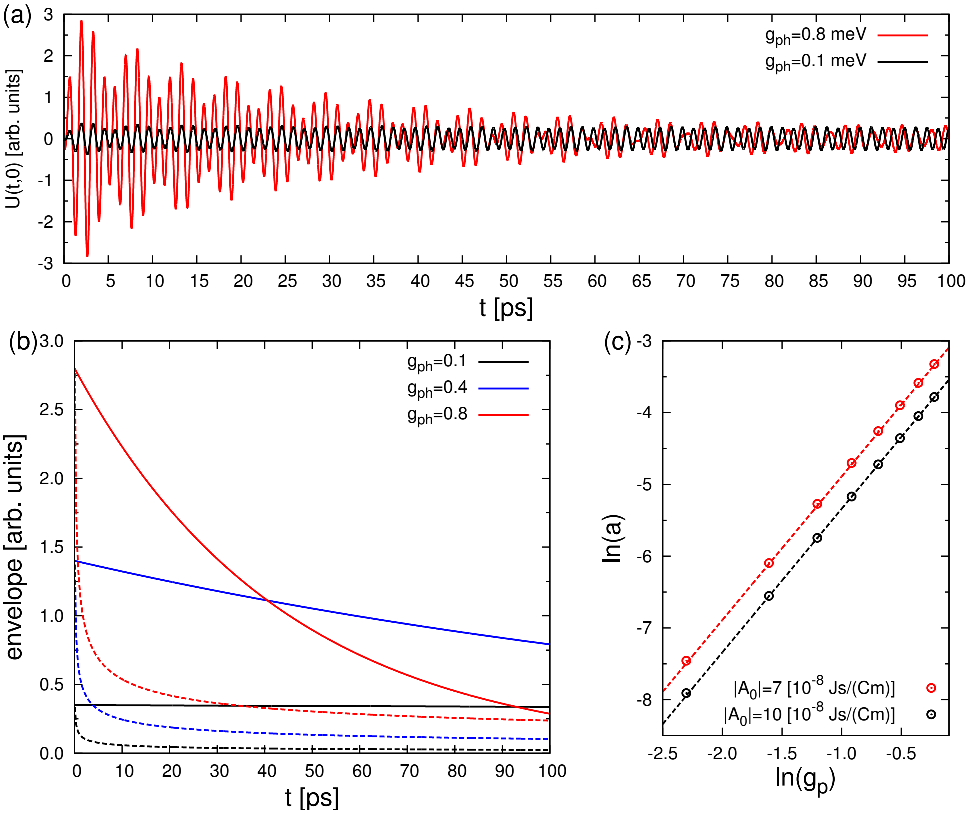

Figure 5.14: (a) Temporal evolution of the lattice displacement $U(t,0)$ for the case $\omega_{\Delta_\infty} < \omega_{\text{ph}} = 3.3\,\text{meV}/\hbar$ and a pump pulse with $\tau_0 = 0.5\,\text{ps}$ and amplitude $|\mathbf{A}_0| = 7{\cdot}10^{-8}\,\text{Js}/(\text{Cm})$. The results for two different coupling stengths are depicted, namely $g_{\text{ph}} = 0.1\,\text{meV}$ and $g_{\text{ph}} = 0.8\,\text{meV}$. (b) The envelope of the oscillation with ω_{ph}, solid lines, and of the oscillation with ω_{Δ_∞}, dashed lines, extracted from a fit of Eq. (5.27) are presented for various coupling strengths. (c) The dependence of the rate a, see Eq. (5.27), on the coupling strength is shown. The data is perfectly describe by $a \propto g_{\text{ph}}^2$ as shown by the dashed lines.

Figure 5.11 shows that the lattice displacement can decay if the phonon energy is larger than the initial gap. This is due to the fact that a phonon can decay into a particle-hole pair in the Bogoliubov quasiparticle basis if $\hbar\omega_{\text{ph}} > 2\Delta_0$. To study this decay in more detail we concentrate on the nonadiabatic regime only, because there is almost no generation of coherent phonons in the two other regimes.

In Fig. 5.14(a), the temporal evolution of two lattice displacements is presented for a pump pulse with $\tau_0 = 0.5\,\text{ps}$ and $|\mathbf{A}_0| = 7 \cdot 10‘{-}8\,\text{Js}/(\text{Cm})$ and different coupling strengths. The phonon energy is set to $\hbar\omega_{\text{ph}} = 3.3\,\text{meV}$. For the larger coupling strength of $g_{\text{ph}} = 0.8\,\text{meV}$ a strong decay of the oscillations of the lattice displacement is visible, but the lattice displacement does not vanish completely. This is caused by the driving force, which is given by the dynamics of the quasiparticle subsystem. The driving force decays only algebraically with $\frac{1}{\sqrt{t}}$ as the order parameter. Only the strong decay at the beginning is presumably caused by an exponential decay of the oscillation with phonon frequency. To test this statement we fit the numerical date with the function

$$U(0,t) = C_1 \exp(-at) \cos(\omega_{\text{ph}} t + \Phi_1) + C_2 t^{-b} \cos(\omega_{\Delta_\infty} t + \Phi_2). \tag{5.27}$$

Here, $C_1, C_2, \Phi_1, \Phi_2, a, b, \omega_{\text{ph}}$, and ω_{Δ_∞} are the fit parameters. In Tab. 5.1 the resulting fit parameters are listed. All in all, the fits match quite well (not explicit shown). For larger values of g_{ph} the fit matches even better. The fitted parameters for the frequencies are in good agreement with the exact values. For the algebraic decay, we expect a fit parameter of $b = 0.5$, the same behavior as for the decay of the order parameter. The fitted parameter b agrees well with this expectation. The deviation can be explained by the fact that the square root decay is very slow and due to the finite computed time interval we are not able to capture the correct behavior within the fits. Furthermore, the rate a increases with increasing coupling strength, namely with $a(g_{\text{ph}}) \propto g_{\text{ph}}^2$. This can be seen in Fig. 5.14(c). Here, the rate a versus g_{ph} in a ln-ln plot is presented. It clearly shows a linear behavior with a slope of 2, as displayed by the dashed lines.

The $g_{\mathbf{p}}^2$-dependence of a is in excellent agreement with Fermi's golden rule [83, 84]. In Fermi's golden rule the transition rate from a state into another state is given by the squared matrix element of the perturbation between both states. In our case the perturbation is given by the Fröhlich Hamiltonian. As a result, the transition rate based on the golden rule is proportional to $\propto g_{\text{ph}}^2$.

The fact that the decay in the lattice displacement can be observed in this low order of truncation is caused by the correlation expansion. As can be seen in Eqs. (4.1) and. (4.8), the phonon dynamics influence the quasiparticle dynamics and vice versa. With this, higher order of g_{ph} are involved in correlation expansion, even though quasiparticle-phonon scattering contributions are neglected in the expansion.

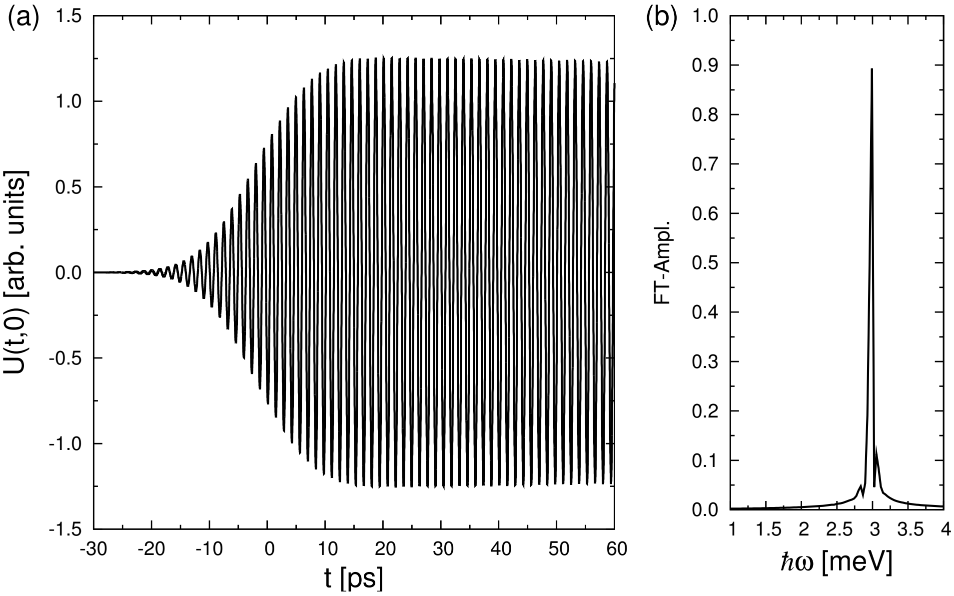

Figure 5.15: (a) Temporal evolution of the lattice displacement $U(t, 0)$ for the adiabatic regime [$\tau_0 = 20\,\mathrm{ps}$, $|\mathbf{A}_0| = 1 \cdot 10^{-8}\,\mathrm{Js/(Cm)}$] in presence of optical phonons in resonance with the pump pulse energy, i.e., $\hbar\omega_0 = \hbar\omega_{\mathrm{ph}}$, and $g_{\mathrm{ph}} = 0.1\,\mathrm{meV}$. (b) Corresponding Fourier spectrum.

Knowing the fit function, we are able to extract the envelopes of the different oscillations of the lattice displacement, see Fig. 5.14(b). This figure shows that for $g_{\mathrm{ph}} \lesssim 0.6$ meV the exponentially decaying envelope prevails the algebraic one. For $g_{\mathrm{ph}} = 0.1$ meV the parameter a is very small, so it might be that Eq. 5.27 does not capture the correct behavior. For $g_{\mathrm{ph}} > 0.6$ meV the algebraically decaying envelope crosses the exponential one. So for large times the lattice displacement oscillates only with the oscillation induced by the driving force. For phonon energy $\hbar\omega_{\mathrm{ph}} \gg 2\Delta_0$ the lattice displacement shows only an oscillation decaying with $\frac{1}{\sqrt{t}}$ with ω_{Δ_∞} induced by the driving force, even for small times.

If the phonon energy is larger than the initial gap, we can set it to resonance with the photon energy, $\hbar\omega_0 = \hbar\omega_{\mathrm{ph}}$. Note, there is no explicit light-phonon coupling taken into account, so that the upcoming investigation has to be treated with care. However, on the experimental side this case is of great interest, because if one knows the phonon energy one is able to tune the photon energy to exact resonance.

As can be seen in Fig. 5.10(b), the nonadiabatic case behaves similar to the case with $\hbar\omega_{\mathrm{ph}} = 3.3\,\mathrm{meV}$ and no special features can be observed. But for the adiabatic regime in resonance the lattice displacement behaves peculiar. In Fig. 5.15 the temporal evolution of the lattice displacement is depicted for a pump pulse with $\tau_0 = 20\,\mathrm{ps}$, $|\mathbf{A}_0| = 1 \cdot 10^{-8}\,\mathrm{Js/(Cm)}$, and a coupling strength of $g_{\mathrm{ph}} = 0.1\,\mathrm{meV}$. The resonant pumping of the phonons leads to undamped coherent phonon oscillations, which persist even after the pump pulse has passed. As can be seen in the Fourier spectra, the lattice displacement oscillates with $\omega_\mathbf{p}$ only.

	$\hbar\omega_{\Delta_\infty}$ [meV]	$\hbar\omega_{\mathrm{ph}}$ [meV]	a	b
reference value	2.542	3.3	-	0.5
$g_{\mathrm{ph}} = 0.1$ meV	2.542731	3.291196	0.000577	0.376857
$g_{\mathrm{ph}} = 0.2$ meV	2.571932	3.291684	0.002251	0.557545
$g_{\mathrm{ph}} = 0.3$ meV	2.542403	3.292517	0.005139	0.370095
$g_{\mathrm{ph}} = 0.4$ meV	2.571345	3.293702	0.009076	0.555516
$g_{\mathrm{ph}} = 0.5$ meV	2.570644	3.295276	0.014161	0.556068
$g_{\mathrm{ph}} = 0.6$ meV	2.570483	3.297269	0.020296	0.559500
$g_{\mathrm{ph}} = 0.7$ meV	2.539838	3.299638	0.027741	0.331318
$g_{\mathrm{ph}} = 0.8$ meV	2.538818	3.302429	0.036021	0.314463
reference value	2.249	3.3	-	0.5
$g_{\mathrm{ph}} = 0.1$ meV	2.249760	3.291095	0.000368	0.380221
$g_{\mathrm{ph}} = 0.2$ meV	2.249798	3.291401	0.001425	0.378953
$g_{\mathrm{ph}} = 0.3$ meV	2.249789	3.291923	0.003199	0.377157
$g_{\mathrm{ph}} = 0.4$ meV	2.249671	3.292679	0.005696	0.374362
$g_{\mathrm{ph}} = 0.5$ meV	2.249399	3.293692	0.008914	0.371589
$g_{\mathrm{ph}} = 0.6$ meV	2.248989	3.294986	0.012839	0.366845
$g_{\mathrm{ph}} = 0.7$ meV	2.248409	3.296585	0.017461	0.361529
$g_{\mathrm{ph}} = 0.8$ meV	2.247688	3.298506	0.022770	0.355451

Table 5.1: Fit parameters for two pump pulses, characterized by $\tau = 0.5\,\mathrm{ps}$ and $|\mathbf{A}_0| = 7 \cdot 10^{-8}\,\mathrm{Js/(Cm)}$ or $|\mathbf{A}_0| = 10 \cdot 10^{-8}\,\mathrm{Js/(Cm)}$, and various electron-phonon-coupling strengths g_{ph}.

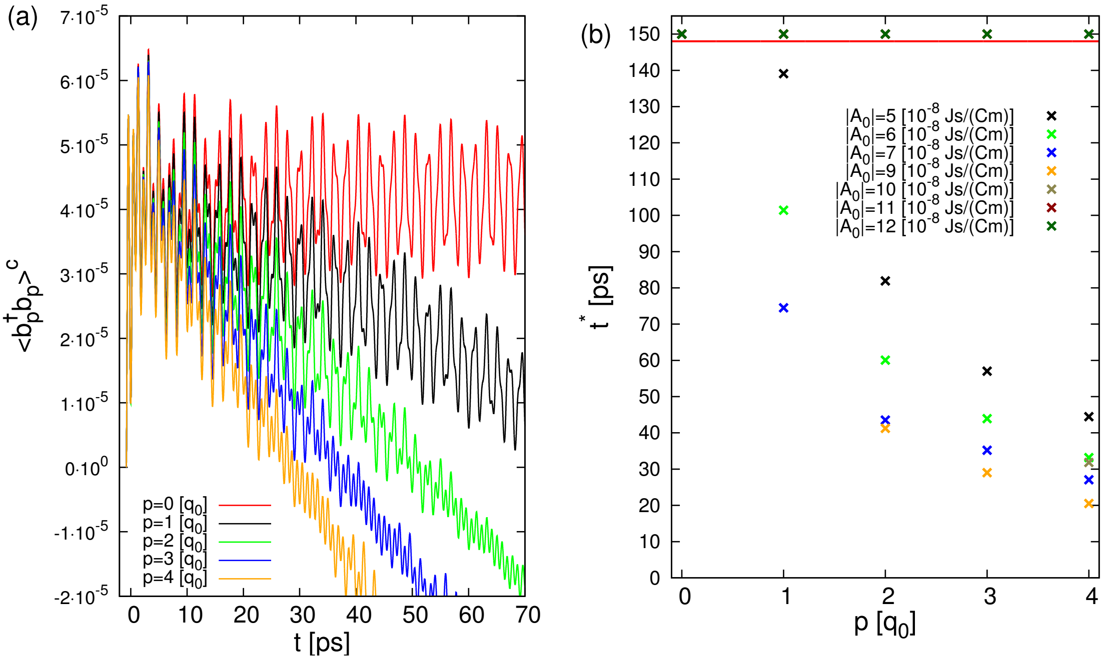

Figure 5.16: The temporal evolution of the incoherent phonon densities $\left\langle b^\dagger_{\mathbf{p}} b_{\mathbf{p}} \right\rangle^c$ is depicted for a pump pulse with $\tau_0 = 0.5\,\mathrm{ps}$ and $|\mathbf{A}_0| = 7 \cdot 10^{-8}\,\mathrm{Js/(Cm)}$ and an electron-phonon coupling of $g_{\mathrm{ph}} = 0.1\,\mathrm{meV}$. The phonon energy is set to $\hbar\omega_{\mathrm{ph}} = 2\,\mathrm{meV}$. In panel (b) the point in time t^* when $\left\langle b^\dagger_{\mathbf{p}} b_{\mathbf{p}} \right\rangle$ becomes negative is shown for various pump pulse amplitudes. The red solid line presents the maximal time up to which is simulated.

5.2.4 Incoherent phonons

Up to now processes, such as electron-phonon or electron-electron scattering, are neglected. In this section, we want to take these processes into account. This maybe will give rise to a finite lifetime of the coherent phonons [33].

To include these processes in the simulations, we go a step further in the correlation expansion, i.e. computing additionally the evolution of the phonon assisted quantities and the incoherent phonon densities. The corresponding equations of motion are given in Sect. 4.1 and App. A.2. Due to the fact that coherent phonons are generated at most in the nonadiabatic regime, we only focus our studies on this regime, i.e., setting $\tau_0 = 0.5\,\mathrm{ps}$. Further, we set the phonon energy to $\hbar\omega_{\mathrm{ph}} = 2\,\mathrm{meV}$ and the coupling strength to $g_{\mathrm{ph}} = 0.1\,\mathrm{meV}$.

As new quantity of interest the incoherent phonon density can be computed. The corresponding equation of motion, see Eq. (4.6), shows that the temporal evolution of the incoherent densities are determined by the temporal evolution of the correction of the phonon assisted quantities.

In Fig. 5.16(a) the incoherent phonon densities are depicted for a pump pulse with $|\mathbf{A}_0| = 7 \cdot 10^{-8}\,\mathrm{Js/(Cm)}$. The simulation shows unphysical results, namely a negative incoherent phonon densities. Incoherent phonon densities for larger momentum become faster unphysical whereas the density for $\mathbf{p} = 0$ remains positive in the simulated time interval. If and how fast the density becomes negative depends on the pump pulse characteristics. In Fig.5.16(b) the point in time t^* when $\left\langle b^\dagger_{\mathbf{p}} b_{\mathbf{p}} \right\rangle$ becomes negative is depicted for various pump pulse amplitudes. Interestingly, if the pump pulse intensity induces a frequency $\omega_{\Delta_\infty} \leq \omega_{\mathrm{ph}}$ the incoherent phonon densities remains positive for all phonon momenta in the simulated time interval.

Due to the unphysical results the simulation of the correlation expansion in second order is not trustable. Hence, we try to discuss why the correlation expansion failed and how we can maybe prevent the unphysical densities. Note, the first order correlation expansion, i.e., computing the generation of coherent phonons, do not show any unphysical results.

First of all, the effect is not caused by possible errors in the implementation of the equations of motion rather it is a uncertainty of the truncation, because the same effect also appears in the simulation of semiconductors [80].

One source of trouble is the chosen initial condition. As initial condition the BCS groundstate without phonons and $\left\langle b^\dagger_{\mathbf{p}} b_{\mathbf{q}} \right\rangle = 0$ is chosen, but this state is not the true groundstate of the coupled system. The argument that this is a good approximation for small coupling strength, which works in the first order, may not be valid anymore. To prevent this error, one may has to use a correct groundstate. It can be computed by an additional diagonalization of the considered Hamiltonian. The Hamiltonian can be diagonalized for example by a Fröhlich transformation [69] or by a **c**ontinuous unitary transformation (CUT) [85–88]. A short discussion of the transformation of an electron-phonon interaction using CUT is given in Ref. [89].

Another source of trouble is that the correlation expansion mixes some expectation values that have renormalized energies with other expectation values without renormalized energies [80]. In the DMF, the energy renormalization is expressed by the feedback of a density matrix on itself, i.e. the density matrix enters in its own equation of motion [52]. For example, in the model the electron-phonon coupling leads to this renormalization.

In order to prevent the mixing Papenkort suggested to change the truncation scheme to the order separation sheme [80]. For the order separation the equation of motion are set up as in the DMF with correlation expansion, but without setting any correlation to zero. In addition, every density matrix gets additionally indices, which denote the order in g_{ph} or in $|\mathbf{A}_0|$. The derivative of such a density depends on contributions of the same order in the coupling strength and vector potential.

We study superconductors instead of semiconductors and due to the mean field description a separation in order of the vector potential is more complicated. Because of that we apply an order separation truncation in g_{ph} only. The corresponding equation of motion is given in Appendix A.3. However, as in the correlation expansion negative densities occurs in this calculation, too. (Not explicitly shown.)

Another possibility to describe the influence of electron-phonon or electron-electron scattering is to change the method. For example, one can use the iterative equation of motion approach as introduced in Sect. 2.2. In this approach we cannot get negative densities per construction. In the iEoM the temporal evolution of an operator is computed. To compute a quasiparticle density one has to multiply an operator with the Hermitian conjugation of it, resulting in a real expectation value. In addition, the toy model calculation in Sect. 2.3 showed that the iEoM leads to more reliable results than the DMF approach if relaxation processes are taken into account.

However, the explicit time dependent Hamiltonian and the second order in g_{ph} make the computation task numerically more costly than the DMF approach. In addition, it is not clear if other complications appear in these computations.

On these grounds the method was not applied in this thesis but it is an interesting task for future projects.

The observed problems in the correlation expansion might be taken as an indication that the simulation in the first order are no longer trustable. However, the results of Sects. 5.2.1- 5.2.3 show no unphysical behavior. Furhter, the toy model calculation shows no hint that the first order is not trustable, see Sect. 2.3. In addition, the generation of coherent phonons in semiconductor computed with the DMF in correlation expansion is in good agreement with experimental results [54,55,80]. All in all, one can trust the results of the first order in the correlation expansion but one has to be careful in the second order.

5.3 Superconductor in presence of acoustic phonons

In this section, we consider acoustic instead of optical phonons. As the investigation of optical phonons shows, the correlation expansion yield only reliable results in the first order. Hence, we will only compute the generation of coherent acoustic phonons. In addition, we only concentrate on the nonadiabatic regime, where the generation of coherent phonons is strongest.

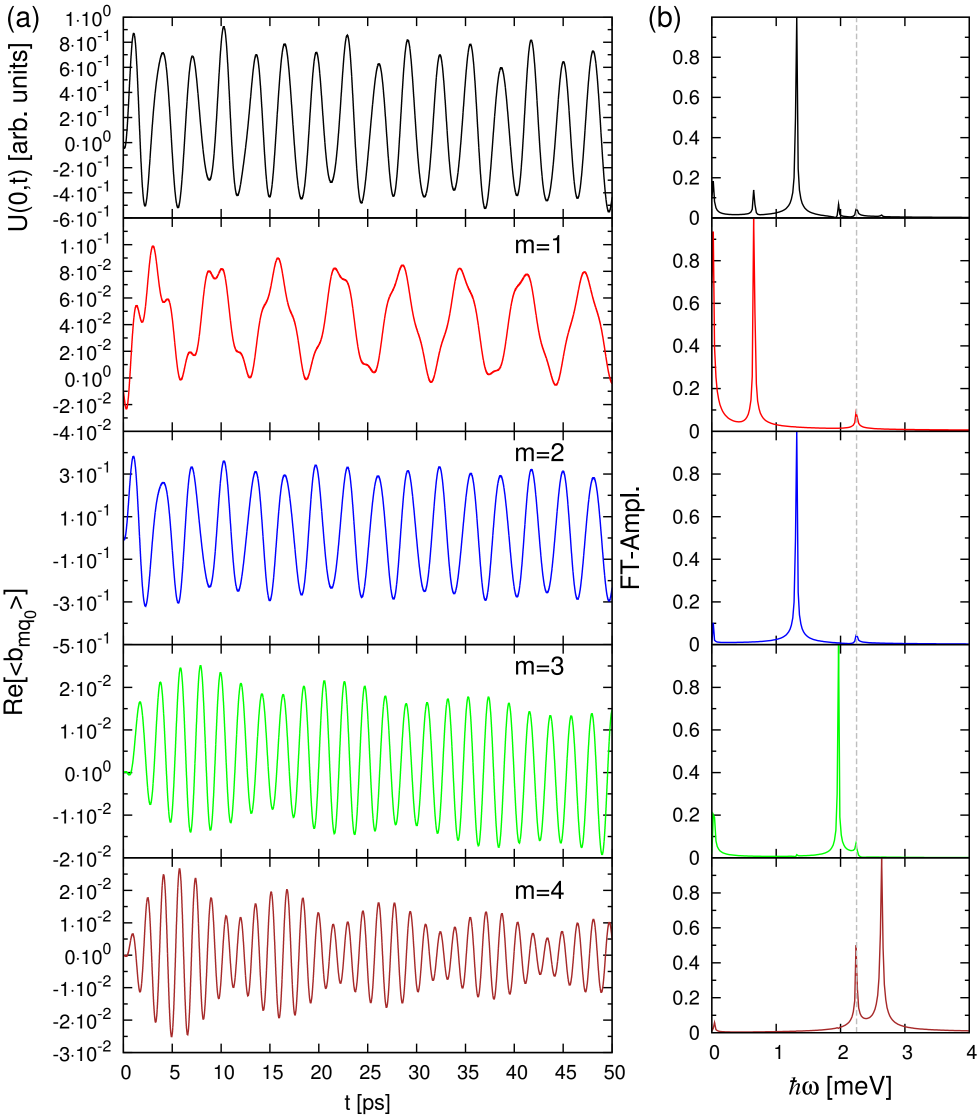

Figure 5.17: Panel (a) shows the temporal evolution of the lattice displacement and the mean phonon amplitudes in the nonadiabatic regime with $\hbar\omega_{\text{max}} = 2.63\,\text{meV}$ and $g_{\text{max}} = 0.5\,\text{meV}$. Panel (b) displays the corresponding Fourier spectra. The gray line denotes ω_{Δ_∞}.

In contrast to the optical phonons in Holstein form, the acoustic phonons possess a momentum dependent frequency and coupling strength. The actual value of this parameter are set as follows.
As discussed in Sect. 4.3, the phonon momentum is given by $\mathbf{p} = m\mathbf{q}_0$ with $|m| \leq 4 = m_{\max}$ thus 9 phonon momenta are taken into account. The frequency of each momentum is set via

$$\omega_{\mathbf{p}} = \frac{\omega_{\max}}{4}|m| \tag{5.28}$$

and the coupling strength is set by

$$g_{\mathbf{p}} = g_{\max}\sqrt{\frac{|m|}{4}}. \tag{5.29}$$

Here, $\omega_{\max}$ and $g_{\max}$ are the maximal value of the frequency and the coupling strength, respectively.
Interestingly, large momenta have the strongest coupling strength but couple to quasiparticle densities which are excited weakest by the pump pulse, see Eq. (4.8).
In the following, we perform a simulation with $\hbar\omega_{\max} = 2.63\,\mathrm{meV}$, $g_{\max} = 0.5\,\mathrm{meV}$, $\tau_0 = 0.5\,\mathrm{ps}$, and $|\mathbf{A}_0| = 10 \cdot 10^{-8}\,\mathrm{Js/(Cm)}$. The temporal evolution of the real part of mean phonon amplitudes $\mathrm{Re}\left[\left\langle b_{\mathbf{p}}\right\rangle\right]$ are depicted in Fig. 5.17. As for optical phonons, each phonon amplitude is described by the forced harmonic oscillator given by Eq. (4.8). Hence, the evolution of $\left\langle b_{\mathbf{p}}\right\rangle(t)$ is given by a superposition of two oscillations. One is oscillating with the frequency of the quasiparticle subsystem ω_{Δ_∞}, see weak peak in the corresponding Fourier spectra. The other one oscillates with the phonon frequency $\omega_{\mathbf{p}}$ as can bee seen by the strong peak in the Fourier spectra. In contrast to the optical phonons, every mean phonon amplitude possess a different phonon frequency depending on the corresponding phonon momentum. Hence, every oscillation of $\mathrm{Re}\left[\left\langle b_{\mathbf{p}}\right\rangle\right]$ behaves differently. For $m = 1$, i.e. small phonon energies, we observe a generation which can be interpreted in terms of the DECP mechanism. For $m = 3$ both frequencies are close to each other, which leads to the resonant generation mechanism. If the phonon energy is larger than the actual gap, see case $m = 4$, we observe again a decay in $\left\langle b_{\mathbf{p}}\right\rangle(t)$.
The corresponding lattice displacements are also depicted in Fig. 5.17. The lattice displacement is a superposition of the oscillation of the mean phonon amplitude. The simulation leads to a finite lattice displacement. Due to the fact that $\left\langle b_{\mathbf{p}}\right\rangle$ oscillates differently for every $\mathbf{p}$, one would expect that the lattice displacement would

vanish due to destructive interference. This is not seen in the simulation, because only a few mean phonon amplitudes become finite. This is caused by the definite wave vector of the vector potential, which is assumed in the simulation. Only specific quasiparticle expectation values become finite, e.g. $\left\langle \alpha^\dagger_{\mathbf{k}} \alpha_{\mathbf{k}+n\mathbf{q}_0} \right\rangle$.
If we consider more realistic pulse shapes with a broader distribution of wave vectors more mean phonon amplitudes can be generated. As a result, the lattice displacement should vanish. But a broader distribution of wave vectors will make the numerical simulation more complicated. One has to construct a new discretization mesh which regards the uncertainties in the momentum. If one constructs such a mesh, the numerical effort will consequently increase due to more discretization points which has to take into account.

6 Nonequilibrium Response

In Sect. 5 we presented the nonequilibrium dynamics of a superconductor. The temporal evolution of the order parameter was one of the main quantities of interest. So it will be of great advantage if we can predict which signatures of a common observable provides information about the dynamics of the system. For that reason, we compute the conductivity $\sigma(\delta t, \omega)$ as it can be measured by the probe pulse. We will show that the conductivity provides signatures as function of delay time, which displays the oscillatory behavior of the order parameter as well as the evolution of the lattice displacement.

Before we discussed the signatures in the conductivity, we explain how the probe pulse is included in the DMF formalism and how the conductivity is actual computed. Next, the results for the s-wave superconductor with and without coupling to coherent phonons will be presented. Parts of the following investigations are published in Ref. [36].

6.1 Conductivity

In order to simulate the pump-probe conductivity, the temporal evolution of the electric current density $\mathbf{j}_{\mathbf{q}_{\mathrm{pr}}}(\delta t, t)$ needs to be known. It is given by [30, 90]

$$\begin{aligned}\mathbf{j}_{\mathbf{q}_{\mathrm{pr}}}(\delta t, t) = {} & \frac{-e\hbar}{2mV} \sum_{\mathbf{k},\sigma} (2\mathbf{k} + \mathbf{q}_{\mathrm{pr}}) \left\langle c^{\dagger}_{\mathbf{k},\sigma} c_{\mathbf{k}+\mathbf{q}_{\mathrm{pr}},\sigma} \right\rangle (\delta t, t) \\ & - \frac{e^2}{mV} \sum_{\mathbf{k},\mathbf{q},\sigma} \mathbf{A}_{\mathbf{q}_{\mathrm{pr}}-\mathbf{q}} \left\langle c^{\dagger}_{\mathbf{k},\sigma} c_{\mathbf{k}+\mathbf{q},\sigma} \right\rangle (\delta t, t),\end{aligned} \tag{6.1}$$

where $\mathbf{q}_{\mathrm{pr}}$ is the wave vector of the probe pulse. For the numerical calculations we neglect the second term in Eq. (6.1) since it only results in a constant offset of the imaginary part of the conductivity spectra [30].

Formally, the current depends on two times, namely the delay time δt between pump and probe pulse and the actual time t at which it is measured or computed, respectively. Then, the pump-probe conductivity $\sigma(\delta t, \omega)$ is obtained from Eq. (6.1) via

$$\sigma(\delta t, \omega) = \frac{j(\delta t, \omega)}{i\omega A(\delta t, \omega)}, \tag{6.2a}$$

where

$$j(\delta t, \omega) = \int_{-\infty}^{\infty} dt\, \hat{\mathbf{e}}_y \cdot \mathbf{j}_{\mathbf{q}_{\mathrm{pr}}}(\delta t, t)\, e^{i\omega t} \tag{6.2b}$$

and

$$A(\delta t, \omega) = \int_{-\infty}^{\infty} dt\, \hat{\mathbf{e}}_y \cdot \mathbf{A}_{\mathbf{q}_{\mathrm{pr}}}(\delta t, t)\, e^{i\omega t} \tag{6.2c}$$

denote the Fourier transformed y-components of the current density $\mathbf{j}_{\mathbf{q}_{\mathrm{pr}}}(\delta t, t)$ and the vector potential $\mathbf{A}_{\mathbf{q}_{\mathrm{pr}}}(\delta t, t)$ of the probe pulse, respectively. Hence, the pump-probe conductivity is fully determined by the time evolution of the expectation values $\langle c^{\dagger}_{\mathbf{k},\sigma} c_{\mathbf{k}+\mathbf{q}_{\mathrm{pr}},\sigma}\rangle(\delta t, t)$, which we numerically compute by integrating the corresponding equations of motion.

In literature, there are also other ways discussed to determine the conductivity, see for instance Ref. [91]. However, in the present context of a pump and a probe pulse the above procedure suggests itself and is closest to what is experimentally done. Consequently, the conductivity is fully determined by the temporal evolution of $\left\langle c^{\dagger}_{\mathbf{k},\sigma} c_{\mathbf{k}+\mathbf{q}_{\mathrm{pr}},\sigma}\right\rangle(\delta t, t)$.

To keep the notation light, we omit the dependence on the delay time in the following, because it is fixed externally. For the numerical computation, the current in terms of Bogoliubov quasiparticle is needed, it is given by

$$\begin{aligned}\mathbf{j}_{\mathbf{q}_{\mathrm{pr}}}(t) = \frac{-e\hbar}{2mV} \sum_{\mathbf{k}} (2\mathbf{k} + \mathbf{q}_{\mathrm{pr}}) \Big[&(u_{\mathbf{k}} v_{\mathbf{k}+\mathbf{q}_{\mathrm{pr}}} - v_{\mathbf{k}} u_{\mathbf{k}+\mathbf{q}_{\mathrm{pr}}}) \big(\langle \alpha^{\dagger}_{\mathbf{k}} \beta^{\dagger}_{\mathbf{k}+\mathbf{q}_{\mathrm{pr}}} \rangle - \langle \beta_{\mathbf{k}} \alpha_{\mathbf{k}+\mathbf{q}_{\mathrm{pr}}} \rangle \big) \\ &+ (u_{\mathbf{k}} u_{\mathbf{k}+\mathbf{q}_{\mathrm{pr}}} + v_{\mathbf{k}} v_{\mathbf{k}+\mathbf{q}_{\mathrm{pr}}}) \big(\langle \alpha^{\dagger}_{\mathbf{k}} \alpha_{\mathbf{k}+\mathbf{q}_{\mathrm{pr}}} \rangle - \langle \beta^{\dagger}_{\mathbf{k}} \beta_{\mathbf{k}+\mathbf{q}_{\mathrm{pr}}} \rangle \big) \Big] .\end{aligned} \tag{6.3}$$

6.2 Implementation

In order to compute the current induced by the probe pulse, we need the temporal evolution of the off-diagonal expectation values $\left\langle \alpha^{\dagger}_{\mathbf{k}} \beta^{\dagger}_{\mathbf{k}+\mathbf{q}_{\mathrm{pr}}} \right\rangle$, $\left\langle \beta_{\mathbf{k}} \alpha_{\mathbf{k}+\mathbf{q}_{\mathrm{pr}}} \right\rangle$, $\left\langle \alpha^{\dagger}_{\mathbf{k}} \alpha_{\mathbf{k}+\mathbf{q}_{\mathrm{pr}}} \right\rangle$, and $\left\langle \beta^{\dagger}_{\mathbf{k}} \beta_{\mathbf{k}+\mathbf{q}_{\mathrm{pr}}} \right\rangle$. All of these off-diagonal terms are zero before the probe pulse is switched on.

Further, we use the following approximation to compute the effects of the probe pulse. Although pump and probe pulse possess different momenta $\mathbf{q}_0 \neq \mathbf{q}_{\mathrm{pr}}$ and by association act on different discretization meshes, we use the same discretization mesh for both pulses. This is done, because the differences between the momenta $\Delta\mathbf{q} = \mathbf{q}_0 - \mathbf{q}_{\text{pr}}$ is irrelevant small compared to the momentum $\mathbf{k}$. Due to this, the previous approximation is well justified. In addition, we approximate for the diagonal elements

$$\left\langle \alpha^\dagger_{\mathbf{k}+\mathbf{q}_{\text{pr}}} \beta^\dagger_{\mathbf{k}+\mathbf{q}_{\text{pr}}} \right\rangle \approx \left\langle \alpha^\dagger_{\mathbf{k}+\mathbf{q}_0} \beta^\dagger_{\mathbf{k}+\mathbf{q}_0} \right\rangle \text{ etc.} \tag{6.4}$$

and restrict the off-diagonal elements to

$$\left\langle \alpha^\dagger_{\mathbf{k}+m\mathbf{q}_{\text{pr}}} \beta^\dagger_{\mathbf{k}+n\mathbf{q}_{\text{pr}}} \right\rangle = 0 \quad \text{if } |m-n| > 1. \tag{6.5}$$

As mentioned in Sect. 3.3, the probe pulse is computed only in linear order in $A_{\text{pr}}(t)$. So we neglect the parts in the equations of motion which are proportional to $\frac{e^2}{2m}$. Additionally, all contributions in linear order of $A_{\text{pr}}(t)$ and the ones proportional to g_{ph}, if phonons are included, simplify due to the approximation in Eq. (6.5). Not every addend in Eq. (4.1) has to be taken into account, because the corresponding expectation value is set to zero. For example, the equations of motion for $\left\langle \alpha^\dagger_{\mathbf{k}} \alpha_{\mathbf{k}+\mathbf{q}_{\text{pr}}} \right\rangle$ without phonons is given by

$$\begin{aligned} i\hbar\frac{\mathrm{d}}{\mathrm{d}t}\left\langle \alpha^\dagger_{\mathbf{k}} \alpha_{\mathbf{k}+\mathbf{q}_{\text{pr}}} \right\rangle &= \left(-R_{\mathbf{k}} + R_{\mathbf{k}+\mathbf{q}_{\text{pr}}}\right)\left\langle \alpha^\dagger_{\mathbf{k}} \alpha_{\mathbf{k}+\mathbf{q}_{\text{pr}}} \right\rangle \\ &+ C_{\mathbf{k}+\mathbf{q}_{\text{pr}}}\left\langle \alpha^\dagger_{\mathbf{k}} \beta^\dagger_{\mathbf{k}+\mathbf{q}_{\text{pr}}} \right\rangle - C^*_{\mathbf{k}}\left\langle \beta_{\mathbf{k}} \alpha_{\mathbf{k}+\mathbf{q}_{\text{pr}}} \right\rangle \\ &+ \frac{e\hbar}{2m} 2\mathbf{k}\mathbf{A}_{\mathbf{q}_{\text{pr}}}\Bigg(- L^+_{\mathbf{k},\mathbf{q}_{\text{pr}}}\left\langle \alpha^\dagger_{\mathbf{k}+\mathbf{q}_0} \alpha_{\mathbf{k}+\mathbf{q}_0} \right\rangle + L^+_{\mathbf{k},\mathbf{q}_{\text{pr}}}\left\langle \alpha^\dagger_{\mathbf{k}} \alpha_{\mathbf{k}} \right\rangle \\ &\quad + M^-_{\mathbf{k},\mathbf{q}_{\text{pr}}}\left\langle \alpha^\dagger_{\mathbf{k}} \beta^\dagger_{\mathbf{k}} \right\rangle + M^-_{\mathbf{k},\mathbf{q}_{\text{pr}}}\left\langle \beta_{\mathbf{k}+\mathbf{q}_0} \alpha^\dagger_{\mathbf{k}+\mathbf{q}_0} \right\rangle \Bigg). \end{aligned} \tag{6.6}$$

6.3 Superconductor in absence of phonons

First, the pump-probe response of the pure s-wave superconductor is presented. Again, we distinguish the three dynamical regimes, namely nonadiabatic, intermediate, and adiabatic regime for instance see Sect. 5. The conductivity is computed for positive and negative delay times. As a reminder the main findings for the dynamics induced by the pump pulse are depicted in the following, as well. A detailed discussion of this dynamics can be found in Sect. 5.

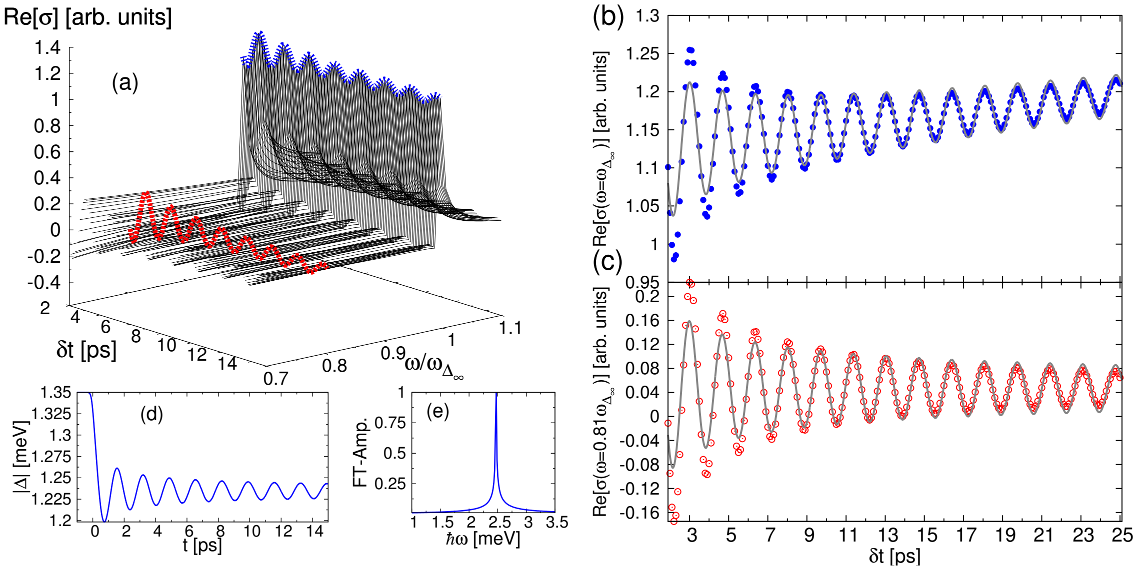

Figure 6.1: (a) Real part of the pump-probe response, $\mathrm{Re}[\sigma(\delta t,\omega)]$, versus ω and $\delta t > 0$ for the nonadiabatic regime, induced by a pulse with $\tau_0 = 0.5$ ps and $|\mathbf{A}_0| = 8 \cdot 10^{-8}$ Js/(Cm). (b), (c) Pump-probe signal $\mathrm{Re}[\sigma(\delta t,\omega)]$ as a function of delay time δt for (b) $\omega = \omega_{\Delta_\infty}$ and (c) $\omega = 0.81\,\omega_{\Delta_\infty}$. The gray lines in panels (b) and (c) represent the best fits of Eq. (6.7) to the numerical data as discussed in the text. (d),(e) Temporal evolution of $|\Delta(t)|$ and spectral distribution of the gap oscillation, respectively, for the same parameters as in panel (a).

6.3.1 Positive delay time

Nonadiabatic regime

The real part of the conductivity versus the delay time and frequency for the nonadiabatic regime is presented in Fig. 6.1. Here, a pump pulse with $\tau_0 = 0.5$ ps and $|\mathbf{A}_0| = 8 \cdot 10^{-8}$ Js/(Cm) is used. The corresponding imaginary part is depicted in Fig. 6.2. First, the results for the real part are discussed; the imaginary part shows similar features.

The oscillatory dynamics of the pumped system, see Sect. 5 or Fig. 6.1(d) and (e), is reflected in the conductivity through an algebraically decaying oscillation as function of delay time depicted in Fig. 6.1(a)-(c). These oscillations are best visible at the frequency ω_{Δ_∞}, where the conductivity exhibits a sharp edge as a function of ω, see Fig. 6.1(a) and (b). The position of the sharp edge at $\omega = \omega_{\Delta_\infty}$ as function of ω is fixed and does not depend on the delay time.

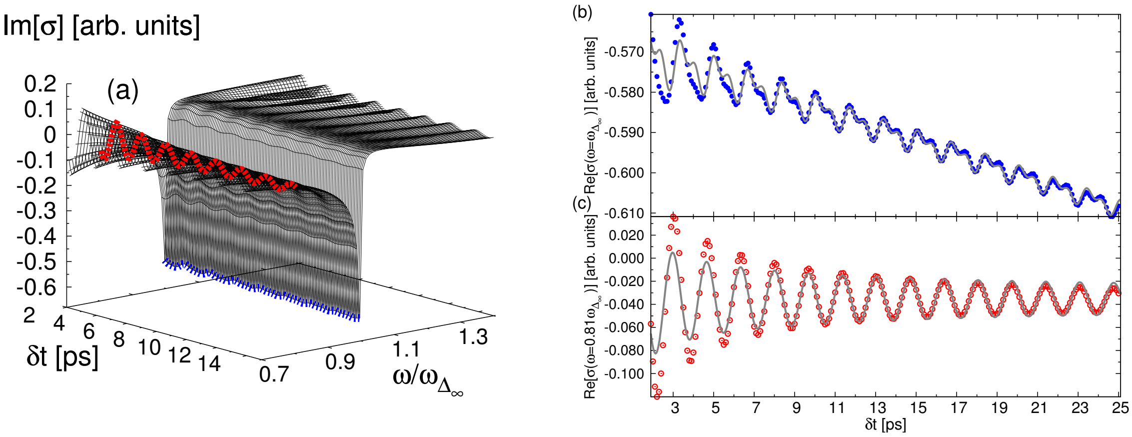

Figure 6.2: (a) Imaginary part of the pump-probe response, $\mathrm{Im}[\sigma(\delta t, \omega)]$, versus ω and $\delta t > 0$ for the nonadiabatic regime, induced by a pulse with $\tau_0 = 0.5$ ps and $|\mathbf{A}_0| = 8 \cdot 10^{-8}$ Js/(Cm). (b), (c) Pump-probe signal $\mathrm{Im}[\sigma(\delta t, \omega)]$ as a function of delay time δt for (b) $\omega = \omega_{\Delta_\infty}$ and (c) $\omega = 0.81\,\omega_{\Delta_\infty}$. The gray lines in panels (b) and (c) represent the best fits of the numerical data with Eqs. (6.8) and (6.7).

The delay-time dependence of $\mathrm{Re}[\sigma(\delta t, \omega_f)]$ for fixed ω_f is approximately given by

$$\mathrm{Re}[\sigma(\delta t, \omega_f)] = A + B\frac{\cos(\omega_{\Delta_\infty}\delta t + \Phi)}{\sqrt{\delta t}} + C\delta t, \tag{6.7}$$

as shown by the excellent fits to the numerical data in Figs. 6.1(b) and 6.1(c). Here, Φ is an overall phase and A, B, and C are fit parameters depending on ω_f. Hence, like the order parameter oscillations, the oscillations in the pump-probe signal are characterized by an amplitude decaying as $1/\sqrt{\delta t}$ and a frequency $\omega_{\Delta_\infty} = 2\Delta_\infty/\hbar$ that is determined by the asymptotic gap value Δ_∞. We note that the linear increase in the pump-probe signal of Fig. 6.1(b) can be attributed to slow oscillations which are related to the finite size of the system. So they are numerical artefacts.

The same signatures, i.e., the oscillatory behavior as a function of δt and the sharp edge at $\omega = \omega_{\Delta_\infty}$ as function of ω, can be detected in the imaginary part of the conductivity in Fig. 6.2. For all frequencies except $\omega = \omega_{\Delta_\infty}$ Eq. (6.7) describes the delay time dependence of the pump probe response. As an example, the conductivity at $\omega = 0.81\omega_{\Delta_\infty}$ is shown in Fig. 6.2(c). Here an almost perfect match of the fit and the data is shown. For $\omega = \omega_{\Delta_\infty}$, where the sharp edge in the conductivity as a function of ω is observed, the oscillation is defined by two frequencies. One is given by ω_{Δ_∞} and the other by $2\omega_{\Delta_\infty}$. This is due to the fact that in the imaginary part of the conductivity we can observe additionally higher harmonics of this oscillation. To describe the delay-time dependence of the conductivity at this frequency, we have to modify Eq. (6.7) in the following way:

$$\mathrm{Im}[\sigma(\delta t,\omega_f)] = A + \frac{B_1\cos(\omega_{\Delta_\infty}\delta t + \Phi_1) + B_2\cos(2\omega_{\Delta_\infty}\delta t + \Phi_2)}{\sqrt{\delta t}} + C\delta t. \tag{6.8}$$

Here, A, B_1, B_2, C, and Φ are again fit parameters. The perfect match of this modified fit shown in Fig. 6.2(b) revealing the excellent approximation.

Due to the fact that the imaginary part of the conductivity provides the same information about the dynamics of the system, we will skip the discussion of the imaginary part for brevity in the following.

All in all, the nonadiabatic BCS state dynamics is clearly visible in $\sigma(\delta t,\omega)$ in terms of oscillations as a function of delay time δt. This is one of the key findings of our investigation. It is in contrast to the statement of Papenkort *et al.*, who claimed that only the value of Δ_∞ can be identified but not the oscillation itself [30, 31, 35]. They stated that the oscillation cannot be observed in the conductivity due to the trade-off between temporal resolution and energy resolution [35]. The time interval, which is needed to energetically resolve the energy gap, must be larger than $\hbar/\Delta_\infty$, but during this interval the oscillation average out [30]. But their look only at the conductivity as function of ω, which in fact shows only signatures reflecting Δ_∞, namely the sharp edge at $\omega = \omega_{\Delta_\infty}$. As we already stated, the information about the oscillation of $|\Delta(t)|$ is provided by the pump probe response as function of delay time.

Further, our results are in qualitative agreement with recent pump-probe experiments [6]. As already mentioned, Matsunaga *et al.* used THz-pump and THz-probe spectroscopy and studied thin $\mathrm{Nb}_{1-x}\mathrm{Ti}_x\mathrm{N}$ films. They used a pulse duration of 90 fs, which induces nonadiabatic dynamics of the superconductor. As observables they studied the change in the transmission of the probe field $\delta E_{\mathrm{probe}}$ and the conductivity. In $\delta E_{\mathrm{probe}}$ they observed oscillations which are algebraically damped and their frequency corresponds to twice the asymptotic gap energy. These dynamics describe the temporal evolution of the order parameter quite well and are in good agreement with our results in Sect. 5.1.

For the conductivity they observed oscillation as function of delay time. They suggested that these oscillation can be interpret as the order parameter oscillation. Our studies shows, that these oscillation are in fact caused by the order parameter oscillation.

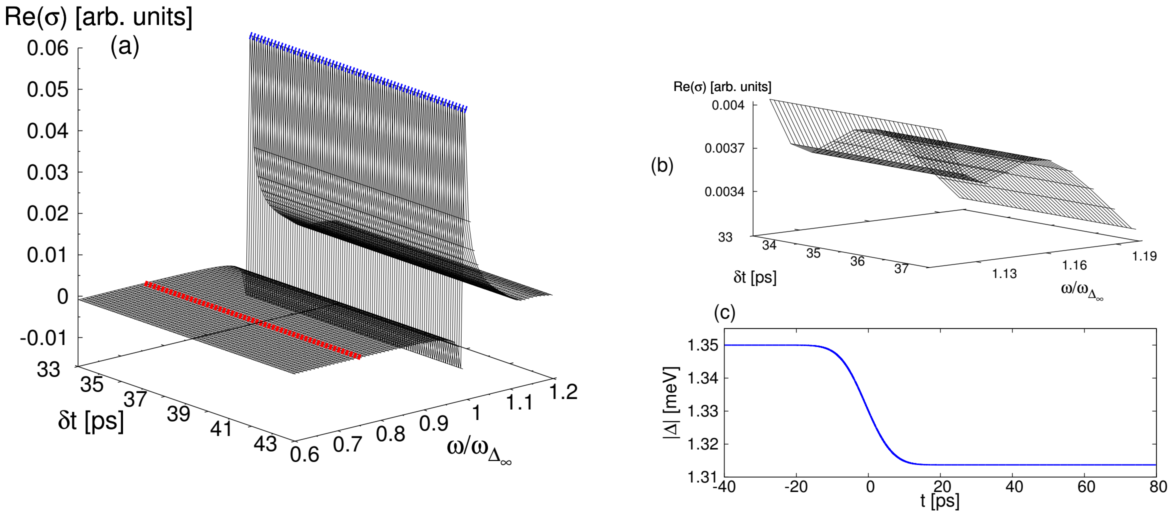

Figure 6.3: (a) Real part of the pump-probe conductivity, $\mathrm{Re}[\sigma(\delta t,\omega)]$, versus ω and $\delta t > 0$ for the adiabatic regime, induced by a pump pulse with $\tau_0 = 20$ ps and $|\mathbf{A}_0| = 0.5\cdot 10^{-8}$ Js/(Cm). Panel (b) shows a detail of the pump-probe response for frequencies just below the pump frequency $\omega_0 = 1.21\omega_{\Delta_\infty}$. The small dip near $\omega \approx 1.15\omega_{\Delta_\infty}$ is due to Pauli blocking. (c) Time dependence of $|\Delta(t)|$ for the same parameters as in panel (a).

Adiabatic regime

The real part of the conductivity for the adiabatic regime as a function of delay time δt and frequency ω is shown in Fig. 6.3(a) for a pump pulse with $\tau_0 = 20\,\mathrm{ps} \gg \tau_\Delta$ and $|\mathbf{A}_0| = 0.5\cdot 10^{-8}$ Js/(Cm). As explained in Sect.5.1, the excited quasiparticle densities remain almost constant after the pump pulse, see Fig. 5.2. Hence, the order parameter $\Delta(t)$ does not oscillate, instead it decreases monotonically towards the asymptotic value Δ_∞ as displayed in Fig. 6.3(c) and already discussed in Sect. 5.1. Correspondingly, the pump-probe signal $\sigma(\delta t,\omega)$ does not exhibit any oscillations as a function of delay time as shown in Fig. 6.3(a). As function of ω, the real part of the conductivity $\mathrm{Re}[\sigma(\delta t,\omega)]$ has a sharp edge at the frequency $\omega = \omega_{\Delta_\infty}$ corresponding to twice the energy of the asymptotic gap value Δ_∞, like the conductivity for the nonadiabatic regime. However, it is almost featureless except for a small dip just below the pump frequency ω_0, see Fig. 6.3(b). This reduced absorption in the vicinity of ω_0 is due to Pauli blocking which leads to a saturation in the narrowly peaked quasiparticle distributions, e.g. see Fig.5.1.

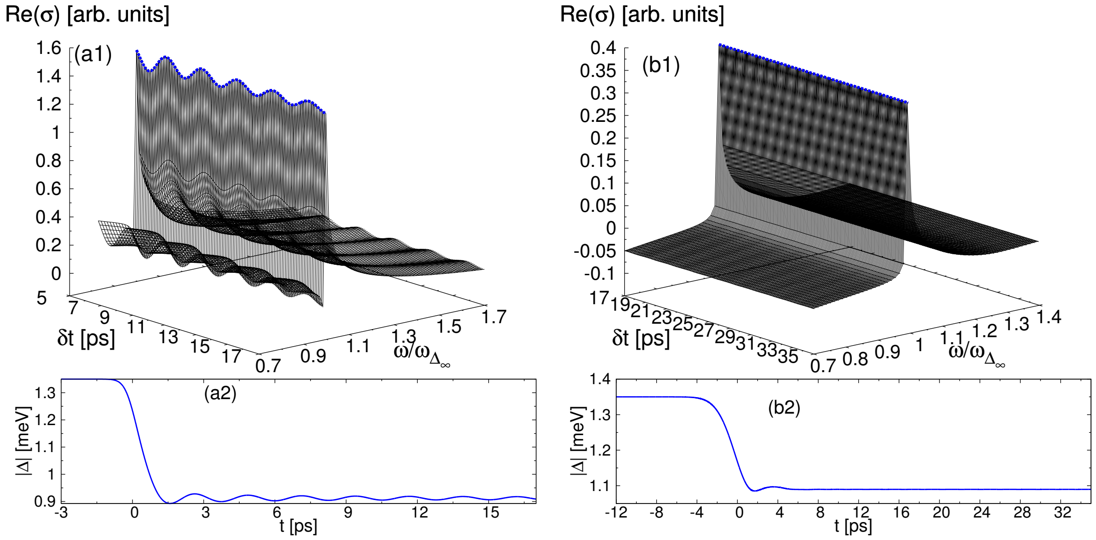

Figure 6.4: (a1) Real part of the pump-probe conductivity, $\mathrm{Re}[\sigma(\delta t,\omega)]$, versus ω and $\delta t > 0$ for the intermediate regime with $\tau_0 = 1.5$ ps and $|\mathbf{A}_0| = 7 \cdot 10^{-8}$ Js/(Cm). (a2) Time dependence of $|\Delta(t)|$ for the same parameters as in panel (a1). (b) same as (a) for a pump pulse width of $\tau_0 = 6$ ps and $|\mathbf{A}_0| = 3 \cdot 10^{-8}$ Js/(Cm)

Intermediate regime

Figure 6.4 shows how the transition between the nonadiabatic and adiabatic regimes is mirrored in the pump-probe response. Here, the real part of the conductivity $\mathrm{Re}[\sigma(\delta t,\omega)]$ are presented exemplarily for $\tau_0 = 1.5$ ps and $\tau_0 = 6$ ps. All pump-probe responses, independent of the pump pulse width, show a sharp edge at $\hbar\omega = 2\Delta_\infty$ as a function of ω. As a function of delay time the conductivity shows an oscillatory behavior of which the amplitude decays $\sim \frac{1}{\sqrt{t}}$, as like in the nonadiabatic regime. For increasing pump pulse width the amplitude of this oscillation gradually decreases leading to the almost featureless shape of the conductivity of the adiabatic regime. In addition, the dip at $\omega \approx \omega_0$ evolves with increasing pump pulse width (not shown). This is in perfect agreement with the transition from a rather broad peak to two sharp peaks in the quasiparticle distributions, see Fig. 5.1.

As a first short conclusion we state, that the pump probe response for positive delay times contains signatures which provides information about the dynamics of the system. For the nonadiabatic regime, the conductivity as function of delay time shows an oscillation which behaves as the oscillation of the order parameter. The frequency with $\omega_{\Delta_\infty} = \frac{2\Delta_\infty}{\hbar}$ as well as the $\frac{1}{\sqrt{t}}$-decay is clearly visible, especially at the absorption frequency $\omega = \omega_{\Delta_\infty}$. For the adiabatic regime instead the conduc-

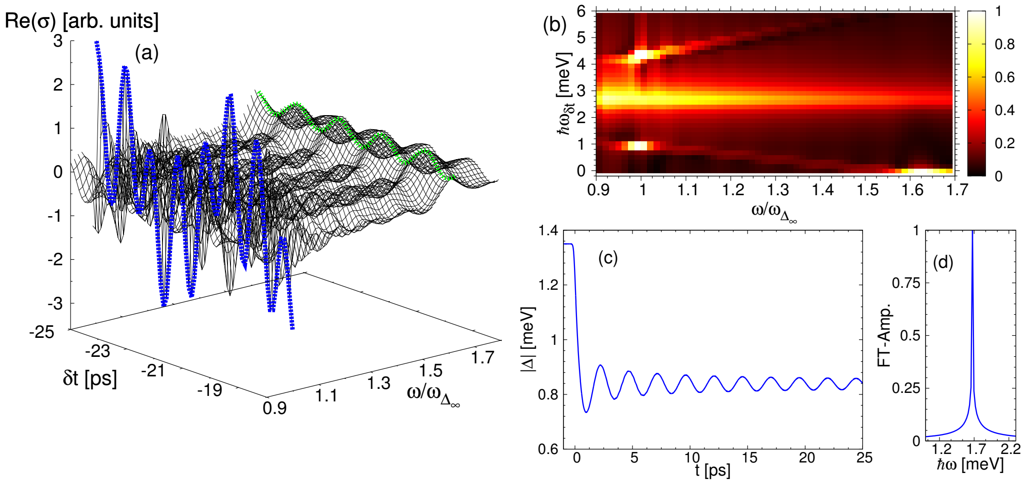

Figure 6.5: (a) Absorption spectrum $\mathrm{Re}[\sigma(\delta t, \omega)]$ versus ω and $\delta t < 0$ for the nonadiabatic regime and negative delay time, induced by a pump pulse with $\tau_0 = 0.5$ ps and $|\mathbf{A}_0| = 13 \cdot 10^{-8}$ Js/(Cm). (b) Fourier transform of the data in panel (a), i.e., $\mathrm{Re}(\sigma)$ as a function of Fourier frequency $\omega_{\delta t}$ and absorption frequency ω. (c), (d) Time dependence of $|\Delta(t)|$ and spectral distribution of the gap oscillation, respectively, for the same parameters as in panel (a).

tivity as function of δt is almost featureless as the corresponding evolution of the order parameter. Even the crossover between the both regimes is reflected in the conductivity as function of delay time.

In contrast, the conductivity as function of ω provides no information, which helps to identify the dynamics of the system. All in all, we state that one has to study the pump-probe response as function of delay time to obtain information about the induced dynamics.

6.3.2 Negative delay time

Here the situation where the probe pulse precedes the pump pulse is considered.

Nonadiabatic regime

In Fig. 6.5(a), the real part of the pump-probe response $\mathrm{Re}[\sigma(\delta t, \omega)]$ is presented versus negative delay time δt and frequency ω for the nonadiabatic regime. We use a pump pulse with $\tau_0 = 0.5$ ps and $|\mathbf{A}_0| = 13 \cdot 10^{-8}$ Js/(Cm).

Both the energy gap before and after the pump pulse are clearly visible in the frequency dependence of $\sigma(\delta t, \omega)$. The pump-probe signal displays two sharp edges as function of frequency, one at twice the initial gap $\hbar\omega_{\Delta_0} = 2\Delta_0 = 2.7$ meV and one at twice the asymptotic gap $\hbar\omega_{\Delta_\infty} = 2\Delta_\infty = 1.677$ meV, see green and blue lines in Fig. 6.5(a). The effect of the pump pulse can be seen due to the fact that the pump pulse modifies the dynamics of the current, which is induced by the preceding probe pulse. The main oscillation of the current is determined by the oscillation frequency of the order parameter $\omega_\Delta = \frac{2\Delta}{\hbar}$. This frequency changes from the initial value to the reduced value provided by the pump pulse. Between the edges the conductivity shows spectral oscillations in ω with a period $\delta\omega$, that is inversely proportional to $\delta\omega \sim (2\pi)/|\delta t|$ [30]. Such spectral oscillation with $\delta\omega \sim (2\pi)/|\delta t|$ are also known and measured in semiconductors [92,93].

As function of delay time the conductivity shows a rich oscillatory behavior with multiple frequencies that depend on the absorption energy $\hbar\omega$. This is revealed most clearly in Fig. 6.5(b), which shows the Fourier transformed response in two-dimensional frequency space, i.e., $\mathrm{Re}(\sigma)$ as a function of the Fourier frequency $\omega_{\delta t}$ of the delay time and of the absorption frequency ω. We observe that for the absorption energy $\hbar\omega$ within the interval $0 < \hbar\omega < \hbar\omega_{\Delta_\infty}$, $\mathrm{Re}[\sigma(\delta t, \omega)]$ oscillates in δt with the frequency ω_{Δ_0}. The oscillatory behavior of $\mathrm{Re}[\sigma(\delta t, \omega)]$ in the interval $\hbar\omega_{\Delta_\infty} < \hbar\omega < \hbar\omega_{\Delta_0}$ is even more intriguing. It shows signatures of how the gap decreases while the pump pulse acts on the sample, see Fig. 6.5(c). In other words, it is found that for these absorption energies $\mathrm{Re}[\sigma(\delta t, \omega)]$ oscillates in δt with three frequencies that are approximately given by ω_{Δ_0}, $\omega_{\Delta_0} + \omega$, and $\omega_{\Delta_0} - \omega$.

Adiabatic regime

The real part of the conductivity $\mathrm{Re}[\sigma(\delta t, \omega)]$ versus negative delay δt time and frequency ω is depicted in Fig. 6.6 for the adiabatic regime.

As for the nonadiabatic case presented in Fig. 6.5 the response as function of ω displays two sharp edges at $\hbar\omega_{\Delta_0}$ and $\hbar\omega_{\Delta_\infty}$ and the spectra oscillation period $\delta\omega \sim (2\pi)/|\delta t|$ in between [30]. As function of delay time the conductivity shows an oscillatory behavior in the interval $\hbar\omega_{\Delta_\infty} \leq \hbar\omega \leq \hbar\omega_{\Delta_0}$ only. Figure 6.6(b) illustrates the Fourier transformed response in two-dimensional frequency space. It shows that $\mathrm{Re}[\sigma(\delta t, \omega)]$ oscillates with $\omega_{\Delta(t_i)} - \omega$. Once more, the pump-probe response for negative delay time shows a signature which reflects how the absolute value of the order parameter decreases during the pump pulse, but compared to the nonadiabatic regime the signature is hardly visible. In addition, we cannot observe an oscillation with frequency ω_{Δ_0} or $\omega_{\Delta_0} + \omega$ as in the nonadiabatic case.

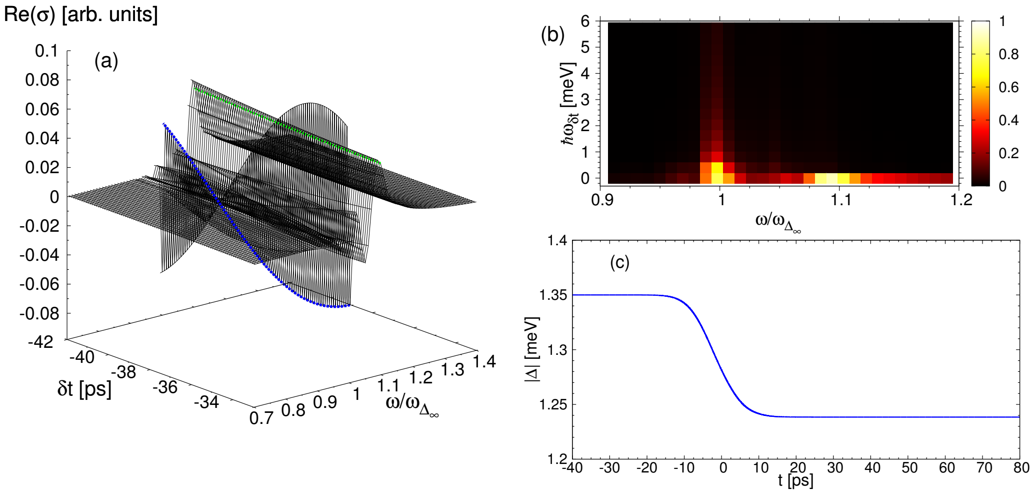

Figure 6.6: (a) Absorption spectrum $\mathrm{Re}[\sigma(\delta t, \omega)]$ versus ω and $\delta t < 0$ for the adiabatic regime and negative delay time, induced by a pump pulse with $\tau_0 = 20$ ps and $|\mathbf{A}_0| = 1 \cdot 10^{-8}$ Js/(Cm). (b) Fourier transform of the data in panel (a), i.e., $\mathrm{Re}(\sigma)$ as a function of Fourier frequency $\omega_{\delta t}$ and absorption frequency ω. (c) Time dependence of $|\Delta(t)|$ for the same parameters as in panel (a).

Intermediate regime

How the crossover between both dynamical regimes is reflected in the conductivity for negative delay time is discussed in this section. The real part of conductivity $\mathrm{Re}[\sigma(\delta t, \omega)]$ between both dynamical regimes shows two sharp edges at $\hbar\omega_{\Delta_0}$ and $\hbar\omega_{\Delta_\infty}$ as a function of ω. In addition, the spectral oscillation with period $\delta\omega \sim (2\pi)/|\delta t|$ can be observed. This is not shown explicitly, but it is presented in Ref. [30].

The oscillatory behavior of $\mathrm{Re}[\sigma(\delta t, \omega)]$ as a function of delay time is more interesting. For illustration the Fourier transformed response in two-dimensional frequency space is depicted in Fig. 6.7 for two different pump pulse with $\tau_0 = 1.5$ ps and $\tau_0 = 6$ ps.

In the nonadiabatic regime we observed three different frequencies $\omega = \omega_{\Delta_0} \pm \omega$ and $\omega = \omega_{\Delta_0}$, see Fig. 6.5. If we increase the pump pulse width, the oscillation with $\omega = \omega_{\Delta_0} + \omega$ is vanished first, see Fig. 6.7(a). By further increase of the pump pulse width the oscillation with $\omega = \omega_{\Delta_0}$ vanishes, too. Only the oscillation with $\omega = \omega_{\Delta_0} - \omega$ remains visible leading the pump-probe response of the adiabatic regime.

In contrast to the results for positive delay times, the results for negative delay time provide not only signatures which reflect the dynamics of the order parameter

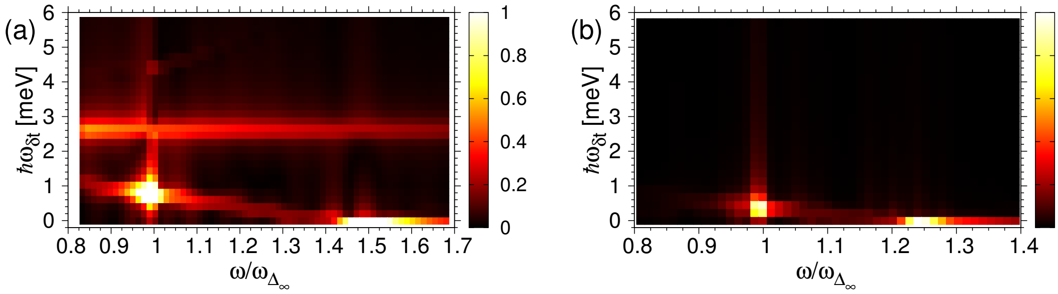

Figure 6.7: (a) Fourier transform of the absorption spectrum $\mathrm{Re}[\sigma(\delta t, \omega)]$ for a pump pulse with $\tau_0 = 1.5$ ps and $|\mathbf{A}_0| = 7 \cdot 10^{-8}$ Js/(Cm), i.e., $\mathrm{Re}(\sigma)$ as a function of Fourier frequency $\omega_{\delta t}$ and absorption frequency ω. (b) same as (a) for a pump pulse with $\tau_0 = 6$ ps and $|\mathbf{A}_0| = 3 \cdot 10^{-8}$ Js/(Cm).

after the pump pulse. The oscillatory behavior of the conductivity as function of δt provides also information about the dynamics of superconductor before and while the pump pulse acts. In order to study the excitation process it can be useful to use negative delay times.

6.4 Superconductor in presence of phonons

In this section, the pump probe response of the superconductor with additional optical phonon is discussed. We study how the dynamics of the lattice is reflected in the pump-probe conductivity. This may lead to an direct comparison to experimental studies. As already mentioned in Sect. 5.2 there are some experimental studies which observed coherent phonons in semiconductors [43, 44, 77], semiconductor quantum wells [78, 79], superlattices [81, 82], and high-temperature superconductcors [14, 46, 47].

For example, Mansart *et al.* observed coherent optical phonons in iron pnictide superconductor $\mathrm{Ba(Fe_{1-x}Co_x)_2As_2}$ [14]. They used the time-resolved pump-probe reflectivity to detect the coherent phonons. More precisely, they observed an oscillation in the reflectivity as function of delay time. This oscillation can be identified as coherent phonon modes by comparison of the measured frequency with standard Raman measurements.

In this thesis, we compute again the conductivity as observable for the pump probe response, but it is possible to compute the reflectivity from the conductivity [94]. As shown in Sect. 5.2 coherent phonons are efficiently generated in the nonadiabatic regime. Thus we concentrate the following studies on this regime. Nevertheless,

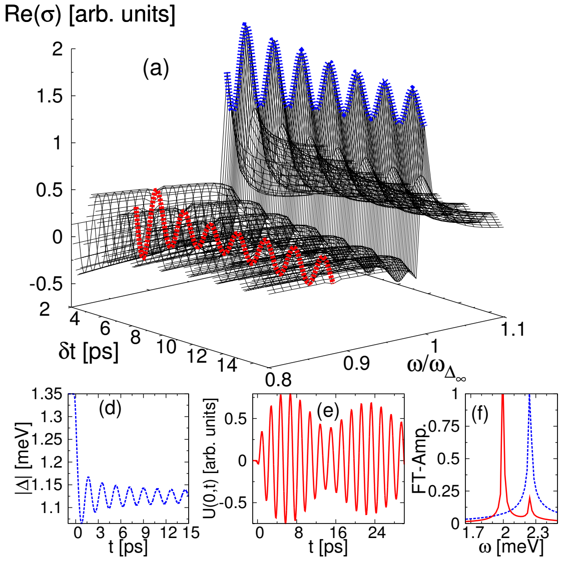

Figure 6.8: Real part of the pump-probe signal, $\mathrm{Re}[\sigma(\delta t, \omega)]$, versus ω and $\delta t > 0$ for the nonadiabatic regime, induced by a pump pulse with $\tau_0 = 0.5$ ps and $|\mathbf{A}_0| = 10 \cdot 10^{-8}$ Js/(Cm), in the presence of an optical phonon mode with energy $\hbar\omega_{\mathrm{ph}} = 2$ meV and coupling strength $g_{\mathrm{ph}} = 0.1$ meV. (b), (c) Pump-probe response $\mathrm{Re}[\sigma(\delta t, \omega)]$ as a function of delay time δt for (b) $\omega = \omega_{\Delta_\infty}$ and (c) $\omega = \omega_{\mathrm{ph}}$. The gray lines in panels (b) and (c) represent the best fits of Eqs. (6.7) and (6.9), respectively, to the numerical data. (d), (e) Time evolution of the order parameter amplitude $|\Delta(t)|$ and the lattice displacement $U(0,t)$, respectively, for the same parameters as in panel (a). (f) Fourier spectra of the order parameter and coherent phonon oscillations are depicted as dashed blue and solid red lines, respectively.

some results concerning the adiabatic regime are also shown. We quit on discussing the intermediate regime due to a lack of interesting new features, see Sect. 5.2. Again, also the pump induced dynamics are presented briefly for sake of completeness.

The pump probe response of a superconductor with additional acoustic phonons is not discussed. As already mentioned in Sect. 5.3 the generation of acoustic phonons is weak. Hence, the signatures which reflect the dynamic of the phonons are almost not visible in the conductivity. As a result, the conductivity looks similar to the case without phonons.

6.4.1 Positive delay time

Nonadiabatic regime

As discussed in Sect. 5.2, the most interesting case corresponds to the situation where the pump pulse drives the quasiparticle oscillation with a frequency that is close to resonance with the phonon frequency. If the two frequencies are close to resonance a beating phenomenon in the lattice displacement can be observed. In Fig. 6.8 the corresponding pump-probe spectra is shown for a pump pulse with $\tau_0 = 0.5$ ps, $|\mathbf{A}_0| = 10 \cdot 10^{-8}$ Js/(Cm). The optical phonon mode is characterized by the energy $\hbar\omega_{\mathrm{ph}} = 2$ meV and coupling strength $g_{\mathrm{ph}} = 0.1$ meV. As for the case without phonons, we concentrate on the real part of the conductivity, because the imaginary part shows the same features. Figures 6.8(d)-(f) serve as a short reminder of the temporal evolution of the system induced by the pump pulse.

We observe two distinct edges in the frequency dependence of $\sigma(\delta t, \omega)$, one at twice the asymptotic gap value $\hbar\omega_{\Delta_\infty} = 2\Delta_\infty = 2.2491$ meV and the other at the phonon energy $\hbar\omega_{\mathrm{ph}} = 2$ meV, see blue and red lines in Fig. 6.8(a). Again, the position of these sharp edges is independent of the delay time. The maxima of these two edges show an oscillatory behavior as a function of delay time, see Figs. 6.8(b) and 6.8(c), reflecting the nonadiabatic dynamics of both the phonon mode and the Bogoliubov quasiparticles. The delay-time evolution of $\mathrm{Re}[\sigma(\delta t, \omega)]$ at ω_{Δ_∞} is well described by Eq. (6.7), as can be seen by the good fit in Fig. 6.8(b). Particularly, $\mathrm{Re}[\sigma(\delta t, \omega_{\Delta_\infty})]$ oscillates with the frequency ω_{Δ_∞} and an amplitude decaying with $1/\sqrt{\delta t}$.

The oscillations at ω_{ph} exhibit a beating phenomenon approximately given by

$$\mathrm{Re}[\sigma(\delta t, \omega_{\mathrm{ph}})] = A + B \cos\left(\omega_+ \delta t + \Phi_1\right) \cos\left(\omega_- \delta t + \Phi_2\right), \tag{6.9}$$

where $\omega_\pm = (\omega_{\Delta_\infty} \pm \omega_{\mathrm{ph}})/2$, and A, B, Φ_1, and Φ_2 are fit parameters. As demonstrated by the gray lines in Fig. 6.8(c), Eq. (6.9) fits the numerical results well. Just as the lattice displacement $U(\mathbf{r}, t)$, $\mathrm{Re}[\sigma(\delta t, \omega_{\mathrm{ph}})]$ exhibits quantum beats, i.e., it oscillates with frequency ω_+ and has an amplitude that is modulated with frequency ω_-. Note that the deviations between the fit function (6.9) and the numerical results of Fig. 6.8(c) for $\delta t \lesssim 7$ ps are due to a transient oscillatory behavior.

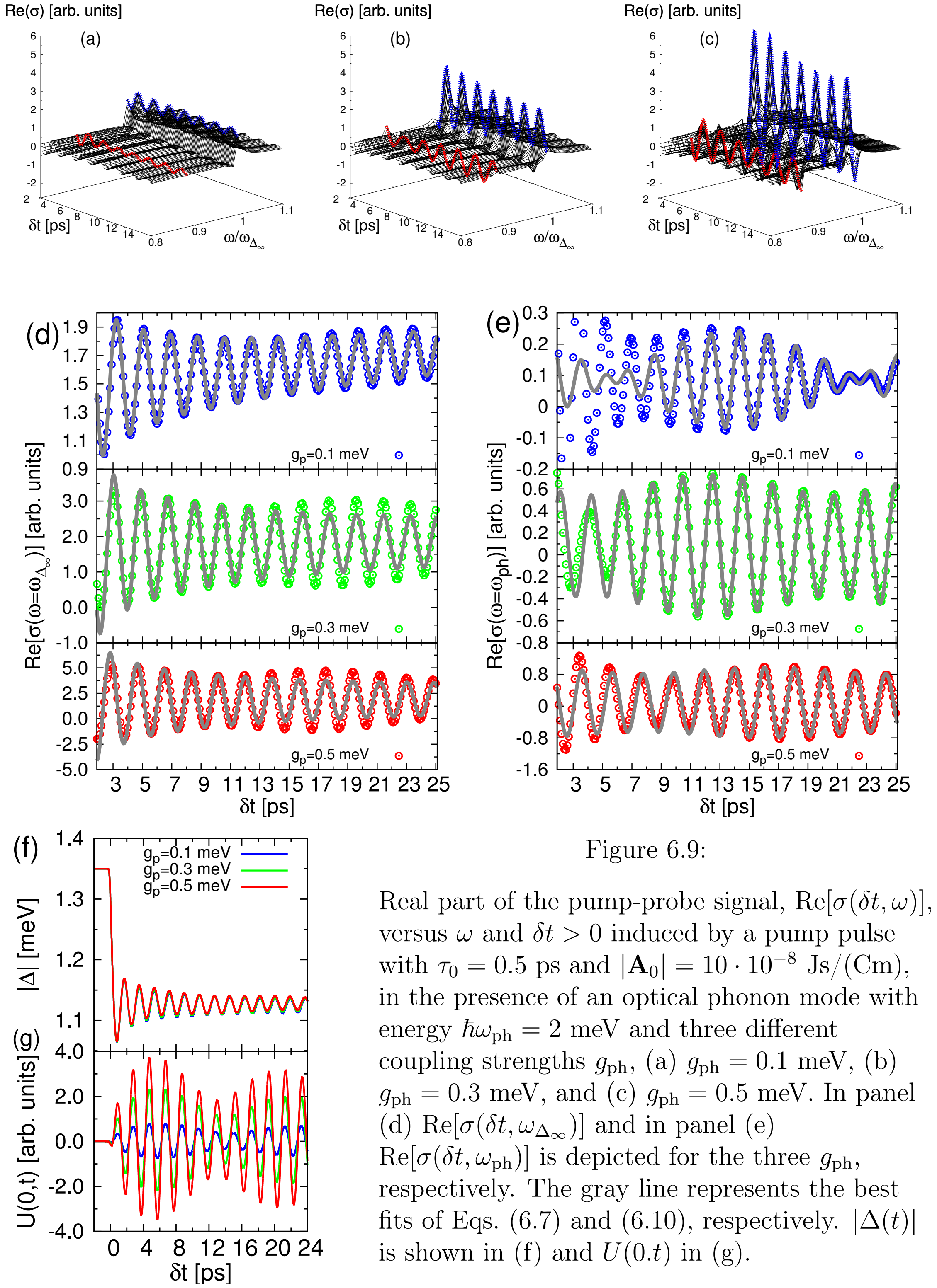

Figure 6.9:

Real part of the pump-probe signal, $\mathrm{Re}[\sigma(\delta t, \omega)]$, versus ω and $\delta t > 0$ induced by a pump pulse with $\tau_0 = 0.5$ ps and $|\mathbf{A}_0| = 10 \cdot 10^{-8}$ Js/(Cm), in the presence of an optical phonon mode with energy $\hbar\omega_{\mathrm{ph}} = 2$ meV and three different coupling strengths g_{ph}, (a) $g_{\mathrm{ph}} = 0.1$ meV, (b) $g_{\mathrm{ph}} = 0.3$ meV, and (c) $g_{\mathrm{ph}} = 0.5$ meV. In panel (d) $\mathrm{Re}[\sigma(\delta t, \omega_{\Delta_\infty})]$ and in panel (e) $\mathrm{Re}[\sigma(\delta t, \omega_{\mathrm{ph}})]$ is depicted for the three g_{ph}, respectively. The gray line represents the best fits of Eqs. (6.7) and (6.10), respectively. $|\Delta(t)|$ is shown in (f) and $U(0.t)$ in (g).

How the conductivity changes with increasing electron-phonon coupling strength g_{ph} is depicted in Fig. 6.9. Here we use the same pump pulse as in Fig. 6.8 and compute $\sigma(\delta t, \omega)$ for two additional coupling strength, namely $g_{\text{ph}} = 0.3\,\text{meV}$ and $g_{\text{ph}} = 0.5\,\text{meV}$.

The real parts of the conductivity, see Fig. 6.9(a)-(c), show a sharp edges at $\omega = \omega_{\text{ph}}$ and $\omega = \omega_{\Delta_\infty}$ as function of ω and an oscillatory behavior as function of δt. However, the edge at the phonon frequency increases with increasing coupling strength. This is caused by a stronger generation of coherent phonons, for instance see the corresponding lattice displacement in Fig. 6.9(g). The conductivity $\text{Re}[\sigma(\delta t, \omega_{\text{ph}})]$ as function of delay time shows an oscillation, which is perfectly captures by Eq. (6.9)

$$\text{Re}[\sigma(\delta t, \omega_{\text{ph}})] = A + B_1 \cos\left(\omega_{\text{ph}}\delta t + \Phi_1\right) + B_2 \cos\left(\omega_{\Delta_\infty}\delta t + \Phi_2\right), \tag{6.10}$$

as demonstrated by the fits in Fig. 6.9(e). In Eq. (6.10) A, B_1, B_2, Φ_1, and Φ_2 are fit parameter. If $B_1 = B_2$ Eq. (6.10) simplifies to Eq. (6.9).

The edge at $\omega = \omega_{\Delta_\infty}$ changes also with increasing coupling strength. The amplitude of the oscillation of $\sigma(\omega_{\Delta_\infty}, \delta)$ increases if g_{ph} increases. In addition, the oscillation are no longer described by Eq. (6.7), as can be seen by the gray lines in Fig. 6.9(d). This change in the conductivity is caused by the feedback of the phonon subsystem on the quasiparticle subsystem. Interestingly, the conductivity is effected more by the phonon subsystem as the order parameter. The order parameter is only slightly changed as can be seen in Fig. 6.9(f), whereas $\sigma(\omega_{\Delta_\infty}, \delta t)$ shows a huge change. This observation can be explained by the influence of the contribution proportional to g_{ph} on the expectation values, which are needed to compute the quantity of interest, in the equations of motion.

To compute the order parameter one needs the expectation values $\left\langle \alpha^\dagger_{\mathbf{k}} \alpha_{\mathbf{k}} \right\rangle$, $\left\langle \beta^\dagger_{\mathbf{k}} \beta_{\mathbf{k}} \right\rangle$, and $\left\langle \alpha^\dagger_{\mathbf{k}} \beta^\dagger_{\mathbf{k}} \right\rangle$. These expectation values are strongly excited by the pump pulse. As a result, the contributions proportional to $g_{\mathbf{p}}$ are weak in relation to the pump pulse effect. Thus, the order parameter is only slightly changed with increasing g_{ph}.

In order to compute the conductivity one needs the expectation values $\left\langle \alpha^\dagger_{\mathbf{k}} \alpha_{\mathbf{k}+\mathbf{q}_{\text{pr}}} \right\rangle$, $\left\langle \beta^\dagger_{\mathbf{k}} \beta_{\mathbf{k}+\mathbf{q}_{\text{pr}}} \right\rangle$, $\left\langle \alpha^\dagger_{\mathbf{k}} \beta^\dagger_{\mathbf{k}+\mathbf{q}_{\text{pr}}} \right\rangle$, and $\left\langle \beta_{\mathbf{k}} \alpha_{\mathbf{k}+\mathbf{q}_{\text{pr}}} \right\rangle$. These values are excited only by the probe pulse. The probe pulse has a weaker intensity than the pump pulse and with this these expectation values are not so strong excited. In addition, these values describe a shift of quasiparticles in $\mathbf{k}$-space. As explained in Sect. 4.3, expectation values which are non-diagonal in $\mathbf{k}$ are weaker excited than the one diagonal in $\mathbf{k}$. Thus, the lower intensity of the probe pulse as well as the shift of quasiprticle in $\mathbf{k}$-space lead to a weaker excitation of $\left\langle \alpha^\dagger_{\mathbf{k}} \alpha_{\mathbf{k}+\mathbf{q}_{\text{pr}}} \right\rangle$, $\left\langle \beta^\dagger_{\mathbf{k}} \beta_{\mathbf{k}+\mathbf{q}_{\text{pr}}} \right\rangle$, $\left\langle \alpha^\dagger_{\mathbf{k}} \beta^\dagger_{\mathbf{k}+\mathbf{q}_{\text{pr}}} \right\rangle$, and

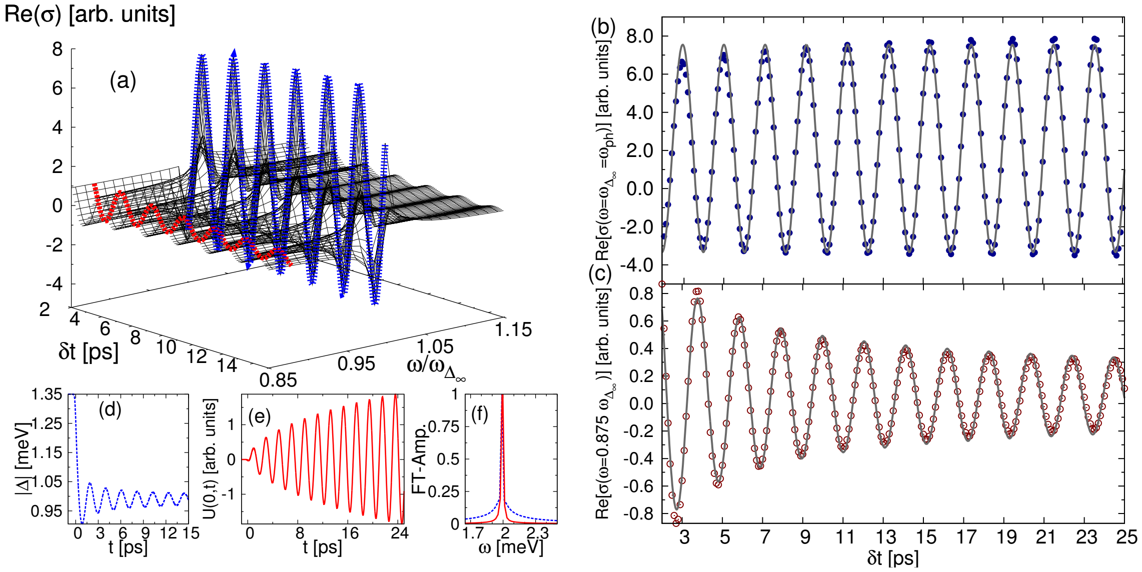

Figure 6.10: (a) Real part of the pump-probe response, $\mathrm{Re}[\sigma(\delta t, \omega)]$, versus ω and $\delta t > 0$ for the nonadiabatic regime, induced by a pump pulse with $\tau_0 = 0.5$ ps and $|\mathbf{A}_0| = 11.64 \cdot 10^{-8}$ Js/(Cm), in the presence of an optical phonon mode with energy at resonance with the order parameter oscillations, i.e., $\omega_{\mathrm{ph}} = \omega_{\Delta_\infty} = 2$ meV. Here the electron-phonon coupling strength is $g_{\mathrm{ph}} = 0.1$ meV. (b), (c) Pump-probe signal $\mathrm{Re}[\sigma(\delta t)]$ as a function of delay time δt for (b) $\omega = \omega_{\Delta_\infty} = \omega_{\mathrm{ph}}$ and (c) $\omega = 0.875\omega_{\Delta_\infty}$. The gray lines in panels (b) and (c) represent the best fits of Eqs. (6.9) and (6.7), respectively, to the numerical data. (d), (e) Time dependence of the order parameter amplitude $|\Delta(t)|$ and the lattice displacement $U(0, t)$, respectively, for the same parameters as in panel (a). (f) Spectral distribution of the order parameter and coherent phonon oscillations are depicted as dashed blue and solid red, respectively.

$\left\langle \beta_{\mathbf{k}} \alpha_{\mathbf{k}+\mathbf{q}_{\mathrm{pr}}} \right\rangle$ than the pump pulse excites $\left\langle \alpha^\dagger_{\mathbf{k}} \alpha_{\mathbf{k}} \right\rangle$, $\left\langle \beta^\dagger_{\mathbf{k}} \beta_{\mathbf{k}} \right\rangle$, and $\left\langle \alpha^\dagger_{\mathbf{k}} \beta^\dagger_{\mathbf{k}} \right\rangle$. As a results, the influence of the contribution proportional to g_{ph} is larger on $\left\langle \alpha^\dagger_{\mathbf{k}} \alpha_{\mathbf{k}+\mathbf{q}_{\mathrm{pr}}} \right\rangle$, $\left\langle \beta^\dagger_{\mathbf{k}} \beta_{\mathbf{k}+\mathbf{q}_{\mathrm{pr}}} \right\rangle$, $\left\langle \alpha^\dagger_{\mathbf{k}} \beta^\dagger_{\mathbf{k}+\mathbf{q}_{\mathrm{pr}}} \right\rangle$, and $\left\langle \beta_{\mathbf{k}} \alpha_{\mathbf{k}+\mathbf{q}_{\mathrm{pr}}} \right\rangle$ than on $\left\langle \alpha^\dagger_{\mathbf{k}} \alpha_{\mathbf{k}} \right\rangle$, $\left\langle \beta^\dagger_{\mathbf{k}} \beta_{\mathbf{k}} \right\rangle$, and $\left\langle \alpha^\dagger_{\mathbf{k}} \beta^\dagger_{\mathbf{k}} \right\rangle$, resulting in a stronger g_{ph} dependence of the conductivity than of the order parameter.

By adjusting the pump-pulse intensity, we can tune the order parameter oscillations into exact resonance with the phonon mode, see Sect. 5.2 or Ref. [33]. This is illustrated in Fig. 6.10, where we plot $\mathrm{Re}[\sigma(\delta t, \omega)]$, $|\Delta(t)|$, and $U(\mathbf{r}, t)$ for a pump pulse with $\tau_0 = 0.5$ ps and $|\mathbf{A}_0| = 11.64 \cdot 10^{-8}$ Js/(Cm). In this resonant case, the lattice displacement oscillates with frequency $\omega_{\mathrm{ph}} = \omega_{\Delta_\infty} = 2$ meV/$\hbar$ and an amplitude that grows like $\sqrt{t}$, see Fig. 6.10(e).

At resonance, the frequency dependence of the pump-probe conductivity $\sigma(\delta t, \omega)$ shows just one sharp edge at $\hbar\omega_{\Delta_\infty} = \hbar\omega_{\mathrm{ph}} = 2$ meV, whose maximum oscillates

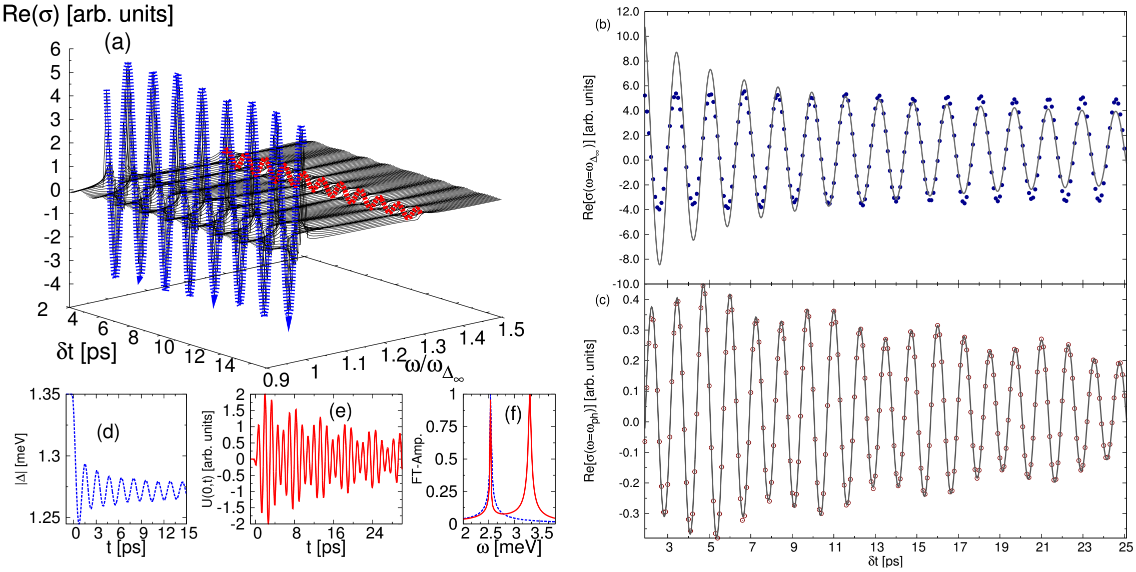

Figure 6.11: (a) Real part of the pump-probe signal, $\mathrm{Re}[\sigma(\delta t, \omega)]$, versus ω and $\delta t > 0$ for the nonadiabatic regime, induced by a pulse with $\tau_0 = 0.5$ ps and $|\mathbf{A}_0| = 7 \cdot 10^{-8}$ Js/(Cm), in the presence of an optical phonon mode with energy $\hbar\omega_{\mathrm{ph}} = 3.3$ meV and coupling strength $g_{\mathrm{ph}} = 0.8$ meV. (b), (c) Pump-probe response $\mathrm{Re}[\sigma(\delta t, \omega)]$ as a function of delay time δt for (b) $\omega = \omega_{\Delta_\infty}$ and (c) $\omega = \omega_{\mathrm{ph}}$. The gray lines in panels (b) and (c) represent the best fits of Eqs. (6.7) and (6.11), respectively, to the numerical data. (d), (e) Time evolution of the order parameter amplitude $|\Delta(t)|$ and the lattice displacement $U(0,t)$, respectively, for the same parameters as in panel (a). (f) Fourier spectra of the order parameter and coherent phonon oscillations depicted as dashed blue and solid red lines, respectively.

as a function of δt, see blue line in Fig. 6.10(a). Remarkably, these oscillations are undamped and their amplitude is considerably larger than in the off-resonant case, compare Fig. 6.8(b) to Fig. 6.10(b). In fact, the δt dependence of $\mathrm{Re}[\sigma(\delta t, \omega)]$ at ω_{Δ_∞} is very well captured by formula (6.9) with $\omega_+ = \omega_{\Delta_\infty}$ and $\omega_- = 0$, as demonstrated by the fits in Fig. 6.10(b).

At absorption energies $\hbar\omega$ different from $\hbar\omega_{\Delta_\infty}$, $\mathrm{Re}[\sigma(\delta t, \omega)]$ shows $1/\sqrt{\delta t}$-decaying oscillations in δt with frequency ω_{Δ_∞}. In Fig. 6.10(c) the delay-time evolution of the conductivity for $\omega \neq \omega_{\Delta_\infty}$ is depicted. It is well described by Eq. (6.7) as the perfect match of the fit shows.

Fig. 6.11 shows the pump probe spectra for a phonon energy larger than the initial gap. Here, a pump pulse with $\tau_0 = 0.5$ ps and $|\mathbf{A}_0| = 7 \cdot 10^{-8}$ Js/(Cm) is used. Further, the phonon energy is set to $\hbar\omega_{\mathrm{ph}} = 3.3$ meV and the coupling strength to $g_{\mathrm{ph}} = 0.8$ meV. As mentioned in Sect. 5.2, the oscillation of the lattice displacement which oscillates with the phonon frequency decays exponentially, whereas the oscillation with ω_{Δ_∞} decays algebraically, see Fig. 6.11(e). This dynamic is also reflected in the pump-probe response as function of delay time. The temporal evolution of the real part of the conductivity $\mathrm{Re}[\sigma(\delta t, \omega)]$ at $\omega = \omega_{\mathrm{ph}}$ shows a decaying oscillations, see Fig. 6.11(c). It is approximately described by

$$\mathrm{Re}[\sigma(\delta t, \omega_{\mathrm{ph}})] = C_1 \exp(-at) \cos(\omega_{\mathrm{ph}} t + \Phi_1) + C_2 t^{-b} \cos(\omega_{\Delta_\infty} t + \Phi_2), \tag{6.11}$$

where $C_1, C_2, \Phi_1, \Phi_2, a$, and b are fit parameters. This function is similar to Eq. (5.27) which describes the evolution of the lattice displacement, see Sect. 5.2. The gray line in Fig. 6.11(c) shows a good agreement of the fit. In addition, the resulting rate $a = 0.03573$ is almost equal to the parameter of the direct lattice displacement fit, see Tab. 5.1.

The delay-time evolution of the conductivity at $\omega = \omega_{\Delta_\infty}$ displays an oscillation with a large amplitude. In addition, this evolution is still described by Eq. (6.7), as demonstrated by the gray lines in Fig. 6.11(b). This is caused by the large coupling strength of $g_{\mathbf{p}} = 0.8\,\mathrm{meV}$ used in the simulation. As it is discussed above in this section, the phonon dynamics influence the dynamics of the quasiparticle densities which are needed to compute $\sigma(\delta t, \omega)$ stronger than the one which are needed to compute Δ. As a consequence, the order parameter is only changed slightly with increasing coupling strength whereas the conductivity shows a huge change.

Adiabatic regime

We contrast the results for the nonadiabatic regime, see Figs. 6.8 - 6.11, with those for the adiabatic case shown in Fig. 6.12(a1). We present the pump-probe signal for a superconductor excited by a long pump pulse with pulse duration $\tau_0 = 20\,\mathrm{ps} \gg \tau_\Delta$. Further, we set $|\mathbf{A}_0| = 0.5 \cdot 10^{-8}$ Js/(Cm), $\hbar\omega_{\mathrm{ph}} = 2$ meV, and $g_{\mathrm{ph}} = 0.1$ meV. As shown in Sect. 5.2 the lattice displacement exhibits large transient oscillations with frequency ω_0 in this regime that occur in the interval $\approx [-\tau_0, +\tau_0]$ while the pump laser acts on the system, see Figs. 6.12(c1) and 6.12(d1). Afterwards, there is only a negligible generation of coherent phonons. The probe signal $\mathrm{Re}[\sigma(\delta t, \omega)]$ is almost featureless as a function of delay time δt. It only displays a sharp edge in the frequency dependence at $\hbar\omega_{\Delta_\infty} = 2\Delta_\infty$ and a small dip just below the pump pulse frequency ω_0 which arises due to Pauli blocking like in the case without phonons. However, since almost no coherent phonons with frequency ω_{ph} are created, $\mathrm{Re}[\sigma(\delta t, \omega)]$ exhibits no feature at the phonon energy $\hbar\omega_{\mathrm{ph}}$, see red line in Fig. 6.12(a1).

For the special case where the pump pulse energy is in resonance with the phonon

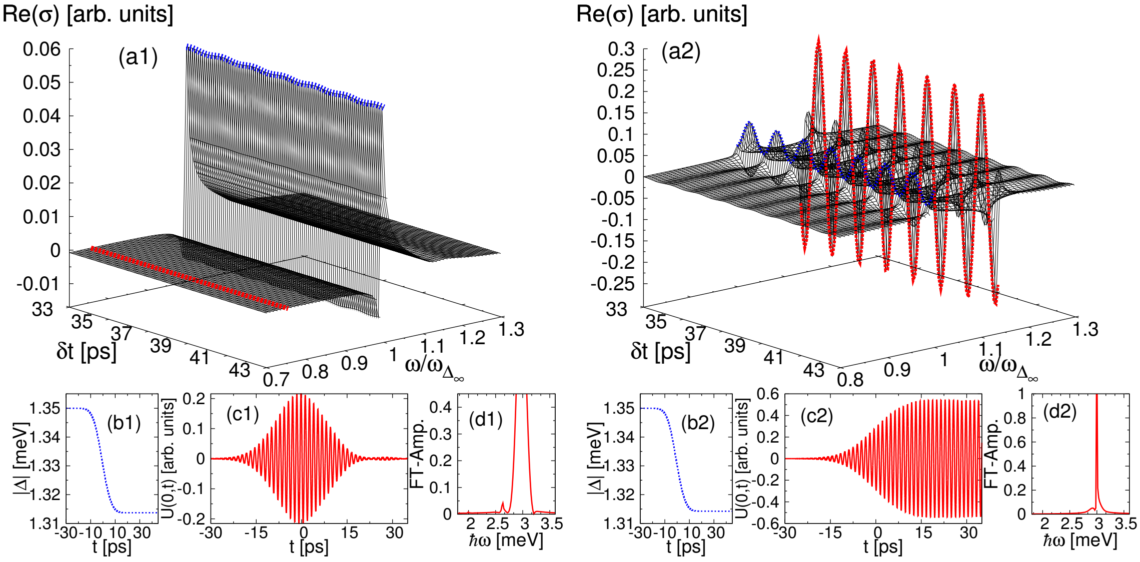

Figure 6.12: Absorption spectrum $\mathrm{Re}[\sigma(\delta t,\omega)]$ versus ω and $\delta t > 0$ for the adiabatic regime, induced by a pump pulse with $\tau_0 = 20$ ps and $|\mathbf{A}_0| = 0.5\cdot 10^{-8}$ Js/(Cm), in the presence of an optical phonon mode with energy $\hbar\omega_{\mathrm{ph}} = 2$ meV (panel a1) or $\hbar\omega_{\mathrm{ph}} = \hbar\omega_0 = 3$ meV (panel a2) and coupling strength $g_{\mathrm{ph}} = 0.1$ meV. (b), (c) Time dependence of the order parameter amplitude $|\Delta(t)|$ and the lattice displacement $U(0,t)$, respectively, for the same parameters as in panel (a). (d) Spectral distribution of the coherent phonon oscillations.

energy, i.e., $\hbar\omega_{\mathrm{p}} = \hbar\omega_{\mathrm{ph}}$, the resonant pumping of the phonon leads to undamped coherent phonon oscillations which persist even after the pump pulse has finished, see Fig. 6.12(c2). This feature is also reflected in the pump probe response. The real part of the pump-probe signal $\mathrm{Re}[\sigma(\delta t,\omega)]$ is presented in Fig. 6.12(a2). Except of the phonon energy we use the same parameter as in Fig 6.12(a1). It shows an enhanced oscillatory behavior in the delay-time dependence of the absorption spectrum $\mathrm{Re}[\sigma(\delta t,\omega)]$ at the phonon frequency ω_{ph}, see red curve in Fig 6.12(a2). In addition, the edge at $\omega = \omega_{\Delta_\infty}$, see blue curves, shows an oscillation as a function of δt. Due to the enhanced phonon dynamics, the influence on the quasiparticle dynamics is larger compared to the off-resonance case, see Fig. 6.12(a1). As already discussed the conductivity is more sensitive to the phonon dynamics than the order parameter.

We shortly conclude, the conductivity as function of positive delay time shows clear signatures which reflect the dynamics of the coherent phonons. The information about the evolution of the lattice displacement is encoded in delay-time evolution of the conductivity at the phonon frequency $\sigma(\delta t,\omega_{\mathrm{ph}})$. It shows for example the same beating phenomena as the lattice displacement.

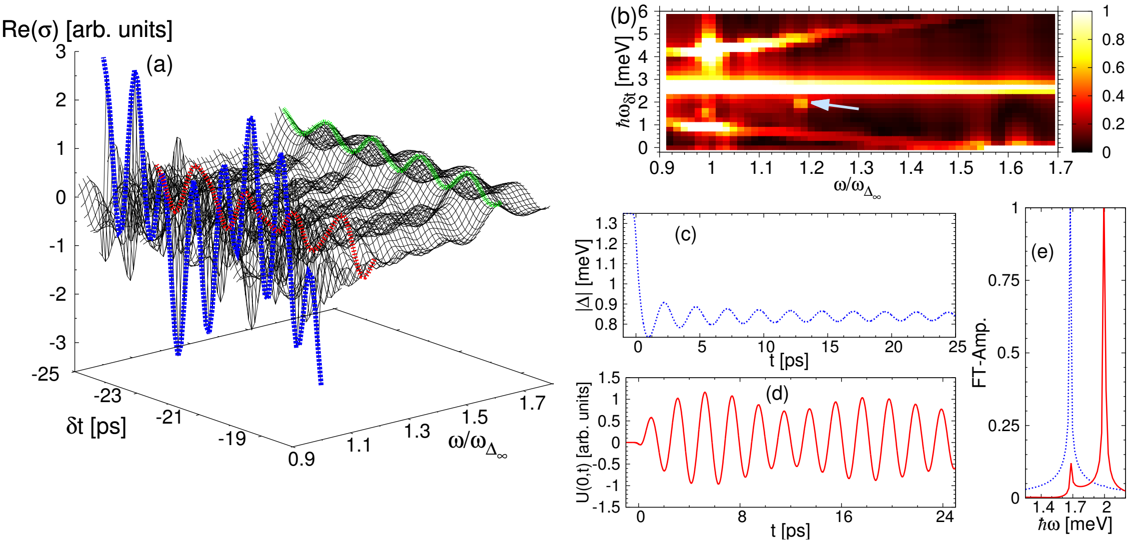

Figure 6.13: (a) Real part of the pump-probe signal, $\mathrm{Re}[\sigma(\delta t, \omega)]$, versus ω and $\delta t < 0$ for the nonadiabatic regime and negative delay time, induced by a pump pulse with $\tau_0 = 0.5$ ps and $|\mathbf{A}_0| = 13 \cdot 10^{-8}$ Js/(Cm), in the presence of a phonon mode with energy $\hbar\omega_{\mathrm{ph}} = 2$ meV $\approx 1.19\,\hbar\omega_{\Delta_\infty}$ and coupling strength $g_{\mathrm{ph}} = 0.1$ meV. (b) Fourier transform of the data in panel (a), i.e., $\mathrm{Re}(\sigma)$ as a function of Fourier frequency $\omega_{\delta t}$ and absorption frequency ω. (c), (d) Time dependence of the order parameter amplitude $|\Delta(t)|$ and the lattice displacement $U(0,t)$, respectively, for the same parameters as in panel (a). (e) Spectral distribution of the order parameter and coherent phonon oscillations as dashed blue and solid red lines, respectively.

The pump probe response can be amplified if the phonon frequency and the order parameter oscillation frequency are in resonance. In this case, the conductivity shows an oscillation with ω_{Δ_∞} and a larger amplitude. This feature can be use to improve the resolution of an experimental measurement.

Another interesting feature is observed in the adiabatic case if $\omega_0 = \omega_{\mathrm{ph}}$. In this case, the conductivity shows a clear oscillation as function of delay time reflecting the enhanced lattice displacement. But as already mentioned, due to the fact that there is no explicit light-phonon coupling taken into account, the results of this case have to be treated with care.

6.4.2 Negative delay time

Nonadiabatic regime

In Fig. 6.13(a), the real part of the pump-probe signal is plotted versus negative delay time δt and frequency ω for a short pump pulse with $\tau_0 = 0.5$ ps and $|\mathbf{A}_0| = 13 \cdot 10^{-8}$

Js/(Cm). In addition we set $\hbar\omega_{\mathrm{ph}} = 2$ meV and $g_{\mathrm{ph}} = 0.1$ meV.

Similar to the case without phonons in Fig. 6.5(a), we observe two sharp edges in the frequency dependence of $\mathrm{Re}[\sigma(\delta t, \omega)]$, one at twice the energy of the asymptotic gap value $\hbar\omega_{\Delta_\infty} = 1.677$ meV and another smaller one at twice the gap energy of the unperturbed superconductor $\hbar\omega_{\Delta_0} = 2\Delta_0 = 2.7$ meV. They are depicted by the blue and green lines in Fig. 6.13(a). In addition, a third edge appears at the phonon frequency $\hbar\omega_{\mathrm{ph}} \approx 1.19\hbar\omega_{\Delta_\infty}$, indicated by the red line in Fig. 6.13(a). As function of delay time the pump-probe signal shows an intricate oscillatory behavior, which reflects the nonadiabatic dynamics of both the Bogoliubov quasiparticle and phonon subsystems. The spectral distribution of these oscillations in δt is depicted in Fig. 6.13(b). It is quite similar to the one without phonons, for comparison see Fig. 6.5. For absorption frequencies ω within the interval $\omega_{\Delta_\infty} < \omega < \omega_{\Delta_0}$, $\mathrm{Re}[\sigma(\delta t, \omega)]$ oscillates in general with three different frequencies, approximately given by ω_{Δ_0}, $\omega_{\Delta_0} + \omega$, and $\omega_{\Delta_0} - \omega$. The oscillations with $\omega_{\Delta_0} \pm \omega$ in this interval reflect how the absolute value of the order parameter reduces during the pump pulse. The oscillation with $\omega_{\Delta_0} = \frac{2\Delta_0}{\hbar}$ reflects the initial value of the order parameter.

The Fourier spectrum of $\mathrm{Re}[\sigma(\delta t, \omega)]$ at the absorption energy $\omega = \omega_{\mathrm{ph}}$ also shows a peak at the phonon energy $\hbar\omega_{\mathrm{ph}} = 2$ meV, see white arrow in Fig. 6.13(b). The oscillation with ω_{ph} of $\sigma(\delta t, \omega_{\mathrm{ph}})$ is a signature of the dynamics of the lattice displacement.

Adiabatic regime

The real part of the conductivity versus negative delay time δt and frequency ω for the adiabatic regime is depicted in Fig. 6.14. Here, we use $\tau_0 = 20$ ps, $|\mathbf{A}_0| = 0.5{\cdot}10^{-8}$ Js/(Cm), $\hbar\omega_{\mathrm{ph}} = 2$ meV, and $g_{\mathrm{ph}} = 0.1$ meV. As for the case without phonons, see Fig. 6.6, two sharp edges in the frequency dependence at $\omega = \omega_{\Delta_\infty}$ and $\omega = \omega_{\Delta_0}$ can be observed, see blue and green curves in Fig. 6.14. Just as the conductivity for positive delay time, the conductivity shows no edge at $\omega = \omega_{\mathrm{ph}}$ in the adiabatic regime. As a function of delay time the pump-probe response oscillates in the frequency interval $\omega_{\Delta_\infty} < \omega < \omega_{\Delta_0}$, which reflects the dynamics of the Bogoliubov quasiparticles, as the Fourier transform in Fig. 6.14(b) shows. The conductivity oscillates with $\omega_{\Delta_0} - \omega$ in this interval. It reflects how the gap reduces during the pump pulse. In addition, even a signature of the large transient oscillation appears in the δt dependence of $\mathrm{Re}[\sigma(\delta t, \omega)]$. At the absorption frequency $\omega = \omega_0$ an oscillation with frequency ω_0 is visible, see white arrow in Fig. 6.14(b).

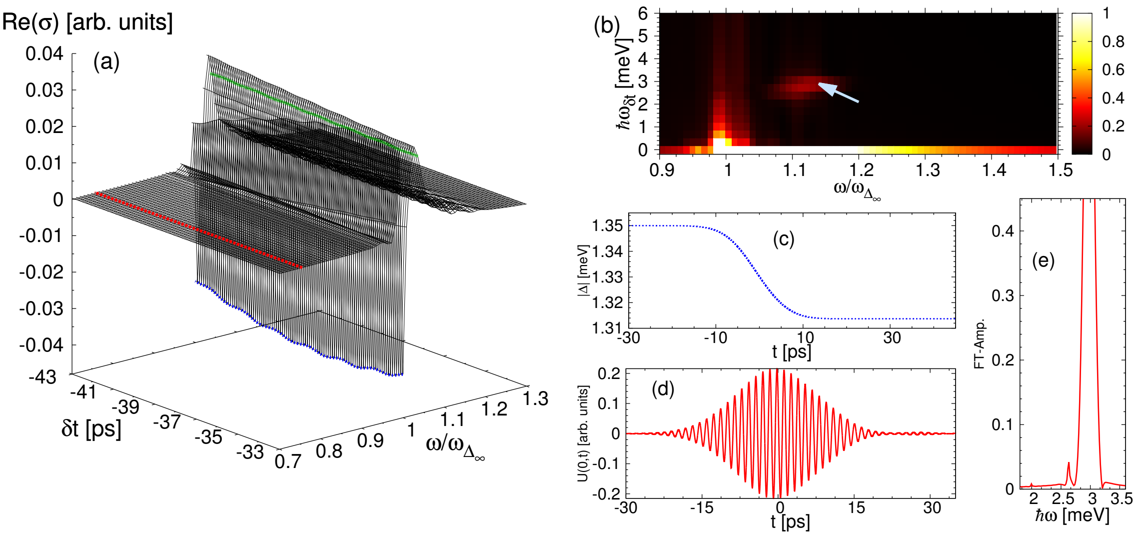

Figure 6.14: (a) Real part of the pump-probe signal, $\mathrm{Re}[\sigma(\delta t,\omega)]$, versus ω and $\delta t < 0$ for the adiabatic regime, induced by a pulse with $\tau_0 = 20$ ps and $|\mathbf{A}_0| = 0.5\cdot 10^{-8}$ Js/(Cm), in the presence of a phonon mode with energy $\hbar\omega_{\mathrm{ph}} = 2$ meV, coupling strength $g_{\mathrm{ph}} = 0.1$ meV, and negative delay time. (b) Fourier transform of the data in panel (a), i.e., $\mathrm{Re}(\sigma)$ as a function of Fourier frequency $\omega_{\delta t}$ and absorption frequency ω. (c), (d) Time dependence of the order parameter amplitude $|\Delta(t)|$ and the lattice displacement $U(0,t)$, respectively, for the same parameters as in panel (a). (e) Spectral distribution of coherent phonon oscillations.

As for the case without phonons, the conductivity for negative delay times provides information about the dynamics of the system before, during, and after the pump pulse. In contrast, the conductivity for positive delay times shows only signatures of the dynamics after the pump pulse.

The conductivity for negative delay times reveals the same signatures such as the one without phonons. In addition the δt evolution of the conductivity at the phonon frequency reflects also the dynamics of the lattice displacement. Especially, the transient oscillation of the lattice displacement in the adiabatic regime is reflected in the conductivity for negative delay times. This features is not visible in the conductivity with positive delay time, because it only appears during the pump pulse.

7 Conclusions and Outlook

7.1 Conclusions

In this thesis, we used the density matrix formalism to simulate the nonequilibrium dynamics of a s-wave BCS superconductor with or without coupled additional phonons. We simulated the temporal evolution of both the quasiparticle and the phonon subsystems. Thereto, we considered different pump pulses, e.g., varying the pulse width and intensity, and different phonon modes, e.g. varying the phonon energy.

All considered pump pulses excite quasiparticle and consequently leads to a lowering of the absolute value of the order parameter during the pump pulse. The temporal evolution of the order parameter afterwards depdens on the pump pulse width. Short pulses excite oscillations of the quasiparticle densities resulting in oscillations of the order parameter. These oscillations display an algebraic $\frac{1}{\sqrt{t}}$ decay. The frequency of the order parameter oscillation $\omega_{\Delta_\infty} = \frac{2\Delta_\infty}{\hbar}$ depends on the pump pulse intensity as well as on the amplitude. In contrast, the order parameter stays almost constant after large pulses.

The dynamics of the quasiparticle densities generate coherent phonons. The generation of coherent phonons is essentially described by a driven oscillator. The corresponding driving force is a function of the Bogoliubov quasiparticle expectation values. We have shown, that coherent phonons are generated most efficiently if the phonon frequency ω_{ph} and frequency of the order parameter oscillation ω_{Δ_∞} are near or at resonance. In the near resonance case, a beating phenomenon is observed in the lattice displacement. At resonance the lattice oscillations are enhanced showing a $\sqrt{t}$-increase. If the phonon energy lies in the interval $0 < \hbar\omega_{\mathrm{ph}} < 2\Delta_0$ we can bring the system into resonance by adjusting the pump pulse intensity. Coherent phonons are mostly generated in the nonadiabatic regime, e.g. short pulses, because a short pulse excite oscillation of the quasiparticle densities. If the phonon energy is larger than the gap it should be possible that a phonon decays into a quasiparticle-hole pair. Also this phenomenon was observed in this thesis. We showed that the oscillation of the lattice displacement which oscillates with the phonon frequency is exponentially decaying. The decay rate increases with the coupling strength with $a \propto g_{\mathrm{ph}}$, which is in perfect agreement with Fermi's golden rule.

In order to study relaxation we include electron-phonon and electron-electron scattering processes into the simulation. However, these simulations resulted in unphysical results. We observed negative phonon densities. The origin of these unphysical results was discussed, e.g. uncertainties of the correlation expansion and the fact that the initial state is not the true groundstate.

In addition to the pump response, e.g. $\Delta(t)$, the pump-probe conductivity was simulated. This allows a direct comparison between experiments and theoretical predictions. We have shown, that the pump pulse absorption spectrum as a function of positive and negative delay times shows clear signatures of the dynamics of both the quasiparticle and the phonon subsystems.

For positive delay times, the absorption spectrum exhibits algebraically decaying oscillations in δt with the same frequency as the order parameter oscillations. This is most visible at twice the frequency of the asymptotic gap value, where the conductivity as function of ω shows a sharp edge. If also phonons are included, the conductivity as function of δt shows the coherent dynamics of the phonons at the phonon frequency. Near resonance the conductivity at ω_{ph} shows a beating phenomenon as a function of δt in the absorption spectrum, as the lattice displacement does. Interestingly, this oscillatory response in the probe spectra can be strongly amplified by tuning the frequency of the order parameter oscillations into resonance with the phonon energy. The above mentioned decay of the lattice displacement of the case $\hbar\omega_{\text{ph}} > 2\Delta_0$ is reflected in the pump probe response at $\omega = \omega_{\text{ph}}$. The temporal evolution of $\sigma(\delta t, \omega_{\text{ph}})$ shows the same dynamics as $U(0,t)$, namely an exponential damping of the oscillation with ω_{ph} and an algebraically decay of the oscillation with ω_{Δ_∞}.

For negative delay times, the pump-probe signal shows an even richer oscillatory response in the delay-time dependence, with multiple frequencies that change as a function of absorption energy. This intricate behavior contains information on how the superconducting condensate is depleted while the pump pulse acts on the sample.

In addition, our theoretical findings are qualitatively consistent with recent pump-probe experiments by Matsunaga *et al.* [6], who have observed order parameter oscillations in the pump-probe conductivity of $\text{Nb}_{1-x}\text{Ti}_x\text{N}$ thin films. They observed oscillation in the conductivity as function of delay time suggesting the oscillation of the order parameter. Our studies show that these oscillation are in fact signatures of the order parameter oscillation.

7.2 Outlook

In this thesis, we perform the simulation in the collisionless regime only, i.e. processes which lead to relaxation are not taken into account. However, relaxation takes place as can be seen in experiments [8]. The relaxation processes remain as an important direction for future research. However, the DMF approach as performed in this thesis is not able to describe relaxation due to unphysical negative densities in the higher order of the expansion. Thus, one is forced either to modify the truncation scheme of the DMF or to use a new method. One candidate is the iterated equation of motion approach. For the presented toy model, the iEoM approach leads to reliable results. In addition, the rising negative phonon densities of the DMF approach are impossible in the iEoM. This is due to the fact, that in this approach the phonon densites are computed by multiplying an operator $b_{\mathrm{ph}}(t)$ with its Hermitian conjugate $b^{\dagger}_{\mathrm{ph}}(t)$. Due to this we get a positive number. These are good reasons to try the iEoM approach for the nonequilibrium dynamics of superconductors. However, the numerical effort is much larger compared to DMF approach. Due to the explicit time dependent Hamiltonian, the operator ansatz and the Hamiltonian become more complicated resulting in more complicated equations of motion.

Beside the relaxation processes other investigations are also of large interest, for example the computation of the pump-probe response of multiband superconductors [95], e.g. iron-based superconductors [96] and MgB_2 [97]. The pump response, e.g. $\Delta(t)$, of such superconductors is already studied in terms of the DMF approach by Akbari *et al.* [34]. With the knowledge of the conductivity, one can compare the recent experimental findings [98, 99] to the theoretically predictions.

In this thesis, we concentrate only on the standard s-wave BCS superconductors, but the nonequilibrium dynamics of high T_c superconductors [100] is also very interesting. For example, one can study the nonequilibrium dynamics of d-wave superconductors. How the order parameter behaves after a nonadiabatic perturbation is an interesting question. Does it oscillate? If yes, what is the frequency of the oscillation and how does the oscillation decay? Certainly, due to the $\mathbf{k}$-dependence of the d-wave order parameter it is no longer valid to use a quasi one dimensional mesh for the simulation. As a results a two dimensional mesh has to be used. If we want to use pump pulse to bring the system out of equilibrium, the numerical effort increases drastically. A quench is suited for a first test, because it is numerically less costly. In addition, a quench induce the same dynamics as a short pump pulse as has been shown for the s-wave superconductor.

In spite of the recent developments on the experimental and on the theoretical side, the field of nonequilibrium dynamics of superconductors is at its infancy. As the outlook shows, there are still a lot of open questions. Consequently, it is still a long journey to the complete understanding of the nonequilibrium dynamics of superconductors, but the first steps are made.

Appendix

A Equations of motion

A.1 Decomposition

In order to apply the correlation expansion we have factorized the higher order density matrices. For the first order of this expansion the phonon assisted quantities have to be factorized, e.g.

$$\left\langle \alpha^\dagger_{\mathbf{k}} \alpha_{\mathbf{q}} b_{\mathbf{p}} \right\rangle = \left\langle \alpha^\dagger_{\mathbf{k}} \alpha_{\mathbf{q}} b_{\mathbf{p}} \right\rangle^c + \left\langle \alpha^\dagger_{\mathbf{k}} \alpha_{\mathbf{q}} \right\rangle \left\langle b_{\mathbf{p}} \right\rangle . \tag{A.1}$$

For the next order new expectation values including four operators have to factorized. The decomposition are given in this section.
First, the expectation values including only fermionic operators are decomposed:

$$\left\langle \alpha^\dagger_{\mathbf{k}} \beta^\dagger_{\mathbf{q}} \alpha^\dagger_{\mathbf{p}} \alpha_{\mathbf{r}} \right\rangle = \left\langle \alpha^\dagger_{\mathbf{k}} \beta^\dagger_{\mathbf{q}} \alpha^\dagger_{\mathbf{p}} \alpha_{\mathbf{r}} \right\rangle^c + \left\langle \alpha^\dagger_{\mathbf{k}} \beta^\dagger_{\mathbf{q}} \right\rangle \left\langle \alpha^\dagger_{\mathbf{p}} \alpha_{\mathbf{r}} \right\rangle - \left\langle \alpha^\dagger_{\mathbf{p}} \beta^\dagger_{\mathbf{q}} \right\rangle \left\langle \alpha^\dagger_{\mathbf{k}} \alpha_{\mathbf{r}} \right\rangle \tag{A.2a}$$

$$\left\langle \alpha^\dagger_{\mathbf{k}} \beta^\dagger_{\mathbf{q}} \beta^\dagger_{\mathbf{r}} \beta_{\mathbf{p}} \right\rangle = \left\langle \alpha^\dagger_{\mathbf{k}} \beta^\dagger_{\mathbf{q}} \beta^\dagger_{\mathbf{r}} \beta_{\mathbf{p}} \right\rangle^c + \left\langle \alpha^\dagger_{\mathbf{k}} \beta^\dagger_{\mathbf{q}} \right\rangle \left\langle \beta^\dagger_{\mathbf{r}} \beta_{\mathbf{p}} \right\rangle - \left\langle \alpha^\dagger_{\mathbf{k}} \beta^\dagger_{\mathbf{r}} \right\rangle \left\langle \beta^\dagger_{\mathbf{q}} \beta_{\mathbf{p}} \right\rangle \tag{A.2b}$$

$$\left\langle \alpha^\dagger_{\mathbf{k}} \beta^\dagger_{\mathbf{q}} \beta_{\mathbf{p}} \alpha_{\mathbf{r}} \right\rangle = \left\langle \alpha^\dagger_{\mathbf{k}} \beta^\dagger_{\mathbf{q}} \beta_{\mathbf{p}} \alpha_{\mathbf{r}} \right\rangle^c + \left\langle \alpha^\dagger_{\mathbf{k}} \beta^\dagger_{\mathbf{q}} \right\rangle \left\langle \beta_{\mathbf{p}} \alpha_{\mathbf{r}} \right\rangle + \left\langle \alpha^\dagger_{\mathbf{k}} \alpha_{\mathbf{r}} \right\rangle \left\langle \beta^\dagger_{\mathbf{q}} \beta_{\mathbf{p}} \right\rangle \tag{A.2c}$$

$$\left\langle \alpha^\dagger_{\mathbf{k}} \beta^\dagger_{\mathbf{q}} \alpha^\dagger_{\mathbf{p}} \beta^\dagger_{\mathbf{r}} \right\rangle = \left\langle \alpha^\dagger_{\mathbf{k}} \beta^\dagger_{\mathbf{q}} \alpha^\dagger_{\mathbf{p}} \beta^\dagger_{\mathbf{r}} \right\rangle^c + \left\langle \alpha^\dagger_{\mathbf{k}} \beta^\dagger_{\mathbf{q}} \right\rangle \left\langle \alpha^\dagger_{\mathbf{p}} \beta^\dagger_{\mathbf{r}} \right\rangle - \left\langle \alpha^\dagger_{\mathbf{p}} \beta^\dagger_{\mathbf{q}} \right\rangle \left\langle \alpha^\dagger_{\mathbf{k}} \beta^\dagger_{\mathbf{r}} \right\rangle \tag{A.2d}$$

$$\left\langle \beta_{\mathbf{k}} \alpha_{\mathbf{q}} \alpha^\dagger_{\mathbf{p}} \alpha_{\mathbf{r}} \right\rangle = \left\langle \beta_{\mathbf{k}} \alpha_{\mathbf{q}} \alpha^\dagger_{\mathbf{p}} \alpha_{\mathbf{r}} \right\rangle^c + \left\langle \beta_{\mathbf{k}} \alpha_{\mathbf{q}} \right\rangle \left\langle \alpha^\dagger_{\mathbf{p}} \alpha_{\mathbf{r}} \right\rangle + \left\langle \beta_{\mathbf{k}} \alpha_{\mathbf{r}} \right\rangle \left(\delta_{\mathbf{p},\mathbf{q}} - \left\langle \alpha^\dagger_{\mathbf{p}} \alpha_{\mathbf{q}} \right\rangle\right) \tag{A.2e}$$

$$\left\langle \beta_{\mathbf{k}} \alpha_{\mathbf{q}} \beta^\dagger_{\mathbf{r}} \beta_{\mathbf{p}} \right\rangle = \left\langle \beta_{\mathbf{k}} \alpha_{\mathbf{q}} \beta^\dagger_{\mathbf{r}} \beta_{\mathbf{p}} \right\rangle^c + \left\langle \beta_{\mathbf{k}} \alpha_{\mathbf{q}} \right\rangle \left\langle \beta^\dagger_{\mathbf{r}} \beta_{\mathbf{p}} \right\rangle + \left\langle \beta_{\mathbf{p}} \alpha_{\mathbf{q}} \right\rangle \left(\delta_{\mathbf{r},\mathbf{k}} - \left\langle \beta^\dagger_{\mathbf{r}} \beta_{\mathbf{k}} \right\rangle\right) \tag{A.2f}$$

$$\begin{aligned} \left\langle \beta_{\mathbf{k}} \alpha_{\mathbf{q}} \alpha^\dagger_{\mathbf{p}} \beta^\dagger_{\mathbf{r}} \right\rangle = {} & \left\langle \beta_{\mathbf{k}} \alpha_{\mathbf{q}} \alpha^\dagger_{\mathbf{p}} \beta^\dagger_{\mathbf{r}} \right\rangle^c + \left\langle \beta_{\mathbf{k}} \alpha_{\mathbf{q}} \right\rangle \left\langle \alpha^\dagger_{\mathbf{p}} \beta^\dagger_{\mathbf{r}} \right\rangle \\ & + \left(\delta_{\mathbf{k},\mathbf{r}} - \left\langle \beta^\dagger_{\mathbf{r}} \beta_{\mathbf{k}} \right\rangle\right)\left(\delta_{\mathbf{q},\mathbf{p}} - \left\langle \alpha^\dagger_{\mathbf{p}} \alpha_{\mathbf{q}} \right\rangle\right) \end{aligned} \tag{A.2g}$$

$$\left\langle \alpha^\dagger_{\mathbf{k}} \alpha_{\mathbf{q}} \alpha^\dagger_{\mathbf{p}} \alpha_{\mathbf{r}} \right\rangle = \left\langle \alpha^\dagger_{\mathbf{k}} \alpha_{\mathbf{q}} \alpha^\dagger_{\mathbf{p}} \alpha_{\mathbf{r}} \right\rangle^c + \left\langle \alpha^\dagger_{\mathbf{k}} \alpha_{\mathbf{q}} \right\rangle \left\langle \alpha^\dagger_{\mathbf{p}} \alpha_{\mathbf{r}} \right\rangle + \left\langle \alpha^\dagger_{\mathbf{k}} \alpha_{\mathbf{r}} \right\rangle \left(\delta_{\mathbf{p},\mathbf{q}} - \left\langle \alpha^\dagger_{\mathbf{p}} \alpha_{\mathbf{q}} \right\rangle\right) \tag{A.2h}$$

$$\left\langle \alpha^\dagger_{\mathbf{k}} \alpha_{\mathbf{q}} \beta^\dagger_{\mathbf{r}} \beta_{\mathbf{p}} \right\rangle = \left\langle \alpha^\dagger_{\mathbf{k}} \alpha_{\mathbf{q}} \beta^\dagger_{\mathbf{r}} \beta_{\mathbf{p}} \right\rangle^c + \left\langle \alpha^\dagger_{\mathbf{k}} \alpha_{\mathbf{q}} \right\rangle \left\langle \beta^\dagger_{\mathbf{r}} \beta_{\mathbf{p}} \right\rangle + \left\langle \alpha^\dagger_{\mathbf{k}} \beta^\dagger_{\mathbf{r}} \right\rangle \left\langle \beta_{\mathbf{p}} \alpha_{\mathbf{q}} \right\rangle \tag{A.2i}$$

$$\left\langle \beta^\dagger_{\mathbf{q}} \beta_{\mathbf{k}} \beta^\dagger_{\mathbf{r}} \beta_{\mathbf{p}} \right\rangle = \left\langle \beta^\dagger_{\mathbf{q}} \beta_{\mathbf{k}} \beta^\dagger_{\mathbf{r}} \beta_{\mathbf{p}} \right\rangle^c + \left\langle \beta^\dagger_{\mathbf{q}} \beta_{\mathbf{k}} \right\rangle \left\langle \beta^\dagger_{\mathbf{r},\mathbf{p}} \beta_{+} \right\rangle \left\langle \beta^\dagger_{\mathbf{q}} \beta_{\mathbf{p}} \right\rangle \left(\delta_{\mathbf{r},\mathbf{k}} - \left\langle \beta^\dagger_{\mathbf{r}} \beta_{\mathbf{k}} \right\rangle\right) \tag{A.2j}$$

Second, the expectation values including two fermionic and two bosonic operators are decomposed:

$$\begin{aligned}\left\langle \alpha^\dagger_{\mathbf{k}} \beta^\dagger_{\mathbf{q}} b_{\mathbf{p}} b_{\mathbf{r}} \right\rangle &= \left\langle \alpha^\dagger_{\mathbf{k}} \beta^\dagger_{\mathbf{q}} b_{\mathbf{p}} b_{\mathbf{r}} \right\rangle^c + \left\langle \alpha^\dagger_{\mathbf{k}} \beta^\dagger_{\mathbf{q}} b_{\mathbf{r}} \right\rangle^c \left\langle b_{\mathbf{p}} \right\rangle + \left\langle \alpha^\dagger_{\mathbf{k}} \beta^\dagger_{\mathbf{q}} b_{\mathbf{p}} \right\rangle^c \left\langle b_{\mathbf{r}} \right\rangle \\ &\quad + \left\langle \alpha^\dagger_{\mathbf{k}} \beta^\dagger_{\mathbf{q}} \right\rangle \left(\left\langle b_{\mathbf{p}} \right\rangle \left\langle b_{\mathbf{r}} \right\rangle + \left\langle b_{\mathbf{p}} b_{\mathbf{r}} \right\rangle^c \right)\end{aligned} \tag{A.3a}$$

$$\begin{aligned}\left\langle \beta_{\mathbf{k}} \alpha_{\mathbf{q}} b_{\mathbf{p}} b_{\mathbf{r}} \right\rangle &= \left\langle \beta_{\mathbf{k}} \alpha_{\mathbf{q}} b_{\mathbf{p}} b_{\mathbf{r}} \right\rangle^c + \left\langle \alpha^\dagger_{\mathbf{k}} \beta^\dagger_{\mathbf{q}} b^\dagger_{\mathbf{r}} \right\rangle^c \left\langle b_{\mathbf{p}} \right\rangle + \left\langle \alpha^\dagger_{\mathbf{k}} \beta^\dagger_{\mathbf{q}} b^\dagger_{\mathbf{p}} \right\rangle^c \left\langle b_{\mathbf{r}} \right\rangle \\ &\quad + \left\langle \beta_{\mathbf{k}} \alpha_{\mathbf{q}} \right\rangle \left(\left\langle b_{\mathbf{p}} \right\rangle \left\langle b_{\mathbf{r}} \right\rangle + \left\langle b_{\mathbf{p}} b_{\mathbf{r}} \right\rangle^c \right)\end{aligned} \tag{A.3b}$$

$$\begin{aligned}\left\langle \beta^\dagger_{\mathbf{q}} \beta_{\mathbf{k}} b_{\mathbf{p}} b_{\mathbf{r}} \right\rangle &= \left\langle \beta^\dagger_{\mathbf{q}} \beta_{\mathbf{k}} b_{\mathbf{p}} b_{\mathbf{r}} \right\rangle^c + \left\langle \beta^\dagger_{\mathbf{q}} \beta_{\mathbf{k}} b_{\mathbf{r}} \right\rangle^c \left\langle b_{\mathbf{p}} \right\rangle + \left\langle \beta^\dagger_{\mathbf{q}} \beta_{\mathbf{k}} b_{\mathbf{p}} \right\rangle^c \left\langle b_{\mathbf{r}} \right\rangle \\ &\quad + \left\langle \beta^\dagger_{\mathbf{q}} \beta_{\mathbf{k}} \right\rangle \left(\left\langle b_{\mathbf{p}} \right\rangle \left\langle b_{\mathbf{r}} \right\rangle + \left\langle b_{\mathbf{p}} b_{\mathbf{r}} \right\rangle^c \right)\end{aligned} \tag{A.3c}$$

$$\begin{aligned}\left\langle \alpha^\dagger_{\mathbf{k}} \alpha_{\mathbf{q}} b_{\mathbf{p}} b_{\mathbf{r}} \right\rangle &= \left\langle \alpha^\dagger_{\mathbf{k}} \alpha_{\mathbf{q}} b_{q} b_{\mathbf{r}} \right\rangle^c + \left\langle \alpha^\dagger_{\mathbf{k}} \alpha_{\mathbf{q}} b_{\mathbf{r}} \right\rangle^c \left\langle b_{\mathbf{p}} \right\rangle + \left\langle \alpha^\dagger_{\mathbf{k}} \alpha_{\mathbf{q}} b_{\mathbf{p}} \right\rangle^c \left\langle b_{\mathbf{r}} \right\rangle \\ &\quad + \left\langle \alpha^\dagger_{\mathbf{k}} \alpha_{\mathbf{q}} \right\rangle \left(\left\langle b_{\mathbf{p}} \right\rangle \left\langle b_{\mathbf{r}} \right\rangle + \left\langle b_{\mathbf{p}} b_{\mathbf{r}} \right\rangle^c \right)\end{aligned} \tag{A.3d}$$

$$\begin{aligned}\left\langle \alpha^\dagger_{\mathbf{k}} \beta^\dagger_{\mathbf{q}} b^\dagger_{\mathbf{p}} b_{\mathbf{r}} \right\rangle &= \left\langle \alpha^\dagger_{\mathbf{k}} \beta^\dagger_{\mathbf{q}} b^\dagger_{\mathbf{p}} b_{\mathbf{r}} \right\rangle^c + \left\langle \alpha^\dagger_{\mathbf{k}} \beta^\dagger_{\mathbf{q}} b_{\mathbf{r}} \right\rangle^c \left\langle b^\dagger_{\mathbf{p}} \right\rangle + \left\langle \beta_{\mathbf{k}} \alpha_{\mathbf{q}} b_{\mathbf{p}} \right\rangle \left\langle b_{\mathbf{r}} \right\rangle \\ &\quad + \left\langle \alpha^\dagger_{\mathbf{k}} \beta^\dagger_{\mathbf{q}} \right\rangle \left(\left\langle b^\dagger_{\mathbf{p}} \right\rangle \left\langle b_{\mathbf{r}} \right\rangle + \left\langle b^\dagger_{\mathbf{p}} b_{\mathbf{r}} \right\rangle^c \right)\end{aligned} \tag{A.3e}$$

$$\begin{aligned}\left\langle \beta^\dagger_{\mathbf{q}} \beta_{\mathbf{k}} b^\dagger_{\mathbf{p}} b_{\mathbf{r}} \right\rangle &= \left\langle \beta^\dagger_{\mathbf{q}} \beta_{\mathbf{k}} b^\dagger_{\mathbf{p}} b_{\mathbf{r}} \right\rangle^c + \left\langle \beta^\dagger_{\mathbf{q}} \beta_{\mathbf{k}} b_{\mathbf{r}} \right\rangle^c \left\langle b^\dagger_{\mathbf{p}} \right\rangle + \left\langle \beta^\dagger_{\mathbf{q}} \beta_{\mathbf{k}} b^\dagger_{\mathbf{p}} \right\rangle^c \left\langle b_{\mathbf{r}} \right\rangle \\ &\quad + \left\langle \beta^\dagger_{\mathbf{q}} \beta_{\mathbf{k}} \right\rangle \left(\left\langle b^\dagger_{\mathbf{p}} \right\rangle \left\langle b_{\mathbf{r}} \right\rangle + \left\langle b^\dagger_{\mathbf{p}} b_{\mathbf{r}} \right\rangle^c \right)\end{aligned} \tag{A.3f}$$

$$\begin{aligned}\left\langle \alpha^\dagger_{\mathbf{k}} \alpha_{\mathbf{q}} b^\dagger_{\mathbf{p}} b_{\mathbf{r}} \right\rangle &= \left\langle \alpha^\dagger_{\mathbf{k}} \alpha_{\mathbf{q}} b^\dagger_{\mathbf{p}} b_{\mathbf{r}} \right\rangle^c + \left\langle \alpha^\dagger_{\mathbf{k}} \alpha_{\mathbf{q}} b_{\mathbf{r}} \right\rangle^c \left\langle b^\dagger_{\mathbf{p}} \right\rangle + \left\langle \alpha^\dagger_{\mathbf{k}} \alpha_{\mathbf{q}} b^\dagger_{\mathbf{p}} \right\rangle^c \left\langle b_{p} \right\rangle \\ &\quad + \left\langle \alpha^\dagger_{\mathbf{k}} \alpha_{\mathbf{q}} \right\rangle \left(\left\langle b^\dagger_{\mathbf{p}} \right\rangle \left\langle b_{\mathbf{r}} \right\rangle + \left\langle b^\dagger_{\mathbf{p}} b_{\mathbf{r}} \right\rangle^c \right)\end{aligned} \tag{A.3g}$$

A.2 Equations of motion

In this section the remaining equations of motion, which are not shown in the main text, are presented.

$$i\hbar\frac{\mathrm{d}}{\mathrm{d}t}\left\langle\beta^\dagger_{\mathbf{k}'}\beta_{\mathbf{k}}\right\rangle = (R_{\mathbf{k}} - R_{\mathbf{k}'})\left\langle\beta^\dagger_{\mathbf{k}'}\beta_{\mathbf{k}}\right\rangle + C_{\mathbf{k}}\left\langle\alpha^\dagger_{\mathbf{k}}\beta^\dagger_{\mathbf{k}'}\right\rangle - C^*_{\mathbf{k}'}\left\langle\beta_{\mathbf{k}}\alpha_{\mathbf{k}'}\right\rangle \tag{A.4a}$$

$$+\frac{e\hbar}{2m}\sum_{\mathbf{q}'=\pm\mathbf{q}_0} 2\mathbf{k}\mathbf{A}_{\mathbf{q}'}\Bigg(- L^+_{\mathbf{k},\mathbf{q}'}\left\langle\beta^\dagger_{\mathbf{k}'}\beta_{\mathbf{k}+\mathbf{q}'}\right\rangle + \tag{A.4b}$$

$$+ L^+_{\mathbf{k}',-\mathbf{q}'}\left\langle\beta^\dagger_{\mathbf{k}'-\mathbf{q}'}\beta_{\mathbf{k}}\right\rangle + M^-_{\mathbf{k},\mathbf{q}'}\left\langle\alpha^\dagger_{\mathbf{k}+\mathbf{q}'}\beta^\dagger_{\mathbf{k}'}\right\rangle - M^-_{\mathbf{k}',-\mathbf{q}'}\left\langle\beta_{\mathbf{k}}\alpha_{\mathbf{k}'-\mathbf{q}'}\right\rangle\Bigg)$$

$$+\frac{e^2}{2m}\sum_{\mathbf{q}'=0,\pm2\mathbf{q}_0}\left(\sum_{\mathbf{q}_i=\pm\mathbf{q}_0}\mathbf{A}_{\mathbf{q}'-\mathbf{q}_i}\mathbf{A}_{\mathbf{q}_i}\right)\Bigg(+ L^-_{\mathbf{k},\mathbf{q}'}\left\langle\beta^\dagger_{\mathbf{k}'}\beta_{\mathbf{k}+\mathbf{q}'}\right\rangle + \tag{A.4c}$$

$$- L^-_{\mathbf{k}',-\mathbf{q}'}\left\langle\beta^\dagger_{\mathbf{k}'-\mathbf{q}'}\beta_{\mathbf{k}}\right\rangle + M^+_{\mathbf{k}',\mathbf{q}'}\left\langle\alpha^\dagger_{\mathbf{k}+\mathbf{q}'}\beta^\dagger_{\mathbf{k}'}\right\rangle - M^+_{\mathbf{k},-\mathbf{q}'}\left\langle\beta_{\mathbf{k}}\alpha_{\mathbf{k}'-\mathbf{q}'}\right\rangle\Bigg)$$

$$+\sum_{\mathbf{p}}\frac{g_{\mathbf{p}}}{\sqrt{N}}\left(\left\langle b^\dagger_{-\mathbf{p}}\right\rangle + \langle b_{\mathbf{p}}\rangle\right)\Bigg(+ L^-_{\mathbf{k},\mathbf{p}}\left\langle\beta^\dagger_{\mathbf{k}'}\beta_{\mathbf{k}+\mathbf{p}}\right\rangle - \tag{A.4d}$$

$$- L^-_{\mathbf{k}',-\mathbf{p}'}\left\langle\alpha^\dagger_{\mathbf{k}'-\mathbf{p}}\alpha_{\mathbf{k}}\right\rangle + M^+_{\mathbf{k},\mathbf{p}}\left\langle\alpha^\dagger_{\mathbf{k}+\mathbf{p}}\beta^\dagger_{\mathbf{k}'}\right\rangle - M^+_{\mathbf{k}',-\mathbf{p}}\left\langle\beta_{\mathbf{k}}\alpha_{\mathbf{k}'-\mathbf{p}}\right\rangle\Bigg)$$

$$+\sum_{\mathbf{p}}\frac{g_{\mathbf{p}}}{\sqrt{N}}\Bigg(+ L^-_{\mathbf{k},\mathbf{p}}\left(\left\langle\beta^\dagger_{\mathbf{k}'}\beta_{\mathbf{k}+\mathbf{p}}b_{\mathbf{p}}\right\rangle^c + \left\langle\beta^\dagger_{\mathbf{k}'}\beta_{\mathbf{k}+\mathbf{p}}b^\dagger_{-\mathbf{p}}\right\rangle^c\right) + \tag{A.4e}$$

$$- L^-_{\mathbf{k}',-\mathbf{p}'}\left(\left\langle\beta^\dagger_{\mathbf{k}'-\mathbf{p}}\beta_{\mathbf{k}}b_{\mathbf{p}}\right\rangle^c + \left\langle\alpha^\dagger_{\mathbf{k}'-\mathbf{p}}\alpha_{\mathbf{k}}b^\dagger_{-\mathbf{p}}\right\rangle^c\right) -$$

$$+ M^+_{\mathbf{k},\mathbf{p}}\left(\left\langle\alpha^\dagger_{\mathbf{k}+\mathbf{p}}\beta^\dagger_{\mathbf{k}'}b_{\mathbf{p}}\right\rangle^c + \left\langle\alpha^\dagger_{\mathbf{k}+\mathbf{p}}\beta^\dagger_{\mathbf{k}'}b^\dagger_{-\mathbf{p}}\right\rangle^c\right) +$$

$$- M^+_{\mathbf{k}',-\mathbf{p}}\left(\left\langle\beta_{\mathbf{k}}\alpha_{\mathbf{k}'-\mathbf{p}}b_{\mathbf{p}}\right\rangle^c + \left\langle\beta_{\mathbf{k}}\alpha_{\mathbf{k}'-\mathbf{p}}b^\dagger_{-\mathbf{p}}\right\rangle^c\right)\Bigg)$$

$$i\hbar\frac{\mathrm{d}}{\mathrm{d}t}\left\langle \alpha^\dagger_{\mathbf{k}}\beta^\dagger_{\mathbf{k}'}\right\rangle = -\left(R_{\mathbf{k}'}+R_{\mathbf{k}}\right)\left\langle \alpha^\dagger_{\mathbf{k}}\beta^\dagger_{\mathbf{k}'}\right\rangle + C^*_{\mathbf{k}'}\left\langle \alpha^\dagger_{\mathbf{k}}\alpha_{\mathbf{k}'}\right\rangle + C^*_{\mathbf{k}}\left(\left\langle \beta^\dagger_{\mathbf{k}'}\beta_{\mathbf{k}}\right\rangle - \delta_{\mathbf{k},\mathbf{k}'}\right) \tag{A.5a}$$

$$+\frac{e\hbar}{2m}\sum_{\mathbf{q}'=\pm\mathbf{q}_0} 2\mathbf{k}\mathbf{A}_{\mathbf{q}'}\Bigg(- L^+_{\mathbf{k},\mathbf{q}'}\left\langle \alpha^\dagger_{\mathbf{k}+\mathbf{q}'}\beta^\dagger_{\mathbf{k}'}\right\rangle + L^+_{\mathbf{k}',-\mathbf{q}'}\left\langle \alpha^\dagger_{\mathbf{k}}\beta^\dagger_{\mathbf{k}'-\mathbf{q}'}\right\rangle \tag{A.5b}$$

$$+ M^-_{\mathbf{k}',-\mathbf{q}'}\left\langle \alpha^\dagger_{\mathbf{k}}\alpha_{\mathbf{k}'-\mathbf{q}'}\right\rangle - M^-_{\mathbf{k},\mathbf{q}'}\left(\left\langle \beta^\dagger_{\mathbf{k}+\mathbf{q}'}\beta_{\mathbf{k}'}\right\rangle - \delta_{\mathbf{k}+\mathbf{q}',\mathbf{k}'}\right)\Bigg)$$

$$+\frac{e^2}{2m}\sum_{\mathbf{q}'=0,\pm2\mathbf{q}_0}\left(\sum_{\mathbf{q}_i=\pm\mathbf{q}_0}\mathbf{A}_{\mathbf{q}'-\mathbf{q}_i}\mathbf{A}_{\mathbf{q}_i}\right)\Bigg(- L^-_{\mathbf{k},\mathbf{q}'}\left\langle \alpha^\dagger_{\mathbf{k}+\mathbf{q}'}\beta^\dagger_{\mathbf{k}'}\right\rangle + \tag{A.5c}$$

$$- L^-_{\mathbf{k}',-\mathbf{q}'}\left\langle \alpha^\dagger_{\mathbf{k}}\beta^\dagger_{\mathbf{k}'-\mathbf{q}'}\right\rangle + M^+_{\mathbf{k}',-\mathbf{q}'}\left\langle \alpha^\dagger_{\mathbf{k}}\alpha_{\mathbf{k}'-\mathbf{q}'}\right\rangle$$

$$- M^+_{\mathbf{k},\mathbf{q}'}\left(-\left\langle \beta^\dagger_{\mathbf{k}'}\beta_{\mathbf{k}+\mathbf{q}'}\right\rangle + \delta_{\mathbf{k}',\mathbf{k}+\mathbf{q}'}\right)\Bigg)$$

$$+\sum_{\mathbf{p}}\frac{g_{\mathbf{p}}}{\sqrt{N}}\left(\left\langle b^\dagger_{-\mathbf{p}}\right\rangle + \left\langle b_{\mathbf{p}}\right\rangle\right)\Bigg(- L^-_{\mathbf{k},\mathbf{p}}\left\langle \alpha^\dagger_{\mathbf{k}+\mathbf{p}}\beta^\dagger_{\mathbf{k}'}\right\rangle + \tag{A.5d}$$

$$- L^-_{\mathbf{k}',-\mathbf{p}'}\left\langle \alpha^\dagger_{\mathbf{k}}\beta^\dagger_{\mathbf{k}'-\mathbf{p}}\right\rangle + M^+_{\mathbf{k},\mathbf{p}}\left(\left\langle \beta^\dagger_{\mathbf{k}'}\beta_{\mathbf{k}+\mathbf{p}}\right\rangle - \delta_{\mathbf{k}',\mathbf{k}+\mathbf{q}'}\right)$$

$$+ M^+_{\mathbf{k}',-\mathbf{p}}\left\langle \alpha^\dagger_{\mathbf{k}}\alpha_{\mathbf{k}'-\mathbf{p}}\right\rangle\Bigg)$$

$$+\sum_{\mathbf{p}}\frac{g_{\mathbf{p}}}{\sqrt{N}}\Bigg(- L^-_{\mathbf{k},\mathbf{p}}\left(\left\langle \alpha^\dagger_{\mathbf{k}+\mathbf{p}}\beta^\dagger_{\mathbf{k}'}b_{\mathbf{p}}\right\rangle^c + \left\langle \alpha^\dagger_{\mathbf{k}+\mathbf{p}}\beta^\dagger_{\mathbf{k}'}b^\dagger_{-\mathbf{p}}\right\rangle^c\right) + \tag{A.5e}$$

$$- L^-_{\mathbf{k}',-\mathbf{p}'}\left(\left\langle \alpha^\dagger_{\mathbf{k}}\beta^\dagger_{\mathbf{k}'-\mathbf{p}}b_{\mathbf{p}}\right\rangle^c + \left\langle \alpha^\dagger_{\mathbf{k}}\beta^\dagger_{\mathbf{k}'-\mathbf{p}}b^\dagger_{-\mathbf{p}}\right\rangle^c\right) -$$

$$+ M^+_{\mathbf{k},\mathbf{p}}\left(\left\langle \beta^\dagger_{\mathbf{k}'}\beta_{\mathbf{k}+\mathbf{p}}b_{\mathbf{p}}\right\rangle^c + \left\langle \beta^\dagger_{\mathbf{k}'}\beta_{\mathbf{k}+\mathbf{p}}b^\dagger_{-\mathbf{p}}\right\rangle^c\right) +$$

$$+ M^+_{\mathbf{k}',-\mathbf{p}}\left(\left\langle \alpha^\dagger_{\mathbf{k}}\alpha_{\mathbf{k}'-\mathbf{p}}b_{\mathbf{p}}\right\rangle^c + \left\langle \alpha^\dagger_{\mathbf{k}}\alpha_{\mathbf{k}'-\mathbf{p}}b^\dagger_{-\mathbf{p}}\right\rangle^c\right)\Bigg)$$

$$
\begin{aligned}
& i\hbar\frac{\mathrm{d}}{\mathrm{d}t}\left\langle \beta^{\dagger}_{\mathbf{k}'}\beta_{\mathbf{k}}b_{\mathbf{p}}\right\rangle^{c} = \\
& (R_{\mathbf{k}} - R_{\mathbf{k}'} + \hbar\omega_{p})\left\langle \beta^{\dagger}_{\mathbf{k}'}\beta_{\mathbf{k}}b_{\mathbf{p}}\right\rangle^{c} + C_{\mathbf{k}}\left\langle \alpha^{\dagger}_{\mathbf{k}}\beta^{\dagger}_{\mathbf{k}'}b_{\mathbf{p}}\right\rangle^{c} - C^{*}_{\mathbf{k}'}\left\langle \beta_{\mathbf{k}}\alpha_{\mathbf{k}'}b_{\mathbf{p}}\right\rangle^{c} \\
& + \frac{e\hbar}{2m}\sum_{\mathbf{q}'=\pm\mathbf{q}_0} 2\mathbf{k}\mathbf{A}_{\mathbf{q}'}\Big(- L^{+}_{\mathbf{k},\mathbf{q}'}\left\langle \beta^{\dagger}_{\mathbf{k}'}\beta_{\mathbf{k}+\mathbf{q}'}b_{\mathbf{p}}\right\rangle^{c} + L^{+}_{\mathbf{k}',-\mathbf{q}'}\left\langle \beta^{\dagger}_{\mathbf{k}'-\mathbf{q}'}\beta_{\mathbf{k}}b_{\mathbf{p}}\right\rangle^{c} \\
& \qquad\qquad - M^{-}_{\mathbf{k}',-\mathbf{q}'}\left\langle \beta_{\mathbf{k}}\alpha_{\mathbf{k}'-\mathbf{q}'}b_{\mathbf{p}}\right\rangle^{c} + M^{-}_{\mathbf{k},\mathbf{q}'}\left\langle \alpha^{\dagger}_{\mathbf{k}+\mathbf{q}'}\beta^{\dagger}_{\mathbf{k}'}b_{\mathbf{p}}\right\rangle^{c}\Big) \\
& + \frac{e^2}{2m}\sum_{\mathbf{q}'=0,\pm2\mathbf{q}_0}\left(\sum_{\mathbf{q}_i=\pm\mathbf{q}_0}\mathbf{A}_{\mathbf{q}'-\mathbf{q}_i}\mathbf{A}_{\mathbf{q}_i}\right)\Big(+ L^{-}_{\mathbf{k},\mathbf{q}'}\left\langle \beta^{\dagger}_{\mathbf{k}'}\beta_{\mathbf{k}+\mathbf{q}'}b_{\mathbf{p}}\right\rangle^{c} \\
& \qquad - L^{-}_{\mathbf{k}',-\mathbf{q}'}\left\langle \beta^{\dagger}_{\mathbf{k}'-\mathbf{q}'}\beta_{\mathbf{k}}b_{\mathbf{p}}\right\rangle^{c} - M^{+}_{\mathbf{k}',-\mathbf{q}'}\left\langle \beta_{\mathbf{k}}\alpha_{\mathbf{k}'-\mathbf{q}'}b_{\mathbf{p}}\right\rangle^{c} + M^{+}_{\mathbf{k},\mathbf{q}'}\left\langle \alpha^{\dagger}_{\mathbf{k}+\vec{}'}\beta^{\dagger}_{\mathbf{k}'}b_{\mathbf{p}}\right\rangle^{c}\Big) \\
& + \sum_{\mathbf{r}}\frac{g_{-\mathbf{q}}}{\sqrt{N}}\Big\{ L^{-}_{\mathbf{k},-\mathbf{p}}\left[\left\langle \beta^{\dagger}_{\mathbf{k}'}\beta_{\mathbf{r}-\mathbf{p}}\right\rangle\left(\delta_{\mathbf{r},\mathbf{k}} - \left\langle \beta^{\dagger}_{\mathbf{r}}\beta_{\mathbf{k}}\right\rangle\right) + \left\langle \alpha^{\dagger}_{\mathbf{r}-\mathbf{p}}\beta^{\dagger}_{\mathbf{k}'}\right\rangle\left\langle \beta_{\mathbf{k}}\alpha_{\mathbf{r}}\right\rangle\right] \\
& \qquad\qquad + M^{+}_{\mathbf{r},-\mathbf{p}}\left[\left\langle \alpha^{\dagger}_{\mathbf{r}-\mathbf{p}}\beta^{\dagger}_{\mathbf{k}'}\right\rangle\left(\delta_{\mathbf{r},\mathbf{k}} - \left\langle \beta^{\dagger}_{\mathbf{r}}\beta_{\mathbf{k}}\right\rangle\right) - \left\langle \beta^{\dagger}_{\mathbf{k}'}\beta_{\mathbf{r}-\mathbf{p}}\right\rangle\left\langle \beta_{\mathbf{k}}\alpha_{\mathbf{r}}\right\rangle\right]\Big\} \\
& + \sum_{q}\frac{g_{\mathbf{q}}}{\sqrt{N}}\Big\{ \\
& + L^{-}_{\mathbf{k},\mathbf{q}}\left[\left\langle \beta^{\dagger}_{\mathbf{k}'}\beta_{\mathbf{k}+\mathbf{q}}b_{\mathbf{p}}\right\rangle^{c}\left(\langle b_{\mathbf{q}}\rangle + \left\langle b^{\dagger}_{-\mathbf{q}}\right\rangle\right) + \left\langle \beta^{\dagger}_{\mathbf{k}'}\beta_{\mathbf{k}+\mathbf{q}}\right\rangle\left(\left\langle b^{\dagger}_{-\mathbf{q}}b_{\mathbf{p}}\right\rangle^{c} + \langle b_{\mathbf{q}}b_{\mathbf{p}}\rangle^{c}\right)\right] \\
& - L^{-}_{\mathbf{k}',-\mathbf{q}}\left[\left\langle \beta^{\dagger}_{\mathbf{k}'-\mathbf{q}}\beta_{\mathbf{k}}b_{\mathbf{p}}\right\rangle^{c}\left(\langle b_{\mathbf{q}}\rangle + \left\langle b^{\dagger}_{-\mathbf{q}}\right\rangle\right) + \left\langle \beta^{\dagger}_{\mathbf{k}'-\mathbf{q}}\beta_{\mathbf{k}}\right\rangle\left(\left\langle b^{\dagger}_{-\mathbf{q}}b_{\mathbf{p}}\right\rangle^{c} + \langle b_{\mathbf{q}}b_{\mathbf{p}}\rangle^{c}\right)\right] \\
& + M^{+}_{\mathbf{k},\mathbf{q}}\left[\left\langle \alpha^{\dagger}_{\mathbf{k}+\mathbf{q}}\beta^{\dagger}_{\mathbf{k}'}b_{\mathbf{p}}\right\rangle^{c}\left(\langle b_{\mathbf{q}}\rangle + \left\langle b^{\dagger}_{-\mathbf{q}}\right\rangle\right) + \left\langle \alpha^{\dagger}_{\mathbf{k}+\mathbf{q}}\beta^{\dagger}_{\mathbf{k}'}\right\rangle\left(\left\langle b^{\dagger}_{-\mathbf{q}}b_{\mathbf{p}}\right\rangle^{c} + \langle b_{\mathbf{q}}b_{\mathbf{p}}\rangle^{c}\right)\right] \\
& - M^{+}_{\mathbf{k}',-\mathbf{q}}\left[\left\langle \beta_{\mathbf{k}}\alpha_{\mathbf{k}'-\mathbf{q}}b_{\mathbf{p}}\right\rangle^{c}\left(\langle b_{\mathbf{q}}\rangle + \left\langle b^{\dagger}_{-\mathbf{q}}\right\rangle\right) + \left\langle \beta_{\mathbf{k}}\alpha_{\mathbf{k}'-\mathbf{q}}\right\rangle\left(\left\langle b^{\dagger}_{-\mathbf{q}}b_{\mathbf{p}}\right\rangle^{c} + \langle b_{\mathbf{q}}b_{\mathbf{p}}\rangle^{c}\right)\right]\Big\}
\end{aligned}
\tag{A.6}
$$

$$
\begin{aligned}
&i\hbar\frac{\mathrm{d}}{\mathrm{d}t}\left\langle\alpha^\dagger_{\mathbf{k}}\beta^\dagger_{\mathbf{k}'}b_{\mathbf{p}}\right\rangle^c = \qquad\qquad\qquad\qquad\qquad\qquad\qquad\qquad\qquad\qquad\qquad\qquad\qquad\text{(A.7)}\\
&(-R_{\mathbf{k}}-R_{\mathbf{k}'}+\hbar\omega_p)\left\langle\alpha^\dagger_{\mathbf{k}}\beta^\dagger_{\mathbf{k}'}b_{\mathbf{p}}\right\rangle^c + C^*_{\mathbf{k}}\left\langle\beta^\dagger_{\mathbf{k}'}\beta_{\mathbf{k}}b_{\mathbf{p}}\right\rangle^c + C^*_{\mathbf{k}'}\left\langle\alpha^\dagger_{\mathbf{k}}\alpha_{\mathbf{k}'}b_{\mathbf{p}}\right\rangle^c\\
&+\frac{e\hbar}{2m}\sum_{\mathbf{q}'=\pm\mathbf{q}_0} 2\mathbf{k}\mathbf{A}_{\mathbf{q}'}\Big(-L^+_{\mathbf{k},\mathbf{q}'}\left\langle\alpha^\dagger_{\mathbf{k}+\mathbf{q}'}\beta^\dagger_{\mathbf{k}'}b_{\mathbf{p}}\right\rangle^c + L^+_{\mathbf{k}',-\mathbf{q}'}\left\langle\alpha^\dagger_{\mathbf{k}}\beta^\dagger_{\mathbf{k}'-\mathbf{q}'}b_{\mathbf{p}}\right\rangle^c\\
&\qquad\qquad\qquad\qquad + M^-_{\mathbf{k}',-\mathbf{q}'}\left\langle\alpha^\dagger_{\mathbf{k}}\alpha_{\mathbf{k}'-\mathbf{q}'}b_{\mathbf{p}}\right\rangle^c - M^-_{\mathbf{k},\mathbf{q}'}\left\langle\beta^\dagger_{\mathbf{k}'}\beta_{\mathbf{k}+\mathbf{q}'}b_{\mathbf{p}}\right\rangle^c\Big)\\
&+\frac{e^2}{2m}\sum_{\mathbf{q}'=0,\pm2\mathbf{q}_0}\left(\sum_{\mathbf{q}_i=\pm\mathbf{q}_0}\mathbf{A}_{\mathbf{q}'-\mathbf{q}_i}\mathbf{A}_{\mathbf{q}_i}\right)\Big(-L^-_{\mathbf{k},\mathbf{q}'}\left\langle\alpha^\dagger_{\mathbf{k}+\mathbf{q}'}\beta^\dagger_{\mathbf{k}'}b_{\mathbf{p}}\right\rangle^c\\
&\qquad - L^-_{\mathbf{k}',-\mathbf{q}'}\left\langle\alpha^\dagger_{\mathbf{k}}\beta^\dagger_{\mathbf{k}'-\mathbf{q}'}b_{\mathbf{p}}\right\rangle^c + M^+_{\mathbf{k}',-\mathbf{q}'}\left\langle\alpha^\dagger_{\mathbf{k}}\alpha_{\mathbf{k}'-\mathbf{q}'}b_{\mathbf{p}}\right\rangle^c + M^+_{\mathbf{k},\mathbf{q}'}\left\langle\beta^\dagger_{\mathbf{k}'}\beta_{\mathbf{k}+\vec{}'}b_{\mathbf{p}}\right\rangle^c\Big)\\
&+\sum_{\mathbf{r}}\frac{g_{-\mathbf{q}}}{\sqrt{N}}\Big\{L^-_{\mathbf{k},-\mathbf{p}}\Big[-\left\langle\alpha^\dagger_{\mathbf{k}}\beta^\dagger_{\mathbf{r}}\right\rangle\left\langle\beta^\dagger_{\mathbf{k}'}\beta_{\mathbf{r}-\mathbf{p}}\right\rangle - \left\langle\alpha^\dagger_{\mathbf{r}-\mathbf{p}}\beta^\dagger_{\mathbf{k}'}\right\rangle\left\langle\alpha^\dagger_{\mathbf{k}}\alpha_{\mathbf{r}}\right\rangle\Big]\\
&\qquad\qquad + M^+_{\mathbf{r},-\mathbf{p}}\Big[-\left\langle\alpha^\dagger_{\mathbf{k}}\beta^\dagger_{\mathbf{r}}\right\rangle\left\langle\alpha^\dagger_{\mathbf{r}-\mathbf{p}}\beta^\dagger_{\mathbf{k}'}\right\rangle + \left\langle\alpha^\dagger_{\mathbf{k}}\alpha_{\mathbf{r}}\right\rangle\left\langle\beta^\dagger_{\mathbf{k}'}\beta_{\mathbf{r}-\mathbf{p}}\right\rangle\Big]\Big\}\\
&+\sum_{q}\frac{g_{\mathbf{q}}}{\sqrt{N}}\Big\{\\
&-L^-_{\mathbf{k},\mathbf{q}}\Big[\left\langle\alpha^\dagger_{\mathbf{k}+\mathbf{q}}\beta^\dagger_{\mathbf{k}'}b_{\mathbf{p}}\right\rangle^c\Big(\langle b_{\mathbf{q}}\rangle + \left\langle b^\dagger_{-\mathbf{q}}\right\rangle\Big) + \left\langle\alpha^\dagger_{\mathbf{k}+\mathbf{q}}\beta^\dagger_{\mathbf{k}'}\right\rangle\Big(\left\langle b^\dagger_{-\mathbf{q}}b_{\mathbf{p}}\right\rangle^c + \langle b_{\mathbf{q}}b_{\mathbf{p}}\rangle^c\Big)\Big]\\
&-L^-_{\mathbf{k}',-\mathbf{q}}\Big[\left\langle\alpha^\dagger_{\mathbf{k}}\beta^\dagger_{\mathbf{k}'-\mathbf{q}}b_{\mathbf{p}}\right\rangle^c\Big(\langle b_{\mathbf{q}}\rangle + \left\langle b^\dagger_{-\mathbf{q}}\right\rangle\Big) + \left\langle\alpha^\dagger_{\mathbf{k}}\beta^\dagger_{\mathbf{k}'-\mathbf{q}}\right\rangle\Big(\left\langle b^\dagger_{-\mathbf{q}}b_{\mathbf{p}}\right\rangle^c + \langle b_{\mathbf{q}}b_{\mathbf{p}}\rangle^c\Big)\Big]\\
&+M^+_{\mathbf{k},\mathbf{q}}\Big[\left\langle\beta^\dagger_{\mathbf{k}'}\beta_{\mathbf{k}+\mathbf{q}}b_{\mathbf{p}}\right\rangle^c\Big(\langle b_{\mathbf{q}}\rangle + \left\langle b^\dagger_{-\mathbf{q}}\right\rangle\Big)\\
&\qquad + \Big(\left\langle\beta^\dagger_{\mathbf{k}'}\beta_{\mathbf{k}+\mathbf{q}}\right\rangle - \delta_{\mathbf{k}',\mathbf{k}+\mathbf{q}}\Big)\Big(\left\langle b^\dagger_{-\mathbf{q}}b_{\mathbf{p}}\right\rangle^c + \langle b_{\mathbf{q}}b_{\mathbf{p}}\rangle^c\Big)\Big]\\
&+M^+_{\mathbf{k}',-\mathbf{q}}\Big[\left\langle\alpha^\dagger_{\mathbf{k}}\alpha_{\mathbf{k}'-\mathbf{q}}b_{\mathbf{p}}\right\rangle^c\Big(\langle b_{\mathbf{q}}\rangle + \left\langle b^\dagger_{-\mathbf{q}}\right\rangle\Big) + \left\langle\alpha^\dagger_{\mathbf{k}}\alpha_{\mathbf{k}'-\mathbf{q}}\right\rangle\Big(\left\langle b^\dagger_{-\mathbf{q}}b_{\mathbf{p}}\right\rangle^c + \langle b_{\mathbf{q}}b_{\mathbf{p}}\rangle^c\Big)\Big]\Big\}
\end{aligned}
$$

$$
\begin{aligned}
&i\hbar\frac{\mathrm{d}}{\mathrm{d}t}\left\langle\beta_{\mathbf{k}}\alpha_{\mathbf{k}'}b_{\mathbf{p}}\right\rangle^{c} = \\
&(R_{\mathbf{k}}+R_{\mathbf{k}'}+\hbar\omega_p)\left\langle\beta_{\mathbf{k}}\alpha_{\mathbf{k}'}b_{\mathbf{p}}\right\rangle^{c} - C_{\mathbf{k}'}\left\langle\alpha^{\dagger}_{\mathbf{k}}\alpha_{\mathbf{k}'}b_{\mathbf{p}}\right\rangle^{c} + C_{\mathbf{k}}\left\langle\beta^{\dagger}_{\mathbf{k}'}\beta_{\mathbf{k}}b_{\mathbf{p}}\right\rangle^{c} \\
&+\frac{e\hbar}{2m}\sum_{\mathbf{q}'=\pm\mathbf{q}_0} 2\mathbf{k}\mathbf{A}_{\mathbf{q}'}\Big(- L^{+}_{\mathbf{k},\mathbf{q}'}\left\langle\beta_{\mathbf{k}+\mathbf{q}'}\alpha_{\mathbf{k}'}b_{\mathbf{p}}\right\rangle^{c} + L^{+}_{\mathbf{k}',-\mathbf{q}'}\left\langle\beta_{\mathbf{k}}\alpha_{\mathbf{k}'-\mathbf{q}'}b_{\mathbf{p}}\right\rangle^{c} \\
&\qquad\qquad + M^{-}_{\mathbf{k}',-\mathbf{q}'}\left\langle\beta^{\dagger}_{\mathbf{k}'-\mathbf{q}'}\beta_{\mathbf{k}}b^{\dagger}_{\mathbf{k}'-\mathbf{q}'}\right\rangle\mathbf{p}^{c} - M^{-}_{\mathbf{k},\mathbf{q}'}\left\langle\alpha^{\dagger}_{\mathbf{k}+\mathbf{q}'}\alpha_{\mathbf{k}'}b_{\mathbf{p}}\right\rangle^{c}\Big) \\
&+\frac{e^2}{2m}\sum_{\mathbf{q}'=0,\pm 2\mathbf{q}_0}\left(\sum_{\mathbf{q}_i=\pm\mathbf{q}_0}\mathbf{A}_{\mathbf{q}'-\mathbf{q}_i}\mathbf{A}_{\mathbf{q}_i}\right)\Big(+ L^{-}_{\mathbf{k},\mathbf{q}'}\left\langle\beta_{\mathbf{k}+\mathbf{q}'}\alpha_{\mathbf{k}'}b_{\mathbf{p}}\right\rangle^{c} \\
&\qquad + L^{-}_{\mathbf{k}',-\mathbf{q}'}\left\langle\beta_{\mathbf{k}}\alpha_{\mathbf{k}'-\mathbf{q}'}b_{\mathbf{p}}\right\rangle^{c} - M^{+}_{\mathbf{k}',-\mathbf{q}'}\left\langle\beta^{\dagger}_{\mathbf{k}'-\mathbf{q}'}\beta_{\mathbf{k}}b_{\mathbf{p}}\right\rangle^{c} - M^{+}_{\mathbf{k},\mathbf{q}'}\left\langle\alpha^{\dagger}_{\mathbf{k}+\vec{\ }}\alpha_{\mathbf{k}'}b_{\mathbf{p}}\right\rangle^{c}\Big) \\
&+\sum_{\mathbf{r}}\frac{g_{-\mathbf{q}}}{\sqrt{N}}\Big\{L^{-}_{\mathbf{k},-\mathbf{p}}\Big[\left\langle\beta_{\mathbf{k}}\alpha_{\mathbf{r}}\right\rangle\Big(\delta_{\mathbf{r}-\mathbf{p},\mathbf{k}'} - \left\langle\alpha^{\dagger}_{\mathbf{r}-\mathbf{p}}\alpha_{\mathbf{k}'}\right\rangle\Big) + \left\langle\beta_{\mathbf{r}-\mathbf{p}}\alpha_{\mathbf{k}'}\right\rangle\Big(\delta_{\mathbf{r},\mathbf{k}} - \left\langle\beta^{\dagger}_{\mathbf{r}}\beta_{\mathbf{k}}\right\rangle\Big)\Big] \\
&+ M^{+}_{\mathbf{r},-\mathbf{p}}\Big[\Big(\delta_{\mathbf{r}-\mathbf{p},\mathbf{k}'} - \left\langle\alpha^{\dagger}_{\mathbf{r}-\mathbf{p}}\alpha_{\mathbf{k}'}\right\rangle\Big)\Big(\delta_{\mathbf{r},\mathbf{k}} - \left\langle\beta^{\dagger}_{\mathbf{r}}\beta_{\mathbf{k}}\right\rangle\Big) - \left\langle\beta_{\mathbf{r}}\alpha_{\mathbf{k}}\right\rangle\left\langle\beta_{\mathbf{r}-\mathbf{p}}\alpha_{\mathbf{k}'}\right\rangle\Big]\Big\} \\
&+\sum_{q}\frac{g_{\mathbf{q}}}{\sqrt{N}}\Big\{ \\
&L^{-}_{\mathbf{k},\mathbf{q}}\Big[\left\langle\beta_{\mathbf{k}+\mathbf{q}}\alpha_{\mathbf{k}'}b_{\mathbf{p}}\right\rangle^{c}\Big(\left\langle b_{\mathbf{q}}\right\rangle + \left\langle b^{\dagger}_{-\mathbf{q}}\right\rangle\Big) + \left\langle\beta_{\mathbf{k}+\mathbf{q}}\alpha_{\mathbf{k}'}\right\rangle\Big(\left\langle b^{\dagger}_{-\mathbf{q}}b_{\mathbf{p}}\right\rangle^{c} + \left\langle b_{\mathbf{q}}b_{\mathbf{p}}\right\rangle^{c}\Big)\Big] \\
&+ L^{-}_{\mathbf{k}',-\mathbf{q}}\Big[\left\langle\beta_{\mathbf{k}}\alpha_{\mathbf{k}'-\mathbf{q}}b_{\mathbf{p}}\right\rangle^{c}\Big(\left\langle b_{\mathbf{q}}\right\rangle + \left\langle b^{\dagger}_{-\mathbf{q}}\right\rangle\Big) + \left\langle\beta_{\mathbf{k}}\alpha_{\mathbf{k}'-\mathbf{q}}\right\rangle\Big(\left\langle b^{\dagger}_{-\mathbf{q}}b_{\mathbf{p}}\right\rangle^{c} + \left\langle b_{\mathbf{q}}b_{\mathbf{p}}\right\rangle^{c}\Big)\Big] \\
&- M^{+}_{\mathbf{k},\mathbf{q}}\Big[\left\langle\alpha^{\dagger}_{\mathbf{k}+\mathbf{q}}\alpha_{\mathbf{k}'}b_{\mathbf{p}}\right\rangle^{c}\Big(\left\langle b_{\mathbf{q}}\right\rangle + \left\langle b^{\dagger}_{-\mathbf{q}}\right\rangle\Big) + \left\langle\alpha^{\dagger}_{\mathbf{k}+\mathbf{q}}\alpha_{\mathbf{k}'}\right\rangle\Big(\left\langle b^{\dagger}_{-\mathbf{q}}b_{\mathbf{p}}\right\rangle^{c} + \left\langle b_{\mathbf{q}}b_{\mathbf{p}}\right\rangle^{c}\Big)\Big] \\
&- M^{+}_{\mathbf{k}',-\mathbf{q}}\Big[\left\langle\beta^{\dagger}_{\mathbf{k}'-\mathbf{q}}\beta_{\mathbf{k}}b_{\mathbf{p}}\right\rangle^{c}\Big(\left\langle b_{\mathbf{q}}\right\rangle + \left\langle b^{\dagger}_{-\mathbf{q}}\right\rangle\Big) \\
&\qquad + \Big(\left\langle\beta^{\dagger}_{\mathbf{k}'-\mathbf{q}}\beta_{\mathbf{k}}\right\rangle - \delta_{\mathbf{k},\mathbf{k}'-\mathbf{q}}\Big)\Big(\left\langle b^{\dagger}_{-\mathbf{q}}b_{\mathbf{p}}\right\rangle^{c} + \left\langle b_{\mathbf{q}}b_{\mathbf{p}}\right\rangle^{c}\Big)\Big]\Big\}
\end{aligned}
\tag{A.8}
$$

$$
\begin{aligned}
i\hbar\frac{\mathrm{d}}{\mathrm{d}t}\left\langle b_{\mathbf{p}}b_{\mathbf{q}}\right\rangle^{c} &= \hbar\left(\omega_{-\mathbf{q}}+\omega_{-\mathbf{p}}\right)\left\langle b_{\mathbf{p}}b_{\mathbf{q}}\right\rangle^{c} \\
&+\frac{1}{\sqrt{N}}\sum_{k}\Big\{g_{-\mathbf{q}}\Big[L^{-}_{\mathbf{k},-\mathbf{q}}\Big(\left\langle\alpha^{\dagger}_{\mathbf{k}-\mathbf{q}}\alpha_{\mathbf{k}}b_{\mathbf{p}}\right\rangle^{c} + \left\langle\beta^{\dagger}_{\mathbf{k}}\beta_{\mathbf{k}-\mathbf{q}}b_{\mathbf{p}}\right\rangle^{c}\Big) \\
&\qquad + M^{+}_{\mathbf{k},-\mathbf{q}}\Big(\left\langle\beta_{\mathbf{k}-\mathbf{q}}\alpha_{\mathbf{k}}b_{\mathbf{p}}\right\rangle^{c} + \left\langle\alpha^{\dagger}_{\mathbf{k}-\mathbf{q}}\beta^{\dagger}_{\mathbf{k}}b_{\mathbf{p}}\right\rangle^{c}\Big)\Big] \\
&\quad + g_{-\mathbf{p}}\Big[L^{-}_{\mathbf{k},-\mathbf{p}}\Big(\left\langle\alpha^{\dagger}_{\mathbf{k}-\mathbf{p}}\alpha_{\mathbf{k}}b_{\mathbf{q}}\right\rangle^{c} + \left\langle\beta^{\dagger}_{\mathbf{k}}\beta_{\mathbf{k}-\mathbf{p}}b_{\mathbf{q}}\right\rangle^{c}\Big) \\
&\qquad + M^{+}_{\mathbf{k},-\mathbf{p}}\Big(\left\langle\alpha^{\dagger}_{\mathbf{k}-\mathbf{p}}\beta^{\dagger}_{\mathbf{k}}b_{\mathbf{q}}\right\rangle^{c} + \left\langle\beta_{\mathbf{k}-\mathbf{p}}\alpha_{\mathbf{k}}b_{\mathbf{q}}\right\rangle^{c}\Big)\Big]\Big\}
\end{aligned}
\tag{A.9}
$$

A.3 Order seperation

In this section, we present the equations of motion for the order separation truncation. For reasons of clarity we introduce not every equation of motion according to Sect. 4.1. The equations of motion which are not shown are similar to the one shown. Further, every expectation value gets an additional index which state the order in $g_{\mathbf{p}}$, e.g. $\left\langle \alpha^{\dagger}_{\mathbf{k}}\alpha_{\mathbf{k}}\right\rangle^{(O(g_{\mathbf{p}}))}$.

$$\begin{aligned}
i\hbar\frac{\mathrm{d}}{\mathrm{d}t}\left\langle \alpha^{\dagger}_{\mathbf{k}}\alpha_{\mathbf{k}'}\right\rangle^{(0)} &= \left(R_{\mathbf{k}'}-R_{\mathbf{k}}\right)\left\langle \alpha^{\dagger}_{\mathbf{k}}\alpha_{\mathbf{k}'}\right\rangle^{(0)} + C_{\mathbf{k}'}\left\langle \alpha^{\dagger}_{\mathbf{k}}\beta^{\dagger}_{\mathbf{k}'}\right\rangle^{(0)} - C^{*}_{\mathbf{k}}\left\langle \beta_{\mathbf{k}}\alpha_{\mathbf{k}'}\right\rangle^{(0)} \qquad \text{(A.10)}\\
&+\frac{e\hbar}{2m}\sum_{\mathbf{q}'=\pm\mathbf{q}_0} 2\mathbf{k}\mathbf{A}_{\mathbf{q}'}\Bigg(- L^{+}_{\mathbf{k},\mathbf{q}'}\left\langle \alpha^{\dagger}_{\mathbf{k}+\mathbf{q}'}\alpha_{\mathbf{k}'}\right\rangle^{(0)} + \\
&\quad + L^{+}_{\mathbf{k}',-\mathbf{q}'}\left\langle \alpha^{\dagger}_{\mathbf{k}}\alpha_{\mathbf{k}'-\mathbf{q}'}\right\rangle^{(0)} - M^{-}_{\mathbf{k}',-\mathbf{q}'}\left\langle \alpha^{\dagger}_{\mathbf{k}}\beta^{\dagger}_{\mathbf{k}'-\mathbf{q}'}\right\rangle^{(0)} + M^{-}_{\mathbf{k},\mathbf{q}'}\left\langle \beta_{\mathbf{k}+\mathbf{q}'}\alpha_{\mathbf{k}'}\right\rangle^{(0)}\Bigg)\\
&+\frac{e^2}{2m}\sum_{\mathbf{q}'=0,\pm2\mathbf{q}_0}\left(\sum_{\mathbf{q}_i=\pm\mathbf{q}_0}\mathbf{A}_{\mathbf{q}'-\mathbf{q}_i}\mathbf{A}_{\mathbf{q}_i}\right)\Bigg(- L^{-}_{\mathbf{k},\mathbf{q}'}\left\langle \alpha^{\dagger}_{\mathbf{k}+\mathbf{q}'}\alpha_{\mathbf{k}'}\right\rangle^{(0)} + \\
&\quad + L^{-}_{\mathbf{k}',-\mathbf{q}'}\left\langle \alpha^{\dagger}_{\mathbf{k}}\alpha_{\mathbf{k}'-\mathbf{q}'}\right\rangle^{(0)} + M^{+}_{\mathbf{k}',-\mathbf{q}'}\left\langle \alpha^{\dagger}_{\mathbf{k}}\beta^{\dagger}_{\mathbf{k}'-\mathbf{q}'}\right\rangle^{(0)} - M^{+}_{\mathbf{k},\mathbf{q}'}\left\langle \beta_{\mathbf{k}+\mathbf{q}'}\alpha_{\mathbf{k}'}\right\rangle^{(0)}\Bigg)
\end{aligned}$$

$$\begin{aligned}
i\hbar\frac{\mathrm{d}}{\mathrm{d}t}\left\langle b_{\mathbf{p}}\right\rangle^{(1)} &= \hbar\omega_{-\mathbf{p}}\left\langle b_{\mathbf{p}}\right\rangle^{(1)} \qquad \text{(A.11)}\\
&+\frac{1}{\sqrt{N}}\sum_{\mathbf{k}} g_{-\mathbf{p}}\Bigg(L^{-}_{\mathbf{k},-\mathbf{p}}\left(\left\langle \alpha^{\dagger}_{\mathbf{k}-\mathbf{p}}\alpha_{\mathbf{k}}\right\rangle^{(0)} + \left\langle \beta^{\dagger}_{\mathbf{k}}\beta_{\mathbf{k}-\mathbf{p}}\right\rangle^{(0)}\right)\\
&\qquad + M^{+}_{\mathbf{k},-\mathbf{p}}\left(\left\langle \alpha^{\dagger}_{\mathbf{k}-\mathbf{p}}\beta^{\dagger}_{\mathbf{k}}\right\rangle^{(0)} + \left\langle \beta_{\mathbf{k}-\mathbf{p}}\alpha_{\mathbf{k}}\right\rangle^{(0)}\right)\Bigg)
\end{aligned}$$

$$
\begin{aligned}
&i\hbar\frac{\mathrm{d}}{\mathrm{d}t}\left\langle\alpha^\dagger_{\mathbf{k}}\alpha_{\mathbf{k}'}b_{\mathbf{p}}\right\rangle^{c,(1)} = \qquad\qquad \text{(A.12)}\\
&(-R_{\mathbf{k}}+R_{\mathbf{k}'}+\hbar\omega_p)\left\langle\alpha^\dagger_{\mathbf{k}}\alpha_{\mathbf{k}'}b_{\mathbf{p}}\right\rangle^{c,(1)}+C_{\mathbf{k}'}\left\langle\alpha^\dagger_{\mathbf{k}}\beta^\dagger_{\mathbf{k}'}b_{\mathbf{p}}\right\rangle^{c,(1)}-C^*_{\mathbf{k}}\left\langle\beta_{\mathbf{k}}\alpha_{\mathbf{k}'}b_{\mathbf{p}}\right\rangle^{c,(1)}\\
&+\frac{e\hbar}{2m}\sum_{\mathbf{q}'=\pm\mathbf{q}_0}2\mathbf{k}\mathbf{A}_{\mathbf{q}'}\Big(-L^+_{\mathbf{k},\mathbf{q}'}\left\langle\alpha^\dagger_{\mathbf{k}+\mathbf{q}'}\alpha_{\mathbf{k}'}b_{\mathbf{p}}\right\rangle^{c,(1)}+L^+_{\mathbf{k}',-\mathbf{q}'}\left\langle\alpha^\dagger_{\mathbf{k}}\alpha_{\mathbf{k}'-\mathbf{q}'}b_{\mathbf{p}}\right\rangle^{c,(1)}\\
&\qquad\qquad-M^-_{\mathbf{k}',-\mathbf{q}'}\left\langle\alpha^\dagger_{\mathbf{k}}\beta^\dagger_{\mathbf{k}'-\mathbf{q}'}b_{\mathbf{p}}\right\rangle^{c,(1)}+M^-_{\mathbf{k},\mathbf{q}'}\left\langle\beta_{\mathbf{k}+\mathbf{q}'}\alpha_{\mathbf{k}'}b_{\mathbf{p}}\right\rangle^{c,(1)}\Big)\\
&+\frac{e^2}{2m}\sum_{\mathbf{q}'=0,\pm2\mathbf{q}_0}\left(\sum_{\mathbf{q}_i=\pm\mathbf{q}_0}\mathbf{A}_{\mathbf{q}'-\mathbf{q}_i}\mathbf{A}_{\mathbf{q}_i}\right)\Big(-L^-_{\mathbf{k},\mathbf{q}'}\left\langle\alpha^\dagger_{\mathbf{k}+\mathbf{q}'}\alpha_{\mathbf{k}'}b_{\mathbf{p}}\right\rangle^{c,(1)}\\
&+L^-_{\mathbf{k}',-\mathbf{q}'}\left\langle\alpha^\dagger_{\mathbf{k}}\alpha_{\mathbf{k}'-\mathbf{q}'}b_{\mathbf{p}}\right\rangle^{c,(1)}+M^+_{\mathbf{k}',-\mathbf{q}'}\left\langle\alpha^\dagger_{\mathbf{k}}\beta^\dagger_{\mathbf{k}'-\mathbf{q}'}b_{\mathbf{p}}\right\rangle^{c,(1)}-M^+_{\mathbf{k},\mathbf{q}'}\left\langle\beta_{\mathbf{k}+\mathbf{q}'}\alpha_{\mathbf{k}'}b_{\mathbf{p}}\right\rangle^{c,(1)}\Big)\\
&+\sum_{\mathbf{r}}\frac{g_{-\mathbf{q}}}{\sqrt{N}}\Big\{L^-_{\mathbf{k},-\mathbf{p}}\left[\left\langle\alpha^\dagger_{\mathbf{k}}\alpha_{\mathbf{r}}\right\rangle^{(0)}\left(\delta_{\mathbf{r}-\mathbf{p},\mathbf{k}'}-\left\langle\alpha^\dagger_{\mathbf{r}-\mathbf{p}}\alpha_{\mathbf{k}'}\right\rangle^{(0)}\right)+\left\langle\alpha^\dagger_{\mathbf{k}}\beta^\dagger_{\mathbf{r}}\right\rangle^{(0)}\left\langle\beta_{\mathbf{r}-\mathbf{p}}\alpha_{\mathbf{k}'}\right\rangle^{(0)}\right]\\
&+M^+_{\mathbf{r},-\mathbf{p}}\left[\left\langle\alpha^\dagger_{\mathbf{k}}\beta^\dagger_{\mathbf{r}}\right\rangle^{(0)}\left(\delta_{\mathbf{r}-\mathbf{p},\mathbf{k}'}-\left\langle\alpha^\dagger_{\mathbf{r}-\mathbf{p}}\alpha_{\mathbf{k}}\right\rangle^{(0)}\right)-\left\langle\alpha^\dagger_{\mathbf{k}}\alpha_{\mathbf{r}}\right\rangle^{(0)}\left\langle\beta_{\mathbf{r}-\mathbf{p}}\alpha_{\mathbf{k}'}\right\rangle^{(0)}\right]\Big\}
\end{aligned}
$$

$$
\begin{aligned}
&i\hbar\frac{\mathrm{d}}{\mathrm{d}t}\left\langle b^\dagger_{\mathbf{p}}b_{\mathbf{q}}\right\rangle^{c,(2)}=\hbar\left(\omega_{-\mathbf{q}}-\omega_{\mathbf{p}}\right)\left\langle b^\dagger_{\mathbf{p}}b_{\mathbf{q}}\right\rangle^{c,(2)} \qquad\qquad \text{(A.13)}\\
&+\frac{1}{\sqrt{N}}\sum_{k}\Big\{g_{-\mathbf{q}}\Big[L^-_{\mathbf{k},-\mathbf{q}}\left(\left\langle\alpha^\dagger_{\mathbf{k}-\mathbf{q}}\alpha_{\mathbf{k}}b^\dagger_{\mathbf{p}}\right\rangle^{c,(1)}+\left\langle\beta^\dagger_{\mathbf{k}}\beta_{\mathbf{k}-\mathbf{q}}b^\dagger_{\mathbf{p}}\right\rangle^{c,(1)}\right)\\
&\qquad\qquad+M^+_{\mathbf{k},-\mathbf{q}}\left(\left\langle\alpha^\dagger_{\mathbf{k}-\mathbf{q}}\beta^\dagger_{\mathbf{k}}b^\dagger_{\mathbf{p}}\right\rangle^{c,(1)}+\left\langle\beta_{\mathbf{k}-\mathbf{q}}\alpha_{\mathbf{k}}b^\dagger_{\mathbf{p}}\right\rangle^{c,(1)}\right)\Big]\\
&\qquad\qquad-g_{\mathbf{p}}\Big[L^-_{\mathbf{k},\mathbf{p}}\left(\left\langle\alpha^\dagger_{\mathbf{k}+\mathbf{p}}\alpha_{\mathbf{k}}b_{\mathbf{q}}\right\rangle^{c,(1)}+\left\langle\beta^\dagger_{\mathbf{k}}\beta_{\mathbf{k}+\mathbf{p}}b_{\mathbf{q}}\right\rangle^{c,(1)}\right)\\
&\qquad\qquad+M^+_{\mathbf{k},\mathbf{p}}\left(\left\langle\alpha^\dagger_{\mathbf{k}+\mathbf{p}}\beta^\dagger_{\mathbf{k}}b_{\mathbf{q}}\right\rangle^{c,(1)}+\left\langle\beta_{\mathbf{k}+\mathbf{p}}\alpha_{\mathbf{k}}b_{\mathbf{q}}\right\rangle^{c,(1)}\right)\Big]\Big\}
\end{aligned}
$$

B iEoM for superconductor

In this section, we set up the equation of motion for the iEoM for a superconductor perturbed by an interaction quench.

To set up the equations of motion we have to consider that the Hamiltonian is explicit time dependent and is given by

$$\tilde{H}_{\mathrm{sc}} = \sum_{\mathbf{k}\in W} \Big(R_{\mathbf{k}}(t) \left(\alpha^{\dagger}_{\mathbf{k}}(t)\alpha_{\mathbf{k}}(t) + \beta^{\dagger}_{\mathbf{k}}(t)\beta_{\mathbf{k}}(t) \right) + C_{\mathbf{k}}(t)\alpha^{\dagger}_{\mathbf{k}}(t)\beta^{\dagger}_{\mathbf{k}}(t) + C^{*}_{\mathbf{k}}(t)\beta_{\mathbf{k}}(t)\alpha_{\mathbf{k}}(t) \Big) . \tag{B.1}$$

The ansatz for the operators is given by

$$\alpha^{\dagger}_{\mathbf{k}}(t) = a_0(t)\alpha^{\dagger}_{\mathbf{k}} + a_1(t)\beta_{\mathbf{k}} \tag{B.2}$$

$$\beta^{\dagger}_{\mathbf{k}}(t) = b_0(t)\beta^{\dagger}_{\mathbf{k}} + b_1(t)\alpha_{\mathbf{k}}, \tag{B.3}$$

with the initial conditions $a_0(0) = 1 = b_0(0)$ and $a_1(0) = 0 = b_1(0)$. With these the Hamiltonian can be rewritten into

$$\begin{aligned}
\tilde{H}_{\mathrm{sc}} = \sum_{\mathbf{k}\in W} \big(&\alpha^{\dagger}_{\mathbf{k}}\alpha_{\mathbf{k}}[R_{\mathbf{k}}(t)\{|a_0(t)|^2 - |b_1(t)|^2\} + C_{\mathbf{k}}(t)a_0(t)b_1(t) + C^{*}_{\mathbf{k}}(t)a^{*}_0(t)b^{*}_1(t)] \\
&+ \beta^{\dagger}_{\mathbf{k}}\beta_{\mathbf{k}}[R_{\mathbf{k}}(t)\{|b_0(t)|^2 - |a_1(t)|^2\} - C_{\mathbf{k}}(t)a_1(t)b_0(t) - C^{*}_{\mathbf{k}}(t)a^{*}_1(t)b^{*}_0(t)] \\
&+ \alpha^{\dagger}_{\mathbf{k}}\beta^{\dagger}_{\mathbf{k}}[R_{\mathbf{k}}(t)\{a_0(t)a^{*}_1(t) - b_0(t)b^{*}_1(t)\} + C_{\mathbf{k}}(t)a_0(t)b_0(t) + C^{*}_{\mathbf{k}}(t)a^{*}_1(t)b^{*}_1(t)] \\
&+ \beta_{\mathbf{k}}\alpha_{\mathbf{k}}[R_{\mathbf{k}}(t)\{a_1(t)a^{*}_0(t) - b_1(t)b^{*}_0(t)\} + C_{\mathbf{k}}(t)a_1(t)b_1(t) + C^{*}_{\mathbf{k}}(t)a^{*}_0(t)b^{*}_0(t)] \\
&+ R_{\mathbf{k}}(t)\{|b_1(t)|^2 + |a_1(t)|^2\} + C_{\mathbf{k}}(t)a_1(t)b_0(t) + C^{*}_{\mathbf{k}}(t)a^{*}_1(t)b^{*}_0(t)\big).
\end{aligned} \tag{B.4}$$

Now, we are able to calculate the equations of motion for the operators $\alpha^{\dagger}_{\mathbf{k}}(t)$ and $\beta^{\dagger}_{\mathbf{k}}(t)$. For this we commute these with $\tilde{H}_{\mathrm{sc}}$. For $\alpha^{\dagger}_{\mathbf{k}}(t)$ we get

$$\begin{aligned}
i\hbar\frac{\mathrm{d}}{\mathrm{d}t}\alpha^{\dagger}_{\mathbf{k}}(t) &= i\hbar\left(\frac{\mathrm{d}}{\mathrm{d}t}\boxed{a_0(t)}\,\alpha^{\dagger}_{\mathbf{k}} + \frac{\mathrm{d}}{\mathrm{d}t}\boxed{a_1(t)}\,\beta_{\mathbf{k}}\right) \\
&= [\alpha^{\dagger}_{\mathbf{k}}(t), \tilde{H}_{\mathrm{sc}}] = [a_0(t)\alpha^{\dagger}_{\mathbf{k}} + a_1(t)\beta_{\mathbf{k}}, \tilde{H}_{\mathrm{sc}}] \\
&= \boxed{-a_0(t)[R_{\mathbf{k}}(t)\{|a_0(t)|^2 - |b_1(t)|^2\} + C_{\mathbf{k}}(t)a_0(t)b_1(t) + C^{*}_{\mathbf{k}}(t)a^{*}_0(t)b^{*}_1(t)]}\,\alpha^{\dagger}_{\mathbf{k}} \\
&\quad \boxed{-a_0(t)[R_{\mathbf{k}}(t)\{a_1(t)a^{*}_0(t) - b_1(t)b^{*}_0(t)\} + C_{\mathbf{k}}(t)a_1(t)b_1(t) + C^{*}_{\mathbf{k}}(t)a^{*}_0(t)b^{*}_0(t)]}\,\beta_{\mathbf{k}} \\
&\quad \boxed{+a_1(t)[R_{\mathbf{k}}(t)\{|b_0(t)|^2 - |a_1(t)|^2\} - C_{\mathbf{k}}(t)a_1(t)b_0(t) - C^{*}_{\mathbf{k}}(t)a^{*}_1(t)b^{*}_0(t)]}\,\beta_{\mathbf{k}} \\
&\quad \boxed{-a_1(t)[R_{\mathbf{k}}(t)\{a_0(t)a^{*}_1(t) - b_0(t)b^{*}_1(t)\} + C_{\mathbf{k}}(t)a_0(t)b_0(t) + C^{*}_{\mathbf{k}}(t)a^{*}_1(t)b^{*}_1(t)]}\,\alpha^{\dagger}_{\mathbf{k}},
\end{aligned} \tag{B.5}$$

and for $\beta^\dagger_{\mathbf{k}}(t)$

$$
\begin{aligned}
&i\hbar\frac{\mathrm{d}}{\mathrm{d}t}\beta^\dagger_{\mathbf{k}}(t) = i\hbar\left(\frac{\mathrm{d}}{\mathrm{d}t}\boxed{b_0(t)}\,\beta^\dagger_{\mathbf{k}} + \frac{\mathrm{d}}{\mathrm{d}t}\boxed{b_1(t)}\,\alpha_{\mathbf{k}}\right) \qquad \text{(B.6)}\\
&= [\beta^\dagger_{\mathbf{k}}(t), \tilde{H}_{\mathrm{sc}}] = [b_0(t)\beta^\dagger_{\mathbf{k}} + b_1(t)\alpha_{\mathbf{k}}, \tilde{H}_{\mathrm{sc}}]\\
&= \boxed{-b_0(t)[R_{\mathbf{k}}(t)\{|b_0(t)|^2 - |a_1(t)|^2\} - C_{\mathbf{k}}(t)a_1(t)b_0(t) - C^*_{\mathbf{k}}(t)a^*_1(t)b^*_0(t)]}\,\beta^\dagger_{\mathbf{k}}\\
&\quad \boxed{+b_0(t)[R_{\mathbf{k}}(t)\{a_1(t)a^*_0(t) - b_1(t)b^*_0(t)\} + C_{\mathbf{k}}(t)a_1(t)b_1(t) + C^*_{\mathbf{k}}(t)a^*_0(t)b^*_0(t)]}\,\alpha_{\mathbf{k}}\\
&\quad \boxed{+b_1(t)[R_{\mathbf{k}}(t)\{|a_0(t)|^2 - |b_1(t)|^2\} + C_{\mathbf{k}}(t)a_0(t)b_1(t) + C^*_{\mathbf{k}}(t)a^*_0(t)b^*_1(t)]}\,\alpha_{\mathbf{k}}\\
&\quad \boxed{+b_1(t)[R_{\mathbf{k}}(t)\{a_0(t)a^*_1(t) - b_0(t)b^*_1(t)\} + C_{\mathbf{k}}(t)a_0(t)b_0(t) + C^*_{\mathbf{k}}(t)a^*_1(t)b^*_1(t)]}\,\beta^\dagger_{\mathbf{k}}.
\end{aligned}
$$

A comparison of the coefficients leads to the equations of motion for the prefactors, see red and green boxes in the equations above.

$$
\begin{aligned}
i\hbar\frac{\mathrm{d}}{\mathrm{d}t}a_0(t) = &-R_{\mathbf{k}}(t)\,\big(a_0(t)\{|a_0(t)|^2 + |a_1(t)|^2 - |b_1(t)|^2\} - a_1(t)b_0(t)b^*_1(t)]\big)\\
&- C_{\mathbf{k}}(t)\,(a_0(t)a_0(t)b_1(t) + a_0(t)b_0(t)a_1(t)) - C^*_{\mathbf{k}}(t)\,\big(b^*_1\{|a_0|^2 + |a_1|^2\}\big)
\end{aligned}
\tag{B.7}
$$

$$
\begin{aligned}
i\hbar\frac{\mathrm{d}}{\mathrm{d}t}a_1(t) = &\,R_{\mathbf{k}}(t)\,\big(a_1(t)\{-|a_0(t)|^2 - |a_1(t)|^2 + |b_0(t)|^2\} + a_0(t)b_1(t)b^*_0(t)]\big)\\
&- C_{\mathbf{k}}(t)\,(a_0(t)a_1(t)b_1(t) + a_1(t)b_0(t)a_1(t)) - C^*_{\mathbf{k}}(t)\,\big(b^*_0\{|a_0|^2 + |a_1|^2\}\big)
\end{aligned}
\tag{B.8}
$$

$$
\begin{aligned}
i\hbar\frac{\mathrm{d}}{\mathrm{d}t}b_0(t) = &\,R_{\mathbf{k}}(t)\,\big(b_0(t)\{|a_1(t)|^2 - |b_1(t)|^2 - |b_0(t)|^2\} + b_1(t)a_0(t)a^*_1(t)]\big)\\
&+ C_{\mathbf{k}}(t)\,(a_0(t)b_0(t)b_1(t) + a_1(t)b_0(t)b_0(t)) + C^*_{\mathbf{k}}(t)\,\big(a^*_1\{|b_0|^2 + |b_1|^2\}\big)
\end{aligned}
\tag{B.9}
$$

$$
\begin{aligned}
i\hbar\frac{\mathrm{d}}{\mathrm{d}t}b_1(t) = &\,R_{\mathbf{k}}(t)\,\big(b_1(t)\{|a_0(t)|^2 - |b_1(t)|^2 - |b_0(t)|^2\} + b_0(t)a_1(t)a^*_0(t)]\big)\\
&+ C_{\mathbf{k}}(t)\,(a_1(t)b_0(t)b_1(t) + a_0(t)b_1(t)b_1(t)) + C^*_{\mathbf{k}}(t)\,\big(a^*_0\{|b_0|^2 + |b_1|^2\}\big)
\end{aligned}
\tag{B.10}
$$

To solve the equations of motion one has also to compute the order parameter, which means that one needs the temporal evolution of the expectation values,e.g. $\left\langle \alpha^\dagger_{\mathbf{k}}\alpha_{\mathbf{k}}\right\rangle$, which can be computed as follows.

$$\begin{aligned}
\left\langle \alpha_c^\dagger(t)\alpha_c(t)\right\rangle &= \left\langle \left(a_0(0,t)\alpha_c^\dagger + a_1(0,t)\beta_c\right)\left(a_0^*(0,t)\alpha_c + a_1^*(0,t)\beta_c^\dagger\right)\right\rangle \qquad \text{(B.11)}\\
&= \left\langle a_0(0,t)\alpha_c^\dagger a_0^*(0,t)\alpha_c\right\rangle + \left\langle a_0(0,t)\alpha_c^\dagger a_1^*(0,t)\beta_c^\dagger\right\rangle\\
&+ \left\langle a_1(0,t)\beta_c a_0^*(0,t)\alpha_c\right\rangle - \left\langle a_1^*(0,t)\beta_c^\dagger a_1(0,t)\beta_c\right\rangle\\
&+ |a_1(0,t)|^2 \left\langle|\right\rangle\\
&\overset{\langle 0|A|0\rangle}{=} |a_1(0,t)|^2\\
\left\langle \beta_c^\dagger(t)\beta_c(t)\right\rangle &\overset{\langle 0|A|0\rangle}{=} |b_1(0,t)|^2 \qquad \text{(B.12)}
\end{aligned}$$

$$\begin{aligned}
\left\langle \alpha_c^\dagger(t)\beta_c^\dagger(t)\right\rangle &= \left\langle \left(a_0(0,t)\alpha_c^\dagger + a_1(0,t)\beta_c\right)\left(b_0(0,t)\beta_c^\dagger + b_1(0,t)\alpha_c\right)\right\rangle \qquad \text{(B.13)}\\
&\overset{\langle 0|A|0\rangle}{=} a_1(0,t)b_0(0,t)\\
\left\langle \beta_c(t)\alpha_c(t)\right\rangle &\overset{\langle 0|A|0\rangle}{=} b_0^*(0,t)a_1^*(0,t) \qquad \text{(B.14)}
\end{aligned}$$

Here, $\langle 0|A|0\rangle$ denotes that we have to compute the expectation value concerning the initial groundstate.

Bibliography

[1] N. B. Kopnin. *Theory of Nonequilibrium Superconductivity.* Calrendon, Oxford, 2001.

[2] J. Orenstein. Ultrafast spectroscopy of quantum materials. *Physics Today*, **65**(9):44–50, 2012.

[3] J. A. Fülöp, L. Pálfalvi, S. Klingebiel, G. Almási, F. Krausz, S. Karsch, and J. Hebling. Generation of sub-mj terahertz pulses by optical rectification. *Opt. Lett.*, **37**(4):557–559, 2012.

[4] R. Matsunaga, N. Tsuji, H. Fujita, A. Sugioka, K. Makise, Y. Uzawa, H. Terai, Z. Wang, H. Aoki, and R. Shimano. Light-induced collective pseudospin precession resonating with higgs mode in a superconductor. *Science*, **345**(6201):1145–1149, 2014.

[5] R. Matsunaga and R. Shimano. Nonequilibrium BCS state dynamics induced by intense terahertz pulses in a superconducting NbN film. *Phys. Rev. Lett.*, **109**:187002, 2012.

[6] R. Matsunaga, Y. I. Hamada, K. Makise, Y. Uzawa, H. Terai, Z. Wang, and R. Shimano. Higgs amplitude mode in the BCS superconductors $\mathrm{Nb}_{1\text{-}x}\mathrm{Ti}_x\mathrm{N}$ induced by terahertz pulse excitation. *Phys. Rev. Lett.*, **111**:057002, 2013.

[7] B. Mansart, J. Lorenzana, A. Mann, A. Odeh, M. Scarongella, M. Chergui, and F. Carbone. Coupling of a high-energy excitation to superconducting quasiparticles in a cuprate from coherent charge fluctuation spectroscopy. *Proc. Natl. Acad. Sci. USA*, **110**(12):4539–4544, 2013.

[8] M. Beck, M. Klammer, S. Lang, P. Leiderer, V. V. Kabanov, G. N. Gol'tsman, and J. Demsar. Energy-gap dynamics of superconducting NbN thin films studied by time-resolved terahertz spectroscopy. *Phys. Rev. Lett.*, **107**:177007, 2011.

[9] M. Beck, I. Rousseau, M. Klammer, P. Leiderer, M. Mittendorff, S. Winnerl, M. Helm, G. N. Gol'tsman, and J. Demsar. Transient increase of the energy gap of superconducting NbN thin films excited by resonant narrow-band terahertz pulses. *Phys. Rev. Lett.*, **110**:267003, 2013.

[10] R. D. Averitt, G. Rodriguez, A. I. Lobad, J. L. W. Siders, S. A. Trugman, and A. J. Taylor. Nonequilibrium superconductivity and quasiparticle dynamics in $YBa_2Cu_3O_{7-\delta}$. *Phys. Rev. B*, **63**:140502, 2001.

[11] R. A. Kaindl, M. A. Carnahan, D. S. Chemla, S. Oh, and J. N. Eckstein. Dynamics of cooper pair formation in $Bi_2Sr_2CaCu_2O_{8+\delta}$. *Phys. Rev. B*, **72**:060510, 2005.

[12] S. Dal Conte, C. Giannetti, G. Coslovich, F. Cilento, D. Bossini, T. Abebaw, F. Banfi, G. Ferrini, H. Eisaki, M. Greven, A. Damascelli, D. van der Marel, and F. Parmigiani. Disentangling the electronic and phononic glue in a high-tc superconductor. *Science*, **335**(6076):1600–1603, 2012.

[13] F. Cilento, S. Dal Conte, G. Coslovich, F. Banfi, G. Ferrini, H. Eisaki, M. Greven, A. Damascelli, D. van der Marel, F. Parmigiani, and C. Giannetti. In search for the pairing glue in cuprates by non-equilibrium optical spectroscopy. *Journal of Physics: Conference Series*, **449**(1):012003, 2013.

[14] B. Mansart, D. Boschetto, A. Savoia, F. Rullier-Albenque, A. Forget, D. Colson, A. Rousse, and M. Marsi. Observation of a coherent optical phonon in the iron pnictide superconductor $Ba(Fe_{1-x}Co_x)_2As_2$ ($x = 0.06$ and 0.08). *Phys. Rev. B*, **80**:172504, 2009.

[15] L. Rettig, R. Cortés, S. Thirupathaiah, P. Gegenwart, H. S. Jeevan, M. Wolf, J. Fink, and U. Bovensiepen. Ultrafast momentum-dependent response of electrons in antiferromagnetic $EuFe_2As_2$ driven by optical excitation. *Phys. Rev. Lett.*, **108**:097002, 2012.

[16] L. Perfetti, P. A. Loukakos, M. Lisowski, U. Bovensiepen, H. Eisaki, and M. Wolf. Ultrafast electron relaxation in superconducting $Bi_2Sr_2CaCu_2O_{8+\delta}$ by time-resolved photoelectron spectroscopy. *Phys. Rev. Lett.*, **99**:197001, 2007.

[17] R. A. Kaindl, M. Woerner, T. Elsaesser, D. C. Smith, J. F. Ryan, G. A. Farnan, M. P. McCurry, and D. G. Walmsley. Ultrafast mid-infrared response of $YBa_2Cu_3O_{7-\delta}$. *Science*, **287**(5452):470–473, 2000.

[18] R. P. Saichu, I. Mahns, A. Goos, S. Binder, P. May, S. G. Singer, B. Schulz, A. Rusydi, J. Unterhinninghofen, D. Manske, P. Guptasarma, M. S.

Williamsen, and M. Rübhausen. Two-component dynamics of the order parameter of high temperature $Bi_2Sr_2CaCu_2O_{8+\delta}$ superconductors revealed by time-resolved raman scattering. *Phys. Rev. Lett.*, **102**:177004, 2009.

[19] A. Pashkin, M. Porer, M. Beyer, K. W. Kim, A. Dubroka, C. Bernhard, X. Yao, Y. Dagan, R. Hackl, A. Erb, J. Demsar, R. Huber, and A. Leitenstorfer. Femtosecond response of quasiparticles and phonons in superconducting $YBa_2Cu_3O_{7-\delta}$ studied by wideband terahertz spectroscopy. *Phys. Rev. Lett.*, **105**:067001, 2010.

[20] E. Abrahams and T. Tsuneto. Time variation of the Ginzburg-Landau order parameter. *Phys. Rev.*, **152**:416–432, 1966.

[21] O. Betbeder-Matibet and P. Nozieres. Transport equations in clean superconductors. *Annals of Physics*, **51**(3):392 – 417, 1969.

[22] A.G. Aronov, Yu.M. Gal'perin, V.L. Gurevich, and V.I. Kozub. The Boltzmann-equation description of transport in superconductors. *Advances in Physics*, **30**(4):539–592, 1981.

[23] E. J. Nicol and J. P. Carbotte. Comparison of *s*- and *d*-wave gap symmetry in nonequilibrium superconductivity. *Phys. Rev. B*, **67**:214506, 2003.

[24] V. V. Kabanov, J. Demsar, and D. Mihailovic. Kinetics of a superconductor excited with a femtosecond optical pulse. *Phys. Rev. Lett.*, **95**:147002, 2005.

[25] J. K. Freericks, V. M. Turkowski, and V. Zlatić. Nonequilibrium dynamical mean-field theory. *Phys. Rev. Lett.*, **97**:266408, 2006.

[26] H. Aoki, N. Tsuji, M. Eckstein, M. Kollar, T. Oka, and P. Werner. Nonequilibrium dynamical mean-field theory and its applications. *Rev. Mod. Phys.*, **86**:779–837, 2014.

[27] S. R. White and A. E. Feiguin. Real-time evolution using the density matrix renormalization group. *Phys. Rev. Lett.*, **93**:076401, 2004.

[28] F. B. Anders and A. Schiller. Real-time dynamics in quantum-impurity systems: A time-dependent numerical renormalization-group approach. *Phys. Rev. Lett.*, **95**:196801, 2005.

[29] M. Moeckel and S. Kehrein. Interaction quench in the Hubbard model. *Phys. Rev. Lett.*, 100:175702, 2008.

[30] T. Papenkort, V. M. Axt, and T. Kuhn. Coherent dynamics and pump-probe spectra of BCS superconductors. *Phys. Rev. B*, **76**:224522, 2007.

[31] T. Papenkort, T. Kuhn, and V. M. Axt. Coherent control of the gap dynamics of BCS superconductors in the nonadiabatic regime. *Phys. Rev. B*, **78**:132505, 2008.

[32] T. Papenkort, T. Kuhn, and V. M. Axt. Nonequilibrium dynamics and coherent control of BCS superconductors driven by ultrashort THz pulses. *Journal of Physics: Conference Series*, **193**(1):012050, 2009.

[33] A. P. Schnyder, D. Manske, and A. Avella. Resonant generation of coherent phonons in a superconductor by ultrafast optical pump pulses. *Phys. Rev. B*, **84**:214513, 2011.

[34] A. Akbari, A. P. Schnyder, D. Manske, and I. Eremin. Theory of nonequilibrium dynamics of multiband superconductors. *Europhys. Lett.*, **101**(1):17002, 2013.

[35] M. Zachmann, M. D. Croitoru, A. Vagov, V. M. Axt, T. Papenkort, and T. Kuhn. Ultrafast terahertz-field-induced dynamics of superconducting bulk and quasi-1d samples. *New Journal of Physics*, **15**(5):055016, 2013.

[36] H. Krull, D. Manske, G. S. Uhrig, and A. P. Schnyder. Signatures of nonadiabatic BCS state dynamics in pump-probe conductivity. *Phys. Rev. B*, **90**:014515, 2014.

[37] A. F. Volkov and Sh. M. Kogan. Colliionless relaxation of the energy gap in superconductors. *Sov. Phys. JETP*, **38**:1018, 1974.

[38] M. H. S. Amin, E. V. Bezuglyi, A. S. Kijko, and A. N. Omelyanchouk. Wigner distribution function formalism for superconductors and collisionless dynamics of the superconducting order parameter. *Low Temperature Physics*, **30**(7):661–666, 2004.

[39] R. A. Barankov, L. S. Levitov, and B. Z. Spivak. Collective rabi oscillations and solitons in a time-dependent BCS pairing problem. *Phys. Rev. Lett.*, **93**:160401, 2004.

[40] E. A. Yuzbashyan, B. L. Altshuler, V. B. Kuznetsov, and V. Z. Enolskii. Nonequilibrium cooper pairing in the nonadiabatic regime. *Phys. Rev. B*, **72**:220503, 2005.

[41] E. A. Yuzbashyan, O. Tsyplyatyev, and B. L. Altshuler. Relaxation and persistent oscillations of the order parameter in fermionic condensates. *Phys. Rev. Lett.*, **96**:097005, 2006.

[42] A. Pashkin and A. Leitenstorfer. Particle physics in a superconductor. *Science*, **345**(6201):1121–1122, 2014.

[43] G. C. Cho, W. Kütt, and H. Kurz. Subpicosecond time-resolved coherent-phonon oscillations in GaAs. *Phys. Rev. Lett.*, **65**:764–766, 1990.

[44] G. A. Garrett, T. F. Albrecht, J. F. Whitaker, and R. Merlin. Coherent thz phonons driven by light pulses and the Sb problem: What is the mechanism? *Phys. Rev. Lett.*, **77**:3661–3664, 1996.

[45] H. J. Zeiger, J. Vidal, T. K. Cheng, E. P. Ippen, G. Dresselhaus, and M. S. Dresselhaus. Theory for displacive excitation of coherent phonons. *Phys. Rev. B*, **45**:768–778, 1992.

[46] L. Rettig, R. Cortés, S. Thirupathaiah, P. Gegenwart, H. S. Jeevan, T. Wolf, U. Bovensiepen, M. Wolf, H. A. Dürr, and J. Fink. Electron-phonon coupling and momentum-dependent electron dynamics in $\mathrm{EuFe_2As_2}$ using time- and angle-resolved photoemission spectroscopy. *ArXiv e-prints*, August 2010.

[47] O.V. Misochko and M.V. Lebedev. Generation of coherent off-diagonal raman-active phonons by femtosecond laser pulses in high-temperature superconductor $\mathrm{YBa_2Cu_3O_{7-x}}$. *Physics of the Solid State*, **43**(7):1195–1198, 2001.

[48] H. P. Breuer. *The Theory of Open Quantum Systems.* Oxford University Press, 2007.

[49] Elsi Laine. Non-Markovian Dynamics of the Spin-Boson Model. Master's thesis, University of Turku, 2009.

[50] S. A. Hamerla and G. S. Uhrig. Dynamical transition in interaction quenches of the one-dimensional Hubbard model. *Phys. Rev. B*, **87**:064304, 2013.

[51] S. A. Hamerla. *Interaction Quenches in Fermionic Hubbard Models: Dynamics of Quenched Fermions in One and Two Dimensions.* PhD thesis, TU Dortmund, 2013.

[52] Fausto Rossi and Tilmann Kuhn. Theory of ultrafast phenomena in photoexcited semiconductors. *Rev. Mod. Phys.*, **74**:895–950, 2002.

[53] M. Herbst, M. Glanemann, V. M. Axt, and T. Kuhn. Electron-phonon quantum kinetics for spatially inhomogeneous excitations. *Phys. Rev. B*, **67**:195305, 2003.

[54] T. Papenkort, T. Kuhn, and V. M. Axt. Resonant generation of coherent lo phonons by charge oscillations in a biased quantum well. *Phys. Rev. B*, **81**:205320, 2010.

[55] T. Papenkort, T. Kuhn, and V. M. Axt. Generation of coherent lo phonons in optically driven biased quantum wells. *physica status solidi (c)*, **8**(4):1121–1124, 2011.

[56] J. Unterhinninghofen, D. Manske, and A. Knorr. Theory of ultrafast nonequilibrium dynamics in *d*-wave superconductors. *Phys. Rev. B*, **77**:180509, 2008.

[57] A. J. Leggett, S. Chakravarty, A. T. Dorsey, M. P. A. Fisher, A. Garg, and W. Zwerger. Dynamics of the dissipative two-state system. *Rev. Mod. Phys.*, **59**:1–85, 1987.

[58] S. A. Hamerla and G. S. Uhrig. One-dimensional fermionic systems after interaction quenches and their description by bosonic field theories. *New Journal of Physics*, **15**(7):073012, 2013.

[59] S. A. Hamerla and G. S. Uhrig. Interaction quenches in the two-dimensional fermionic Hubbard model. *Phys. Rev. B*, **89**:104301, 2014.

[60] W. H. Press, S. A. Teukolsky, W. T. Vetterling, and B. P. Flannery. *Numerical Recipes.* Cambridge University Press, 2007.

[61] L. Viola and S. Lloyd. Dynamical suppression of decoherence in two-state quantum systems. *Phys. Rev. A*, **58**:2733–2744, 1998.

[62] G. S. Uhrig. Keeping a quantum bit alive by optimized π-pulse sequences. *Phys. Rev. Lett.*, **98**:100504, 2007.

[63] G. S Uhrig. Exact results on dynamical decoupling by π pulses in quantum information processes. *New Journal of Physics*, **10**(8):083024, 2008.

[64] R. Bulla, H.-J.. Lee, N.-H. Tong, and M. Vojta. Numerical renormalization group for quantum impurities in a bosonic bath. *Phys. Rev. B*, **71**:045122, 2005.

[65] J. Bardeen, L. N. Cooper, and J. R. Schrieffer. Theory of superconductivity. *Phys. Rev.*, **108**:1175–1204, 1957.

[66] G. Czycholl. *Theoretische Festkörperphysik.* Springer, 2007.

[67] N. N. Bogoliubov. *Soviet physics Journal of Experimental and Theoretical Physics*, 7:41, 1958.

[68] N. N. Bogoliubov. *Nuovo Cimento*, 7:794, 1958.

[69] H. Fröhlich. Interaction of electrons with lattice vibrations. *Phys. Roy. Soc. Lond.*, **A215**:291, 1952.

[70] W. Nolting. *Grundkurs Theoretische Physik 7.* Springer Berlin Heidelberg, Berlin, Heidelberg, 2005.

[71] C. P. Poole, H. A. Farach, R. J. Creswick, and R. Prozorov. *Superconductivity.* Academic Press, New York, 2007.

[72] E. A. Yuzbashyan, B. L. Altshuler, V. B. Kuznetsov, and V. Z. Enolskii. Solution for the dynamics of the BCS and central spin problems. *Journal of Physics A: Mathematical and General*, **38**(36):7831, 2005.

[73] P. W. Anderson. Random-phase approximation in the theory of superconductivity. *Phys. Rev.*, **112**:1900–1916, 1958.

[74] R. W. Richardson and N. Sherman. Exact eigenstates of the pairing-force Hamiltonian. *Nuclear Physics*, **52**(0):221 – 238, 1964.

[75] V. B. Kuznetsov. Quadrics on real Riemannian spaces of constant curvature: Separation of variables and connection with Gaudin magnet. *Journal of Mathematical Physics*, **33**(9):3240–3254, 1992.

[76] E. K. Sklyanin. Separation of variables: New trends. *Progress of Theoretical Physics Supplement*, **118**:35–60, 1995.

[77] T. K. Cheng, J. Vidal, H. J. Zeiger, G. Dresselhaus, M. S. Dresselhaus, and E. P. Ippen. Mechanism for displacive excitation of coherent phonons in Sb, Bi, Te, and Ti_2o_3. *Applied Physics Letters*, **59**(16), 1991.

[78] T. Dekorsy, A. M. T. Kim, G. C. Cho, H. Kurz, A. V. Kuznetsov, and A. Förster. Subpicosecond coherent carrier-phonon dynamics in semiconductor heterostructures. *Phys. Rev. B*, **53**:1531–1538, 1996.

[79] O. Kojima, K. Mizoguchi, and M. Nakayama. Enhancement of coherent longitudinal optical phonon oscillations in a GaAs/AlAs multiple quantum well due to intersubband energy tuning under an electric field. *Phys. Rev. B*, **70**:233306, Dec 2004.

[80] T. Papenkort. *Coherent and sqeezed phonons in semiconductor quantum wells*. PhD thesis, WWU Münster, 2012.

[81] T. Dekorsy, A. Bartels, H. Kurz, K. Köhler, R. Hey, and K. Ploog. Coupled Bloch-phonon oscillations in semiconductor superlattices. *Phys. Rev. Lett.*, **85**:1080–1083, 2000.

[82] A. W. Ghosh, L. Jönsson, and J. W. Wilkins. Bloch oscillations in the presence of plasmons and phonons. *Phys. Rev. Lett.*, **85**:1084–1087, Jul 2000.

[83] P. A. M. Dirac. The quantum theory of the emission and absorption of radiation. *Proceedings of the Royal Society of London. Series A*, **114**(767):243–265, 1927.

[84] G. Wentzel. Über strahlungslose Quantensprünge. *Zeitschrift für Physik*, **43**(8):524–530, 1927.

[85] F. Wegner. Flow-equations for Hamiltonians. *Ann. Phys.*, **506**(2):77–91, 1994.

[86] S. D. Głazek and K. G. Wilson. Renormalization of Hamiltonians. *Phys. Rev. D*, **48**:5863, 1993.

[87] S. D. Głazek and K. G. Wilson. Perturbative renormalization group for Hamiltonians. *Phys. Rev. D*, **49**:4214, 1994.

[88] S. Kehrein. *The Flow Equation Approach to Many-Particle Systems*, volume 217 of *Springer Tracts in Modern Physics*. Springer, Berlin, 2006.

[89] H. Krull, N. Drescher, and G. Uhrig. Enhanced perturbative continuous unitary transformations. *Phys. Rev. B*, **86**:125113, 2012.

[90] G Rickayzen. *Theory of superconductivity.* Interscience Publ., New York, 1965.

[91] M. Eckstein, M. Kollar, and P. Werner. Interaction quench in the Hubbard model: Relaxation of the spectral function and the optical conductivity. *Phys. Rev. B*, **81**:115131, 2010.

[92] T. Guenther, C. Lienau, T. Elsaesser, M. Glanemann, V. Axt, T. Kuhn, S. Eshlaghi, and A. Wieck. Coherent nonlinear optical response of single quantum dots studied by ultrafast near-field spectroscopy. *Phys. Rev. Lett.*, **89**:057401, 2002.

[93] J. Sokoloff, M. Joffre, B. Fluegel, D. Hulin, M. Lindberg, S. Koch, A. Migus, A. Antonetti, and N. Peyghambarian. Transient oscillations in the vicinity of excitons and in the band of semiconductors. *Phys. Rev. B*, **38**:7615–7621, 1988.

[94] J. D. Jackson. *Klassiche Elektrodynamik.* de Gruyter, Berlin, New York, 2002.

[95] H. Suhl, B. T. Matthias, and L. R. Walker. Bardeen-Cooper-Schrieffer theory of superconductivity in the case of overlapping bands. *Phys. Rev. Lett.*, **3**:552–554, 1959.

[96] Y. Kamihara, T. Watanabe, M. Hirano, and H. Hosono. Iron-based layered superconductor La[$O_{1-x}F_x$]FeAs (x = 0.05-0.12) with Tc = 26 k. *Journal of the American Chemical Society*, **130**(11):3296–3297, 2008.

[97] J. Nagamatsu, N. Nakagawa, T. Muranaka, Y. Zenitani, and J. Akimitsu. Superconductivity at 39 K in magnesium diboride. *Nature*, **410**(63), 2001.

[98] J. Demsar, R. D. Averitt, A. J. Taylor, V. V. Kabanov, W. N. Kang, H. J. Kim, E. M. Choi, and S. I. Lee. Pair-breaking and superconducting state recovery dynamics inMgB_2. *Phys. Rev. Lett.*, **91**:267002, 2003.

[99] T. Mertelj, V. V. Kabanov, C. Gadermaier, N. D. Zhigadlo, S. Katrych, J. Karpinski, and D. Mihailovic. Distinct pseudogap and quasiparticle relaxation dynamics in the superconducting state of nearly optimally doped $SmFeAsO_{0.8}F_{0.2}$ single crystals. *Phys. Rev. Lett.*, **102**:117002, 2009.

[100] J.G. Bednorz and K.A. Müller. Possible highTc superconductivity in the Ba-La-Cu-O system. *Zeitschrift für Physik B Condensed Matter*, **64**(2):189–193, 1986.

Publications

H. Krull, N. A. Drescher, and G. S. Uhrig (**2012**)
Enhanced Perturbative Continuous Unitary Transformations , Phys. Rev. B **86**, 125113

Parts of this work have been published in:

H. Krull, D. Manske, G. S. Uhrig, and A. P. Schnyder (**2014**)
Signatures of nonadiabatic BCS state dynamics in pump-probe conductivity , Phys. Rev. B **90**, 014515

List of Figures

List of Tables

Danksagung

An dieser Stelle möchte ich mich bei den Menschen bedanken, die zum Gelingen dieser Arbeit beigetragen haben.
Besonderer Dank gilt Herrn Prof. Dr. Götz Uhrig für die Vergabe des interessanten Themas, die hervorragende Betreuung, die hilfreichen Diskussionen und wertvollen Anregungen.
Herrn Prof. Dr. Dirk Manske danke ich, dass er sich Zeit genommen hat die Zweitkorrektur dieser Arbeit zu übernehmen. Des Weiteren danke ich Ihm für die Möglichkeit meine Arbeit am Max-Planck-Institut für Festkörperforschung zu beenden. Auch für die vielen hilfreichen Diskussionen und wertvollen Anregungen danke ich sehr.
Ein weiterer großer Dank gebührt Dr. Andreas Schnyder. Durch seine hervorragende Betreuung und den vielen Diskussion hat er einen sehr großen Anteil am Gelingen dieser Arbeit.
Dem kompletten Lehrstuhl T1 danke ich für die schöne, lustige und produktive Zeit während meiner Arbeit.
Der Abteilung Quanten-Vielteilchensysteme des Max-Planck-Instituts in Stuttgart danke ich, dass sie mich so herzlich aufgenommen haben und mir die Zeit fern von der Heimat so erleichtert haben.
Meiner Familie und meinen Freunden danke ich für die Unterstützung und die angenehme Zeit fern ab vom Promotionsstress und Physik.
Meiner Verlobten Dominique Handschak danke ich für die Durchsicht der Arbeit und für die großartige Unterstützung während der Promotion. Insbesondere für das Verständnis für meine Zeit in Stuttgart danke ich sehr.